TKK Dissertations 209
Espoo 2010

LIGHTNING-INDUCED OVERVOLTAGES IN MEDIUM VOLTAGE DISTRIBUTION SYSTEMS AND CUSTOMER EXPERIENCED VOLTAGE SPIKES

Doctoral Dissertation

Nehmdoh A. Sabiha

Aalto University
School of Science and Technology
Faculty of Electronics, Communications and Automation
Department of Electrical Engineering

TKK Dissertations 209
Espoo 2010

LIGHTNING-INDUCED OVERVOLTAGES IN MEDIUM VOLTAGE DISTRIBUTION SYSTEMS AND CUSTOMER EXPERIENCED VOLTAGE SPIKES

Doctoral Dissertation

Nehmdoh A. Sabiha

Dissertation for the degree of Doctor of Science in Technology to be presented with due permission of the Faculty of Electronics, Communications and Automation for public examination and debate in Auditorium S4 at the Aalto University School of Science and Technology (Espoo, Finland) on the 18th of March, 2010, at 12 noon.

Aalto University
School of Science and Technology
Faculty of Electronics, Communications and Automation
Department of Electrical Engineering

Aalto-yliopisto
Teknillinen korkeakoulu
Elektroniikan, tietoliikenteen ja automaation tiedekunta
Sähkötekniikan laitos

Distribution:
Aalto University
School of Science and Technology
Faculty of Electronics, Communications and Automation
Department of Electrical Engineering
P.O. Box 13000
FI - 00076 Aalto
FINLAND
URL: http://sahkotekniikka.tkk.fi/
Tel. +358-9-470 25384
Fax +358-9-470 25012
E-mail: nehmdoh.sabiha@tkk.fi

ISBN 978-952-60-3045-6
ISBN 978-952-60-3046-3 (PDF)
ISSN 1795-2239
ISSN 1795-4584 (PDF)
URL: http://lib.tkk.fi/Diss/2010/isbn9789526030463/

TKK-DISS-2719

Picaset Oy
Helsinki 2010

AALTO UNIVERSITY
SCHOOL OF SCIENCE AND TECHNOLOGY
P. O. BOX 13000, FI-00076 Aalto, Finland.

ABSTRACT OF DOCTORAL DISSERTATION

Author Nehmdoh A. Sabiha

Name of the dissertation

Lightning-Induced Overvoltages in Medium Voltage Distribution Systems and Customer Experienced Voltage Spikes

Manuscript submitted 3 September 2009 | Manuscript revised 15 December 2009

Date of the defense 18 March 2010

☒ Monograph ☐ Article dissertation (summary + original articles)

Faculty Electronics, Communications and Automation
Department Electrical Engineering
Opponent Prof. Maria Teresa Correia de Barros, Technical University of Lisbon, Portugal
Supervisor Prof. Matti Lehtonen, Aalto University School of Science and Technology, Finland

Abstract: In Finland, distribution transformers are frequently subjected to lightning strokes for which they are continuously protected by spark-gaps. So, the breakdown probability of medium voltage (MV) spark-gaps is modeled using the Gaussian distribution function under an impulse voltage test in accordance with the IEC 60060-1 standard. The model is presented in the form of the well-known Gaussian tail probability. Accordingly, a modified probabilistic model is proposed to study the effect of impulse voltage superimposed on the ac voltage on the breakdown probability of MV spark-gaps. The modified model is verified using experimental data, where the experimental setup is arranged to generate a range of impulse voltages superimposed on the ac voltages. The experimental verification shows evidence of the efficacy of the proposed probabilistic model. Furthermore, the proposed model is used to evaluate single-phase, two-phase and three-phase spark-gap breakdown probabilities in the case of lightning induced overvoltages. These breakdown probabilities are used along with the simplified Rusck expression to evaluate the performance of MV overhead lines above a perfectly conducting ground under lightning-induced overvoltages using a statistical approach.

In order to study the overvoltages propagating through the transformer to its low voltage side, the high frequency model of the transformer is investigated. First, the investigation is carried out using model introduced by Piantini at no-load condition. This model is modified to take more than one resonance frequency into consideration. Therefore, the frequency response of the simulated transient voltage is improved. A verification of the modified model is carried out through the comparison between the experimental and simulation results, in which the time domain simulation is carried out using ATP/EMTP while MATLAB is used to identify the model parameters. As this model is found suitable only for unloaded transformer, an accurate and simplified model is proposed concerning unloaded and loaded conditions as well. The proposed high frequency transformer model is experimentally verified under different balanced load conditions considering two different practical distribution transformers. Then the impact of low voltage (LV) network feeder numbers, lengths, types and loads on the lightning-induced overvoltage reached at the service entrance point is investigated with and without MV spark-gap operation. The high frequency model representation of the distribution transformer and low voltage network are combined in a single arrangement in the environment of ATP/EMTP. A simplified low voltage surge arrester model is represented and verified. Finally, a study is carried out to mitigate the overvoltages by allocating the surge arrester at secondary side of the distribution transformer with concerning MV spark-gap operation.

Keywords: MV spark-gap, distribution function, lightning-induced overvoltage, statistical approach, high frequency transformer model, LV surge arrester.

ISBN (printed)	978-952-60-3045-6	ISSN (printed)	1795-2239
ISBN (pdf)	978-952-60-3046-3	ISSN (pdf)	1795-4584
Language	English	Number of pages	xviii + 178 p.

Publisher: Aalto University School of Science and Technology, Faculty of Electronics, Communications and Automation, Department of Electrical Engineering.

Print distribution: Department of Electrical Engineering

☒ The dissertation can be read at http://lib.tkk.fi/Diss/2010/isbn9789526030463/

Acknowledgements

First of all, I would like to raise unlimited thanks to God, the Most Gracious, the Most Merciful, Who said in His Holy Quran:

"It is He who shows you lightning, as a fear and as a hope (for those who wait for rain). And it is He who brings up (or create) the clouds, heavy (with water) (12). And the thunder glorifies and praises Him, and so do the angles because of His awe. He sends thunderbolts, and therewith He strikes whom He wills, yet they (disbelievers) dispute about Allah. And He is mightily in strength and severe in punishment (13)."
Translation of the meanings of Surah Ar-R´ad (The Thunder).

I would like to take this opportunity to acknowledge the faithful guidance and unlimited encouragement by Professor Matti Lehtonen. His excellent supervision was the main source of providing this work in its presented outline where several ideas in this dissertation have been benefited from his insightful discussions. Also, I would like to thank Dr. Nagy I. Elkalashy for a lot of faithful discussions during this work and I acknowledge his help during the experimental measurements.

I would like to express my appreciation for the financial support from Graduate School in Electrical Engineering (GSEE) during two and half years and the encouragements from Fortum Säätiö and Ella & Georg Ehrnrooth Säätiö.

I would like to acknowledge the collaboration with Dr. Naser Tarhuni and Dr. Petri Hyvönen in the mathematical modeling and experiments of spark-gap operation, respectively. I would like to gratefully appreciate the assistance with the experimental measurements by Mr. Jouni Mäkinen, Mr. Hannu Kokkola and Mr. Veli-Matti Niiranen. I would like to thank Mr. Tapio Tuomi for providing this work by statistical data of lightning current distribution in Finland. I would like to thank Professor Alexandre Piantini, Professor Carlo Alberto Nucci and Professor Hans Høidalen for their positive response regarding some of their unavailable publications. I would like to thank Dr. John Millar for checking the language of the paper published in IEEE/TDEI. I also would like to acknowledge the discussion with Dr. Pirjo Heine and to thank Professor Liisa Haarla for her interest to encourage me at the beginning of my study. I also would like to thank the department secretaries for their help. I would like to express my appreciation to the pre-examiners Professor Carlo Alberto Nucci and Dr. Kari Luoma for their honest and faithful comments.

At the last, but not least, I cannot forget to express my warmest gratitude to dear father, mother, brothers and sisters, mother-in-law, beloved husband and sons Ibrahim and Mohamed for their patience and endless support.

Aalto University School of Science and Technology, February 2010.

Nehmdoh A. Sabiha

Author's Contribution

The author of this thesis has had the main responsibility for all contents of the thesis, for doing all analyses and simulations of the shown results and for developing and writing the corresponding published papers. Professor Matti Lehtonen, he is the supervisor of this work and he has contributed in selecting the research topic, in presenting the work outline and in discussing the simulated results. Dr. Naser Tarhuni helped with the mathematics in chapter 2 as well as Dr. Petri Hyvönen, Dr. Nagy I. Elkalashy and Mr. Jouni Mäkinen helped with the experimental setups and measurements.

Table of Contents

List of Symbols and Abbreviations

E	The crest value of the voltage waves on the line,
e_i	The generated voltage due to bound charge collapse,
q	Bound charge per unit length of line,
C_1	Capacitance between the cloud and the line,
C_2	Capacitance between the line and the ground,
C	Capacitance per unit length of line,
V	Ground potential rise,
xx	Distance from the lightning striking point,
$(RLC)_d$	Resistance, inductance and capacitance of distributed circuit model for lightning return stroke current,
$i(0,t)$	Channel base current,
$i(z',t)$	Current along lightning channel,
z'	Height at any point z′ along the lightning channel,
t	Time,
v	Return stroke velocity,
I_u	A uniform current,
E_{close}	The close electric field,
H	Current channel height,
ε_0	Free space permittivity,
i_p	A breakdown pulse current,
λ_p	Decay constant of the breakdown pulse current,
i_c	A corona current,
λ_c	Decay constant of the corona current,
λ	Decay constant,
z''	Height at any point z′′ from a corona source,
i_{cs}	The corona current due to a corona source,
I_o, α and β	The parameters which determine the assumed double exponential shape of the single corona source,
t_{on}	The zero to peak time of the breakdown pulse current,
c	Light speed,
i_{bd}	Breakdown current,
i_c	Corona current,
v^*	Current wave propagation speed ,
g	The Heaviside function,
$P(z')$	The height dependent current attenuation factor,
ϕ	The total induced scalar potential in the line,
ϕ^i	The scalar potential,
$i(x,t)$	The total line current,
L' and C'	The inductance and capacitance per unit length, respectively,

$u(x,t)$	The total induced voltage on the line,
R_0 *and* R_L	Overhead power line termination resistances,
L	Overhead power line length,
h	The height of the conductor,
A_z^i	The vertical component of the incident vector potential,
U_{max}	The peak induced overvoltage in a power line in the point closest to the strike,
μ_0	Free space permeability,
Z_0	Characteristic impedance of the overhead power line,
I_0	The lightning peak current,
d	The closest distance between the lightning strike and the line,
E_z^i	The vertical incident electric field,
B_y^i	The transverse incident magnetic induction field,
E_x^i	The horizontal incident electric field,
u^s	The scattered voltage,
E_z^s	The vertical component of the scattered electric field,
u^i	The incident voltage,
i^s	The scattered current,
N_g	Ground flash density,
N_f	The number of flashovers of insulator strings induced by a direct lightning strike,
D_{min}	The minimum distance,
D_{max}	The maximum distance,
AB	The nodes correspond to spark-gap terminals,
d_s	Half distance between the two electrodes of spark-gap,
ΔU	Spaced voltage levels,
Uj	Starting voltage,
U_{50}	The voltage which leads to 50 % probability of discharge,
U_{10}	The voltage which leads to 10 % probability of discharge,
U_{16}	The voltage which leads to 16 % probability of discharge,
N_d	The number of times breakdown occurred,
N_t	The total number of times of applied voltage,
θ	Inception angle,
$P(U)$	Breakdown probability,
m	The mean of random variable,
σ	The standard deviation,
U_m	The applied AC peak value,
U_0	Voltage level at the impulse time,
N	Number of spark-gaps,
$\overline{P}$	The average breakdown probability per spark-gap,
P_{1ph}	The average probability of a single breakdown,
P_{2ph}	The average probability of the simultaneous breakdown of two spark-gaps,

P_{3ph}	The average probability of three spark-gaps simultaneously breaking down,
Pr_{1ph}	Probability of single phase fault type,
Pr_{2ph}	Probability of double-phase fault type,
Pr_{3ph}	Probability of three-phase fault type,
U_{arr}, U_n	Arrester rated voltage,
C_{s1}, C_{s2}, C_{sm}	Winding-to-winding and winding-to-enclosure capacitance,
Z_{skin}	Skin effects of winding conductors and an iron core,
Y_1, Z_2	Block indicating multiple resonances due to the combination of winding inductance and turn-to-turn capacitance,
Y_{mag}	Saturation and hysteresis effects of an iron core,
i_S	Stroke current injected into the system,
i_A	Surge arrester discharge current,
i_{pG}	Current entering the earth at the transformer pole ground,
i_{HG}	Current entering the earth at the house ground,
i_{X2}	Current into terminal of the distribution transformer,
i	Current in the interconnection path between the neutral conductors of the primary and secondary systems,
Lp, Ls	Leakage inductances,
Lm	Magnetizing inductance,
Rp and Rs	Resistive losses and the losses in the ferrite core at the lowest frequency,
Rm	Frequency dependent and represents the hysteresis losses in the core,
Cp and Cs	Distributed elements between turns of each winding,
Cps	The capacitance between the primary and secondary windings,
Z_{11}	Input impedance of the quadripole,
Z_{12}= Z_{21}	Transfer impedance of the quadripole,
Z_{22}	Output impedance of the quadripole,
$Z1$	Impedance between the primary and the ground,
$Z2$	Impedance between the secondary and the ground,
$Z3$	Impedance between the primary and the secondary,
U_1	Primary voltage,
U_2	Secondary voltage,
I_1	Input current of transformer,
R, L, C	Resistance, inductance and capacitance,
Z_1	Winding leakage impedance of each phase,
Z_m	Winding magnetizing impedance of each phase,
$y_{xy,\pi}$	Admittance between two nodes x and y in π- equivalent of the transformer,
$\Re$	The magnetic reluctance,
Ni	Ampere-turn,
Φ	Flux,
(C_1, C_2)	Capacitances between winding and mass,
(C_{12_1}, C_{12_2})	Capacitance between inner side of HV and outer side of LV windings,
ABC, abcn	The nodes correspond to the terminals at the HV and LV, respectively,
U_c	The highest power frequency voltage (continuous operating voltage),
I_n	The nominal discharge current,

I_{max}	Maximum discharge current,
U_o	Line-to-neutral voltage of the low-voltage system,
U_p	Voltage protection level,
U_{ps}	Simulated residual voltage (Simulated voltage protection level),
P [.]	Probability of event [.],
$(N)n$	The total number of possibilities,
$\binom{N}{n}$	The number of k-combinations of n objects,
$S, X, n_0, n_1, n, N, k, xi$	Events or Random variables,
f	The probability distribution function,
F	The cumulative distributions function,
$\overline{Y}$	The mean of the data,
σ^2	The variance,
ND	The number of data points,
Q	Q-function or the tail probability of the normalized Gaussian distribution,
$\phi(x)$	The cumulative distribution function of the normal Gaussian distribution,
erf	Error function or Gauss error function,
$erfc$	The complementary error function,
b	The width of the line,
Sf	Shielding factor,
h_{11}	Short-circuit input impedance,
h_{12}	Open-circuit reverse voltage gain,
h_{21}	Short-circuit forward current gain,
h_{22}	Open-circuit output admittance,
A	Open-circuit voltage ratio,
B	Negative short-circuit transfer impedance,
C	Open-circuit transfer admittance,
D	Negative short-circuit current ratio,

TKK	Helsinki University of Technology,
MV	Medium Voltage,
LV	Low Voltage,
YLE	Finnish Broadcasting Company,
GPR	Ground Potential Rise,
EMC	Electromagnetic Compatibility,
BG model	Bruce-Golde model of the lightning return stroke current,
TL model	Transmission Line model of the lightning return stroke current,
MULS model	Master, Uman, Lin and Standler model,
TCS model	Travelling Current Source model,
MTL model	Modified Transmission Line model,
MTLE model	Modified Transmission Line with Exponentially Decay Model,
DU	Diendorfer-Uman Model,
NEMP	Nuclear Electromagnetic Pulse,
ICLRT	International Center for Lightning Research and Testing,
LEMP	Lightning Electromagnetic Impulse,

CLAs	Current Limiting Arresters,
EMTP	Electromagnetic Transient Program,
ATP	Alternative Transient Program,
pdf	Probability Density Function,
cdf	Cumulative Distribution Function,
sdf	Survival Density Function,
CLED	Coincident Lightning Events Detector,
CT	Current Transformer,
RC	The waveform digital memory device for measuring current,
VD	The capacitance divider made of insulators,
LIOV	Lightning Induced Overvoltage,
DSO	Fast Digitizing Oscilloscope,
PC	Personal Computer,
BIL	Basic Insulation Level,
ANN	An Artificial Neural Networks,
HV	High Voltage,
IEC	International Electrotechnical Commission,
GFD	Ground Flash Density,
CH	Channel,
T	Transformer,
PLC	Power Line Communication,
MF model	Medium Frequency model,
HF model	High Frequency model,
SPD	Surge Protective Device,
IEEE	Institute of Electrical and Electronics Engineers,
WG	Working Group,
MCOV	Maximum Continuous Operating Voltage,
r.m.s	Root Mean Square,
ABB	Asea Bronu Boveri,
LOVOS	The product name of the LOw VOltage Surge arrester given by ABB,
NA	Not Available,
TT, TN-C, TN-S, IT	Different earthing schemes.
AMKA	Overhead cable type,
XLPE/PVC	Underground cable type,
OHC	Overhead Cable,
UGC	Underground Cable,

1- Introduction

Lightning is an important meteorological process, it is a dangerous natural phenomenon which causes disturbances in our life, and it has a bad effect on mankind. So a great attention has been taken towards this phenomenon. From electrical power systems point of view, these systems should be protected against this phenomenon, where large parts of the power system exposed to lightning. System components can be exposed to lightning-induced overvoltages; these overvoltages have high magnitude comparing with any voltage level of distribution network, so flashover is generated causing damage to the equipment when insufficient protection against this phenomenon is used. This directly affects on power quality and system reliability.

1.1 Lightning Phenomenon

The lightning is a natural phenomenon generated during thunderstorm by electrostatic discharge which produced electromagnetic radiations. The lightning is occasionally associated with thunder due to the electric current passing through the lightning channel [1]. The main source of lightning is rainstorms and it is rarely occurred during snowstorms.

1.1.1 Types of Lightning

Lightning discharges can be classified into three main types [2-4]:

1. Intracloud discharge,
2. Cloud-to-cloud discharge and
3. Cloud-to-ground discharge.

From the power system point of view, cloud-to-ground discharge is the frequent type that generates lightning overvoltages on overhead distribution lines. The process explanation of the cloud to ground discharge is discussed in the following subsection.

1.1.2 Lightning Process

Figure 1.1 shows induced charges on transmission line when the thunder cloud located above the transmission line. In Figure 1.1.a, the distribution of negative and positive charges of the charged thunder cloud is depicted with different temperature values. In the base of the thunder cloud, the negative charges center is at temperature -5 ^{o}C and located in the lower part of the cloud. At higher elevation, there is a positive charging center with temperature less than -20 ^{o}C. In the circumstances of many neighbor storm clouds, there are generated positive charges in a small region at the cloud base as depicted in Figure 1.1.a [5]. This small region temperature is around 0 ^{o}C.

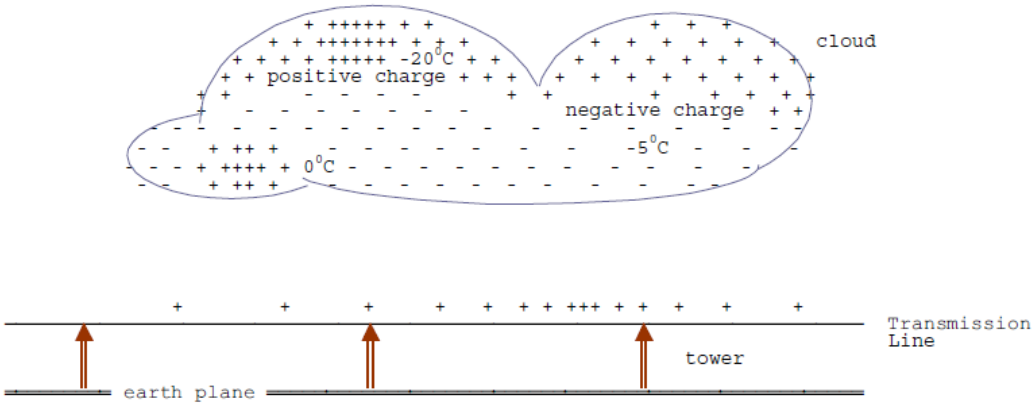

a. Induced charges with different temperature.

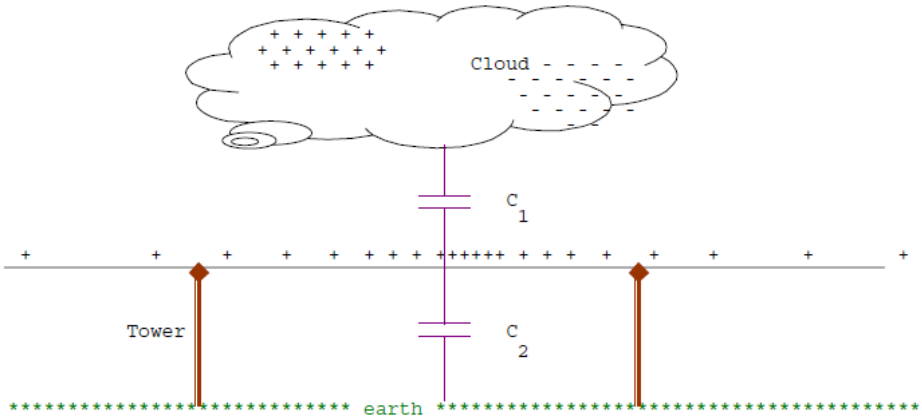

b. Induced charges indicating the calculation of the potential.

Figure 1.1 Induced charges on transmission line [5].

Figure 1.1.b shows the induced charge in the line through the down coming leader charge. These induced charges travel along the line with approximately the light velocity when the cloud is discharged. Otherwise, the induced charges remain at their positions without any traveling. The travelling of the induced charges along the line generates voltage surge in both sides of the line. This voltage is dependent on the lightning stroke location where it can be evaluated using the form:

$$e_i = -E.\frac{C_2}{C_1 + C_2} = \frac{q}{C} \tag{1.1}$$

where E is the peak value of the voltage waves on the line, C_1 is the capacitance between the cloud and the line, C_2 is the capacitance between the line and the ground, q is the bound charge per unit length of the line, C is the capacitance per unit length of the line.

The induced overvoltage process can be simply interpreted considering principles of electrostatic induction and electromagnetic induction [6]. These principles are discussed below.

A. Electrostatic Induction

Figure 1.2 shows the electrostatic induction process. In Figure 1.2.a, the positive charges are electrostatistically induced on the line when the thunder cloud elevated above it with negative charges at its lower part. Discharging between clouds and ground or between clouds themselves cause disappearing of the negative charges in the lower part of the thunder cloud. Then, the overvoltage is generated on both direction of the line due to travelling of the line positive charges along the line as shown in Figure 1.2.b.

B. Electromagnetic Induction

The dynamic process of the electromagnetic induction is shown in Figure 1.3. A magnetic field is generated by discharging the cloud to ground nearby the line. This generated magnetic field is due to the surge current associated with the discharging process. Considering such electromagnetic coupling, the overvoltage is induced and then travels over the line.

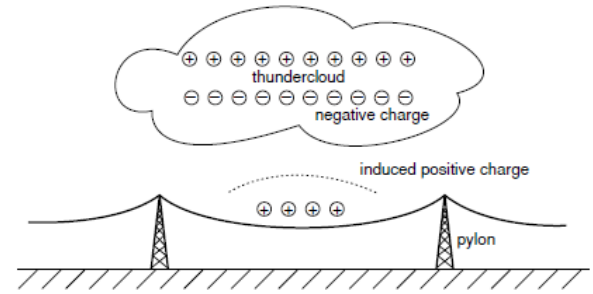

a. Bound charges

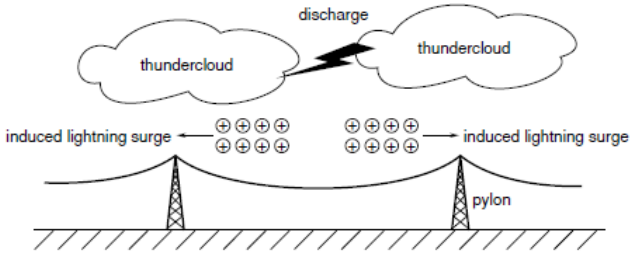

b. Discharge process

Figure 1.2 Electrostatic induction processes [6].

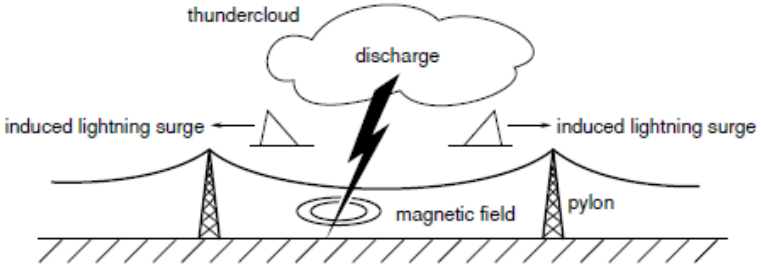

Figure 1. 3 Electromagnetic induction processes [6].

1.1.3 Lightning Channel

A streamer is generated from the thunder cloud to the ground when the electric field of the negative charges center reached 10 kV/cm. This streamer propagates with high velocity (one-tenth the light speed). A second streamer is generated after the occurrence of first streamer taking the same path of the first one. Therefore, the ionized channel is propagated a little more. This process continued several times (stepped leader stroke), in each time, the ionized channel length is increased by 10 to 100 m. The sequence of the streamers elongation is shown in Figure 1.4. Finally, when the stepped leader becomes near to the earth in a range of 15 to 50 m, an electric field is generated with a sufficient value to produce an upward streamer crossing the gap. The stepped leader produces high neutralized current flowing through the ionized channel to neutralize the charge. This current is called return stroke current and its value is high where it can reach to 200 kA. However, its average is statistically evaluated 20 kA [5]. In Finland, this average statistic value is around 15 kA.

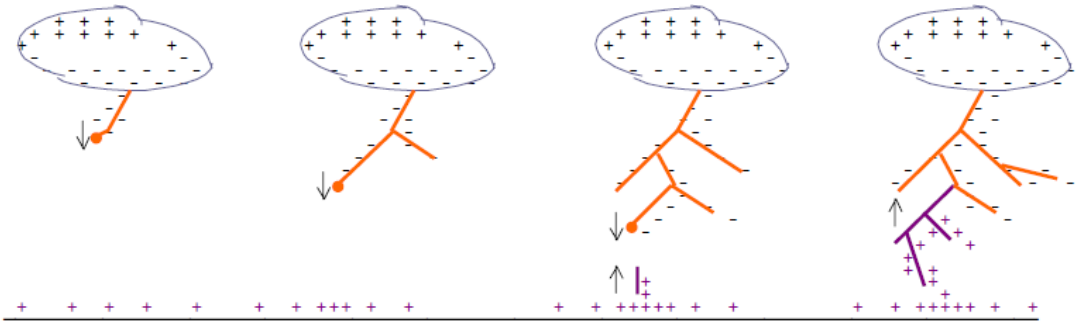

Figure 1.4 Propagation of lightning channel [5].

1.2 Difference between Direct and Indirect Lightning Strokes

Either direct or indirect lightning strokes cause overvoltages and therefore outages of the transmission lines are possibly increased. In case of indirect strokes, the return stroke current in nearby lines generates electromagnetic field which produces lightning-induced overvoltage [7].

1.2.1 Direct Stroke

Lightning direct stroke can be defined as the lightning stroke that directly hit any part of the electrical network. In most cases in power distribution lines, the insulation flashover is occurred although the return stroke current is small due to the high generated overvoltage which is very high comparing with the overhead distribution lines insulation level. For example, when the stroke current is 10 kA, the generated overvoltage can be 2000 kV [4]. Also, direct strokes cause faults in the high voltage lines due to the overvoltage and therefore flashover across the insulator strings [7,8].

1.2.2 Indirect Stroke

Indirect lightning stroke can be defined as the lightning stroke that does not directly hit any part of the electrical network; however, the induced overvoltage is generated and travelled over the network. This type of strokes is responsible for many of lightning outages of low insulation lines. Most of the flashes hitting near to the line produce overvoltages less than 300 kV [4].

Although the indirect strokes generate induced overvoltage with small amplitude comparing with generated overvoltage by direct stroke, they are frequently occurred affecting on the performance of overhead distribution lines. In the medium voltage distribution lines, indirect stroke is the main source of recorded faults as reported in [7,8].

1.3 Lightning Problems

As it is well-known, the lightning is coming from natural discharges and therefore generating overvoltages. However, these overvoltages can appear in different manners such as overhead line overvoltages and ground potential rises. These overvoltages are discussed in the following subsections.

1.3.1 Transmission Line Overvoltages

As aforementioned in section 1.1.2, the unmoved positive charges in the line are induced due to the presence of negative charges at the thunder cloud lower part. Then lightning discharge excited these positive charges on the line causing travelling of these charges along the line. Figure 1.5 shows different paths causing surges on the line. The overvoltage is generated in the line through three discharging paths as explained below in brief referring to Figure 1.5 [5].

A. Induced Overvoltage due to Nearby Lightning Stroke

Path (1) is the discharging between the leader core and the earth. Such path is occurred rapidly. However, the discharging between the leader core and earth wire as well as the conductor are occurred by travelling wave action which takes very longer time developing a voltage across insulator string .

B. Back-Flashover Mode

Path (2) is when the discharging is occurred between the leader core and the earth wire. In this case, there is voltage difference across the insulator, which is sufficient to cause back flashover from the tower back to the conductor.

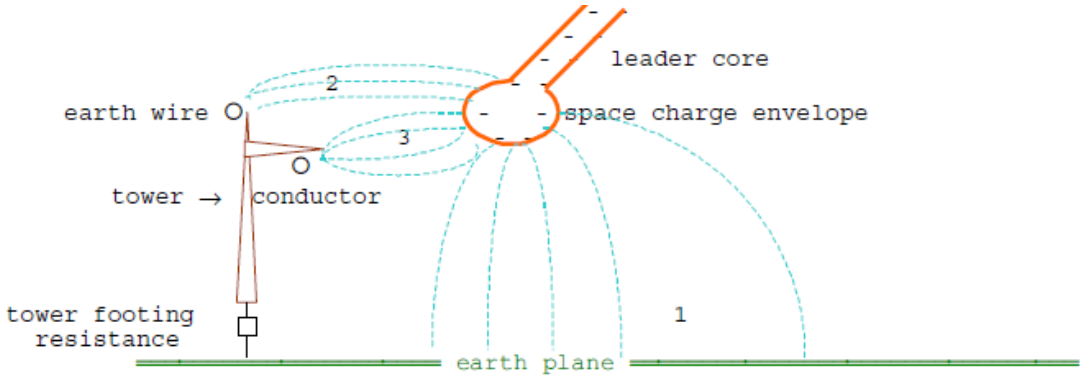

Figure 1.5 Geometry of lightning leader stroke and transmission line [5].

C. Shielding Failure or Direct Stroke to the Phase Conductor.

Path (3) is when the discharging is occurred between the leader core and the phase conductor injecting discharge current to the phase conductor. Therefore, the voltage is generated across the insulator string. Also, there is discharging path from the leader core to the earth via the tower.

1.3.2 Ground Potential Rise (GPR)

The ground potential rises due to flow of high current to the ground, which results from direct strokes to the building or to the rod allocated over the building. For example, there are two equipments as shown in Figure 1.6.a; one of them allocated close to lightning rod and the other one is far from the rod. When the lightning hits the lightning rod, there is potential rise at the first equipment. This potential rise travels over the cable to the second equipment [6]. On the other hand, if there is a building electrostatically charged as shown in Figure 1.6.b, these charges travel to earth when the discharging occurred between clouds or between cloud and ground. Therefore, there is a ground potential rise higher at one building than the other one. Such differences in ground potentials can produce surge travelling.

It is addressed in [9] that ground potential rise has been estimated under the assumption of uniformly flowing of the lightning current into the ground through a ground electrode or a tree as illustrated in Figure 1.7. The ground potential rise (GPR) at distance *xx* from the location of lightning stroke is given by the form:

$$V(xx) = V(0)/xx \qquad (1.2)$$

where $V(xx)$ is the ground potential rise at distance *xx* and $V(0)$ is the potential rise at the lightning striking point ($xx = 0$).

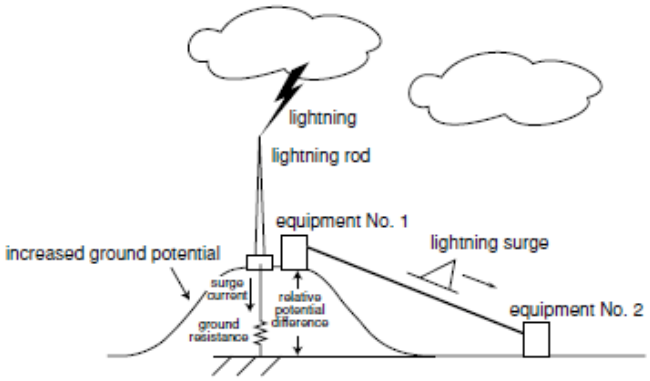

a. Lightning strikes a lightning rod.

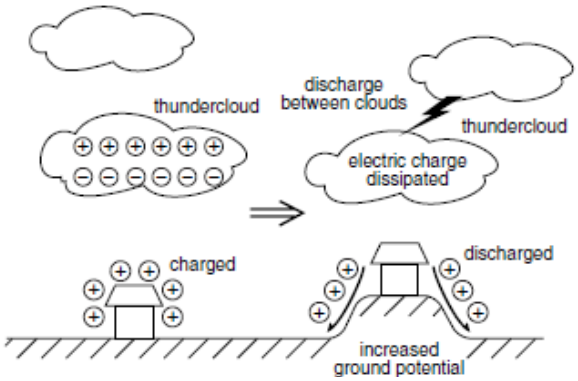

b. Electric charge on building directed to the ground.

Figure 1.6 Ground potential rise illustration [6].

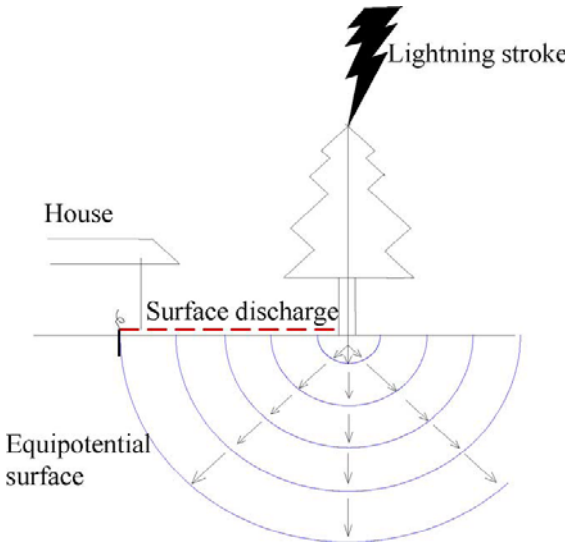

Figure 1.7 A simplified model of lightning hit to ground associated with voltages in residence [9].

From the comparison point of view between the voltage of ground potential rise and the lightning-induced overvoltage, the difference between them concerning low voltage circuit can be studied concerning the peak value, the direction and the duration. The two overvoltage types have approximately the same peak value while they have opposite direction. The lightning-induced overvoltage duration is shorter than the voltage by ground potential rise. Since the voltage generated by the ground potential rise has longer duration than the induced overvoltage, the voltage of ground potential rise generates large energy where it is more dangerous for the home appliances [9].

The soil resistivity is an important factor affecting on the ground potential rise. Increasing soil resistivity increases the ground potential rise. Therefore, this factor cannot be ignored and another factor should be considered that electromagnetic field deformation radiated from the return stroke [9,10].

1.4 Lightning-Induced Overvoltage on Power Lines

Indirect lightning-induced overvoltages on overhead lines are frequently occurred and they can cause damage to power systems, communication networks, electronic control and management systems. Therefore, indirect lightning estimation is very essential for the lightning protection design and insulation coordination of overhead lines. The powerful electromagnetic radiation occurs during the return stroke phase and then, the lightning-induced overvoltage is produced [11,12]. Higher voltages reaching up to few hundreds of kVs produce flashovers between the network conductor, in particularly, over the network insulator string. If the line terminal is protected by spark-gap, the overvoltages are discharged to the earth via spark-gap. Therefore, the protection relays can detect the spark-gap breakdown as short circuit although it is overvoltage protection. Accordingly, the corresponding breakers interrupt to isolate this recorded fault. This interruption scenario occurs because of spark-gap operation as it is evaluated in chapter 2. The magnitude and the shape of the induced overvoltage are dependent on lightning return stroke parameters of the ground, distance and relative position with respect to the transmission line and the line terminations [11,13,14]. The lightning-induced overvoltages can be evaluated considering the following two steps [15]:

I. Using lightning return stroke current where the electromagnetic field generated by the lightning return stroke current is calculated through employment of the return stroke current model. This model describes the lightning return stroke current as a function of height and time along over the channel.

II. Using an appropriate coupling model to attain the interaction between the electromagnetic field, which calculated in the previous step, and the line conductor and therefore the overvoltage is calculated.

1.4.1 Lightning Return Stroke Current Models

Lightning return stroke models are categorized into four classes. They are gas dynamic or physical models, electromagnetic models, distribution circuit or $(RLC)_d$ transmission line models and engineering models. For more information, deep discussions are reported in

[16,17]. The most frequent used models for computing the lightning return stroke current are the engineering models and therefore, they are discussed in the following subsections.

1.4.2 Engineering Models

According to the principles of this model category, the lightning electromagnetic fields are expressed as a function in return-stroke current models. These models are such as [15]:

A. Bruce-Golde (BG) Model

In this model, the current is in the form [18]:

$$i(z',t)=\begin{cases} i(0,t) & z' \le vt \\ 0 & z' \succ vt \end{cases} \tag{1.3}$$

where $i(0,t)$ is the current at ground beneath the wave front of the upward-moving return stroke at time t, z' represents any point along the lightning channel, v is the propagation speed of the return stroke wave front. The return stroke current propagating-upward by this model is depicted in Figure 1.8. The Bruce-Golde model is not physically recommended for the lightning stroke current where it is uncomfortable to have the Bruce-Golde model characteristics due to the discontinuity at the return stroke wave front.

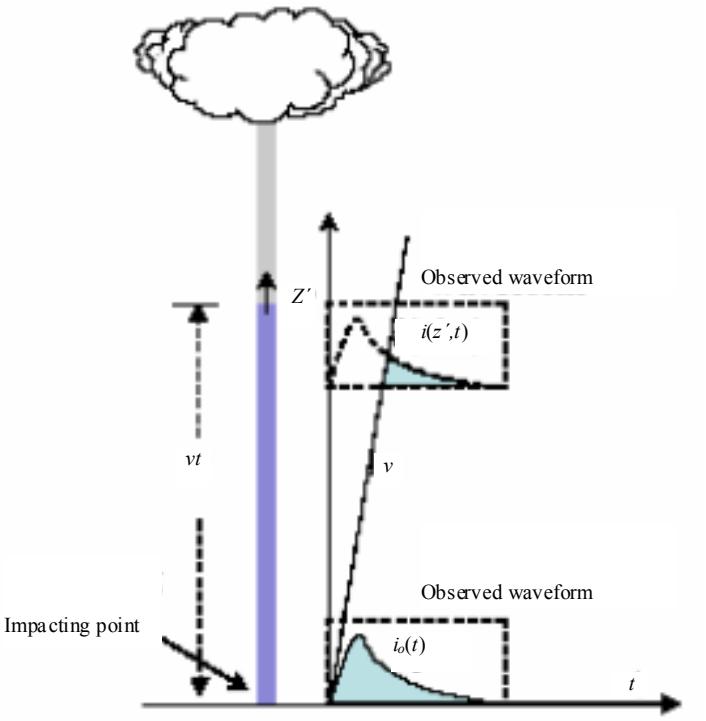

Figure 1.8 Return stroke current propagating-upward by BG model [16, 19].

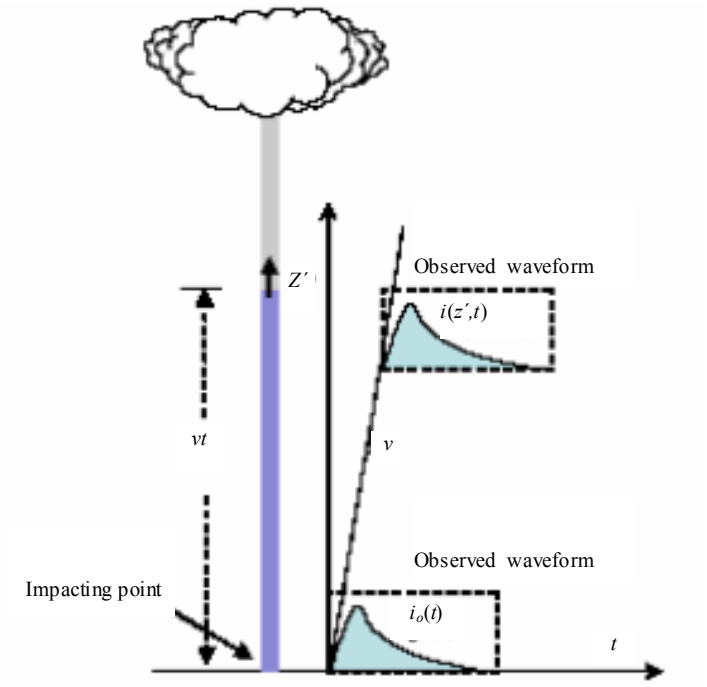

Figure 1.9 Return stroke current propagating-upward according to the TL Model [16,19].

B. Transmission line (TL) Model

In this model, the current waveform at the ground is assumed propagated upward at a constant speed without any distortion or attenuation. Based on this model, the current is in the form [20]:

$$i(z',t)=\begin{cases} i(0,t-z'/v) & z' \leq vt \\ 0 & z' \succ vt \end{cases} \tag{1.4}$$

In this model, the charge transfers from the bottom of the channel to the top without any removal of net charge from the channel [16,21]. The return stroke current propagating-upward according to the transmission line model is shown in Figure 1.9.

C. Master, Uman, Lin and Standler (MULS) Model

This model was introduced in [22] and then modified in [23]. During the lightning return stroke current process, there are three different types of current. These types are:

1. A uniform current (I_u) presents a leader current feeding from a thunder cloud at a fixed height H using the close electric field E_{close} (r equal to 1upto10 km) as reported in [22]. This current can be written in the form:

$$I_u = \frac{2\pi\varepsilon_0 (H^2+r^2)^{3/2}}{H} \frac{dE_{close}(r,t)}{dt} \tag{1.5}$$

2. A breakdown pulse current (i_p) describes the combination between the current upward propagating pulse and the upward propagating electrical breakdown at the return-stroke wave front. It is in the form [24]:

$$i_p(z',t) = \begin{cases} i_p(0, t - z'/v)\exp(-z'/\lambda_p) & z' \leq vt \\ 0 & z' \succ vt \end{cases} \quad (1.6)$$

where λ_p is the decay constant of the breakdown pulse current.

3. A corona current i_c is estimated considering radial opposite movement of the charge initially stored in the corona sheath around the leader channel. This current due to the corona source at altitude z′′ is in the form:

$$di_{cs}(z'',t) = \begin{cases} 0 & t \leq t' \\ I_0 \exp(z''/\lambda_c) \times \{\exp[-\alpha(t-t')] - \exp[-\beta(t-t')]\} dz & t \succ t' \end{cases} \quad (1.7)$$

where I_0, a and β are parameters determining the assumed double exponential shape of the single corona source, λ_c is the decay constant, $t' = z''/v + t_{on}$, and t_{on} is the zero to peak time of the breakdown pulse current. The drawbacks of this model are its mathematical complexity as well as the absence of channel base current from its original formulation.

D. Travelling Current Source (TCS) Model

This model assume that the current source propagate from ground to cloud at speed v and at height z'. More assumption is that the current is injected and propagated with the light speed c down the channel. This model current is in the form [25]:

$$i(z',t) = \begin{cases} i(0, t + z'/c) & z' \leq vt \\ 0 & z' \succ vt \end{cases} \quad (1.8)$$

The Bruce-Golde model can be deduced from the travelling current source model when the speed of the flowing current to ground is an infinite.

E. Modified Transmission Line (MTL) Model

In this model, the lightning current intensity is in the form [26]:

$$i(z',t) = \begin{cases} i(t - z'/v)\exp(-z'/\lambda) & z' \leq vt \\ 0 & z' \succ vt \end{cases} \quad (1.9)$$

where v is the return stroke velocity and λ is the decaying constant. The removal of the net charge from the leader channel can be occurred considering a good agreement with experimental results.

F. Modified Transmission Line with Exponentially Decay (MTLE) Model

The corona current of this model can be described as a modified transmission line model current moving upward with exponentially decaying as in the form [27]:

$$i_c(z',t) = \begin{cases} i_c(t - z'/v)\exp(-z'/\lambda_c) & z' \le vt \\ 0 & z' \succ vt \end{cases} \quad (1.10)$$

where λ_c is the decay constant.

G. Modified Transmission Line with Linear Current Decay (MTLL) Model

In this model, another modification of the transmission line model has been added where the current pulse decreases linearly while propagating up the channel. The current intensity can be expressed mathematically by the form [16, 28]:

$$i(z',t) = \begin{cases} i(0,t - z'/v)(1 - z'/H) & z' \le vt \\ 0 & z' \succ vt \end{cases} \quad (1.11)$$

where H is the total channel height.

H. Diendorfer-Uman (DU) Model

This model assumes that there are two independent processes for leader discharging; these processes are [29]:

1. Discharge the core of the leader channel which is highly ionized with very small time constant (1μs or less).
2. Discharge the corona envelope with a larger time constant (some of ms).

Therefore, the current at the ground can be expressed as a summation of the breakdown current and the corona current as given by:

$$i(z',t) = i_{bd}(0,t_m) - i_{bd}(0,z'/v^*)exp(-t_e/\tau_{bd}) + i_c(0,t_m) - i_c(0,t+z'/v^*)exp(-t_e/\tau_c) \quad (1.12)$$

where $t_m = t+z'/c$, $v^* = 1/(1/v+1/c)$, $t_e = (t-z'/v)$ and $i(0,t) = i_{bd}(0,t)+i_c(0,t)$

I. Generalization of the Engineering Models

The generalized current equation has been introduced by Rakov [16,30]. It is in the form:

$$i(z', t) = g(t - z'/v^*)P(z')i(0, t - z'/v^*) \quad (1.13)$$

where g is the Heaviside function equal to unity for $t \ge z'/v$ and zero otherwise, v^* is the current wave propagation speed and $P(z')$ is the height dependent current attenuation factor. Generally, this model is mathematically more proper and furthermore the Heaviside function g can enhance the field estimations.

The field, at very early times of lightning discharge occurrence, is not accurately modeled using all of the above models because all of them ignore the attachment process of the lightning discharge. Therefore, further experimental data are required to overcome such a drawback. Also, further theoretical and experimental activities are needed to include the presence of an elevated strike object at ground level or to include the channel bent in the models [16]. From

the above illustration, other simple and reliable models are required to compensate the shortcomings. This comment provides evidence to continue to discuss models such as the coupling models summarized in the following subsection.

1.4.3 Coupling Models

Electromagnetic fields are generated by the lightning current stroke. These fields can destroy the electrical network [31]. The coupling between the stroke and the lines are achieved using various models concerning field to line coupling. These models will be briefly described assuming that the conductors are located above a perfectly conducting ground and considering the geometry presented in Figure 1.10 [14].

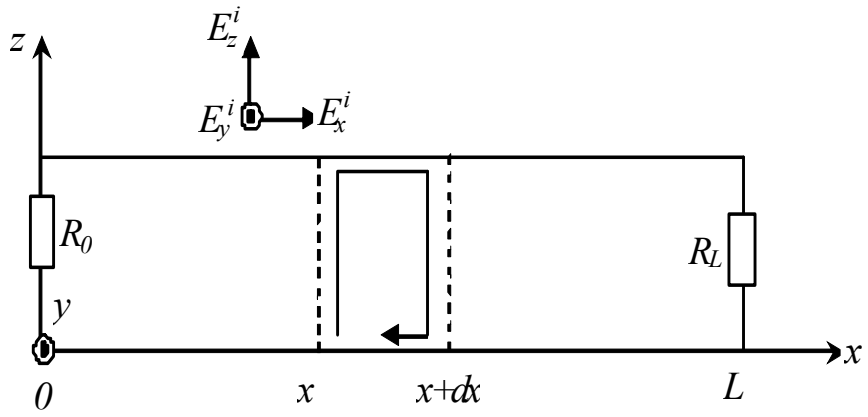

Figure 1.10 Geometry used for the calculation of overvoltages induced on an overhead power line by an indirect lightning return stroke (a lossless single-conductor overhead line parallel to the x-axis and contained in the xz plane terminated to two resistances R_0 and R_L [14].

A. Rusck Model

The transmission lines equations associated with the Rusck model were derived relating the total electric field on the conductor surface to the scalar and vector potentials. The corresponding transmission line coupling equations derivative by Rusck are listed in the following forms [14,32]:

$$\frac{\partial \phi(x,t)}{\partial x} + L'.\frac{\partial i(x,t)}{\partial t} = 0 \tag{1.14}$$

$$\frac{\partial i(x,t)}{\partial x} + C'\frac{\partial \phi(x,t)}{\partial t} = C'.\frac{\partial \phi^i(x,t)}{\partial t} \tag{1.15}$$

where ϕ is the total induced scalar potential in the line due to the scalar potential (ϕ^i) of the incident field, $i(x,t)$ is the total line current and L' and C' are the corresponding line inductance

and line capacitance per unit length, respectively. The total induced voltage *u(x,t)* on the line is given by:

$$u(x,t) = \phi(x,t) + \int_0^h \frac{\partial A_z^i(x,z,t)}{\partial t}.dz \tag{1.16}$$

where *h* is the height of the conductor and A_z^i is the vertical component of the incident vector potential. Therefore, the boundary conditions for the transmission corresponding to equations (1.14) and (1.15) are:

$$\phi(0,t) = -R_0.i(0,t) - \int_0^h \frac{\partial A_z^i(0,z,t)}{\partial t}.dz \tag{1.17}$$

$$\phi(L,t) = R_L.i(L,t) - \int_0^h \frac{\partial A_z^i(l,z,t)}{\partial t}.dz \tag{1.18}$$

From the abovementioned coupling line equations, the forcing functions are the scalar potential of the incident field and the vertical component of the incident vector potential at the line terminations. In other words, the line is excited by the scalar potential of the incident field which generates a vertical component of the electric field [33]. The peak induced overvoltage in a power line closest to the lightning strike has been estimated by Rusck using a simplified equation depending on stroke location and amplitude as reported in [34,4]. The corresponding form is:

$$U_{\max} = \frac{Z_0 I_0 h}{d}\left(1 + \frac{1}{\sqrt{2}}\frac{v}{c}\frac{1}{\sqrt{1-\frac{1}{2}\left(\frac{v}{c}\right)^2}}\right) \tag{1.19}$$

where Z_0 is the characteristic impedance $(1/(4\pi)\sqrt{\mu_0/\varepsilon_0})$, I_0 is the lightning peak current and *d* is the closest distance between the lightning strike and the line. However, this equation (1.19) does not give a complete description of the lightning induced overvoltage where it provides only the peak value. Also, there are restrictions for applying this equation where it is only applied under perfect ground conductivity and perpendicular lightning channel to the ground. Figure 1.11 depicts the transmission line representation of the Rusk model.

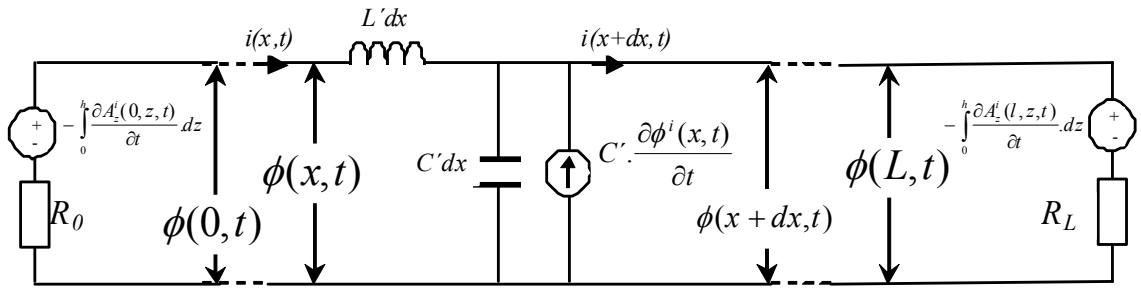

Figure 1.11 Transmission line coupling circuit associated with Rusck model.

The model (1.19) can be simplified by substituting the value of Z_0 by 30 Ω where the speed of the measured lightning return stroke for natural lightning varies between 0.29×10^8 m/s and 2.4×10^8 m/s as addressed in [35]. By assuming the return-stroke velocity is 1.2×10^8 m/s, the model takes the form:

$$U_{\max} = 38.8\frac{I_0 h}{d} \quad [kV] \tag{1.20}$$

As aforementioned, the shortcoming of this model is that it provides no information regarding the front and decay times of lightning-induced overvoltages [31].

B. Taylor et al. Model

Another model derived in terms of the distributed voltage and current sources was presented by Taylor et al. [36,37]. Transmission line equations have been proposed in terms of total line voltage and line currents as in the form:

$$\frac{\partial u(x,t)}{\partial x} + L'.\frac{\partial i(x,t)}{\partial t} = -\frac{\partial}{\partial t}\int_0^h B_y^i(x,z,t).dz \tag{1.21}$$

$$\frac{\partial i(x,t)}{\partial x} + C'.\frac{\partial u(x,t)}{\partial t} = -C'.\frac{\partial}{\partial t}\int_0^h E_z^i(x,z,t).dz \tag{1.22}$$

The boundary conditions can be expressed as:

$$u(0,t) = -R_0\, I(0) \tag{1.23}$$

$$u(L,t) = -R_L\, I(L) \tag{1.24}$$

In this case two forcing sources (functions) are used. These functions are the exciting vertical electric field (B_z^i) and the exciting transverse magnetic induction (B_y^i), unlike Rusk model. The corresponding transmission line representation associated with the Taylor et al. model is presented in Figure 1.12 by distributed parallel current source and distributed series voltage source. The interaction between nuclear electromagnetic pulse (NEMP) and transmission lines has been described by the Taylor formulation [36,38].

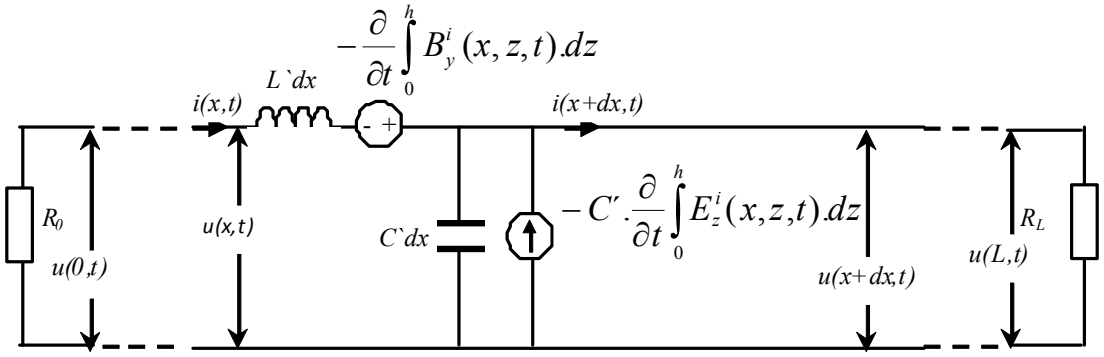

Figure 1.12. Transmission line coupling circuit associated with Taylor, Satterwhite and Harrison model.

C. Agrawal et al. Model

In this model, scattered voltage is used to describe the transmission line equations. In this case Maxwell's equations have been integrated along the integration path defined in Figure 1.10, and are expressed in terms of scattered voltage as in the form [14,38,39]:

$$\frac{\partial u^s(x,t)}{\partial x} + L' \frac{\partial i(x,t)}{\partial t} = E_x^i(x,h,t) \tag{1.25}$$

$$\frac{\partial i(x,t)}{\partial x} + C' \frac{\partial u^s(x,t)}{\partial t} = 0 \tag{1.26}$$

where $E_x^i(x,h,t)$ is the horizontal component of the incident electric field along the *x* axis at the conductor's height. $u^s(x,t)$ is the scattered voltage where it is defined by the form:

$$u^s(x,t) = -\int_0^h E_z^s(x,z,t)dz \tag{1.27}$$

where $E_z^s(x,z,t)$ is the vertical component of the scattered electric field.

The total line voltage $u(x,t)$ can be expressed in terms of scattered voltage as in the following form:

$$u(x,t) = u^s(x,t) + u^i(x,t) \tag{1.28}$$

Therefore, the total voltage at a given point along the line is the summation of the scattered voltage coming from the solution of (1.25) and (1.26) and the incident voltage which is defined by:

$$u^i(x,t) = -\int_0^h E_z^i(x,z,t)dz \tag{1.29}$$

where *h* is the height of the conductor and $E_z^i(x,z,t)$ is the incident vertical electric field.

The scattered voltage boundary conditions are:

$$u^s(0,t) = -R_0 i(0,t) - u^i(0,t) \tag{1.30}$$

$$u^s(L,t) = R_L i(L,t) - u^i(L,t) \tag{1.31}$$

It can be concluded that the horizontal incident electric field E_x^i along the line and the vertical incident electric field E_z^i at the line terminations generates the scattered voltage. The equivalent coupling circuit according to the Agrawal model is shown in Figure 1.13 where there are distributed voltage sources and two voltage sources at the line terminations. These terminated voltage sources are called risers.

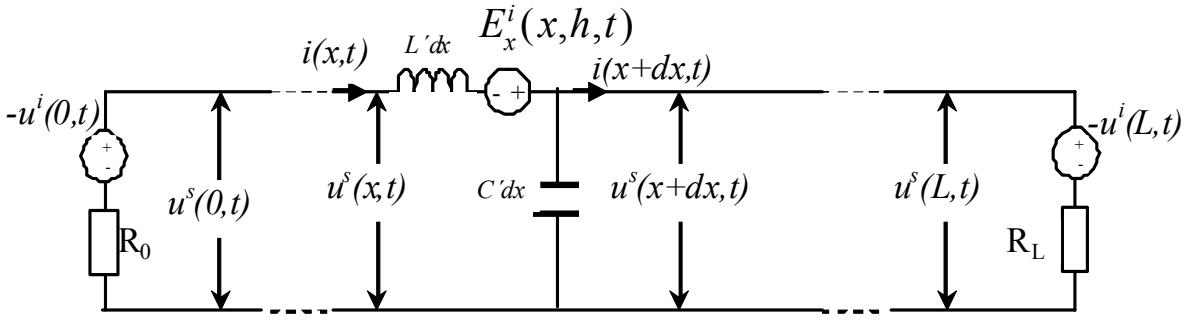

Figure 1.13 Transmission line coupling circuit associated with Agrawal et al. model.

D. Rachidi Model

It is addressed in [40] the formulation of the field to transmission line coupling equations derived by Rachidi. In Rachidi model, the magnetic excitation field is the main core for its derivation. This model is equivalent to models such as the Agrawal et al. and the taylor et al. The corresponding transmission line equations based on Rachidi coupling model are in the form [36,40]:

$$\frac{\partial u(x,t)}{\partial x} + L' \frac{\partial i^s(x,t)}{\partial t} = 0 \tag{1.32}$$

$$\frac{\partial i^s(x,t)}{\partial x} + C' \frac{\partial u(x,t)}{\partial t} = \frac{1}{L'} \int_0^h \frac{\partial B_x^i(x,z,t)}{\partial y} .dz \tag{1.33}$$

The total current in the line at point x and at the corresponding time t can be expressed in terms of the total scattered current as in:

$$i(x,t) = i^s(x,t) - \frac{1}{L'} \int_0^h B_y^i(x,z,t).dz \tag{1.34}$$

The boundary conditions at the line terminations are:

$$i^s(0,t) = -\frac{u(0,t)}{R_0} + \frac{1}{L'} \int_0^h B_y^i(0,z,t).dz \tag{1.35}$$

$$i^s(L,t) = -\frac{u(L,t)}{R_L} + \frac{1}{L'} \int_0^h B_y^i(l,z,t).dz \tag{1.36}$$

Field to transmission line coupling can be evaluated from the magnetic field components. Generally, the measurement of the magnetic fields is much easier than the measurement of the electric fields. Therefore, this model is more interesting because the magnetic field is only measured and used in the model [40]. Figure 1.14 shows the transmission line representation of the Rachidi model.

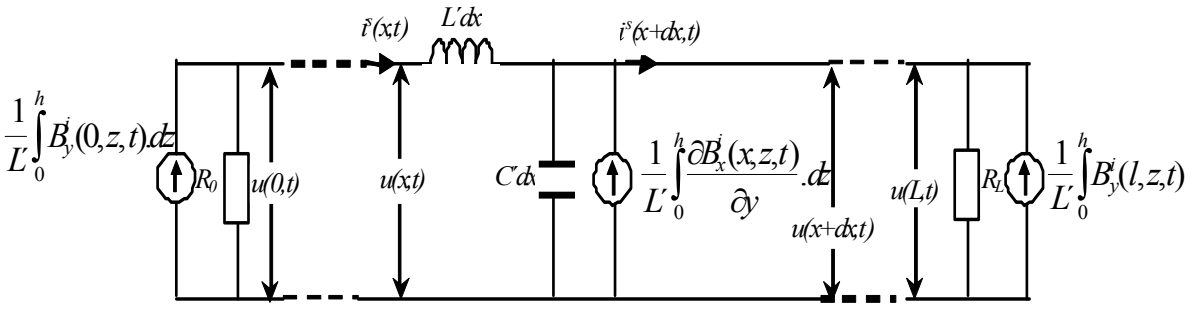

Figure 1. 14 Transmission line coupling circuit associated with Rachidi model.

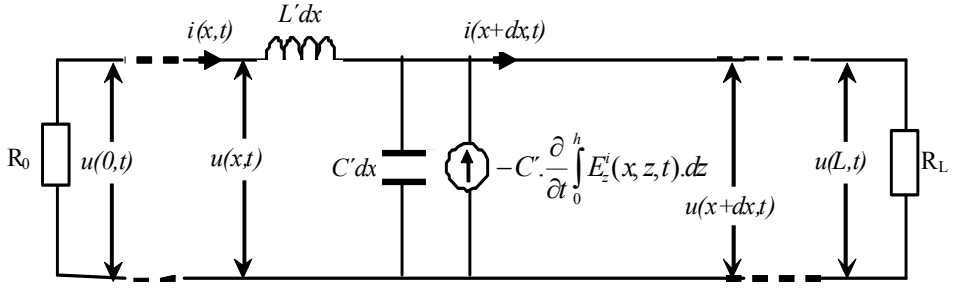

Figure 1.15 Transmission line coupling circuit associated with Chowdhuri - Gross model.

E. Chowdhuri Model

The transmission line equations presented by Chowdhuri and Gross [41] are similar to those of the Rusck model [32]. However, the total line voltage and incident inducing voltages are used in the model instead of total line voltage and incident scalar potentials [14,42]. The Chowdhuri transmission line equations are in the form:

$$\frac{\partial u(x,t)}{\partial x} + L'.\frac{\partial i(x,t)}{\partial t} = 0 \tag{1.37}$$

$$\frac{\partial i(x,t)}{\partial x} + C'.\frac{\partial u(x,t)}{\partial t} = -C'.\frac{\partial}{\partial t}\int_0^h E_z^i(x,z,t).dz \tag{1.38}$$

where E_z^i is the vertical component of incident electric field. The boundary conditions for the above set of equations are:

$$u(0,t) = -R_0.i(0,t) \tag{1.39}$$

$$u(L,t) = R_L.i(l,t) \tag{1.40}$$

The equivalent transmission line representation based on Chowdhuri coupling model is shown in Figure 1.15.

In the aforementioned coupling models, there are two models found superior and they are frequently used to estimate the lightning-induced overvoltages in power lines. They are Rusck model [32] and Agrawal et al. model [38]. Therefore, a comparison has been carried out between them as reported in [33]. This comparison showed that the Rusck model neglects the vector potential contribution and use only the portion of the horizontal electric field which causing it to be source dependent. Therefore, Rusck model can give accurate results, although it is incomplete computing lightning parameters. This accuracy is achieved with neglecting the contribution from the vector potential. Using single phase transmission line in [43], the lightning-induced overvoltage resulting from Rusk model has been evaluated with both the experimental measurements reported in [44] and the computed maximum induced overvoltage using Agrawal coupling model presented in [45].

These aforementioned models are still in the research because there are shortages as channel branches, lightning current attachment processes and relevant effects on the radiated electromagnetic field are still not taken into considerations [36]. In this work, lightning-induced overvoltage is evaluated by the simplified Rusck formula due to its simplicity and it produces good accuracy only for low values of soil resistivity. Therefore, it can be reliable under this condition as reported in [4].

1.5 Lightning Experiments

It is traditionally to experimentally accomplish lightning tests using impulse generators. However, there are limitations of the source ratings in such experiments and therefore they cannot be sufficient for heavily injecting of the experimental prototyped lightning current. Due to such experimental sophistications in accomplishing the lightning testing, artificial triggering of natural lightning strikes has been carried out in open field area exploiting network established. The lightning stroke point is controlled with exploiting the natural clouds. The striking point is controlled by launching a small rocket earthed by thin wires when the rocket is released and move with speed 200 m/s towards a charged cloud [46]. The consequences, when the rocket is at about height about 200 to 300 m, are that the field enhancement near the rocket tip launches a positively charged leader that propagates upward toward the cloud. Therefore, the trailing wire is vaporized and initial continuous current of the order of several hundred amperes is started. Consequently, negative charge moved from the cloud charge source to the designated point. The other lightning initiation approach is the ungrounded wire technique where the triggering wire not attached to the ground.

The Camp Blanding lightning triggering site, called the International Center for Lightning Research and Testing (ICLRT), occupies a flat, open field since 1994 and operated under an agreement between the University of Florida and the Camp Blanding Florida Army National Guard Base. The site is extended to include a 0.8 km test underground power cable, a 0.7 km test overhead power line.

1.6 Factors Affecting on Lightning-Induced Overvoltage

A. Multi-Conductor

The induced overvoltages due to nearby strokes are affected by the multi-conductor tower structure. This effect significantly depends on the line configuration where it becomes more extensive for vertical line configuration. However, in the horizontal line configuration, it depends on the distance of the strike point with respect to separation distances between the conductors [42]. The induced overvoltages on one conductor in a multi-conductor line are reduced by the effect of the other conductors. This reduction could be between 15 or 40% lower than those corresponding to a single line. Other study found that, due to the presence of multi-conductor, the induced overvoltage is reduced by 15 to 25% on each conductor comparing with single conductor [36,47]. Increasing the number of conductors increases the reduction of the induced overvoltage reaching to the highest reduction at the line end [48]. As the number of conductors is increased, a mutual shielding comes into effect, thereby reducing the induced overvoltage. However, this effect is nullified for the induced overvoltage at the location perpendicular to the lightning stroke [49].

B. Ground Wire/Shield Wire

The induced overvoltage is reduced when ground wires are used. This reduction depends on the position of the ground wire with respect to the phase conductors or ungrounded conductors [42]. Shield wires help in reducing the magnitude of induced overvoltages by a factor of about 20 to 40 % as addressed in [12,32,47,50]. The effectiveness of shielding wires is mostly affected by the spacing between two adjacent grounding points [51].

C. Ground Conductivity

The magnitude of the induced overvoltage in case of finite ground conductivity is function in the calculation point along the line. The induced overvoltage is increased at the midpoint of the line while it decreased at the line termination [49]. For lower conductor's heights (less than 10 m), the finite ground conductivity has a significant effect on the induced overvoltage magnitudes as well as its wave shape. Increasing the ground conductivity contributes to decrease the induced overvoltage [48,53]. However, for higher conductors, the finite ground conductivity has no effect on induced overvoltage [52]. Under finite ground conductivity assumption, the induced overvoltage at the midpoint of the line is increased while it is decreased at the line terminations. More information can be found in [54].

D. Lightning Strike Point

The induced overvoltage magnitude is decreased with increasing the incident angle. For striking point far away from the line, the induced overvoltage magnitude is decreased [48]. For the same return stroke parameters and assuming a perfectly conducting ground, the induced overvoltage at a given point along the line can be approximately assumed to decrease inversely proportional to the distance [10]. The delay time also increases with an increase in the distance as addressed in [53].

E. Transmission Line Height

The influence of the transmission line height is on the induced overvoltage amplitude and front steepness where they are increased with increasing the height of the line [53]. The induced overvoltage magnitude is nearly proportional to the line height for a perfectly conducting ground [36,47,55]. In case of perfectly ground conductivity, there is a nearly proportional between the magnitude of the induced overvoltage and the height of the line. However, in case of finite ground conductivity, the induced overvoltage increases as a function of the ground conductivity, the position of the stroke location and also the observation point along the line.

F. Transmission Line Length

The coupling between the lightning electromagnetic impulse (LEMP) and the transmission line can be neglected for the line length more than 2 km. The maximum value of the voltage amplitude remains constant with the line length for the lossless line. While, the maximum value of the voltage amplitude decreased clearly then slightly in case of small conducting ground [36,56].

G. Corona

The induced overvoltage affected by corona depends on the type of the lightning stroke (direct or indirect strokes). The induced overvoltage amplitude increased in case of indirect stroke. However, it decreased in case of direct stroke. The increasing of the induced overvoltage can be explained as the line capacitance is increased by corona. Therefore, the lightning-induced overvoltage propagation speed is decreased and it increases the total induced overvoltage. Generally, the corona has an effect on the induced overvoltage as significant as the finite ground conductivity. However, in case of direct stroke, the corona affects more on the induced overvoltage than the finite ground conductivity. In addition to, at the presence of corona, the induced overvoltage rise time is increased while its front steepness is decreased [57]. Corona affects on the mutual coupling between conductors where the induced overvoltage amplitude is increased in the most exposed conductors. However, it is decreased in the less exposed lines. In case of mutual coupling between lines, the corona should be taken into consideration [58].

H. Lightning Parameters

1. Front time

The induced overvoltages amplitude decreases when the lightning front time increases [48,59], having greater effect on the middle of the line. Generally, the induced overvoltage is inversely proportional with the front time. The other important parameter in the induced overvoltages is its front time that is proportional to the lightning front time [48].

2. Decay time

It doesn't affect the induced overvoltages where it is just observed a small variation on the induced overvoltage amplitude when the decay time is varied and the front time is lower than 1 μs [24]. The variation of time to half-value of the return stroke current has little effect upon the induced overvoltage amplitude [59].

3. Amplitude Current

It is common sense that the induced overvoltage is proportional to the current amplitude along the whole line without any affect from other parameters. However, the current amplitude has no impact on the induced overvoltage front time [48,59].

4. Return stroke velocity

The return stroke velocity affects on induced overvoltage magnitude, front time and decay time. Its influence is different along the line and depends on lightning strike location and ground conductivity. Greater variations of induced overvoltage magnitude could be observed at the end of the line when the ground conductivity is low [48]. The return stroke velocity affects on the induced overvoltage amplitude as well as on its wave shape, in particular on its front steepness. The induced overvoltage amplitude is decreased and its wave shape front steepness is increased by increasing the return stroke velocity [59]. The induced overvoltage peak is approximately proportional to the return stroke velocity for faraway stroke locations. However the induced overvoltages at these distances are not high. For near stroke locations, the return stroke velocity has no effect on the induced overvoltage [36,55,60].

1.7 Research Motivation

In different parts of Uusimaa in Southern Finland on Wednesday, the 22nd of August, 2007, about 18,000 households in the east of Helsinki and 20,000 homes in the southeast of Espoo were without electricity and furthermore broadcasting companies were influenced [61]. The disturbance source was powerful thunderstorm causing electrical blackouts. This provides evidence of necessary to do more research for better protection of the customers from lightning overvoltage spikes.

As the Finnish distribution networks are frequently subject to lightning-induced overvoltages, small distribution transformers (< 200 kVA) are traditionally protected with spark-gaps, and bigger ones with surge arresters. Appendix A shows the average ground flash density (GFD) per 100 km^2 in Finland from 1998-2008 collected on thunderstorm days [62]. The protected equipment by spark-gap should withstand the deep front lightning voltages and chopping due spark-gap breakdown.

Lightning overvoltages in distribution networks often cause igniting of all the spark-gaps of the three phases, which contribute to record three phase short-circuit by digital relays (usually with ground connection) and hence to reclosing operations in order to reconnect the feeder. In addition, voltage dip occurs during spark-gap breakdowns in all the feeders connected to the

same busbar in the substation. The deepness of the dip depends on the position of the sparking gaps because their position affecting on the short circuit current value. The other factor is the weakness of the network feeding the busbar or in other words the busbar short circuit impedance.

In Finland, many utilities have been planned to replace the spark-gaps with current limiting arresters (CLAs). This replacement can improve the equipment protection level in addition to decrease the amount of short interruptions and voltage dips which result from spark-gap operation [63]. Regarding this installation, there are two types of protection strategy. The first type is called the full protection strategy, which aims to protect all small transformers (less than 200 kVA) with current limiting arresters and large transformers with surge arresters. The second type is called partial protection strategy, which aims to protect all small transformers with current limiting arresters and large transformers with surge arresters up to certain distance from the substation. This distance depends on the minimum residual voltage during a three-phase short circuit. The traditional strategy is used in this case to protect the rest of the line. Using the partial strategy, the occurrence of the voltage dip can be prevented. However, Distribution transformers have traditionally been protected, and a major part is still protected, using protective spark-gaps [64].

When a MV spark-gap operates in order to dissipate the induced overvoltage, a steep voltage change is occurring, which creates a voltage spike transferred through the transformer to the low voltage side. However, there is usually no protection against this kind of overvoltages in low voltage networks as it is generated from a protection device. Therefore, it is worth to study the spark-gap characteristics and its impact on the induced overvoltages at the customer entrance.

From the literature point of view, the spark-gap characteristics have been described when it is only subject to surges but in the reality the surges are combined with ac voltages. So, this dissertation introduces a probabilistic model for spark-gap characteristics suitable for combined waveforms. However, there is an ac phase shift of 120^{o} between phases and lightning-induced overvoltages which induced equally in phases. This circumstance provides an instantaneous different voltage value of each phase. Therefore, probability of spark-gap operation of each phase is different. This motivates to modify the introduced model in order to take into account the ac phase shift in the three phases and therefore, to introduce the probability of single-phase, two-phase and three-phase spark gap operation.

As there is a probability of spark-gaps to be ignited and therefore discharge the overvoltage, there is a probability of induced overvoltage transferring over the distribution transformer to the secondary side due to the voltage waveform chopping. Therefore, these overvoltages can reach to the customer socket. In order to study how to protect against these overvoltages, the distribution transformers are to be accurately modeled in the high frequency domain. This high frequency transformer model is suitable to study the transformer under overvoltage transients due to lightning, switching and voltage waveform chopping. This transformer model provides an opportunity to evaluate the overvoltages at the customer entrance. Therefore, suitable protection system can be designed to prevent arrivals of overvoltages at appliances connected at the customer sockets.

1.8 Dissertation Objective

The mentioned motivations in previous section provide evidence of the work objectives. These objectives can be divided into two categories. The first one is to model spark-gap characteristics for combined waveforms of lightning overvoltage and ac voltage. Therefore, the probability of single-phase, two-phase and three-phase spark-gap operation is computed. The second one is to model the distribution transformer in the high frequency domain where this model helps to evaluate the transmitted overvoltages from the primary to the secondary side of the transformer. Then, an appropriate overvoltage protection device can be installed in low voltage networks to prevent the overvoltages. These two objectives are briefly described as follows.

The Gaussian distribution function is used as recommended in the IEC 60060-1 standard to model the breakdown probability of MV spark-gaps. The function is modified and introduced for the first time to predict the breakdown probability under impulse voltage superimposed on ac voltage. Experiments are used to investigate the proposed probabilistic model accuracy. The proposed model is used to evaluate single-phase, two-phase and three-phase spark-gap breakdown probabilities under lightning-induced overvoltage. This is then combined with the probability density function of the induced overvoltage in order to estimate the fault types due to lightning-induced overvoltage in MV networks.

Also, a very simple transformer model for unloaded as well as loaded conditions is presented to study the performance of the distribution transformer under lightning strokes. The transformer frequency response using experimental measurements is investigated in order to find the model parameters. The experimental setup is accomplished to measure the transient features due to impulse signals. The proposed model is verified concerning two practical distribution transformers. The proposed model is competitive to the Piantini model as it is presented in a simple way. Furthermore it is more accurate as two resonance frequencies are considered in computing the transformer model parameters.

Then, this accurate model with a simple high frequency circuit for transformer is used to study the response of the low voltage network due to both lightning-induced overvoltages in MV networks and the flashover of MV spark-gap connected at the primary terminal of the distribution transformer. Concerning these two different scenarios of induced overvoltages, the effect of the low voltage network configuration, number of overhead cables, lengths, load and types is investigated concerning the peak voltage profile along the feeder. Finally, the lightning protection for low voltage distribution network is suggested. The surge arrester operation is evaluated by comparing the dissipated energy in the two scenarios. It is found that the MV sparkgap operations provide higher induced overvoltages which are sever to the customers and their protection should be installed even if the network is underground cables.

1.9 Dissertation Outline

The dissertation consists of six chapters. The first chapter is the current one which is an Introduction. The second chapter introduces a probabilistic model for MV spark-gap characteristics concerning lightning-induced overvoltage superimposed on AC voltage. The model is verified using experimental statistical for the spark-gap flashovers. The third chapter investigates a proposed high frequency transformer model. The model accuracy is experimentally evaluated in time and frequency domains concerning the impulse waveform chopping due to spark-gap operation. In the fourth chapter, the surge arrester is modeled for LV network protection where the model accuracy is ascertained using surge arrester data sheet. The fifth chapter investigates lightning-induced overvoltages transmitted to customer side under spark-gap operation. Consequently, the mitigation is discussed using the surge arrester modeled in the fourth chapter. The last chapter is the conclusions.

2- Probabilistic Model for MV Spark-Gap Characteristics with Lightning-Induced Overvoltage Superimposed on AC Voltage

As one of the main objectives of this thesis is to study the overvoltages transferred to the low voltage network due to voltage collapse caused by the MV spark-gap operation, this chapter introduces the breakdown probability model of MV spark-gap when it is subjected to impulse voltage superimposed on the AC voltage. Then, the performance of MV overhead lines above a perfectly conducting ground under lightning-induced voltages using a statistical approach is evaluated.

The normal distribution is of fundamental importance in many statistical estimates and tests. In high voltage engineering, the processes of breakdown in air, flashover over insulators and other insulation arrangement are randomly occurred. The normal distribution is commonly used in such statistical applications of high voltage engineering due to its easiest handled by an engineer [65].

Another random behavior point of view is that applying voltage stress to the insulation individually as well as collectively and then measuring the random performance of insulation breakdown or withstand. Generally, the parameters describing the insulation characteristics are handled using statistical approaches [66]. From this point of view, the breakdown probability of the spark-gap is very important to study. The random nature of the appearance of breakdown can be modeled by considering a large number of stress applications where the probability of breakdown represents one of the insulation conditions [67]. Also, the breakdown probability is used for the coordination of spark-gaps with zinc-oxide arresters [68]. More declaration regarding the probability can be found in [69-74] and it is summarized in Appendix B.

2.1 Statistical Point of View of Overhead Lines under Lightning Strokes

Lightning is one of the major causes for outages in electric distribution and transmission networks. This lightning is random phenomena. Therefore, many statistical studies have been carried out on line performance under lightning [75-79]. In order to carry out such studies, instrumentation has been developed to differentiate between outages caused by lightning and those caused by other phenomena [75]. The lightning caused operation as well as non-lightning caused operation of the circuit breaker operations have been categorized by the coincident lightning events detector (CLED). A block diagram describing this process is shown in Figure 2.1. The lightning faults for both direct and indirect lightning strokes were recorded by the coincident lightning events detector for the same time periods as the ground flash density (N_g). More details about relation between N_g and number of strikes in the distribution networks are addressed [80] and summarized in Appendix C. There are buildings, houses and tress nearby the distribution line which is shorter than them and in such cases, the shielding wire should be used. Therefore, Eriksson's equation which is reported in [81] was modified to account for shielding from other nearby structures to modify the number of strokes to the line.

Another study has been carried out in order to describe four-phase and five-phase grounding faults caused by the lightning on a 154 kV overhead transmission line [76]. Insulator voltages and currents flowing along the ground wire and the tower have been measured as shown in Figure 2.2. There are installed Current transformers CT_1, CT_2, CT_3, and CT_4, in which they are allocated as shown in the figure. The transformer CT_1 is used to measure the lightning stroke currents flowing through the 1.2 m lightning rod. The transformers CT_2 and CT_3 are to measure the current in the ground wire. The transformer CT_4 is a cluster of four transformers and it is used to measure the current flowing through the upper part of the tower. RC is the waveform digital memory device for measuring current. The voltage divider VD is the capacitance divider made of insulators. Also, the lightning strokes to the transmission line and flashovers between the arcing horns have been photographed and the fault phases at substations have been examined. However, measurements of current and voltage waveforms caused by natural lightning on the transmission lines is extremely difficult because in general there is only a very slight chance of lightning striking a tower where measuring equipment has been installed.

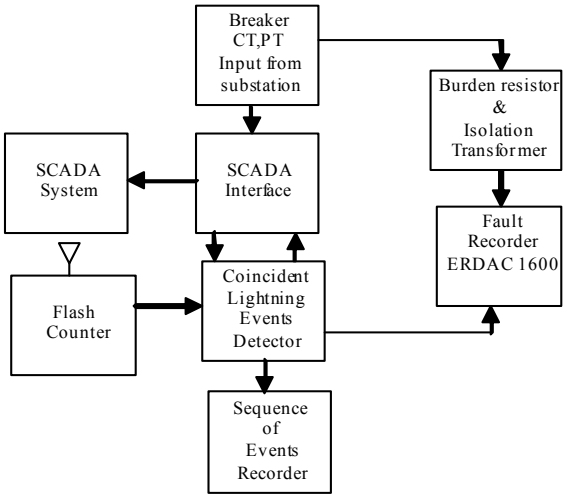

Figure 2.1 Instrumentation block diagram [75].

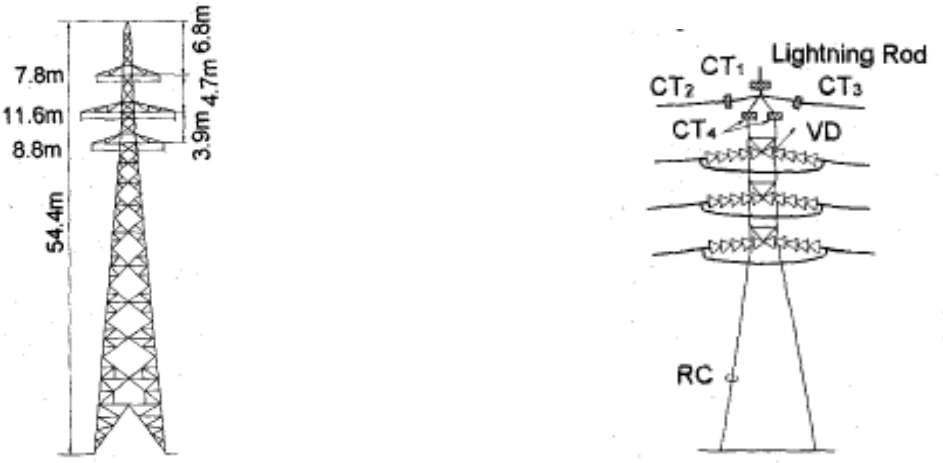

a. Structure b. Arrangement of equipment

Figure 2.2 Tower structure and arrangement of the equipment [76].

A study of the probability that a lightning flash detected by a lightning location system has been evaluated statistically [82]. An improved evaluation of the lightning performance of distribution lines overvoltages has been introduced based on the Monte Carlo method as reported in [77]. In this evaluation, the LIOV (Lightning-Induced Overvoltage) code has been used for the calculation of the lightning-induced overvoltages and Monte Carlo method has been used for the statistical evaluation of the line performance. Additional features have been added such as the steady-state voltage and the coupling factor changes between the line conductors and the ground at the location where flashovers take place. In this method, the lightning-induced overvoltage along a multi conductor line has been calculated as a function of lightning return-stroke channel-base current wave shape, return-stroke velocity, line geometry, stroke location, ground resistivity, relative permittivity and termination impedance.

In [78], stochastic approaches towards the assessment of lightning performance of overhead lines have been introduced using a combination of systematic EMTP simulations and the probability distribution functions. Two types of stochastic lightning performance characteristics are considered. The aim of the first one is to produce the number of flashover probability of the insulator strings due to direct strokes. The second type is done in order to produce the probability of fault types resulting from lightning strokes. Finally, the probabilities of fault types can assess the lightning performance of different line configuration

A number of insulation failures in distribution networks caused by direct and indirect strokes have been statistically evaluated as addressed in [79]. The estimation of overhead line and substation insulation failure rate resulting from the lightning-induced overvoltages has been described as well as another issue is to study the reduction of the direct lightning strike flashover rate resulting from the shielding effect of the nearby objects. As shown in Figure 2.3, the variation of the lightning stroke location has been performed from the minimum distance D_{min}, which is limiting the equivalent line attractive area, to the maximum distance D_{max} where lightning discharge can still cause the insulation flashover. The overhead line conductor can be directly strike when the lightning strokes are closer than D_{min}. On the other hand, the induced overvoltage is small to cause insulation failure when strokes are away from D_{max}. The distance D_{max} depends on the line basic insulation level (BIL). The analyses of the influence of the shielding effect by nearby objects have been performed. An estimation of flashover rate due to direct strokes has been analyzed taking into consideration the distance between the nearby object and the overhead line and the height of the object. The flashover rate of the medium voltage line is significantly reduced when they placed in the wood area comparing with the clear area due to shielding effect.

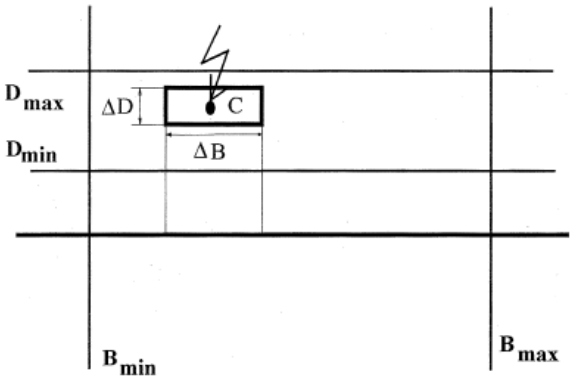

a. Limits in which the indirect lightning strike locations are varied.

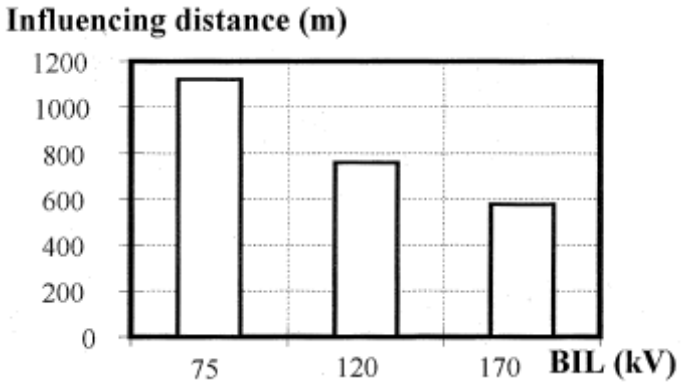

b. Maximum distance where the indirect lightning strikes can cause insulation flashover for various line insulation levels.

Figure 2.3 Indirect lightning strike location range [79].

The lightning performance of overhead distribution lines has been analyzed using a neural network in [83]. An artificial neural networks (ANNs) have been used to calculate lightning flashover rates of distribution lines, where the neural network architectures have been developed and trained to discriminate between strokes to the line and strokes to ground (with and without shielding wire) and to calculate the lightning overvoltage caused by each type of stroke using different algorithms. Therefore, the outputs of the model are the stroke type and the lightning induced overvoltage. The stroke type can be direct to phase conductor, nearby to ground with and without shielding wires and direct to shield wire. In this model, ANN has been trained using the calculated overvoltage produced from the lightning strokes which are randomly generated. The impact location (line or ground) has been deduced before induced overvoltage calculation. Finally, the lightning performance for any distribution line is duplicated using ANN. The model input variables are the return stroke velocity, the peak current, the height of the line and the closest distance from the stroke channel to the line with and without shielding wires. Furthermore, the shield wire height and the footing resistance for shield wire should be defined for the model. However, the validation of ANN performance depends on the range of the input data during the learning process.

The surge arresters or spark-gaps have been used for overvoltage protection purposes in medium voltage networks. In these networks, the effective protection using the shield wire is insignificant due to the small clearance between the ground wire and the conductor which leads to strike the phase conductor as well [84,85]. Therefore, it is worth to study the spark-gap breakdown characteristics. In practice, an impulse voltage does not exist alone in the field. Therefore, the impulse voltage should be superimposed on the AC voltage. Impulse breakdown superimposed on AC voltage has been combined in a study of several insulations [86-90]. However, none of these studies investigated the spark-gap breakdown probability model subjected to a combined waveform.

2.2 Experimental Work

2.2.1 Experimental Setup

Experiments were performed to determine the breakdown probability of an MV spark-gap under different impulse voltage values as well as to measure the impact of the AC voltage. The experiments were carried out at the High Voltage Laboratory, Helsinki University of Technology (TKK), Finland. The instruments used were:

1. Impulse voltage source,
2. Voltage divider,
3. Double spark-gap device (horn to horn type),
4. Current limiting resistor,
5. AC voltage source,
6. Fast digitizing oscilloscope (DSO) captured voltage trace,
7. PC with commercial software in order to interface the DSO with the PC for computerized data acquisition.

The experimental configuration is shown in Figure 2.4 and the corresponding equipment parameters are detailed in Appendix D. There were two considered setup configurations: the first configuration, shown in Figure 2.4a, was used to measure the spark-gap characteristics with impulse voltages only. The second configuration, shown in Figure 2.4b, was used to measure the spark-gap characteristics for combined voltages. In the second configuration, two sources, impulse and AC, were connected at the spark-gap terminals A and B, respectively. However, a small current limiting resistor was connected for safety reasons.

The distance between the two electrodes of the spark-gap was adjusted to 2 × 40 mm. The spark-gap configuration and its dimensions are specified in Appendix E.

All measurements reported here are for positive polarity impulses for which the breakdown voltage is lower than that of negative impulses for the gaps used. The tests were made during a period when the atmospheric pressure, temperature and humidity in the HV laboratory were very close to the standard values; hence correction factors had no impact.

For a statistical study, there are three test procedures [63,91]. They are summarized as follows.

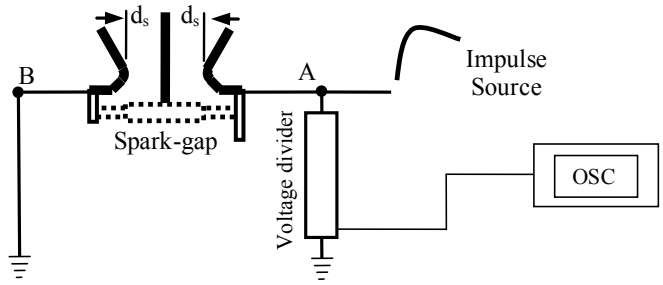

a. Impulse voltage test.

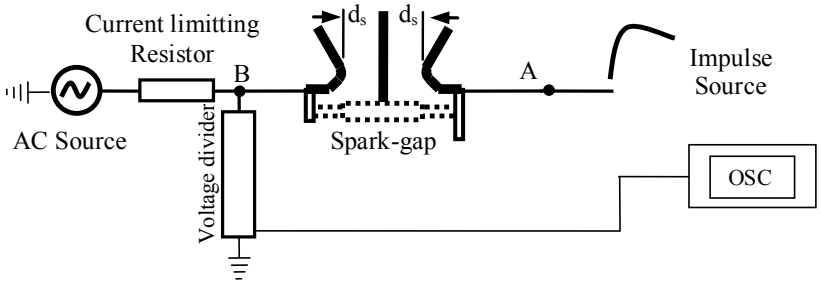

b. Combined voltage test.

Figure 2.4 Experimental setup configurations.

A. Up-and-Down Tests.

Up-and down test starts the first shot using voltage (U_j) close to the expected flashover value. Then, step voltage change *(*ΔU) is considered where this change is either up or down with respect to the first chosen voltage. The up or down is depending on the measured performance of the spark-gap at the voltage U_j. For example, if there is a breakdown, the next shot is down which means apply voltage U_j - ΔU. Accordingly, the parameters U_{50} (50 % probability) and U_{10} (10 % probability) can be extracted using these measured data where the probability of withstand are plotted against the voltage U_j. Then U_{50} and U_{10} are directly obtained from the graph. As relatively few shots can help to find the model parameters, this test concept is frequently used by industry. However, it is not very accurate in determining standard deviation (σ). The U_{10} can be expressed as a function of U_{50} as in the form:

$$U_{10} = 0.96\ U_{50} \tag{2.1}$$

More details on the up-and-down tests are addressed in [66].

B. The extended up-and-down method.

The concept of up-and-down is extended as following. A suitable number of impulses are applied at a certain voltage level to find the probability at this voltage level. If none causes discharge or the probability is less than 50%, the voltage is increased by a suitable step voltage change. If the attained probability is greater than 50%, the voltage is reduced by suitable voltage change. The 50 % probability of discharge is given by the form:

$$0.5 = 1-(1-p)^n \quad (2.2)$$

where n is a number of series shots would have 50 % probability of giving at least one flashover.

C. *Multiple-level tests*.

The steps of multiple-level tests are as following:

- At predefined voltage levels, a certain number of pulses (n) are applied on the spark-gap at each level,
- At each voltage level, the number (x) of spark-gap operations is defined,
- Draw fitted line on the plotted measured points of $p(U)$ (xj/n) against U (kV),
- At $P(U)$= 50 %, U_{50} is identified,
- and σ is defined by $\sigma = U_{50\%} - U_{16\%}$.

This test method is generally preferred for researching and live-line testing. In this chapter, the multiple-level test concept is applied as it is the general testing method used to study breakdown probability.

2.2.2 Impulse Voltage Tests

When the spark-gap was only subjected to the impulse voltage waveforms, the setup configuration shown in Figure 2.4a was considered. The impulse voltages were applied to terminal A of the spark-gap while terminal B was connected to the ground. The impulse voltages were varied from 81.66 kV to 116.31 kV. The front time 1.6 μs and tail time 50 μs were used in order to verify the proposed model. The corresponding breakdown probability of the spark-gap is summarized in Table 2.1. During the measurements, fourteen different values of impulse voltage were applied experimentally. Each impulse voltage value was applied about twenty times (or less), from which the breakdown probability can be calculated. This table is used to find the probabilistic model parameters discussed in subsection 2.3.1.

Table 2.1 Breakdown probability for impulse voltage tests.
U is the impulse voltage peak value, N_d is the number of times breakdown occurred, N_t is the total number of times of applied voltage and $P = N_d / N_t$ is the breakdown probability.

U (kV)	N_d	N_t	$P(U) = N_d/N_t$
81.66	0	20	0
81.73	0	10	0
82.99	0	12	0
84.78	3	20	0.15
81.68	4	20	0.20
85.69	6	20	0.30
86.69	8	20	0.40
86.92	10	20	0.50
86.90	11	20	0.55
89.04	16	20	0.8
89.06	18	20	0.9
90.54	20	20	1
91.13	20	20	1
116.31	20	20	1

2.2.3 Combined Voltage Tests

In order to study the impact of the AC voltage on the breakdown probability, the AC voltage source was added, as depicted in the setup configuration shown in Figure 2.4b. In this case, the experiment scenario is as follows:

1. The voltage divider was connected at point A to measure the value of impulse voltages.
2. Due to a shortage in the number of suitable voltage dividers, the connection of used one was moved from point A to point B, as shown in Figure 2.4b, and then the performance of the spark-gap breakdowns was captured through the oscilloscope.
3. A small current limiting resistor of 50 kΩ was used. Figure 2.5 shows samples of captured signals measured at point B, where the impulse voltage is applied at 5 ms. If there is a spark-gap breakdown, the impulse voltage becomes superimposed on the AC voltage at an inception angle (θ), as the AC voltage value at the impulse instant is described by $U_m \sin(\theta)$ (U_m is the applied AC peak value).
4. The oscillation in the signals in Figure 2.5 comes from the resonance between the voltage divider capacitance and the transformer inductances. This oscillation can be eliminated by increasing the current limiting resistor to a very high value but in practice this is not a point of concern.
5. Statistically, the considered impulse voltages were varied from 72 kV to 101 kV as summarized in Table 2.2, where the applied AC peak voltage was equal to 17.0 kV. Seven different impulse voltage values were applied to the spark-gap and were repeated one hundred times. The proposed probabilistic model for the combined voltage tests is verified using these results, as discussed in subsection 2.3.2.

Table2.2 Breakdown probability for combined voltage tests.

U (kV)	N_d	N_t	$P(U)= N_d/N_t$
72	29	100	0.29
76	33	100	0.33
81.5	51	100	0.51
91	64	100	0.64
95	78	100	0.78
98	80	100	0.8
101	89	100	089

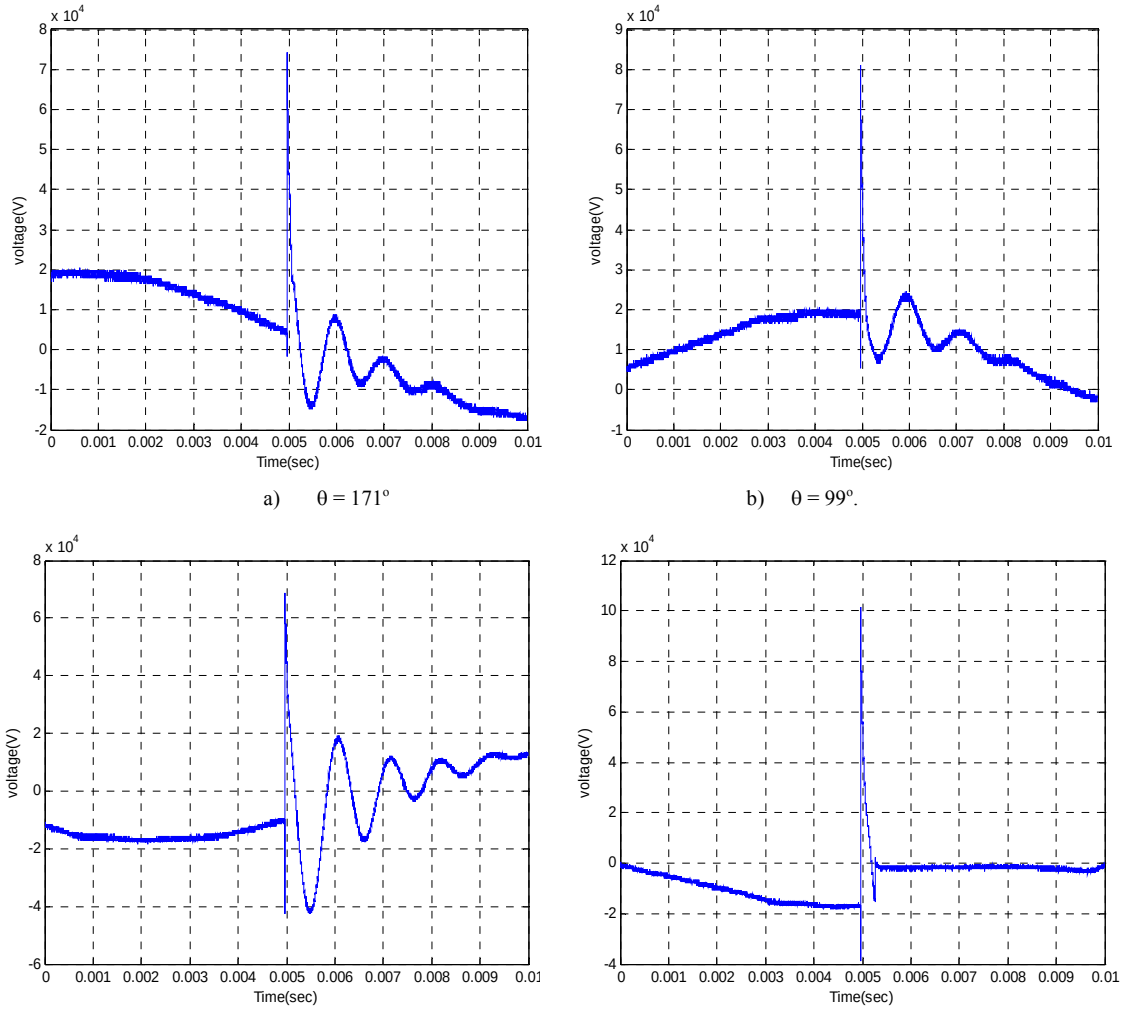

Figure 2.5 Voltage waveforms measured at different inception angles θ.

2.3 Probabilistic Model

2.3.1 Probabilistic Breakdown Model

In order to investigate the spark-gap breakdown probability, the most commonly used distribution function is the normal (Gaussian) distribution; another frequently used distribution function for representing breakdown probability is the Weibull function. Both the Gaussian and the Weibull functions produce similar results in the range $0.01 \leq P(U) \leq 0.99$, where $P(U)$ is the breakdown probability of the applied impulse voltage U [66].

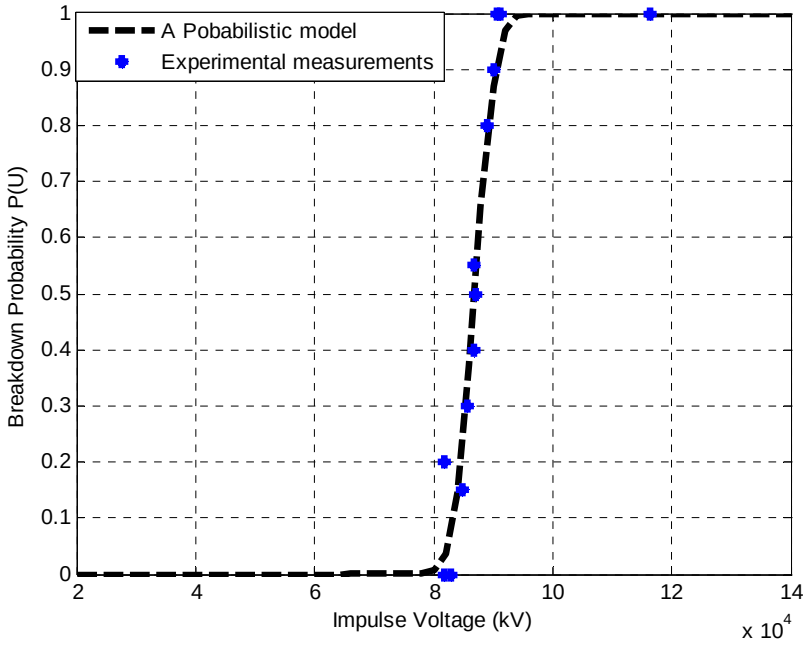

Figure 2.6 Comparison of the probabilistic model with the experimental results when the spark-gap is only subjected to impulse voltages.

When an earthed spark-gap is subjected to impulse voltage tests as depicted in Figure 2.4a, the probability of breakdown $P(U)$ at a voltage level of U is the integral of the Gaussian distribution function in the form [91]:

$$P(U) = \frac{1}{\sqrt{2\pi}\sigma}\int_{-\infty}^{U} e^{-\frac{(u-m)^2}{2\sigma^2}}\, du \tag{2.3}$$

where m is the mean and σ is the standard deviation.

Let $w = \frac{u-m}{\sigma}$, and $dw = \frac{du}{\sigma}$. Then equation (2.3) is rewritten as:

$$P(U) = \frac{1}{\sqrt{2\pi}}\int_{-\infty}^{\frac{U-m}{\sigma}} e^{-\frac{w^2}{2}}\, dw \tag{2.4}$$

which reduces to the following compact form,

$$P(U) = 1 - Q\left(\frac{U-m}{\sigma}\right) \tag{2.5}$$

where the Q- function, which quantifies the area under the normalized Gaussian probability density function tail, is:

$$Q(k) = \frac{1}{\sqrt{2\pi}}\int_{k}^{\infty} e^{-\frac{w^2}{2}}\, dw \tag{2.6}$$

Equation (2.5) describes the breakdown probability as a function of the applied voltage level in terms of the Q-function.

From the results of Table 2.1 in subsection 2.2.2, the standard deviation σ and the mean m of the impulse voltage breakdowns are found 2.75 kV and 86.9 kV, respectively. Considering these parameters, the probabilistic model in equation (2.5) is implemented using Matlab, as shown in Appendix F. The corresponding theoretical results are compared with the experimental measurements of Table 2.1, as depicted in Figure 2.6. The figure shows a good agreement between the theoretical model and experimental results.

Actually, the impulse voltage could not exist alone in the field but its impact on the spark-gap is in the form of its superimposition on the AC voltages. Therefore, in the following subsections this situation is thoroughly analyzed and the corresponding average breakdown probability is evaluated.

2.3.2 Proposed Model for Combined Voltages

As the impulse voltage duration is very short with respect to the period of the AC waveforms, the AC value during the time of applying the impulse voltage can be considered constant. If the time instant of the impulse voltage is exactly known, then the value of the AC voltage can be determined. If the AC voltage level at the impulse time is denoted by U_0, then the breakdown probability is similar to equation (2.5), by taking into account the reduction of the applied voltage to the spark-gap terminals by U_0. So, the breakdown probability is [92]:

$$P(U) = 1 - Q\left(\frac{(U - U_0) - m}{\sigma}\right) \tag{2.7}$$

However, in a real power system case, the time instant of the applied impulse is not known, therefore equation (2.7) is modified by including the sinusoidal term with a random phase angle θ. The phase angle is distributed according to a uniform probability density function over 0 to 2π. This is a reasonable assumption meaning that it is uncertain at what time the lightning may strike. The resultant breakdown probability is now given as:

$$P(U) = 1 - Q\left(\frac{(U - U_m \sin(\theta)) - m}{\sigma}\right) \tag{2.8}$$

where U_m is the peak value of the sinusoidal AC voltage. The result given in equation (2.8) is also a random variable and averaging over the random phase is applied to get an average breakdown probability of,

$$\overline{P}(U) = 1 - \frac{1}{2\pi}\int_0^{2\pi} Q\left(\frac{(U - U_m \sin\theta) - m}{\sigma}\right) d\theta \tag{2.9}$$

Equation (2.9) is easily solved numerically using Matlab, as depicted in Appendix F. Using the previously evaluated mean and standard values, and the applied AC peak voltage U_m, which is equal to 17.0 kV, a comparison of the theoretical results using (2.9) and the experimental measurements tabulated in Table 2.2 is shown in Figure 2.7. The solid line is the theoretical result from the model in (2.9) and the dashed line is the result of the impulse voltage test model (2.5). Figure 2.7 shows a good agreement between theoretical and experimental results. Small shift of the theoretical curve to the right relative to the measured values is believed to be due to the small current limiting resistance introduced to protect the measurement equipment.

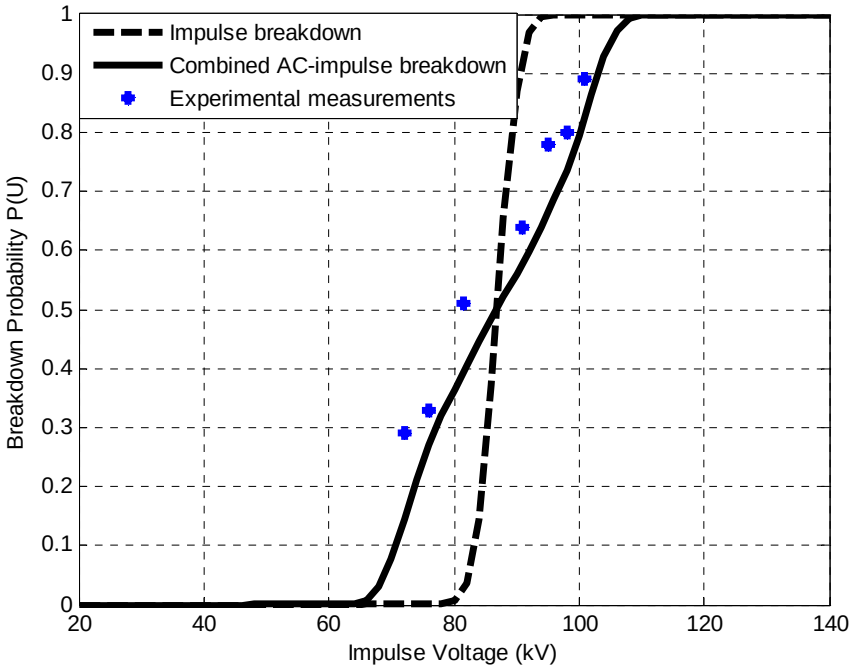

Figure 2.7 Breakdown probability for applying combined waves.

2.3.3 The Model for Multi-Phase Breakdowns

For a total number of N independent and identical spark-gaps, the average probability of $n \le N$ simultaneous breakdowns can be evaluated using the binomial distribution [92]:

$$P_n(U) = \binom{N}{n} \overline{P}(U)^n \left[1 - \overline{P}(U)\right]^{N-n} \tag{2.10}$$

where $\overline{P}(U)$ is the average probability per spark-gap at a voltage level of U, and is evaluated using (2.9). The model in (2.10) is used to find the simultaneous breakdown probability of n spark-gaps when there are N spark-gaps allocated along the feeder phase.

More specifically, assuming N = 3 spark-gaps connected to a three-phase system as shown in Figure 2.8, assuming the lightning stroke is nearby the MV line and assuming an identical induced overvoltage to all phases, the model in (2.10) can help to get the formula of probability of n spark-gaps simultaneously breaking down, where n=1, 2 or 3; however, the phase voltages are not instantaneously equal, meaning that if a phase voltage is a function of the random angle θ, the other voltages are dependent and there is a phase shift of $\pm 120^{o}$. For example, the average probability of a single breakdown considering model (2.10), where $N = 3$ and $n = 1$, is:

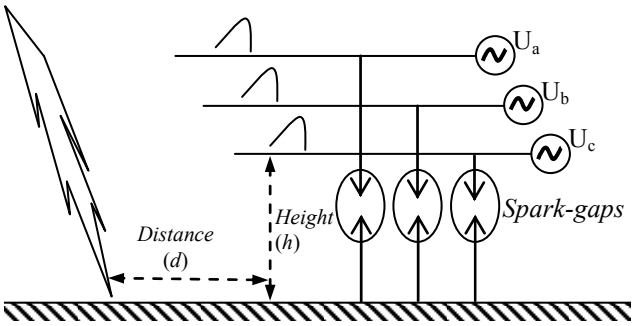

Figure 2.8 Three phase system with identical spark-gaps and induced overvoltages.

$$P_{1ph}(U)=\frac{3}{2\pi}\int_0^{2\pi}\left[\begin{array}{l}(1-Q(\frac{U-U_m\sin\theta-m}{\sigma}))\\ \times Q(\frac{U-U_m\sin(\theta-120°)-m}{\sigma})\\ \times Q(\frac{U-U_m\sin(\theta+120°)-m}{\sigma})\end{array}\right]d\theta \tag{2.11}$$

Similarly, the average probability of the simultaneous breakdown of two spark-gaps, where $n = 2$, is in the form:

$$P_{2ph}(U)=\frac{3}{2\pi}\int_0^{2\pi}\left[\begin{array}{l}(1-Q(\frac{U-U_m\sin\theta-m}{\sigma}))\\ \times(1-Q(\frac{U-U_m\sin(\theta-120°)-m}{\sigma}))\\ \times Q(\frac{U-U_m\sin(\theta+120°)-m}{\sigma})\end{array}\right]d\theta \tag{2.12}$$

Also, the average probability of three spark-gaps simultaneously breaking down, where $n = 3$, is:

$$P_{3ph}(U)=\frac{1}{2\pi}\int_0^{2\pi}\left[\begin{array}{l}(1-Q(\frac{U-U_m\sin\theta-m}{\sigma}))\\ \times(1-Q(\frac{U-U_m\sin(\theta-120°)-m}{\sigma}))\\ \times(1-Q(\frac{U-U_m\sin(\theta+120°)-m}{\sigma}))\end{array}\right]d\theta \tag{2.13}$$

Figure 2.9 shows the model results using (2.11), (2.12) and (2.13), illustrated by dotted, dashdot and dashed curves, respectively, as well as the solid line represents the combined wave case reproduced from Figure 2.7 as a reference. Figure 2.9 illustrates the probability of spark-gap operations for lightning-induced overvoltage. Considering Figure 2.8, the operation can be single-phase, two-phase or three-phase, due to number of spark-gap breakdowns. When the overvoltage is less than the mean, which is equal to 86.9 kV, the single-phase breakdown probability, shown by the dotted line, is the highest. However, when the applied voltage increases, the single-phase breakdown probability decreases, and at the same time the two-phase simultaneous breakdown probability, shown by the dash-dot

line, increases. Finally, for an impulse voltage higher than the mean plus the standard deviation and AC peak voltage, the two-phase simultaneous breakdown probability is reduced to zero, as the probability of three-phase simultaneous breakdown increases considerably, reaching one. However, the models in (2.11), (2.12) and (2.13) do not describe a complete scenario of the fault type due to spark-gap breakdown caused by lightning strokes. The reason is that the lightning-induced overvoltage is a function of stroke distance and the lightning current, which has a statistical distribution as discussed in the following section.

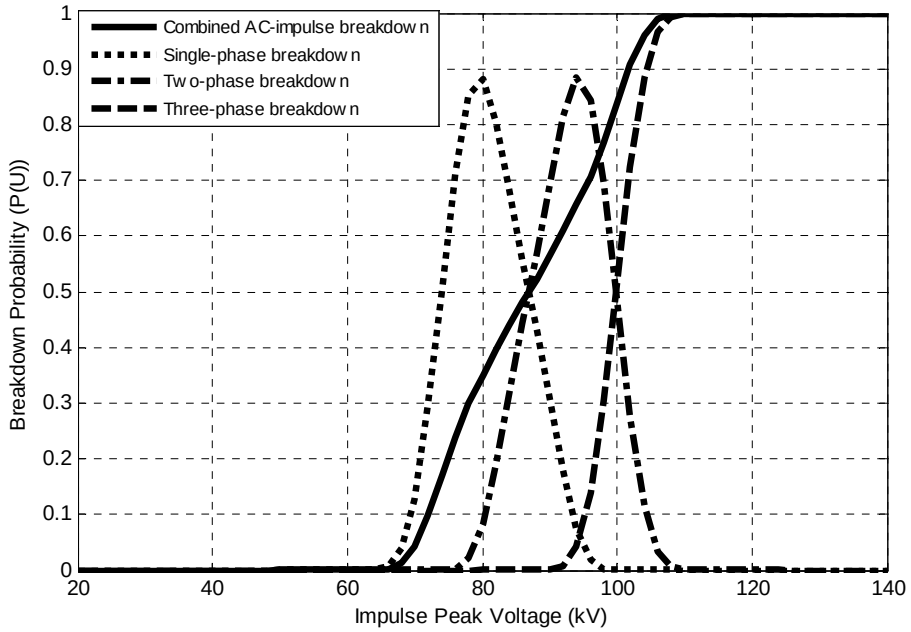

Figure 2.9 Theoretical breakdown probability for different cases.

2.4 Fault Type Modeling of Indirect Lightning-Induced Overvoltage

Spark-gap breakdowns due to lightning contribute to outages recorded in digital relays as faults. Such faults are transient faults and they are associated with the frequency of thunderstorm activity or ground flash density (GFD) in the region where the transmission line is located. The flash density distributions in Finland for the period from 1998 to 2008 are shown in color with a 10 km grid in Appendix A. These distributions provide evidence that Finland is frequently exposed to lightning strokes. In this section, the induced overvoltage equation due to lightning hitting nearby overhead lines is discussed and then the fault type probability is investigated.

2.4.1 Induced Overvoltage Flashovers

There are two adequate theoretical models for induced overvoltage that describe the interaction of electromagnetic fields with power lines. These models were introduced by Rusck [32] and Agrawal et al. [38]. In this work, the simplified Rusck formula is chosen for

induced overvoltages calculations because of its simplicity and because it has been shown to be mathematically correct and somewhat consistent with experimental results [4]. In order to take into account the effect of ground resistivity, which in some cases can enhance the induced overvoltage amplitude, an improved model has been addressed in [13], but is not considered in this study.

As discussed in subsection 1.4.3 and according to Rusck [34,4], assuming a return stroke speed of 1.2×10^8m/s and assuming a step-like wave shape for the lightning current, the maximum induced overvoltage in a power line at the point closest to the strike may be estimated by:

$$U_0 = 38.8\frac{h}{d}I_0 \tag{2.14}$$

where I_0 is the lightning peak current (kA), h is the average height (m) of the line over the ground level and d is the closest distance (m) between the line and the lightning stroke. Since the peak current is randomly distributed, the induced overvoltage is also randomly distributed. For the sake of handling a probabilistic distribution of current peak values in a simple way, according to the Anderson approximation [4,93], the following expression is adopted, where its survival density function (sdf) is:

$$P(I_0 \geq I) = \frac{1}{1+(I/I_{50})^a} \tag{2.15}$$

Equation (2.15) is the probability that any peak return-stroke in any given flash will exceed I (kA). I_0 is the random lightning peak current (kA) and I_{50} is the 50% lightning current. The values of I_{50} and a differ from one place to another.

In order to find the type of fault or breakdown, we need to average the results in (2.11), (2.12), and (2.13) over the probabilistic distribution function (pdf) of the induced overvoltage. The pdf of the induced overvoltage can be easily evaluated by finding the cumulative distribution function (cdf) of the peak current, which is given from (2.15) by:

$$F_{I_0}(I) = 1 - P(I_0 \geq I) = \frac{(I/I_{50})^a}{1+(I/I_{50})^a} \tag{2.16}$$

Then, the cdf of the maximum induced overvoltage is,

$$F_{U_0}(U) = 1 - P(U_0 \geq U)$$

$$= 1 - P(38.8\frac{h}{d}I_0 \geq U) = 1 - P(I_0 \geq \frac{I_{50}}{U_{50}}U)$$

Therefore,

$$F_{U_0}(U) = \frac{(U/U_{50})^a}{1+(U/U_{50})^a} \tag{2.17}$$

where $U_{50} = 38.8\frac{h}{d}I_{50}$.

Differentiating (2.17), the pdf of maximum induced overvoltage is:

$$f_{U_0}(U) = \frac{a(U/U_{50})^{a-1}}{U_{50}\left[1+(U/U_{50})^{a}\right]^2} \tag{2.18}$$

To specify the maximum induced overvoltage pdf, the following parameters should be estimated.

1. I_{50} and a are identified using statistical lightning current measurements, as the aforementioned values of I_{50} and exponential a differ from one country to another according to their ground flash density (GFD). For example, the values of these parameters are 15 kA and 3.09, respectively, according to lightning observations in Finland [94]. In Ireland, these parameter values become 7.8125 kA and 1.6, [78]. According to [93], Anderson obtained values equal to 31 kA and 2.6.
2. h is considered equal to 10 m.
3. d is considered to be different multiples of 50 m until a 500 m maximum closest distance, as addressed in [95].

Therefore, the effect of the distribution of the maximum induced overvoltage on the fault type probability can be evaluated, as discussed in the following subsection. However, the induced overvoltages have a time to half value much shorter than that of the lightning current, as reported in [84]. Accordingly, the waveform time parameter effect is expected to be on the model parameters of (2.3), which are the standard deviation σ and the mean m. Considering a 0.9/9.4 μs impulse voltage to imitate the lightning-induced overvoltage, it is experimentally found that σ = 2.0 kV and m = 94.5 kV. These new parameters are considered in results discussed in the following subsection.

2.4.2 Probability of Fault Type

As the number of conductors is increased, a mutual shielding comes into effect, thereby reducing the induced overvoltage. This effectively increases as the travelling distance is increased over the conductors up to the spark-gap locations [49]. However, this effect is nullified for the induced overvoltage at the location perpendicular to the lightning stroke. Such sophistications can be considered in the computed induced overvoltage. Assuming that the spark-gap location is near to the point on the conductors that is closest to lightning stroke, the fault type probability, (2.11), (2.12), and (2.13) can be averaged over the pdf of U in accordance with Rusck model as in the forms [92]:

$$\mathrm{Pr}_{1ph} = \int_{-\infty}^{\infty} P_{1ph}(U) f_{U_0}(U) dU \tag{2.19}$$

$$\mathrm{Pr}_{2ph} = \int_{-\infty}^{\infty} P_{2ph}(U) f_{U_0}(U) dU \tag{2.20}$$

$$\mathrm{Pr}_{3ph} = \int_{-\infty}^{\infty} P_{3ph}(U) f_{U_0}(U) dU \tag{2.21}$$

Based on statistical lightning information in Finland, I_{50} = 15 kA and a = 3.09. Considering these values, Figure 2.10 shows survival density function for lightning current (sdf) and its corresponding cumulative density function (cdf) and probability density function (pdf). sdf and cdf curves are computed using Equations (2.15) and (2.16),

respectively and pdf is computed by differentiating Equation (2.16). Figure 2.11 shows the pdf of U (f_{U_0}) (red line) as well as P_{1ph}, P_{2ph} and P_{3ph} reproduced from Figure 2.9 (black lines). The multiplications of $P_{1\,ph} f_{U_0}$, $P_{2\,ph} f_{U_0}$ and $P_{3\,ph} f_{U_0}$ (blue lines) are also shown, where the y-axis is in a log scale. Figure 2.11 visually helps to predict the behavior of the induced overvoltage and the effect of its pdf on the fault type. When the lightning distance is d = 50 m (Figure 2.11a), the area under the $P_{3\,ph} f_{U_0}$ curve is the highest, indicating a higher probability of 3-phase simultaneous discharge. This is expected, since the distance is short and there is a high probability that the induced overvoltage is high enough to cause breakdown of three spark-gaps. However, when the distance is increased, for example d = 150 m as shown in Figure 2.11b, the area under $P_{3\,ph} f_{U_0}$ decreases significantly while that of $P_{1\,ph} f_{U_0}$ and $P_{2\,ph} f_{U_0}$ is less affected. Figure 2.11c shows these results for a distance of 250 m.

The numerical values of these probabilities are summarized in Table 2.3. The maximum distance is considered to be 500 m and divided into ten sections. This means that the probability of lightning hitting each section is assumed to be equally distributed. The information from Table 2.3 is that the fault type average probability due to a single lightning stroke at the farthest distance 500 m is 0.0247 for a 1-phase fault, 0.0193 for a 2-phase fault and 0.0748 for a 3-phase fault.

Cigre parameters (I_{50} = 31 kA and a = 2.6) and Ireland parameters (I_{50} = 7.8125 and a = 1.6), the probability fault type distribution are shown in Figures 2.12 and 2.13 and tables 2.4 and 2.5 respectively. Comparing Figures 2.11 and 2.12, as the I_{50} is higher, the U_{50} is increased and therefore the three-phase simultaneous discharge probability is expected to increase. However, for Irland, the I_{50} is lower and therefore U_{50} is reduced as it can be show by comparing Figures 2.11 and 2.13.

This confirms the fault probability due to lightning-induced overvoltages in MV networks protected by spark-gaps and that they can be cleared by isolating and then using autoreclosure. Furthermore, there is a probability of voltage wave chopping in single-phase, two-phase and three-phase, due to the spark-gap breakdown protecting the network from lightning-induced overvoltages. This chopping is sharp, due to spark-gap breakdown, causing the generated high frequencies to reach consumers over the distribution transformers, as studied in the following chapters.

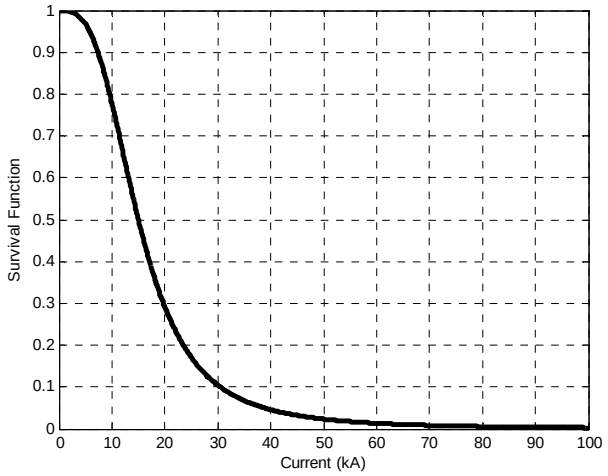

a. sdf.

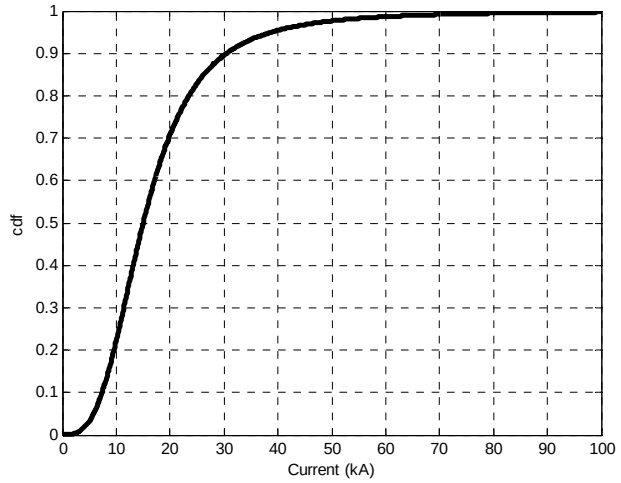

b. cdf.

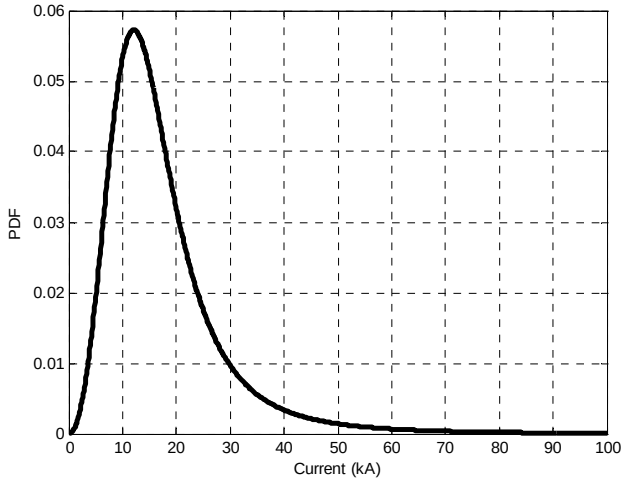

c. pdf.

Figure 2.10 sdf, cdf and pdf for Finland.

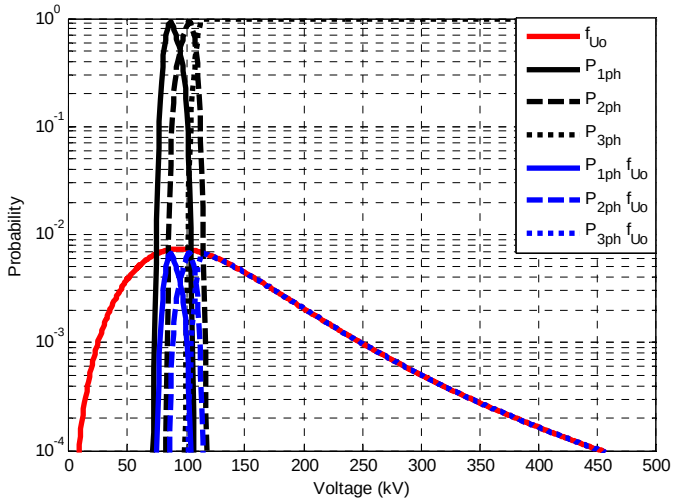

a. *d*=50 m.

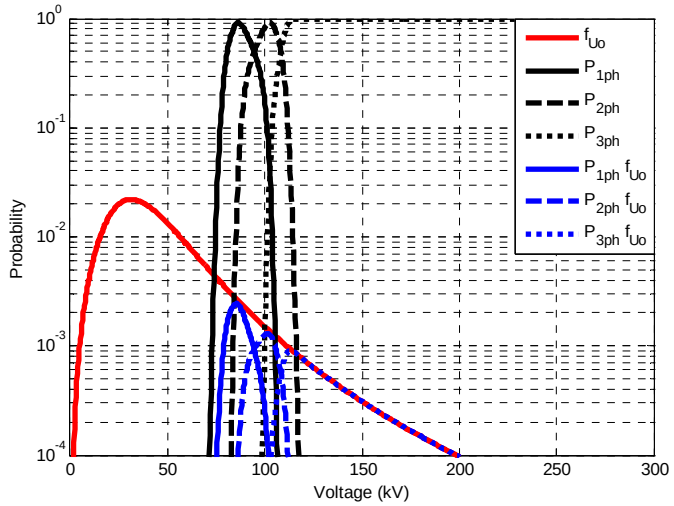

b. *d* =150 m.

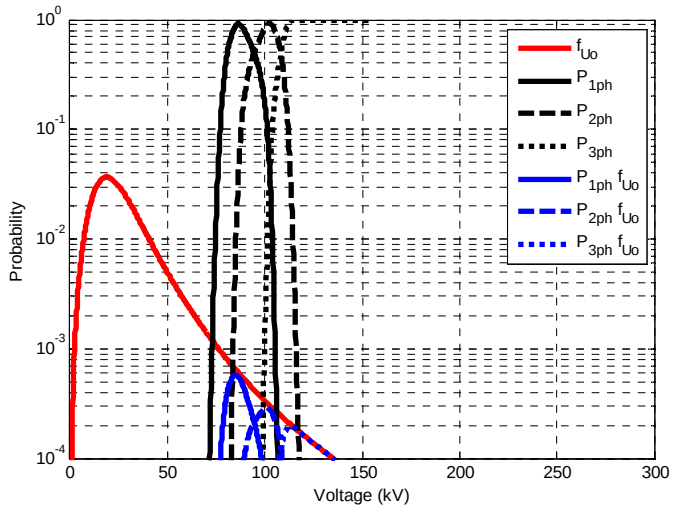

c. *d* =250 m.

Figure 2.11 Declarations for the fault type probability distribution (I_{50} = 15 kA and a = 3.09).

Table 2.3 The probability of fault type over the closest distance of 500 m (Finnish data).

Distance	1-ph probability	2-ph probability	3-ph probability
50	0.00980	0.00981	0.05584
100	0.00824	0.00561	0.01281
150	0.00336	0.00206	0.00385
200	0.00152	0.00090	0.00146
250	0.00079	0.00046	0.00060
300	0.00046	0.00027	0.00022
350	0.00029	0.00016	3.1302e-005
400	0.00018	4.1997e-005	1.2624e-011
450	6.9972e-005	4.9701e-007	0
500	2.9542e-006	2.5945e-016	0
Average Probability	0.0247	0.0193	0.0748

2.5 Model Modification for Special Cases

As aforementioned, this chapter presents a probabilistic model for the spark-gap characteristics. However, it will be more interesting to study the proposed model when the overvoltage is affected by line transverse discontinuities such as those caused by periodically-grounded shielding wires or by surge arresters. Adding a shielding wire will reduce the induced overvoltage across the spark-gap by a factor which depends on the grounding and proximity of the ground conductor to the phase conductor [4]. Simply, this factor can be considered in the proposed model by its multiplication in Equation (2.14).

For discontinuities due to surge arresters, the arrester limits the overvoltage on the equipment to a certain value [4]. This value is denoted in the following equations as U_{arr}. Such behavior can be described in the pdf of U in Equation (2.18) as follows:

1. The spark-gap will be subjected to an overvoltage equal to:

$$\hat{U} = \begin{cases} U_0 & U \le U_{arr} \\ U_{arr} & U > U_{arr} \end{cases} \tag{2.22}$$

2. Let $\hat{f}_{U_0}(U)$ be a truncated version of $f_{U_0}(U)$, i.e,

$$\hat{f}_{U_0}(U) = \begin{cases} f_{U_0}(U) & U \le U_{arr} \\ 0 & U > U_{arr} \end{cases} \tag{2.23}$$

3. Then the corresponding pdf of $\hat{U}$ will be:

$$f_{\hat{U}}(U) = \hat{f}_{U_0}(U) + \delta(U - U_{arr}) P_{ro}(U > U_{arr}) \tag{2.24}$$

where $$P_{ro}(U > U_{arr}) = \int_{U_{arr}}^{\infty} f_{U_0}(U)\,dU \tag{2.25}$$

Therefore, the limited voltage behavior of the surge arrester is considered in the pdf of the overvoltage over the spark-gap. The new pdf will be substituted in the models (2.19), (2.20) and (2.21) to present the fault type concerning the arrester dynamic behavior on the overvoltage amplitude. However, the waveform time parameter effect is expected to be on the model parameters of (2.3), which are the standard deviation σ and the mean m.

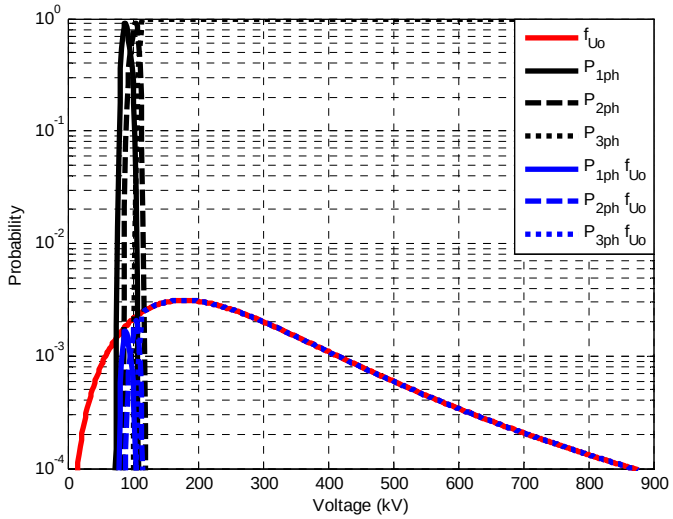

a. d= 50 m.

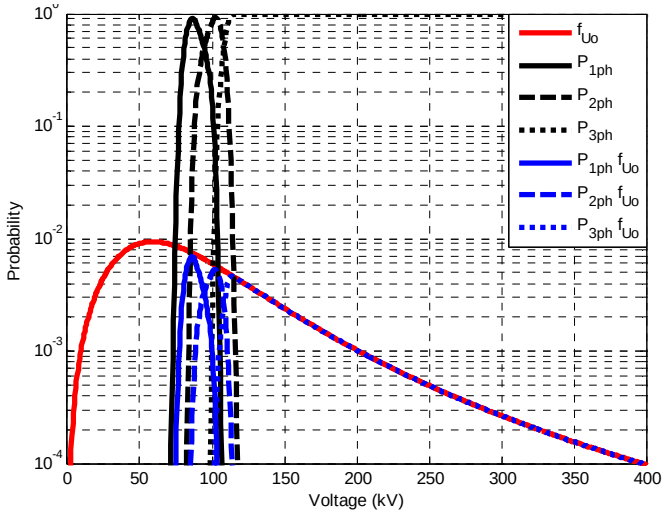

b. d = 150 m.

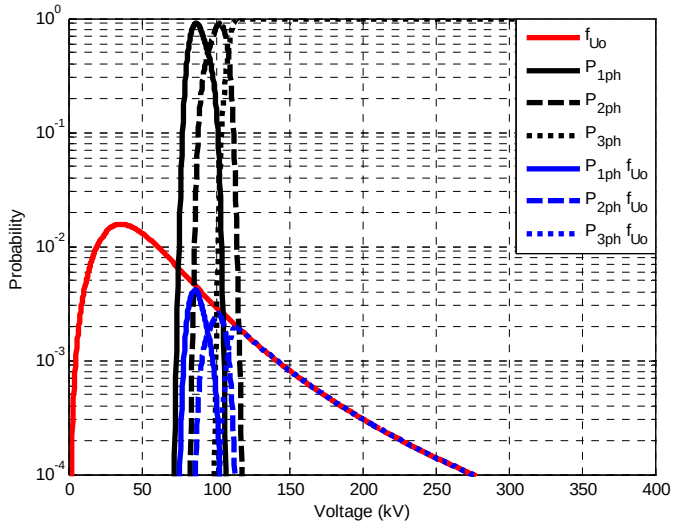

c. d =250 m.

Figure 2.12 Declarations for the fault type probability distribution (I_{50} = 31 kA and a = 2.6).

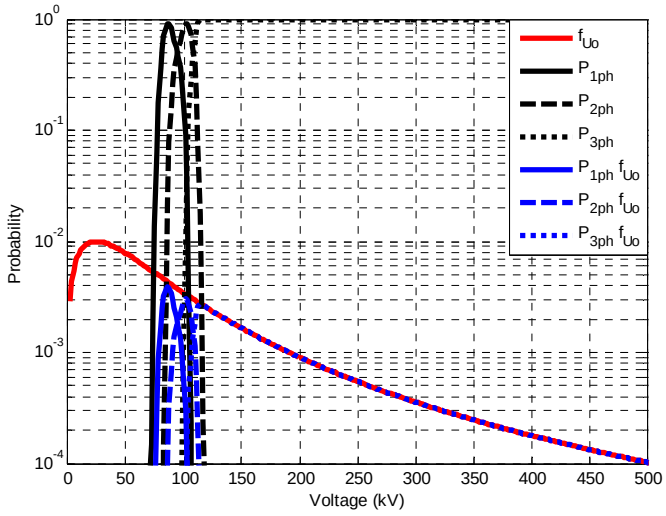

a. d = 50 m.

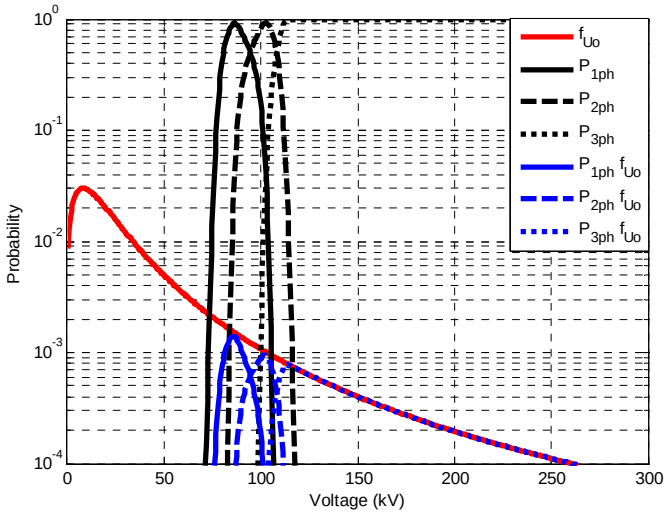

b. d =150 m.

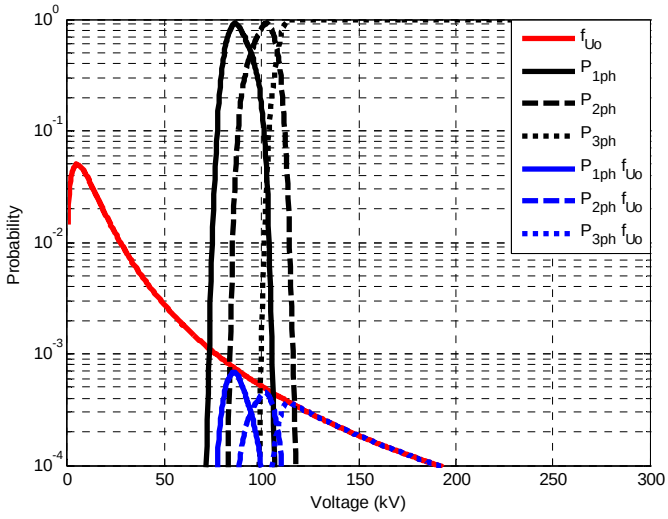

c. d = 250 m.

Figure 2.13 Declarations for the fault type probability distribution (I_{50} = 7.8125 kA and a = 1.6).

Table 2.4 The probability of fault type over the closest distance of 500 m (Cigre data).

Distance	1-ph probability	2-ph probability	3-ph probability
50	0.00253	0.00295	0.08824
100	0.00844	0.00825	0.05648
150	0.00985	0.00808	0.03107
200	0.00798	0.00587	0.01735
250	0.00581	0.00401	0.01025
300	0.00416	0.00277	0.00639
350	0.00302	0.00197	0.00414
400	0.00225	0.00144	0.00144
450	0.00171	0.00108	0.00184
500	0.00133	0.00084	0.00123
Average Probability	0.0471	0.0373	0.2184

Table 2.5 The probability of fault type over the closest distance of 500 m (Irish data).

Distance	1-ph probability	2-ph probability	3-ph probability
50	0.00567	0.00463	0.02803
100	0.00325	0.00244	0.01111
150	0.00198	0.00145	0.00590
200	0.00134	0.00097	0.00362
250	0.00097	0.00070	0.00240
300	0.00074	0.00053	0.00167
350	0.00059	0.00042	0.00119
400	0.00048	0.00034	0.00086
450	0.00040	0.00028	0.00062
500	0.00034	0.00024	0.00044
Average Probability	0.016	0.012	0.059

3- High Frequency Transformer Models

In order to know the impact of the lightning overvoltages in MV networks when they are transferred to the LV networks, an accurate model of the distribution transformer is necessary. This model can enhance the lightning protection design, many researchers in this field, assuming that the lightning surges transferred to the customers in the LV networks through the interwinding capacitance of the distribution transformer [96]. There are two ways for obtaining the model which describes the transformer frequency behavior. The first method uses the mechanical description of the transformer to calculate the reactances and capacitances which together give the model. The main problem of this method is that a detailed mechanical description of the transformer must be known and calculation is extremely difficult. The second way is an experimental method where measurements are carried out on the transformers and from these results the transformer model can be build up. The advantage of this method is that every transformer can be modeled when it is measured first. In this chapter, the experimental method is adopted.

3.1 Transformer Models at Unloaded Conditions

A study has been done in [97] to provide a method for the development of a high frequency transformer model for use in an electromagnetic transient program (EMTP). This complex model used the modal analysis to convert the measured results to a digital EMTP-model. The EMTP high frequency transformer model is shown in Figure 3.1, where each part consists of:

- Two ideal transformers with transfer ratio's μ and λ,
- Three components R_k, L_k and C_k determined from the modal parameters,
- Three components R, L and C determined from the modal parameters and the components R_k, L_k and C_k respectively,
- Capacitor C_o represents the capacitive behavior of the transformer.

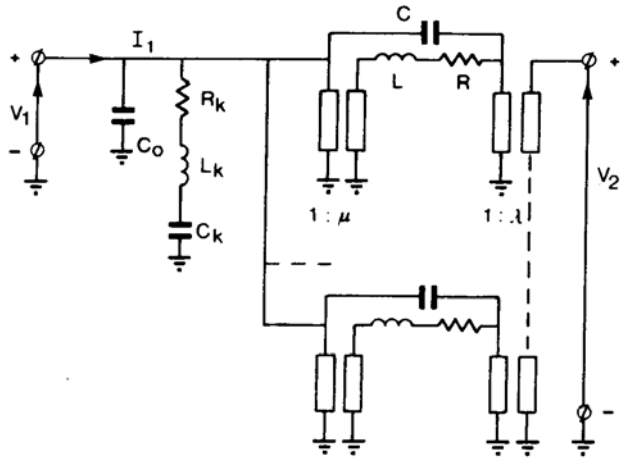

Figure 3.1 the EMTP high frequency transformer model [97].

A simple model suitable for unloaded transformer has been developed in [98] taking into account the compromise between accuracy and simplicity. This model enables the calculation of transferred voltages to the secondary side in case of lightning discharge close to a line. The transformer model is shown in Figure 3.2, the values of the circuit parameters are derived from the transformer input impedance and frequency response.

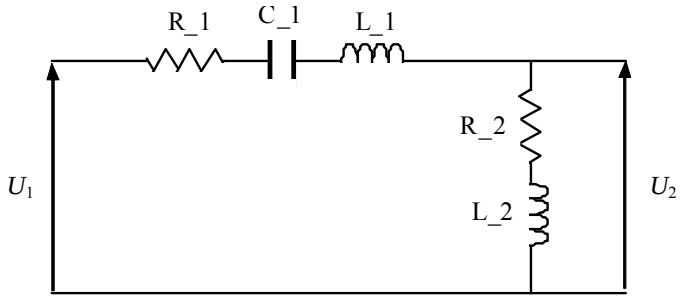

Figure 3.2 Transformer model for calculating transferred voltages (under no-load condition), when lightning strikes close to an overhead line [98].

As mentioned before, this model compromise between accuracy and simplicity, however its parameters calculation is carried out at only one resonance frequency to calculate the transformer parameters under lightning strokes. In this chapter, this model is modified to take the two resonance frequencies into consideration instead of the one of the highest amplitude only as shown in the next subsection. Therefore, more accurate results of frequency response of the transient voltages are attained. The proposed model accuracy is verified using experimental measurements.

3.1.1 Experimental Procedure and Measurements

Experiments have been performed to measure the high frequency characteristics of the distribution transformer under lightning strokes. These measurements contribute to determine the parameters of the simple equivalent circuit of the transformer. As in general, lightning-induced voltages on overhead lines are practically the same in all phases, all tests are made with the HV terminals interconnected. These experiments were carried out at the High Voltage Laboratory, Helsinki University of Technology (TKK), Finland.

Figure 3.3 illustrates the experimental configuration. The voltages U_1 and U_2 and the current I_1 are measured at the point CH_1, CH_2 and CH_3, respectively. The experimental tests were made for two transformers using the same experiment configuration in Figure 3.3. The first transformer (T1) has a rating of 100 kVA and the other one (T2) has a rating of 50 kVA. The experiment procedure is very simple as the input impulse voltage (U_1) is applied on the primary terminal, and therefore, input voltage (U_1), input current (I_1) and transferred voltage to the secondary side (U_2) were simultaneously measured. The devices used in the experimental setup are indicated in Appendix G.

The signals U_1, I_1 and U_2 were measured for unloaded transformers T1 and T2 considering the experiment configuration shown in Figure 3.3. The voltages and currents traces were captured through the oscilloscope attaining the signals depicted in Figures 3.4 to 3.6. The input signal shown in Figure 3.4 is 940 V, 0.87/50 μsec. Figures 3.5 and 3.6 illustrate the current I_1 and voltage U_2 for the two transformers T1 and T2, respectively.

These measurements were accomplished to determine the transformer input impedance (U_1 / I_1) and the ratio U_2 / U_1 in the frequency domain and therefore, to model the transformer by a simple circuit described by Piantini et al. addressed in the following section.

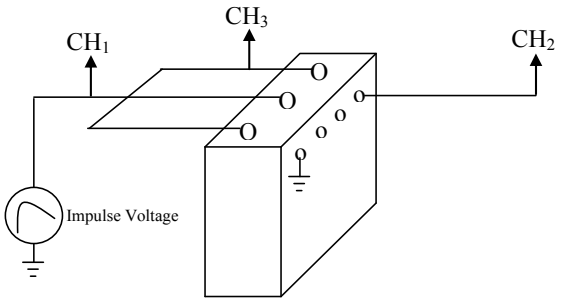

Figure 3.3 Experimental configurations.

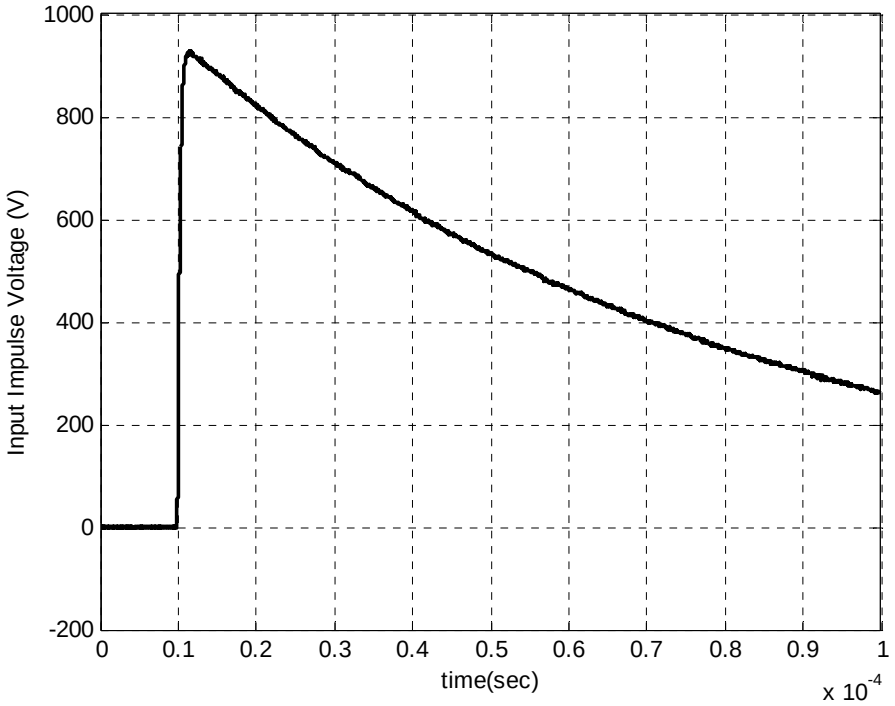

Figure 3.4 Input impulse voltage for the two transformers (T1 and T2).

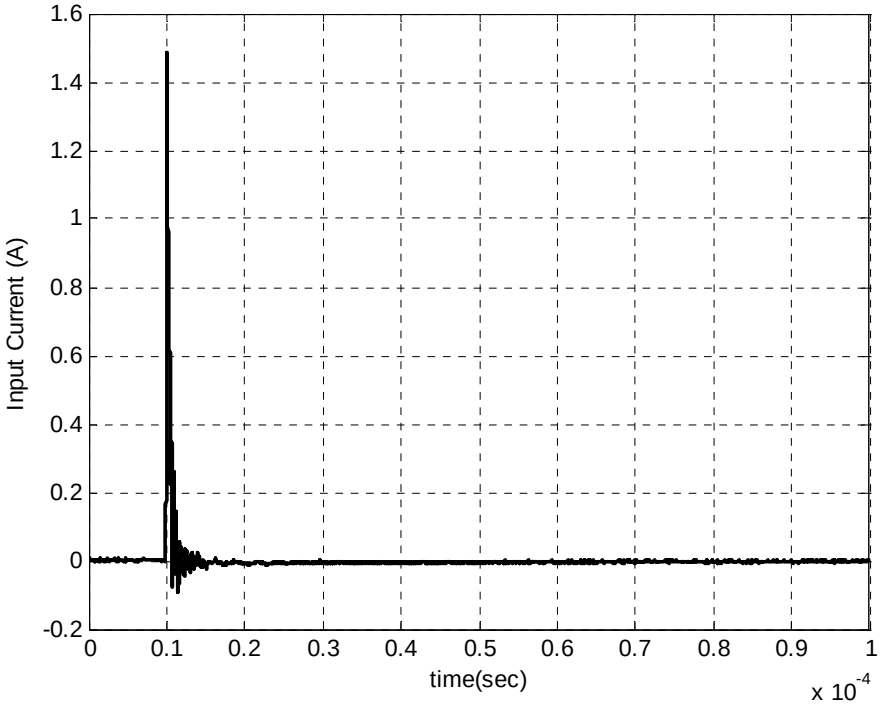

a. Current I_1.

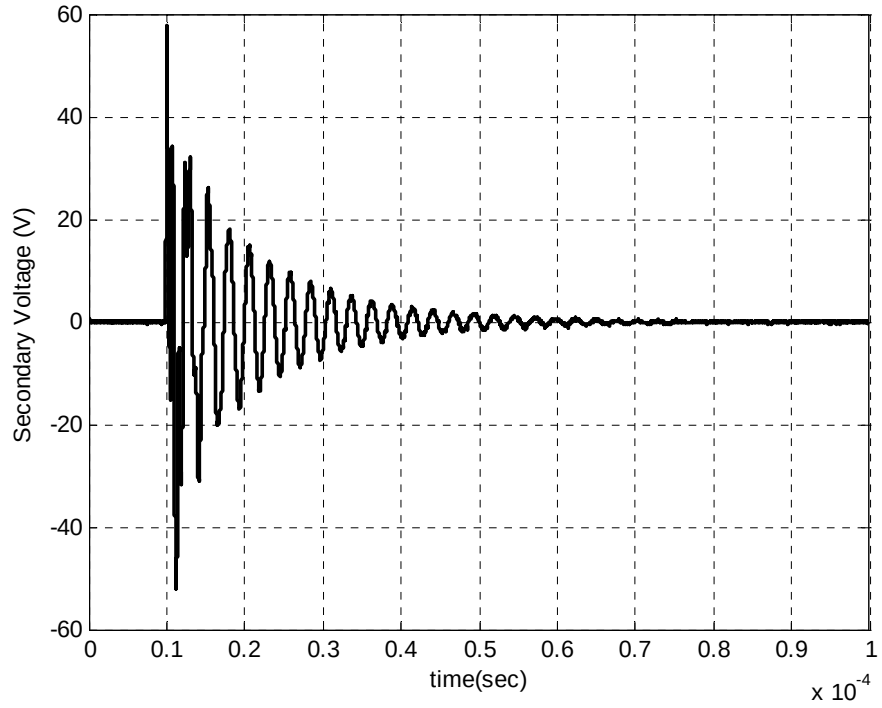

b. Voltage U_2.

Figure 3.5 Measured signals of the transformers T1.

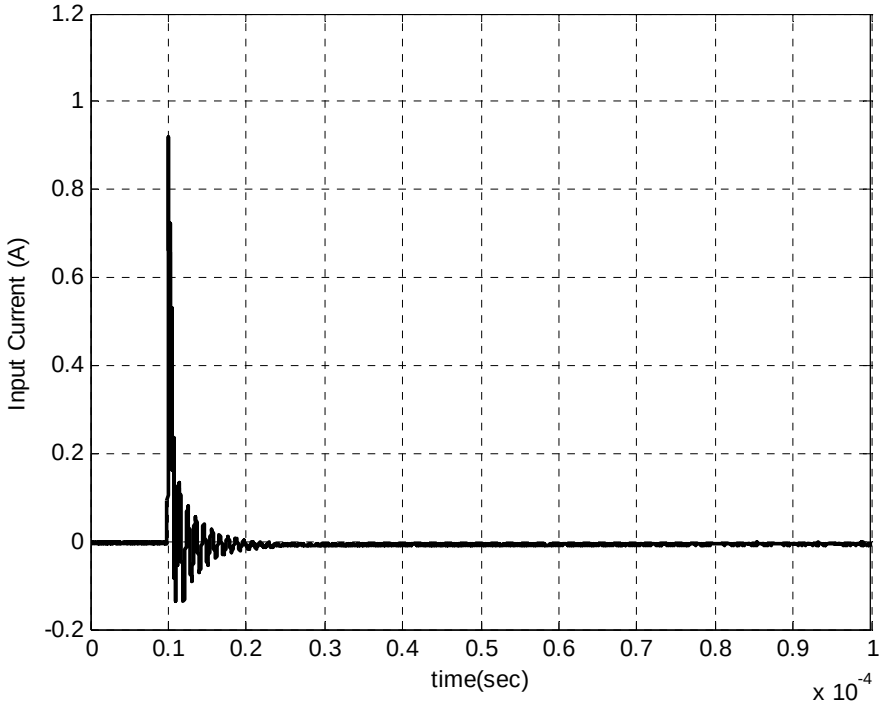

a. Current I_1.

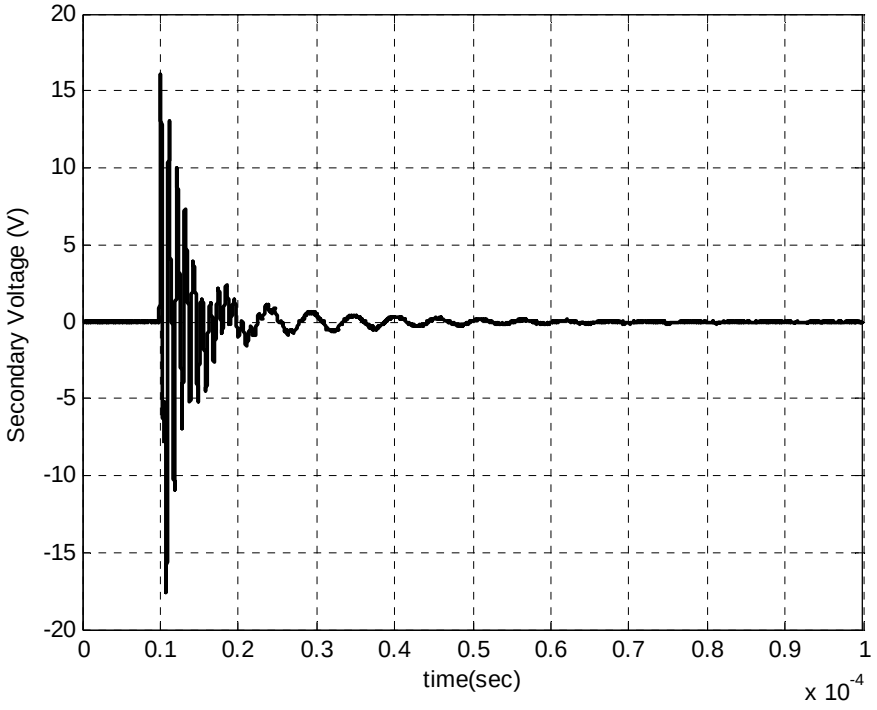

b. Voltage U_2.

Figure 3.6 Measured signals of the transformers T2.

3.1.2 Modeling by Piantini et al.

The transformer transient model proposed by Piantini et al. is the shown in Figure 3.2 [98]. The values of the circuit elements are derived as following. First the FFT algorithm is applied on the experimental measured voltages and current signals (U_1, U_2 and I_1) shown in Figures 3.4 to 3.6 where they are measured during testing the power transformers T1 and T2. In the frequency domain, the input impedance and transformer response (secondary voltage / primary voltage) are analyzed. The model parameters identification procedure is summarized in Appendix H [99]. It is found for T1 that R_1 = 485.83 Ω, R_2 = 60.968 Ω, L_1= 2.25686 mH, L_2= 0.122 mH and C_1= 0.0732 nF. For T2, its parameters are R_1= 295.8Ω, R_2= 1 μΩ, L_1= 0.312 mH, L_2= 0.01 mH and C_1= 0.085 nF [100].

The ATP/EMTP simulation circuit shown in Figure 3.2 is realized by ATPDraw which is a graphical interface used to simplify the ATP/EMTP processing [101]. The ATPDraw circuit is shown in Figure 3.7. The applied voltage to the primary terminals in the simulations is identical to the measured one depicted in Figure 3.4. The simulated transient voltage U_2 is exported to MATLAB in order to compare with the measured signals. The time and frequency domains of the transient voltage U_2 during impulse test are computed for the two transformers T1 and T2 as shown in Figures 3.8 and 3.9, respectively. Therefore, the model evaluation can be performed.

The comparison between the experimental and simulated results show a good agreement for the transformer T1 as illustrated in the time domain comparison depicted in Figure 3.8a, where the solid line is for experimental results and the dashed one is for the simulated results. However when this transient voltage is analyzed in frequency domain as shown in Figure 3.8b, only the resonance frequency of the highest amplitude appeared in the simulation results although the experimental frequency analysis of the transferred voltage shows more than one resonance frequency. The reason is that the first resonance frequency value is considered, as it is the highest value, to identify the model parameters. However, the comparison, in the time domain, considering the second transformer T2 is not in a good agreement as shown in Figure 3.9a. The reason is that the second frequency value is considered to identify the model parameters where it is selected as the highest amplitude as shown in Figure 3.9b and the other lower frequency has significant amplitude. For accurate transformer representation, the model is modified as addressed in the next subsection.

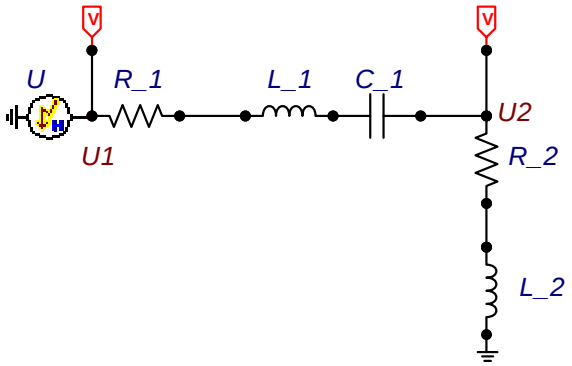

Figure 3.7 ATPDraw simple high frequency transformer model.

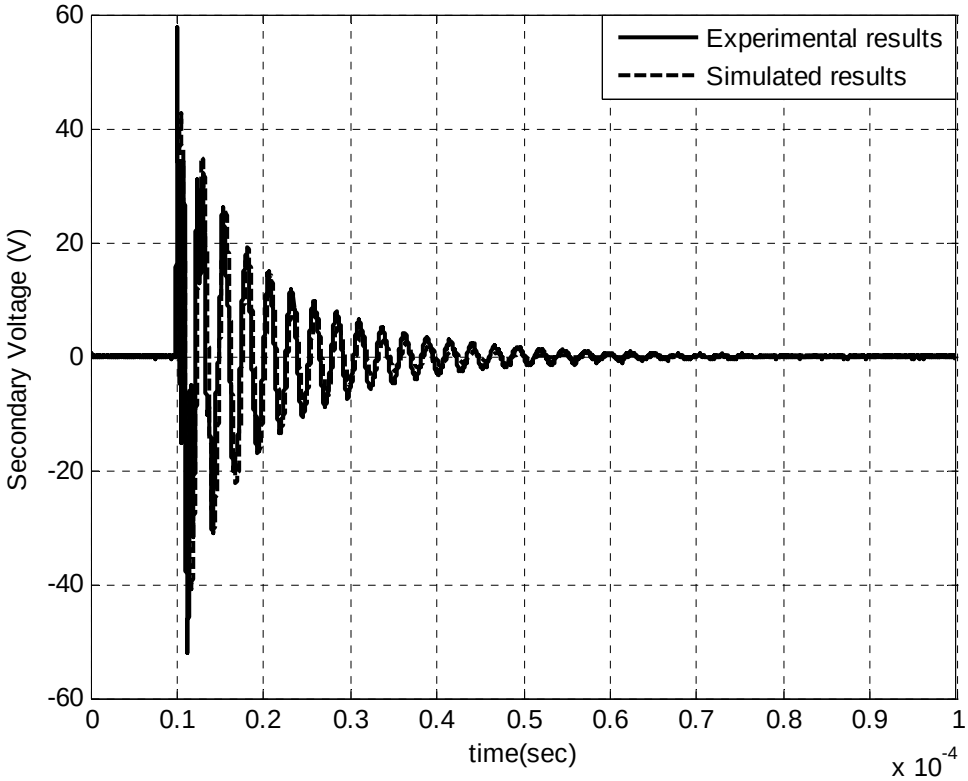

a. Time response.

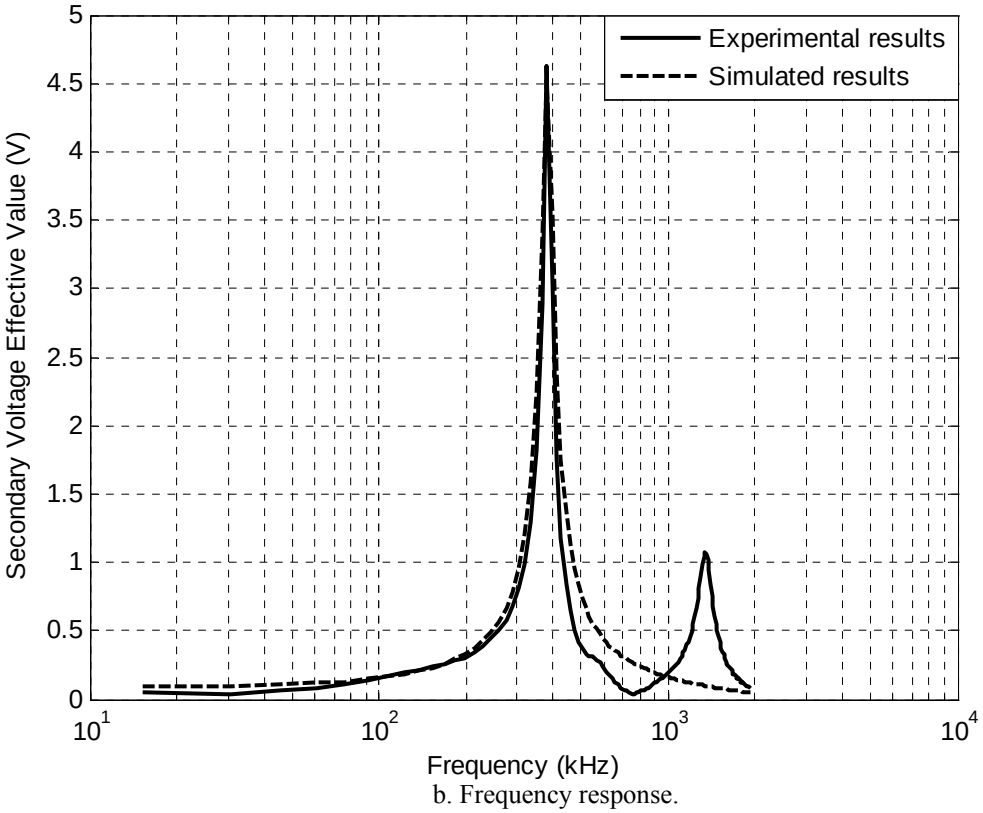

b. Frequency response.

Figure 3.8 Secondary transferred voltage under unloaded condition (T1).

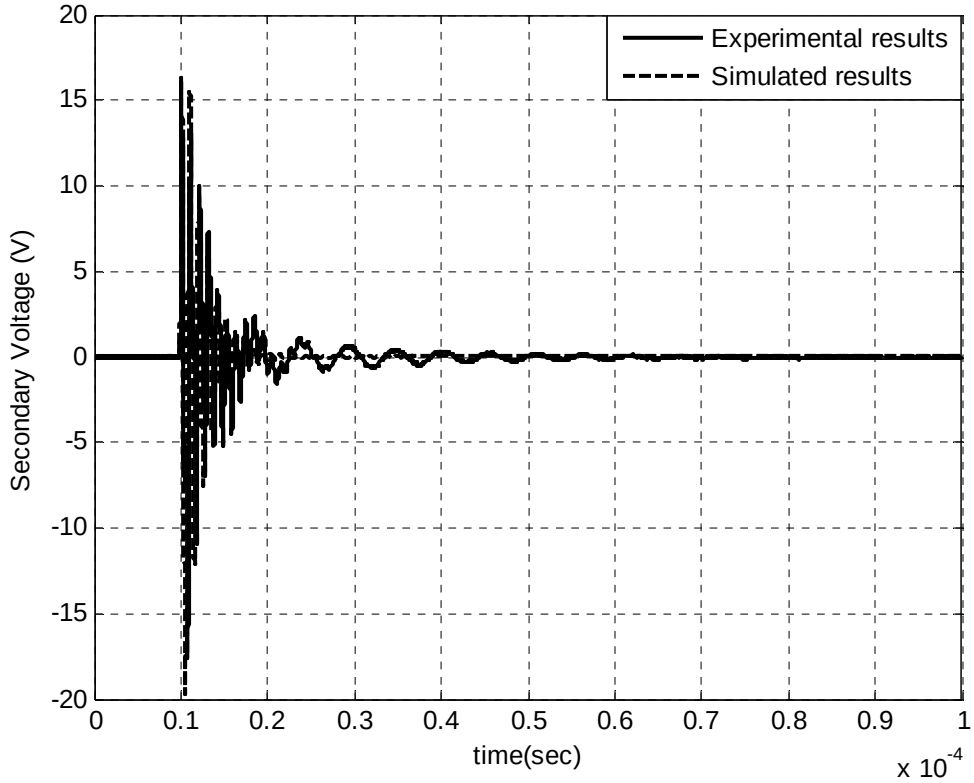

a. Time response.

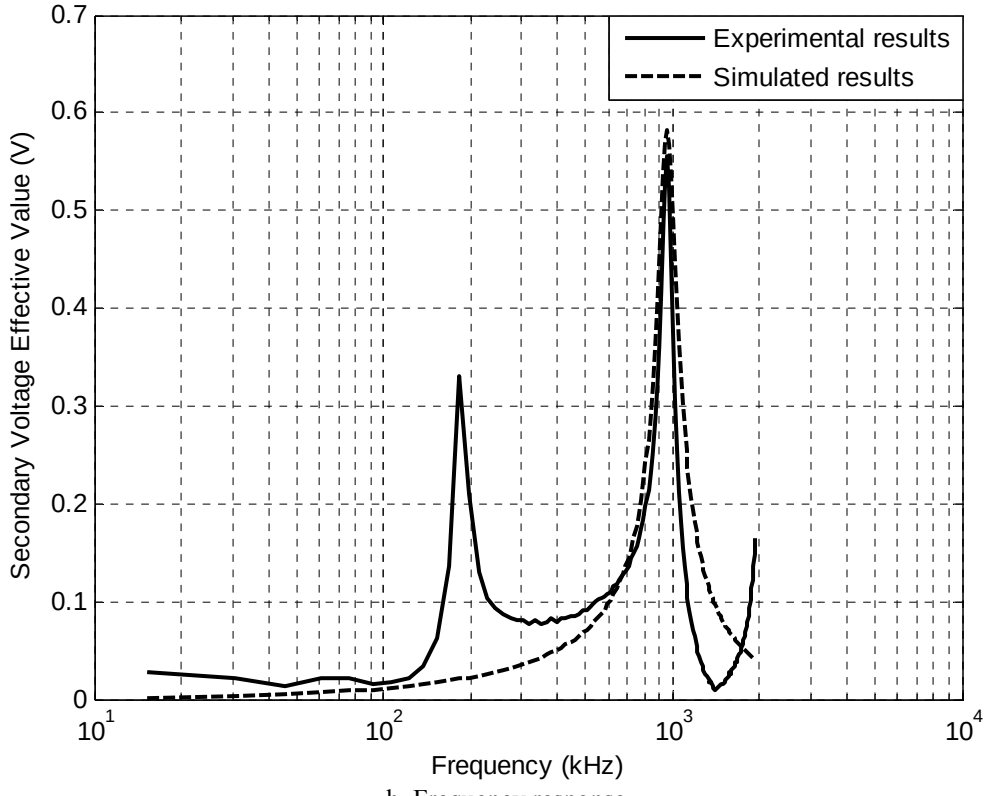

b. Frequency response.

Figure 3.9 Secondary transferred voltage under unloaded condition (T2).

3.1.3 Proposed Model for Unloaded Transformer

In this subsection, a modification is carried out on the Piantini et al. model in order to take into account two resonance frequencies which appeared in Figures 3.8 and 3.9 [100]. This modification is obtained by following the same procedure which was suggested by Piantini et al. [98], however, the first consequently two resonance frequencies are considered in the model circuit calculation. The derivation of the transformer parameters under lightning stroke in the modified model is carried out through two steps:

1. Based on the Piantini model procedure, the derivation of the transformer parameters using the measured data at the resonance frequency of the highest amplitude (the first resonance frequency for transformer T1 and the second resonance frequency for transformer T2 as aforementioned) is done. From this derivation, the circuit elements shown in Figure 3.7 are seemingly obtained, in which this network is a part of the network shown in Figure 3.10.
2. To overcome the shortcoming of Piantini model, a branch of R, L and C is added as shown in Figure 3.10. The derivation of theses parameters is done following the same procedure suggested by Piantini et al. but using the second resonance frequency (the resonance frequency of next amplitude, for example the second resonance frequency in transformer T1 and the first resonance frequency in transformer T2). Also, these elements are formed only in one branch connected as shown in Figure 3.10 not two branches as done using the highest amplitude resonance frequencies as described in above step. Accordingly, the added branch parameters are found R=50 Ω, L= 0.2421 mH and C= 0.038 nF for transformer T1. While for transformer T2, it is found that R=1 μΩ, L= 0.018 mH and C= 26 nF with changing R_1=195.8 Ω, for T2.

The comparison between the results of the modified model and experimental results indicate good agreements between the simulated and experimental results as shown in Figures 3.11 and 3.12 for transformers T1 and T2, respectively. From these figures, the model accuracy is achieved as well as keeping on the model simplicity.

From these results, the high frequency transformer model has been modified. This modification has improved the transient voltage waveforms as taking more than one resonance frequency into consideration in the modelling process. The results have ensured the proposed model accuracy as well as the model simplicity is still achieved.

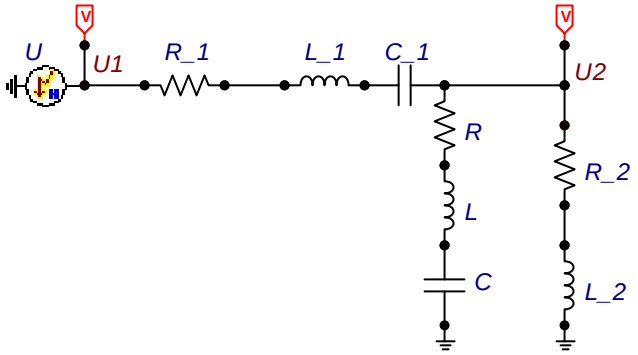

Figure 3.10 ATPDraw circuit of the modified model.

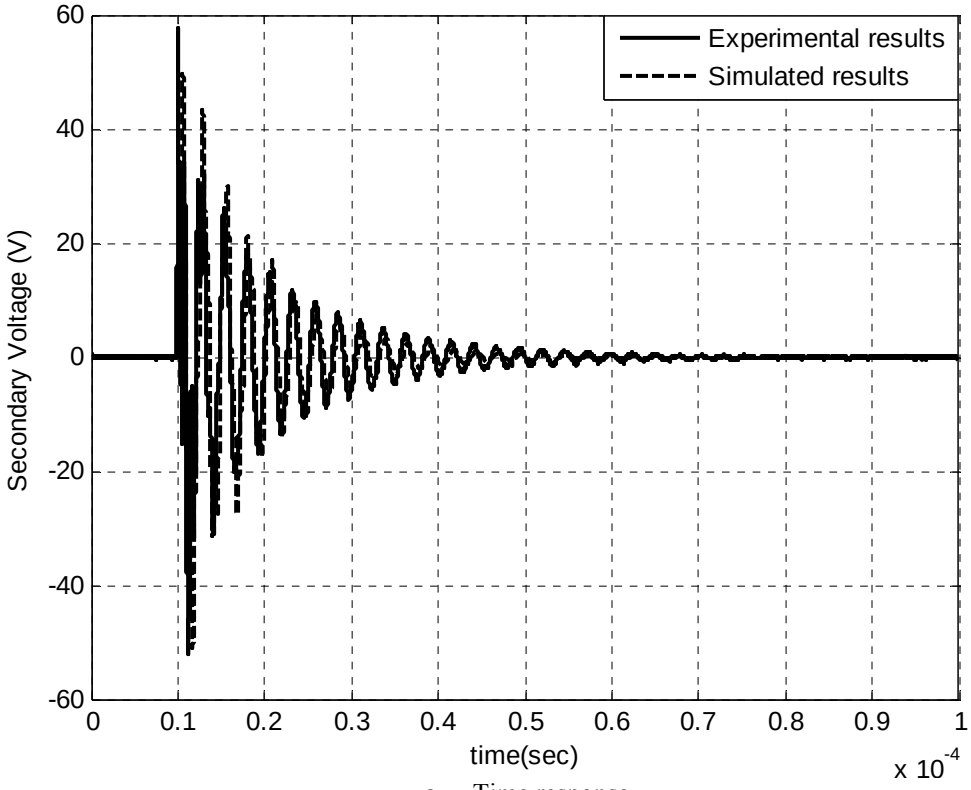

a. Time response.

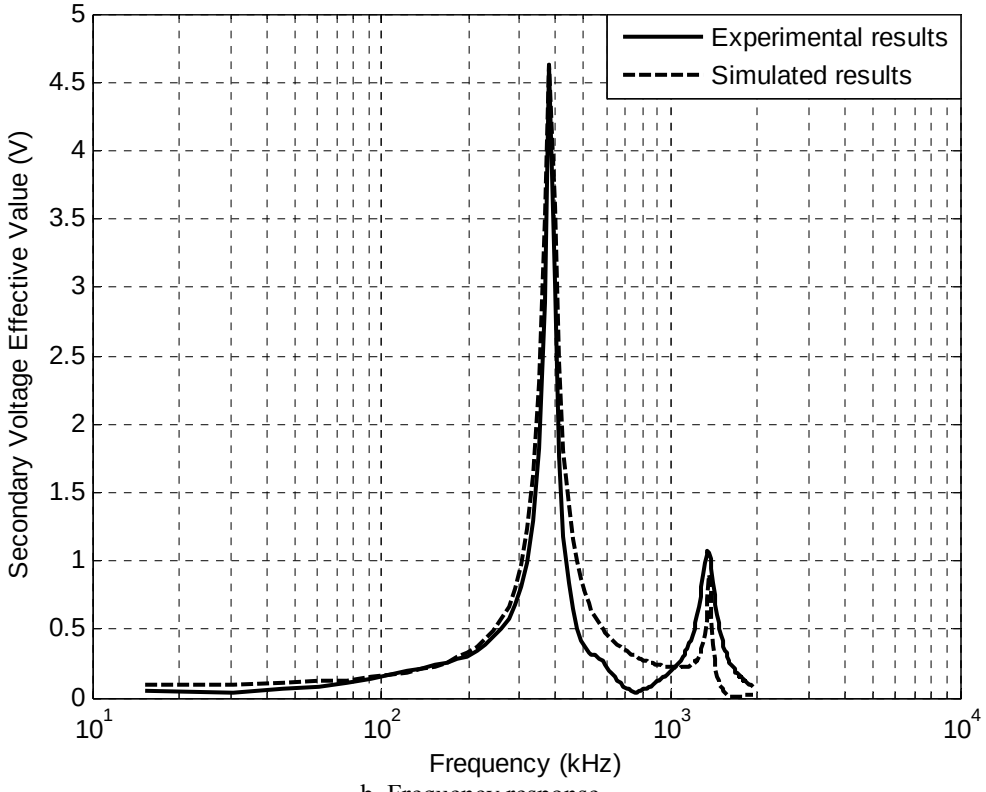

b. Frequency response.

Figure 3.11 Secondary transferred voltage under unloaded condition (T1).

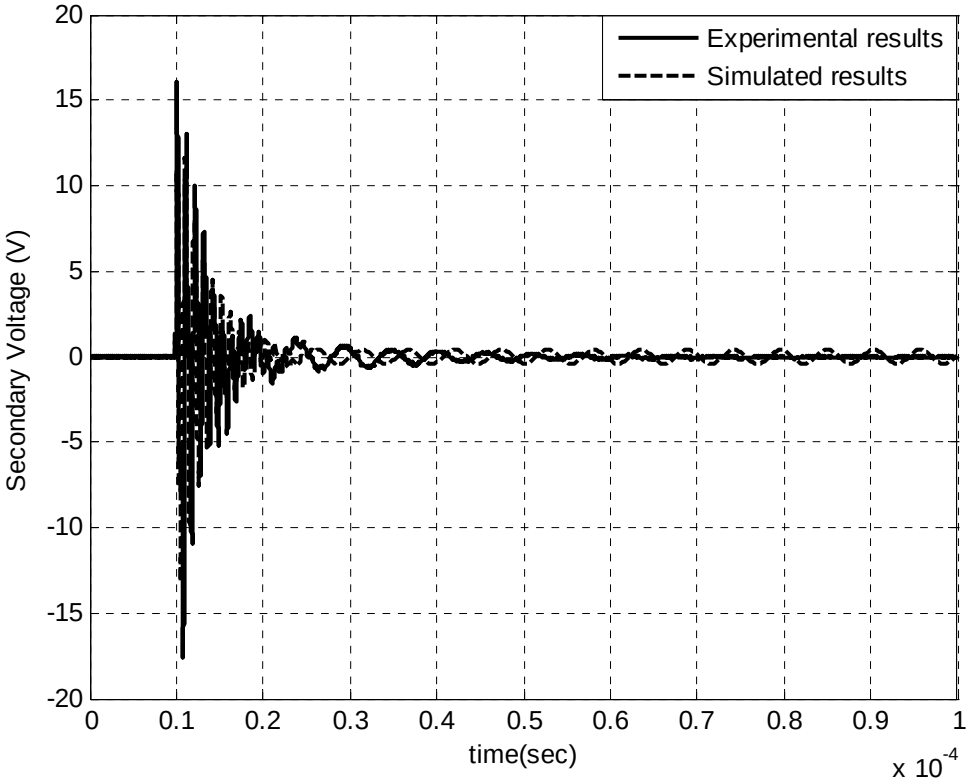

a. Time response.

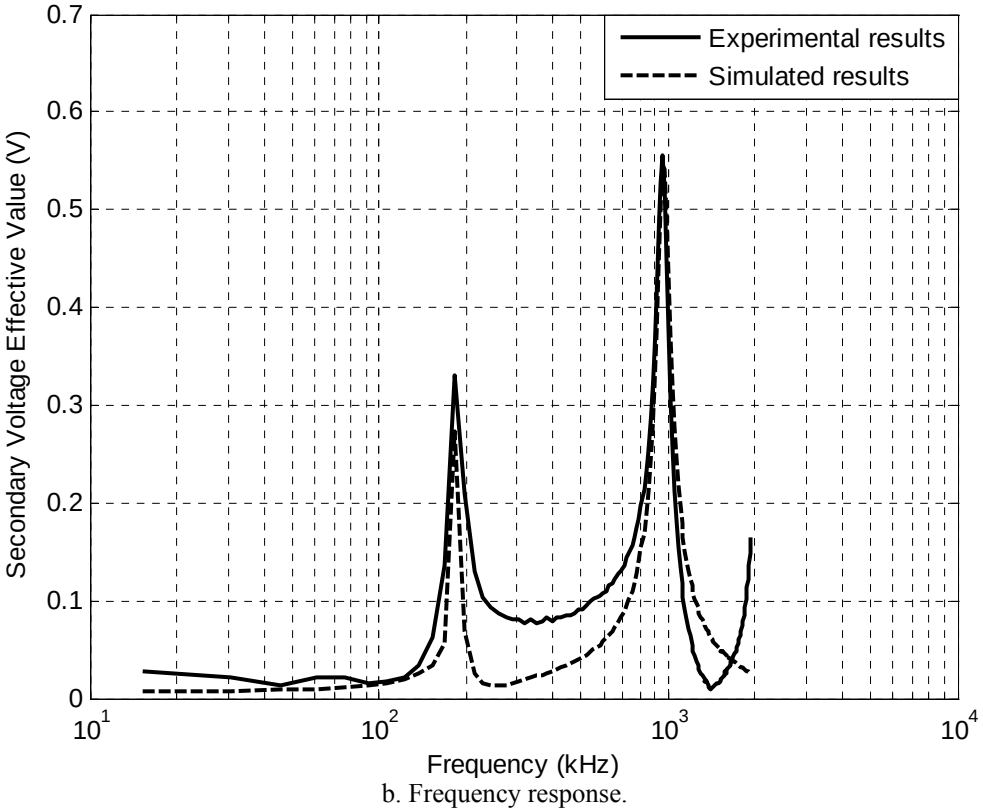

b. Frequency response.

Figure 3.12 Secondary transferred voltage under unloaded condition (T2).

3.2 Transformer Models at Loaded Conditions

As this work is going to investigate lightning impact reached at the service entrances, the transformer load should be considered. So, it is worthy to model the transformer at loaded conditions where the aforementioned models are used only in case of unloaded transformer.

3.2.1 Models in Literature

From the literature review, the high frequency transformer models were divided into two categories. The first category concentrated on modelling the transformer windings [102-112]. However, most of these models are very complex and need details of the transformer construction. Furthermore, most models of this category aim to know the electrical stresses to which the winding can be exposed during transient oscillations and not to study the effect of lightning strokes on the voltage transferred to the secondary side. The second category models aim to study the effect of the lightning strokes on the voltage transferred to the transformer secondary side.

A transformer model using electromagnetic transient studies has been introduced in [113]. Using the frequency-characteristics measurements recorded by the impedance analyzer, the model parameters have been determined with neglecting both the hysteresis and iron core effects where this model aim to study the lightning surges. The following effects have been presented by this model:

1. Capacitances between windings themselves and between winding and enclosure,
2. Winding conductors and iron core skin effects,
3. The combination between winding inductance and the capacitance between turns which lead to multiple resonances.

As shown in Figure 3.13, the transformer fundamental equivalent circuit is formed from an ideal transformer, leakage inductance, winding resistance and magnetizing admittance. This model has been modified to be suitable for lightning surges studies. This modification has been carried out by adding blocks evaluating the aforementioned factors effects in addition to the iron core saturation and hysteresis effects can be inserted. This model has been used in order to evaluate the lightning surge propagation from a distribution line to a consumer entrance via a pole-mounted transformer where such scenario is shown in Figure 3.14 [114].

An accurate R-L-C model of the shell type power transformer has been presented in [115] where R-L-C parameters were calculated with analytical and numerical methods (Finite Elements). However, this model is not easy to be used in addition to the equivalent network of the transformer contains many electrical elements. For example the 600 MVA autotransformer, the windings (36 coils) are represented by a circuit including 72 nodes and 210 elements. Part of R, L and C equivalent circuit of transformer winding is shown in Figure 3.15.

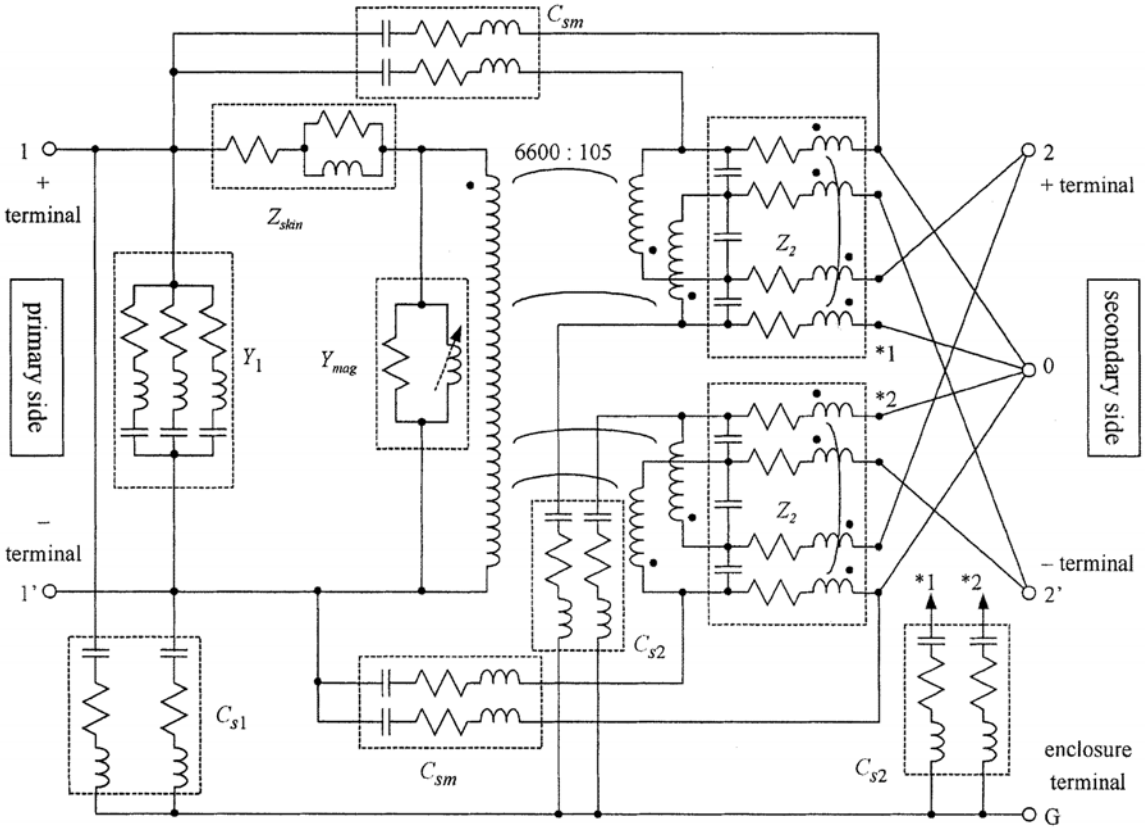

Figure 3.13 Transformer model (equivalent circuit). (1) Winding-to-winding and winding-to-enclosure capacitance: C_{s1}, C_{s2}, C_{sm}. (2) Skin effects of winding conductors and an iron core: Z_{skin}. (3) Multiple resonances due to the combination of winding inductance and turn-to-turn capacitance: Y_1, Z_2. (4) Saturation and hysteresis effects of an iron core: Y_{mag} [113].

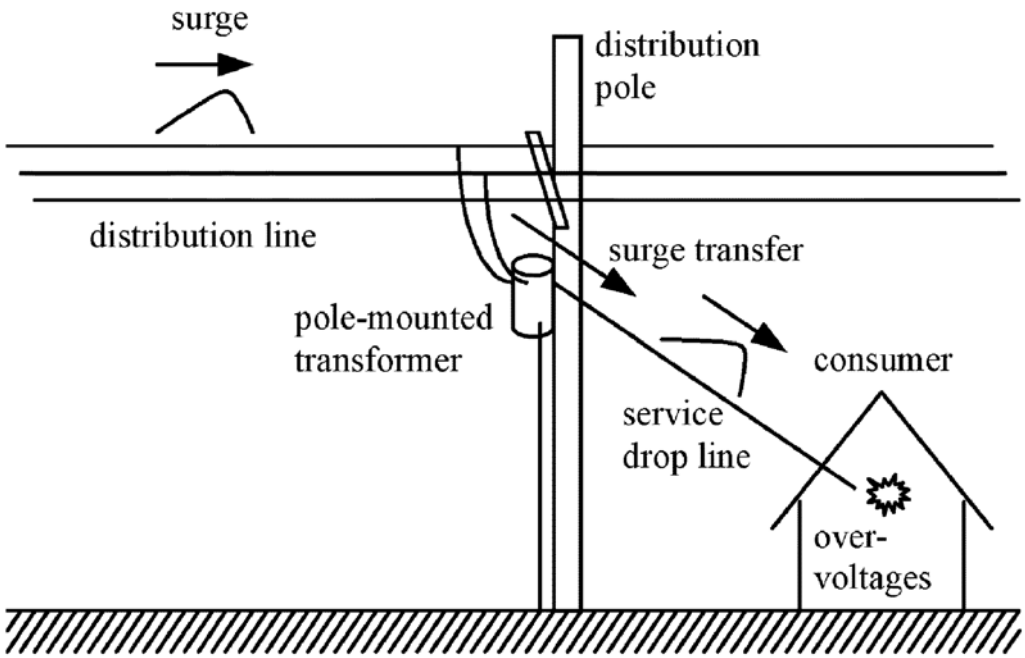

Figure 3.14 Surge transfer from a distribution line to a consumer entrance via a pole-mounted transformer [114].

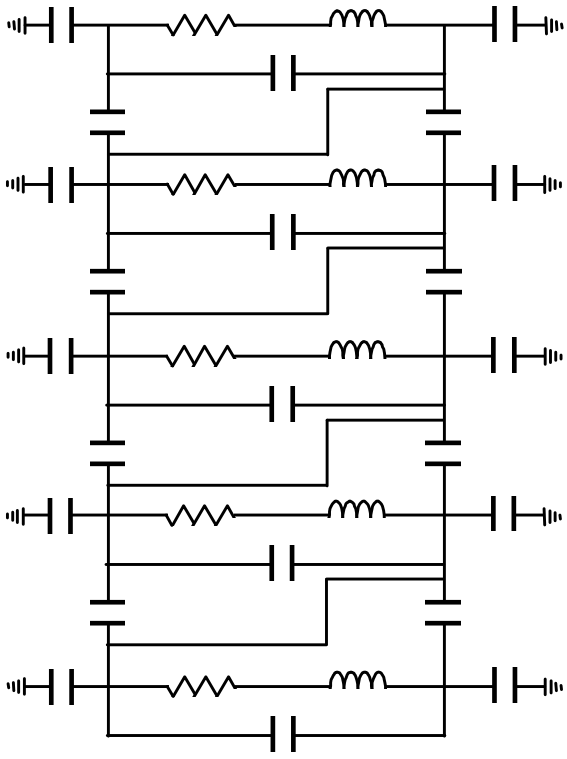

Figure 3.15 Part of R, L and C equivalent network of transformer winding [115].

A simplified lumped parameter model for the distribution transformer and associated distribution system has been described in [116] depending on the stroke current as shown in Figure 3.16, where Figure 3.16a represents single phase system and transformer and Figure 3.16b represents the simplified lumped parameter model for the system shown in Figure 3.16a, where, i_S is the stroke current injected into the system at terminal H1, i_A is the surge arrester discharge current, i_{pG} is the current entering the earth at the transformer pole ground, i_{HG} is the current entering the earth at the house ground, i_{X2} is the current into terminal X2 of the distribution transformer and i is the current in the interconnection path between the neutral conductors of the primary and secondary systems.

Scattering Matrix theory has been used in [117] to model the transformer, where the corresponding network using this method is shown in Figure 3.17. The network is represented by electrical elements (capacitance, inductance and resistance) in addition to ideal transformer. As shown in Figure 3.17, Lp and Ls are the leakage inductances, Lm is the magnetizing inductance. Rp and Rs are the resistive losses and the losses in the ferrite core at the lowest frequency. Rm is the hysteresis losses in the core, Cp and Cs are distributed capacitances between turns of each winding. Cps is the capacitance between the primary and secondary windings. These model parameters were obtained using the parameter extraction technique. The main scope of this technique is to modify the data iteratively with evaluating the correlation between the calculated S-parameters and the measured ones. However, this method was used to describe and directly calculate the total power losses in the transformer. The model was not tested for transferred voltage to the secondary side.

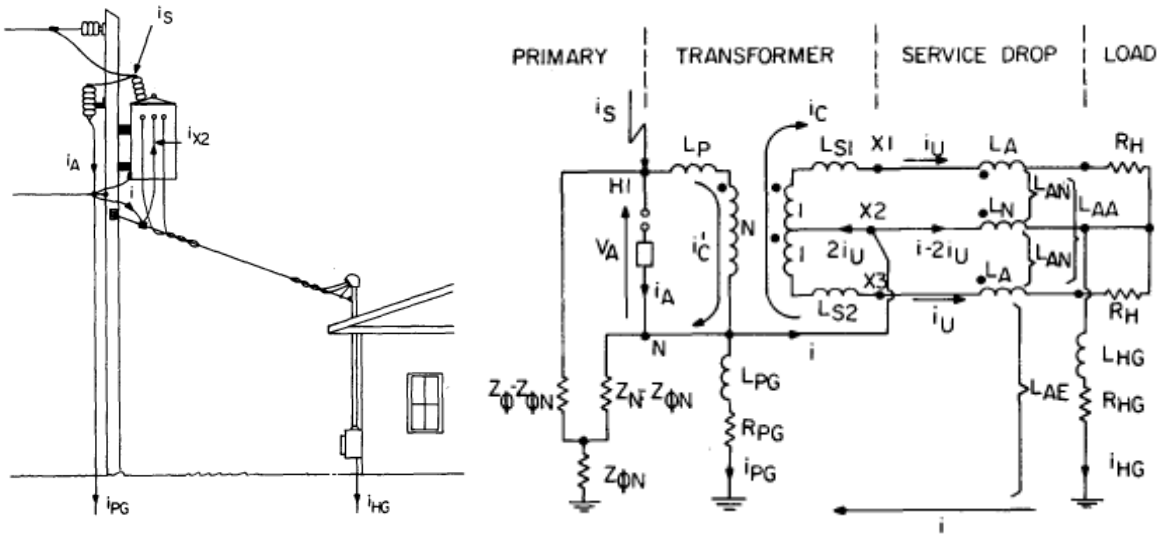

a. Single-phase system and transformer. b. Model for the single-phase system and transformer.

Figure 3.16 Configuration of Single-phase system and transformer and its model [116].

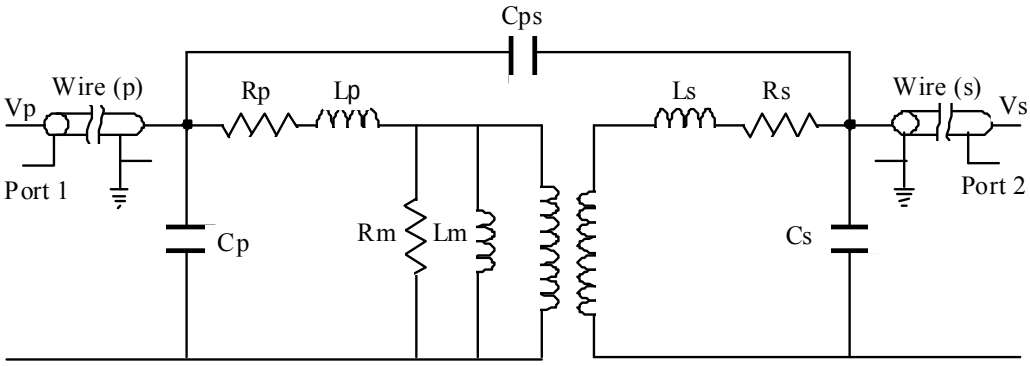

Figure 3.17 Two-port transformer representation [117].

Modeling the transformer from the frequency response has been presented in [118] where the transformer parameters were calculated using mathematical procedure which needs the module of the impedance with certain behavior. A model based on a classical model has been constructed as shown in Figure3.18a, where each cell was represented by R, L and C elements. On the other hand, this model took the following effects into consideration using three cells:

Cell set 1: The core effects.

Cell set 2: The major winding effects.

Cell set 3: The minor winding effects.

However this behavior is not available for all transformers. Each cell should be participated only at its assigned frequency and neglected at the rest of frequencies. This behavior can be granted by choosing the suitable cells topology. There are four suitable cells can be used as shown in Figure 3.18b.

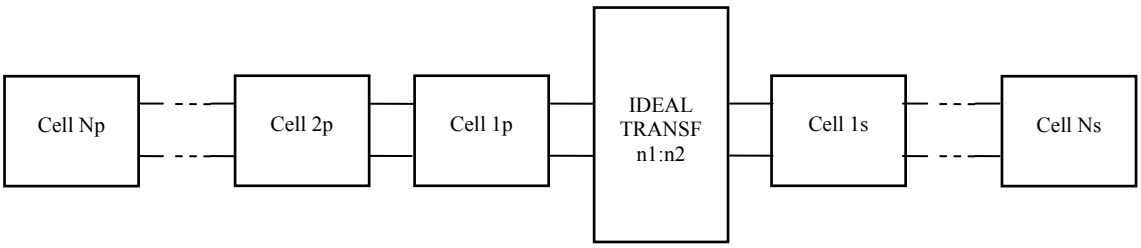

a. Wide bandwidth model for a two winding magnetic component.

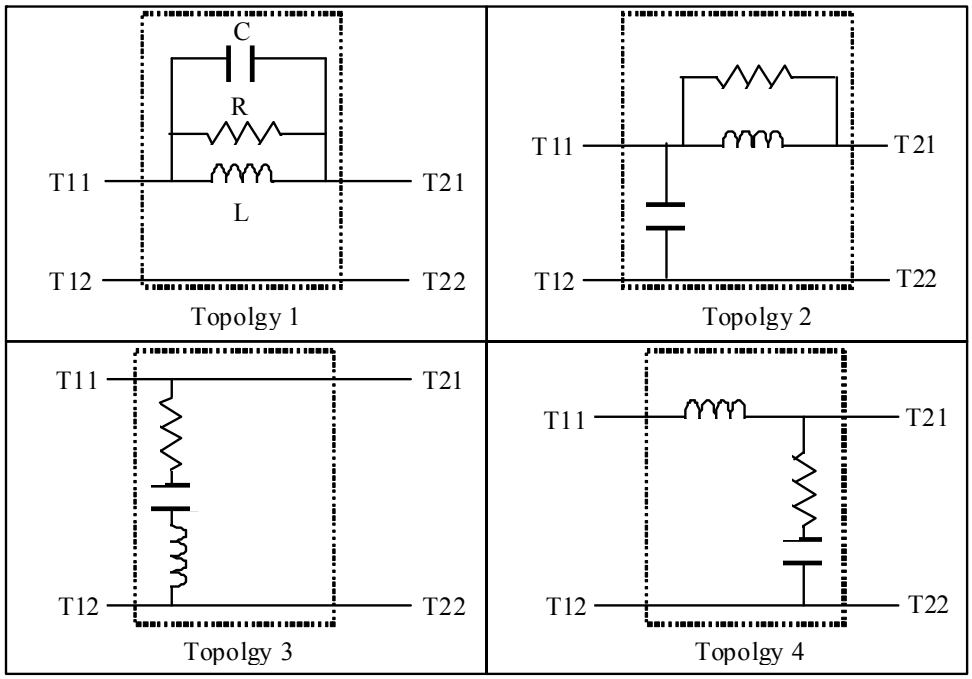

b. Suitable topology for the basic cells.
Figure 3.18 cells arrangement and their topology [118].

Concerning simple modeling category, a transformer model was introduced in [119] with equivalent circuit shown in Figure 3.19. This model has been modified and the methodology of the modified model was established in [120] based on the frequency response of distribution transformer. In this study, the distribution transformer has been considered as a two-port network and the frequency response of the equivalent impedances were determined. Considering linear and time invariant two-port network, the following equation can be obtained as:

$$U_1=Z_{11}I_1+Z_{12}I_2 \quad (3.1)$$

$$U_2=Z_{21}I_1+Z_{22}I_2 \quad (3.2)$$

where Z_{11} is the two-port input impedance, $Z_{12}= Z_{21}$ is the two-port transfer impedance, Z_{22} is the two-port output impedance.

Based on the equations (3.1) and (3.2), an equivalent circuit of the distribution transformer is shown in Figure 3.20a where, Z1 is the input impedance, Z2 is the output impedance, Z3 is the transfer impedance between primary and secondary.

The frequency characteristics of each impedance Z1, Z2 and Z3 have been evaluated. Then, the transformer equivalent circuit has been computed and implemented using resistance, inductance and capacitance elements. This equivalent circuit is shown in Figure 3.20b. The model shown in Figure 3.20 has been modified in [121] and the new equivalent circuit is shown in Figure 3.21.

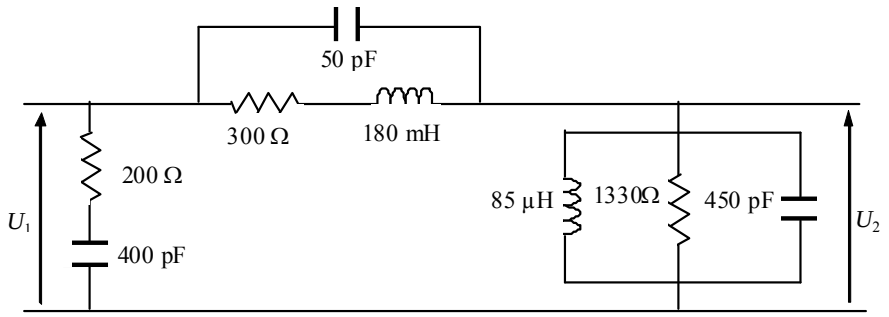

Figure 3.19 Transformer model for calculation of transferred surges [119].

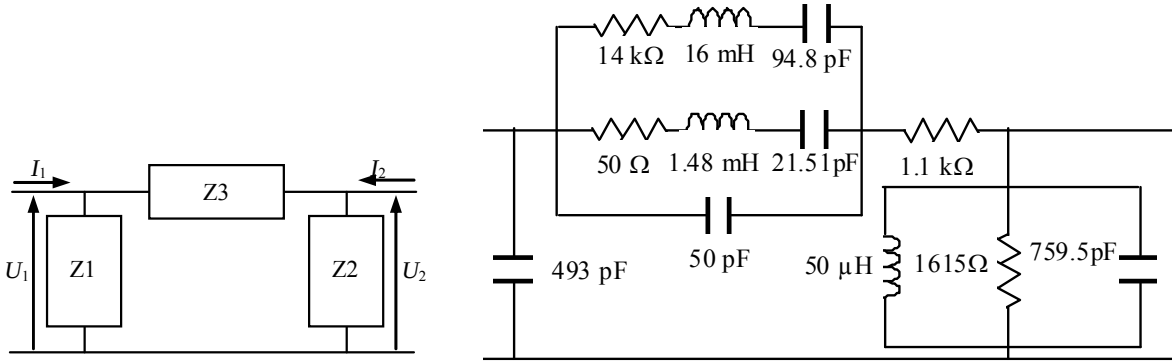

a. Equivalent circuit of the quadripole. b. equivalent circuit.

Figure 3.20 Transformer model [120].

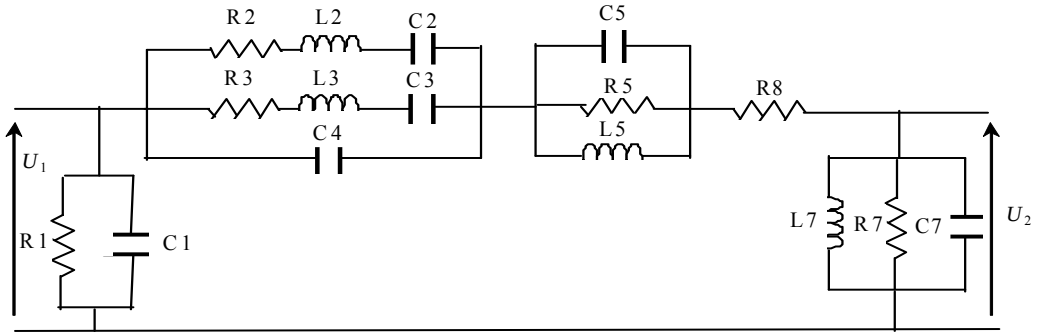

Figure 3.21 equivalent circuit of the transformer [121].

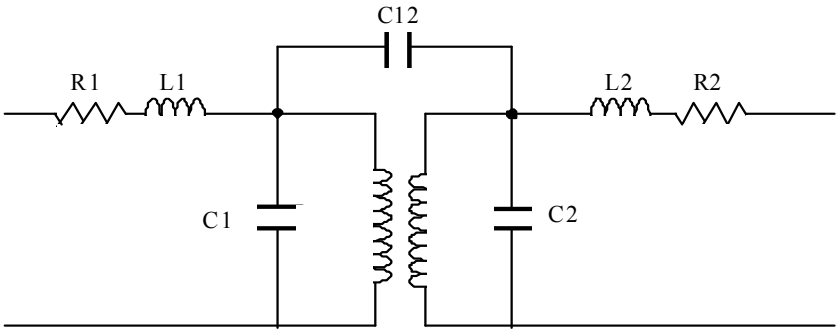

Figure 3.22 First order model [122].

A transformer model has been developed to study the transferred voltages, using simple testing parameters and the ATP (Alternative Transient Program) [122]. The transformer model to simulate the transferred surge behavior is shown in Figure 3.22. However this model did not achieve a better approach for the transferred voltage peak and shape.

The frequency characteristics of the transformer admittance matrix between its terminals have been used in [123] to model a high frequency transformer over a frequency range up to 1 MHz. This model presented an equivalent circuit of the transformers over the frequency range of interest provided that its admittance matrix matches the nodal admittance matrix of the original transformer. The parameters of a multi-terminal π-equivalent shown in Figure 3.23 can be calculated from its nodal admittance matrix where the nodal admittance matrix parameters have been estimated using rational function. However, this model has large nodal admittance matrix.

The interaction between electric and magnetic quantities of the transformer has been reproduced using high frequency transformer model introduced in [124]. Therefore, the equivalent circuit was composed of a magnetic circuit as shown Figure 3.24a and an electric interface as depicted in Figure 3.24b [124]. However, the characteristics of the magnetic material and the geometry of the winding and core are needed which sometimes represent difficult to be obtained.

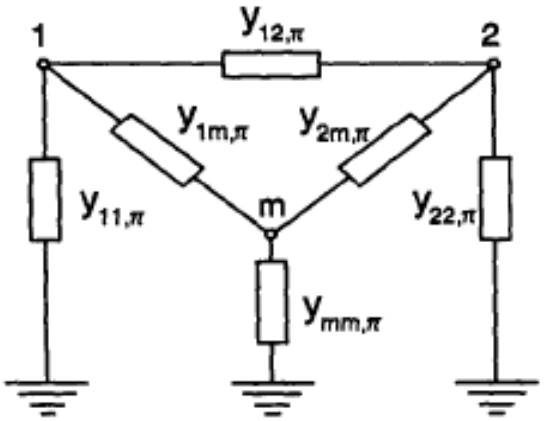

Figure 3.23 Single line diagram of a multi-terminal π-equivalent [123].

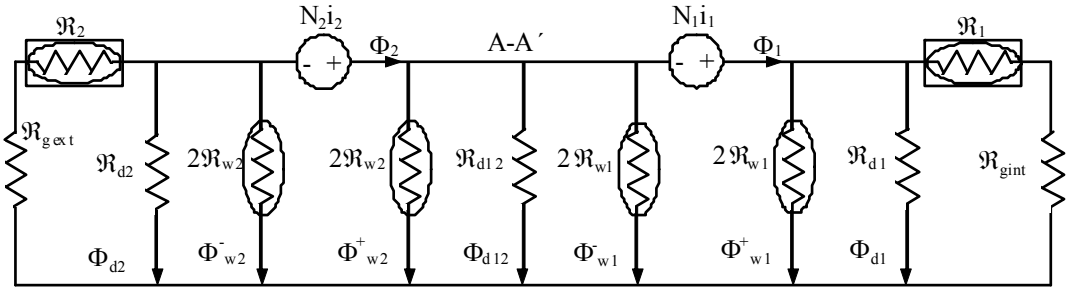

a. Magnetic part, nonlinear and frequency-dependent components are, respectively, enclosed in a rectangle and in an ellipse.

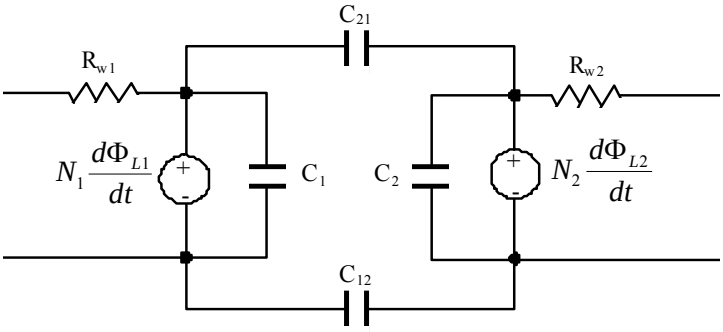

b. Electric part.

Figure 3.24 High frequency model reported in [124].

Distribution power transformer has been modeled with the frequency up to 10 MHz for Power Line Communication (PLC) applications [125]. This model has been represented by the simple R, L, C circuits and having two MF and HF models which are separately modeled. The difference between these models is the participation of the iron core effects where it has been taken into account in case of MF model through the ideal transformer. However, in HF model it does not include due to the absence of the ideal transformer. MF model for this model is shown in Figure 3.25a, where, the HV and LV terminals are defined by ABC and abcn, respectively, Z_1 is the leakage impedance of the wingding/phase, Z_m is the magnetizing impedance of the winding/phase, C_1 and C_2 are the capacitances between winding and mass and C_{12_1} and C_{12_2} are the capacitances between inner side of HV and outer side of LV windings. Using frequency characteristics measurements of the impedance at the transformer terminals, all of these parameters have been calculated, where three kinds of measurements are carried out such as open-circuit, short-circuit, and capacitance measurement.

The HF of this model is shown in Figure 3.25b, where the same resonance and capacitance have been taken into consideration for both HF and MF models. However in HF model, C_{12} has been presented by pure capacitance in addition to the ideal transformer has been neglected. Only measurement to evaluate the resonance was needed to determinate the parameters of the HF model.

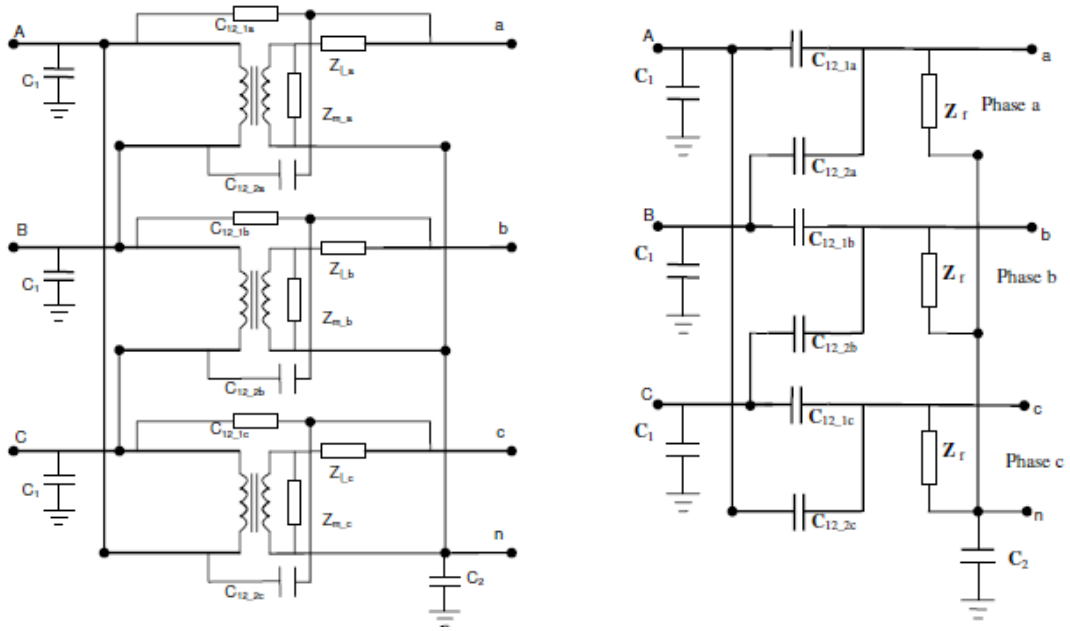

a. The model of transformer in MF. b. The model of transformer in HF.

Figure 3.25 Model of transformer [125].

3.2.2 Proposed Transformer Model

In this subsection, an accurate and simplified distribution transformer model for overvoltage transfer under lightning strokes is presented using its frequency response. The model is suitable for unloaded and loaded conditions as well [126]. The proposed model is based on two-port network theory. It is experimentally verified under different balanced load conditions considering two different practical distribution transformers. The corresponding models are simulated using ATP/EMTP in order to verify the proposed model.

There are four types of the port-type networks. They are impedance parameters, admittance parameters, hybrid parameters and transmission parameters networks where their details are depicted in Appendix I [127]. The simplest one is the impedance parameters network as the open circuit tests are needed to compute the network parameters. Therefore, this impedance parameters two-port network is considered for the proposed model. The transformer can be modeled using a two-port network as shown in Figure 3.26. The network can be described as in Equations (3.1) and (3.2) as addressed in [127,128].

The impedance parameters (Z_{11}, Z_{12}, Z_{21} and Z_{22}) can be evaluated by setting $I_1 = 0$ (input port open circuited) or $I_2 = 0$ (output port open circuited). Therefore, the impedance parameters are obtained as:

$$Z_{11} = \left.\frac{U_1}{I_1}\right|_{I_2=0}, \quad Z_{12} = \left.\frac{U_1}{I_2}\right|_{I_1=0}, \quad Z_{22} = \left.\frac{U_2}{I_2}\right|_{I_1=0} \text{ and } \quad Z_{21} = \left.\frac{U_2}{I_1}\right|_{I_2=0} \tag{3.3}$$

where Z_{11} is the open-circuit input impedance, Z_{12} is the open circuit transfer impedance from port 1 to port 2, Z_{21} is the open circuit transfer impedance from port 2 to port 1, Z_{22} is the open-circuit output impedance.

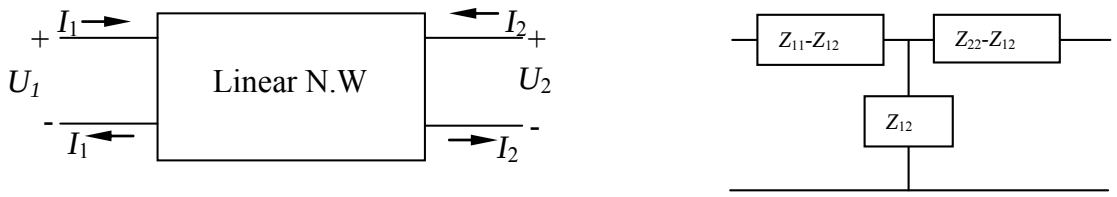

a. two-port network. b. T equivalent circuit.

Figure 3.26 Impedance parameters two-port network.

In order to describe the high frequency model using these impedance parameters, the impulse voltage was applied on the primary side when the secondary was opened (I_2= 0), then the impulse voltage was applied on the secondary side when the primary was open (I_1= 0) as the experiments declared in following subsection.

3.2.3 Experimental Measurements and Model Calculation

The experimental measurements have been carried out on two different practical transformers. The input impulse signal was 450 V, 0.87/50 μsec. The experimental measuring was carried out on two distribution transformers T1 100 kVA and T2 50 kVA considering the following two steps.

Step1: The impulse voltage was applied on the interconnected high voltage side when the transformer was unloaded to measure the primary voltage (U_1), primary phase current (I_1) and secondary voltage (U_2) through channels CH_1, CH_2 and CH_3, respectively as shown in Figure 3.27a. These voltages and currents traces are captured and stored in time domain through a four-channel oscilloscope.

Step2: The impulse voltage was applied on the interconnected low voltage side when the high voltage side was opened to measure the primary voltage (U_1), the secondary current (I_2) and secondary voltage (U_2) through channels CH_1, CH_2 and CH_3, respectively as shown in Figure 3.27b.

The Fourier algorithm was applied on the measured voltages and currents. Then the impedance parameters in Equations (3.1) and (3.2) were evaluated using the relations in Equation (3.3) for obtaining these impedance parameters as a function of frequency. Finally, the frequency domain of T equivalent circuit impedances is shown in Figure 3.28 for transformer T1. Figures 28.a, b and c, show the amplitude and the angle of Z_{11}-Z_{12}, Z_{12} and Z_{22}-Z_{12}, respectively. Similarly, Figure 3.29 illustrates the frequency domain impedances of transformer T2.

After investigating the frequency response of the T-equivalent circuit impedance parameters (magnitude and angle) of the two transformers, each of these impedances can be converted to R, L and C elements according to its behavior in frequency domain [129]. For each transformer, the calculations of their elements are carried out taking into account the first and second resonance frequencies in a wide range of frequency, and then these elements are tuned to match the measured results in case of unloaded and loaded

conditions. Such tuning is considerable in order to compensate Fourier Transform (FT) performance used for calculating the transformer transfer function as addressed in [130].

For both transformers and concerning two resonances, the same equivalent circuit was obtained as following. The impedance (Z_{11}-Z_{12}) was represented by only capacitance at each resonance frequency, where these capacitances (C_5 and C_6) are connected in parallel. The impedance (Z_{12}) was represented by parallel R, L and C circuit at each resonance frequency and these circuits are connected in series. The impedance (Z_{22}-Z_{12}) was represented by parallel R, L and C circuit at first resonance frequency and series R, L and C circuit at second resonance frequency and these circuits are connected in series. In the equivalent circuit R_5 and R were considered for tuning purposes for impedances (Z_{11}-Z_{12}) and (Z_{12}) respectively, where R_5 was used under unloaded conditions only and R was used under loaded conditions only. The procedure of the parameter determination is discussed in Appendix J. The corresponding transformer model is shown in Figure 3.30 for unloaded transformer. However the load is added to the terminal U_2 for loaded transformer. The elements values are shown in Table 3.1 for each transformer.

The validation of the proposed high frequency transformer model was obtained through both time and frequency domains of the voltage transferred to the secondary side. The comparison between experimental and simulation of the voltage transferred to the secondary side shows a good agreement for unloaded and balanced loaded conditions as ascertained in Figures 3.31, 3.32 and 3.33 for transformer T1 and confirmed in Figures 3.34 and 3.35 for transformer T2. The transformers are directly loaded at the secondary terminals using different loads such as pure resistance equal to 50 Ω and then the resistance was paralleled with capacitance equal to 1200 pF. The simulations were carried out using ATP/EMTP [101] where the ATPDraw program is used as preprocessor.

From these results, the high frequency transformer model has been proposed under unloaded as well as balanced loaded conditions. The model compromises between the simplicity and also accuracy. A very simple circuit to evaluate the transformer performance under lightning strokes was taken, in addition to a very easy procedure was achieved to determine the model parameters at two different frequencies. Concerning two resonance frequencies in the transformer modeling has enhanced the model accuracy. The proposed model showed a good agreement between the experimental and the simulated results. So, it can be used to study the behavior of the transformer and the connected low voltage network under lightning strokes as discussed in chapter 5.

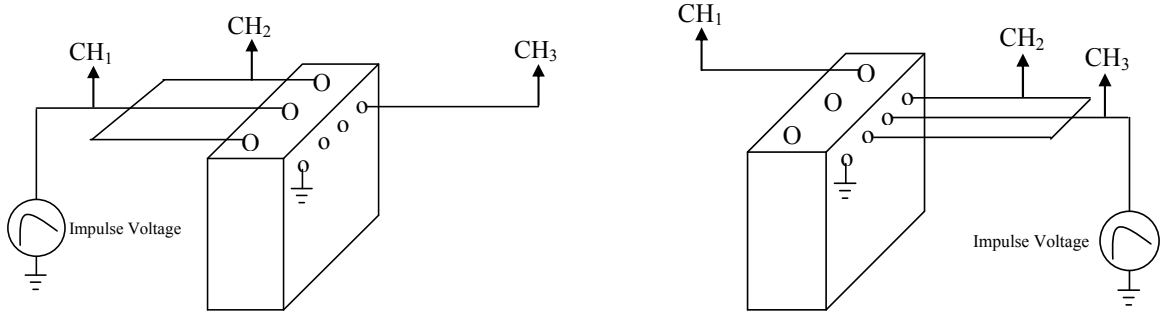

a. Impulse voltage on primary. b. Impulse voltage on secondary.

Figure 3.27. Experimental Configuration.

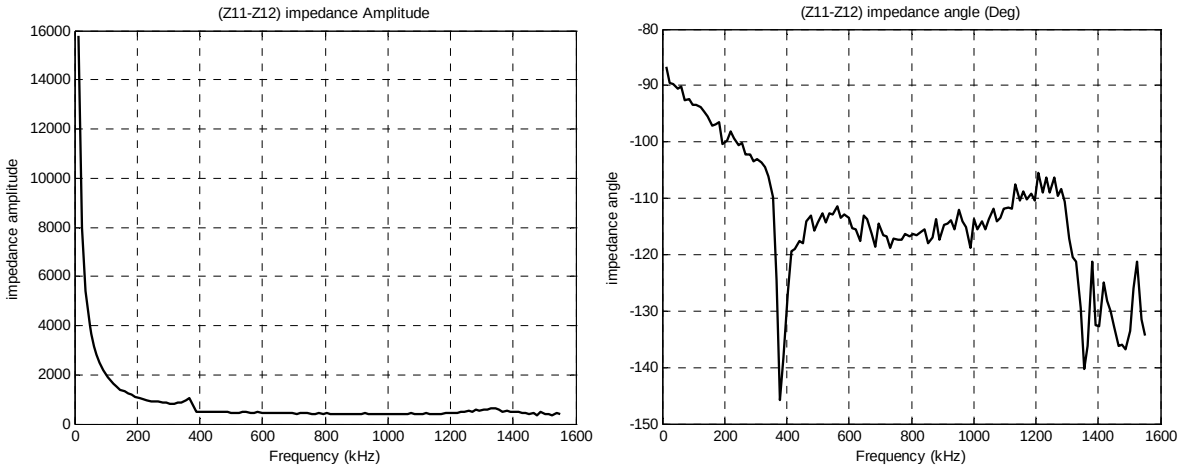

a. Z_{11}-Z_{12} frequency response.

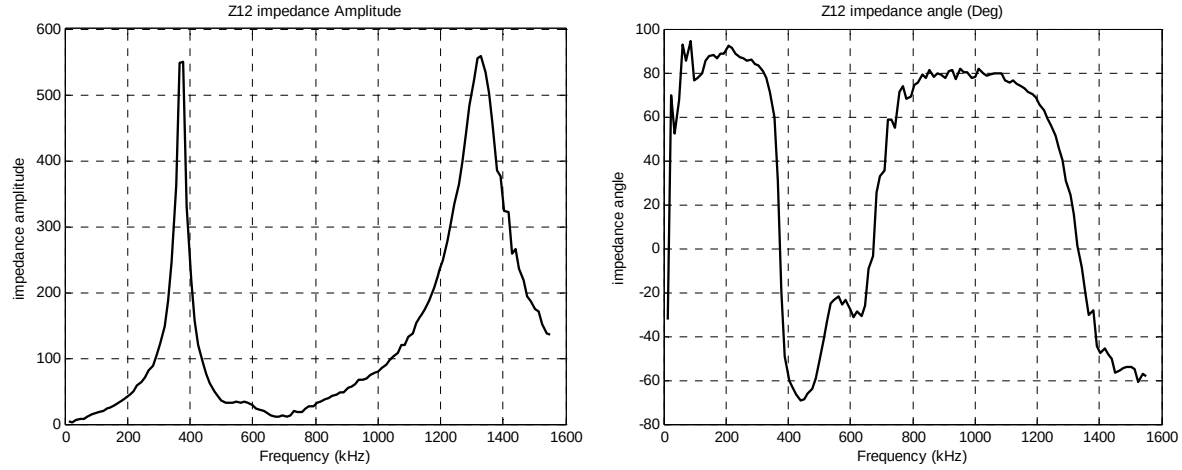

b. Z_{12} frequency response.

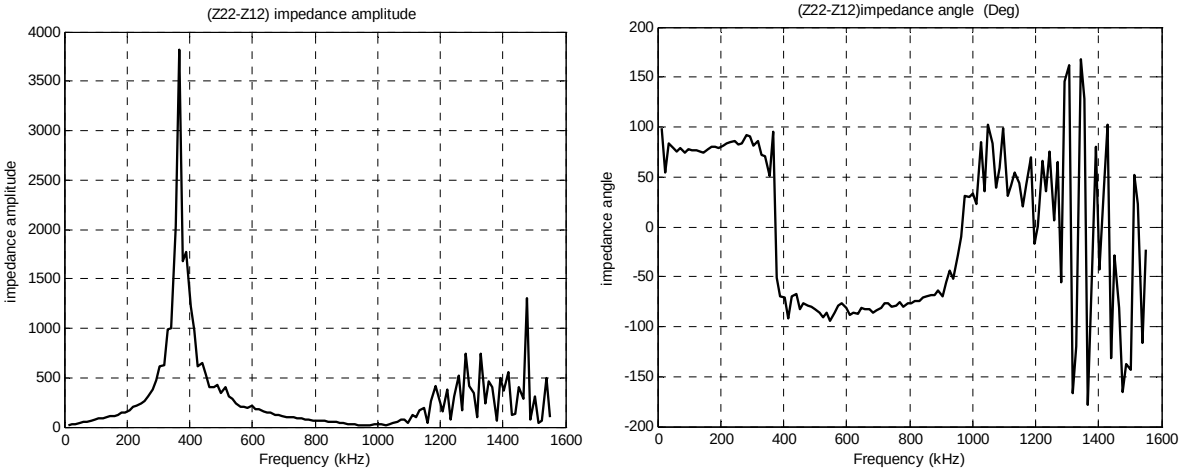

c. Z_{22}-Z_{12} frequency response.

Figure 3.28 frequency response of T-equivalent circuit impedance parameters for T1 (100 kVA).

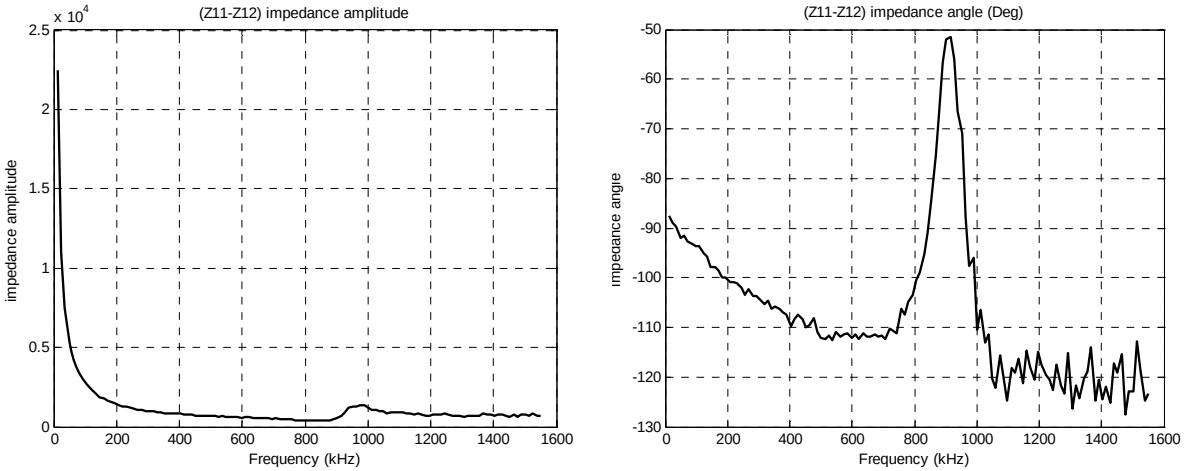

a. Z_{11}-Z_{12} frequency response.

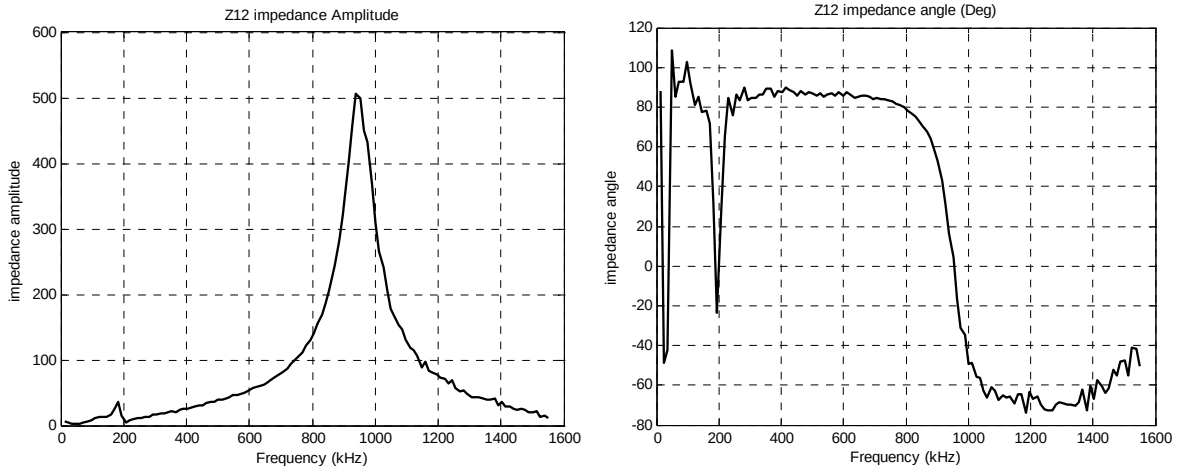

b. Z_{12} frequency response.

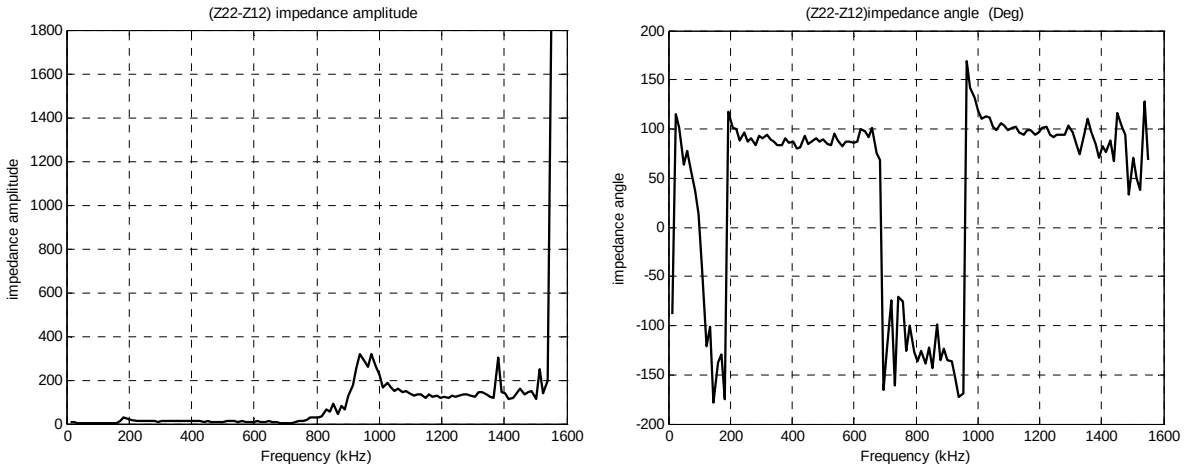

c. Z_{22}-Z_{12} frequency response.

Figure 3.29 frequency response of T-equivalent circuit impedance parameters for T2 (50 kVA).

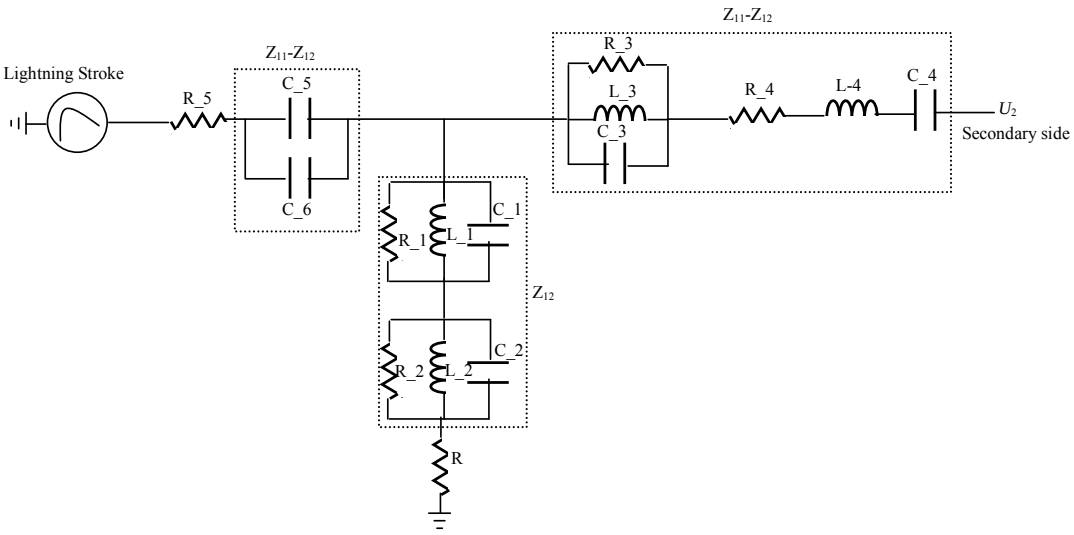

Figure 3.30 High Frequency Transformer Model.

Table 3.1 Elements values for T1 and T2.

Elements	T1 (100 kVA)	T2 (50 kVA)
R_1 (Ω)	500	5.6839
R_2 (Ω)	558.5405	906.7085
R_3 (Ω)	1000	529.0657
R_4 (Ω)	1E-6	130.1928
R_5 (Ω)	50	500
R (Ω)	1500	50
L_1 (mH)	0.00856	0.23964
L_2 (mH)	0.0046	0.006497
L_3 (mH)	0.036897	0.0173762
L_4 (mH)	0.048296	0.091127
C_1 (μF)	0.021063	1.91546
C_2 (μF)	0.00302967	0.0035155(loaded) 0.0051155(unloaded)
C_3 (μF)	0.00512	0.000739
C_4 (μF)	0.00022167	0.00115
C_5 (μF)	0.0004221	0.000551916
C_6 (μF)	0.00019152	0.000485187

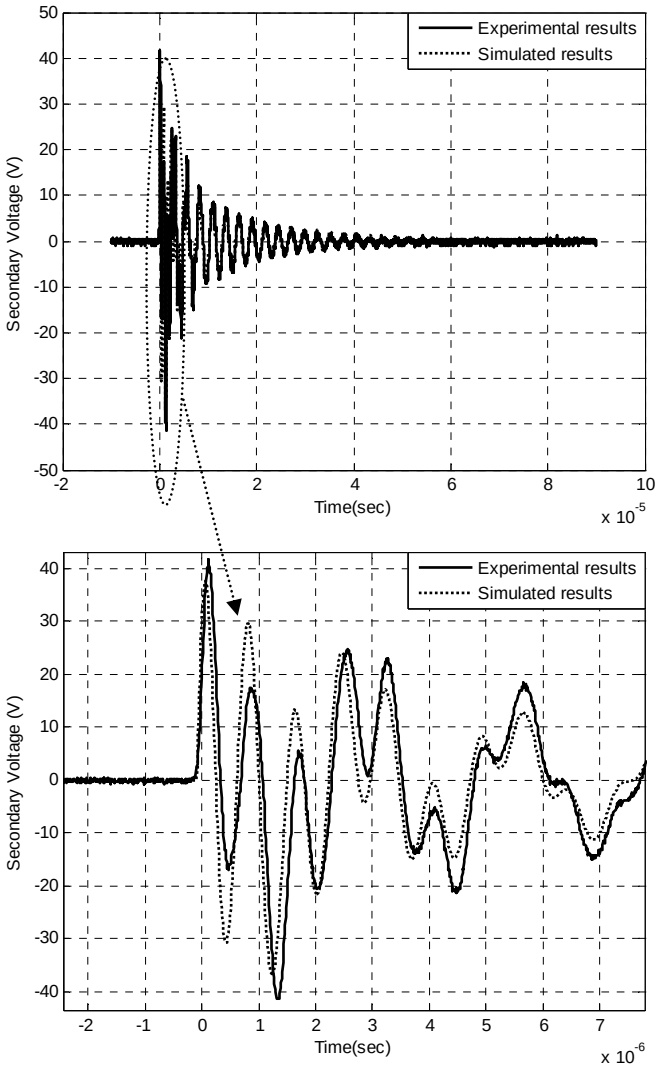

a. Time response of voltage transferred to the Secondary side.

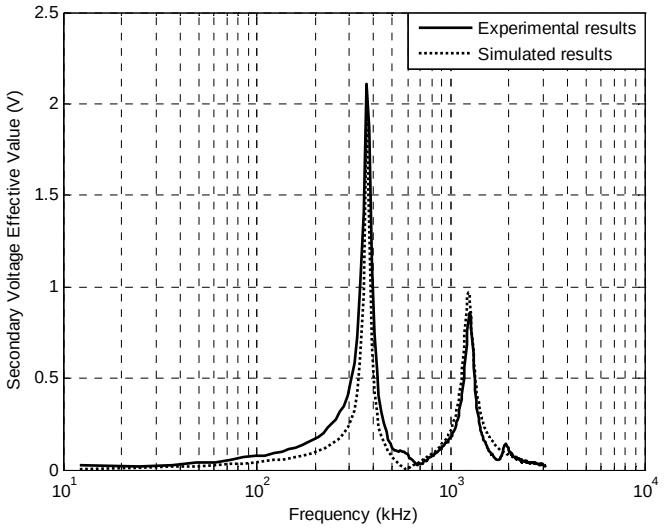

b. Frequency response of voltage transferred magnitude.

Figure 3.31 Secondary transferred voltage under unloaded condition for T1.

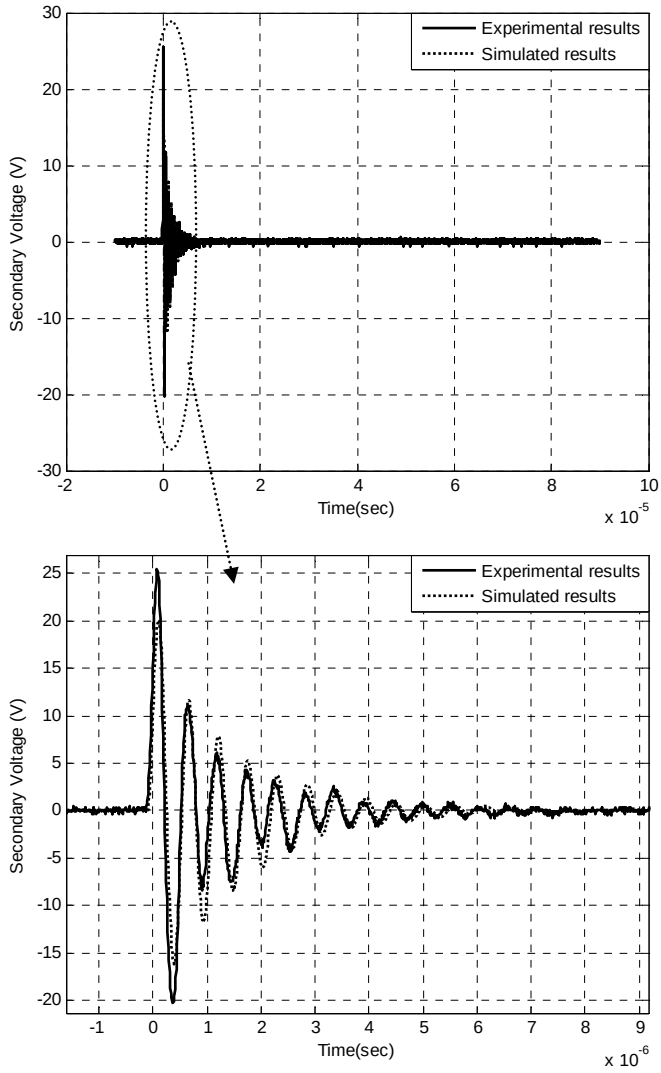

a. Time response of voltage transferred to the Secondary side.

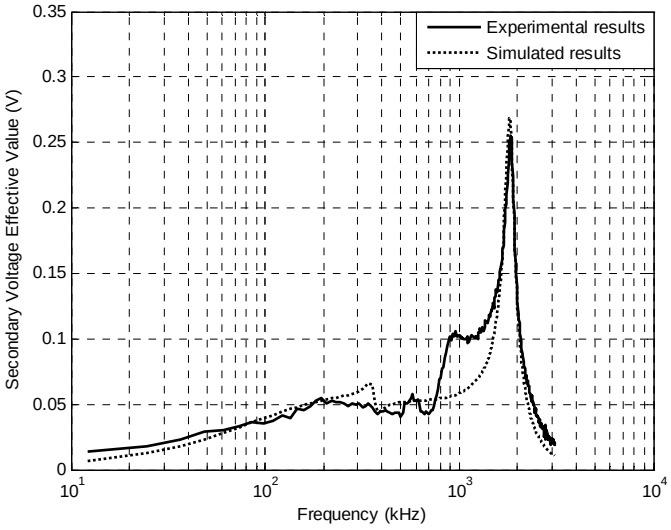

b. Frequency response of transfer voltage magnitude.

Figure 3.32 Secondary transferred voltage under resistive load for T1.

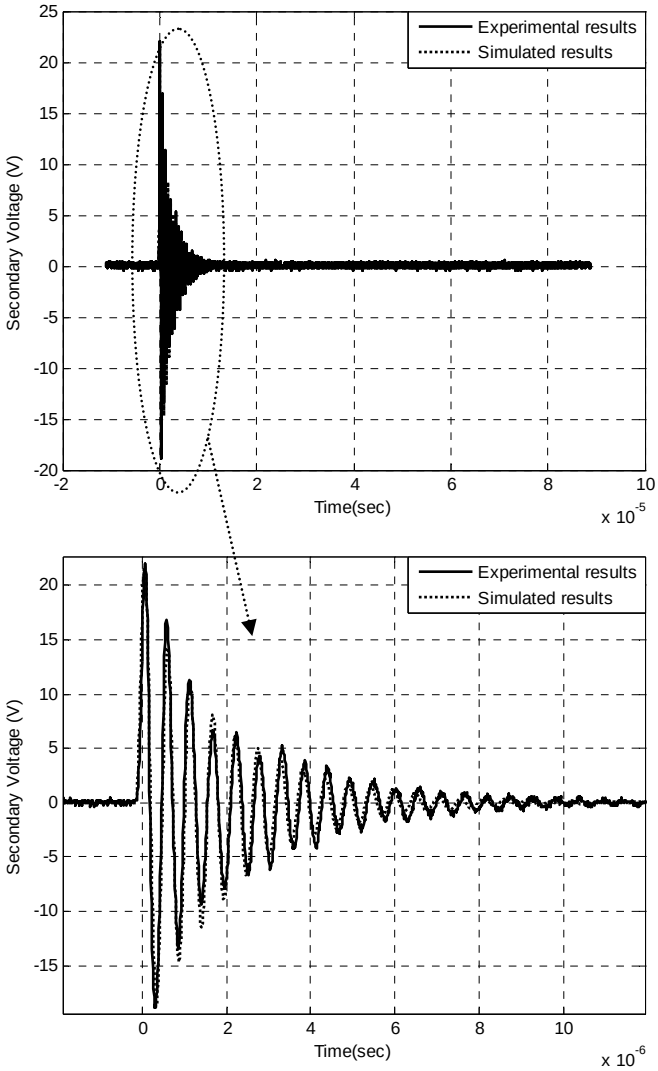

a. Time response of voltage transferred to the Secondary side.

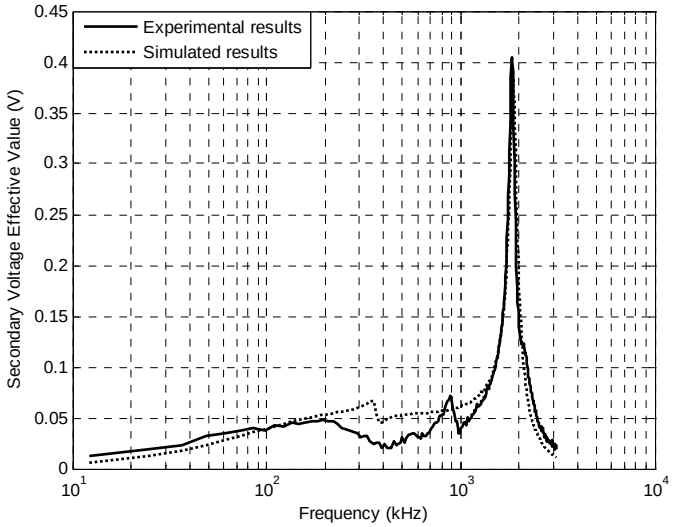

b. Secondary voltage magnitude as a function of frequency.

Figure 3.33 Secondary transferred voltage under paralleled resistive-capacitive load for T1.

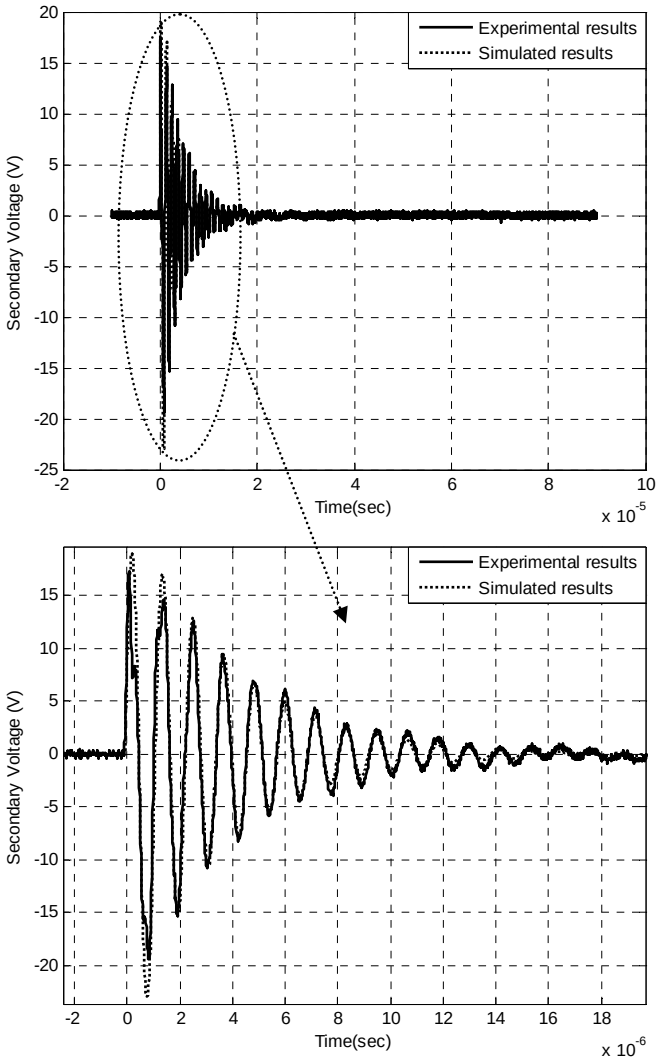

a. Time response of voltage transferred to the Secondary side.

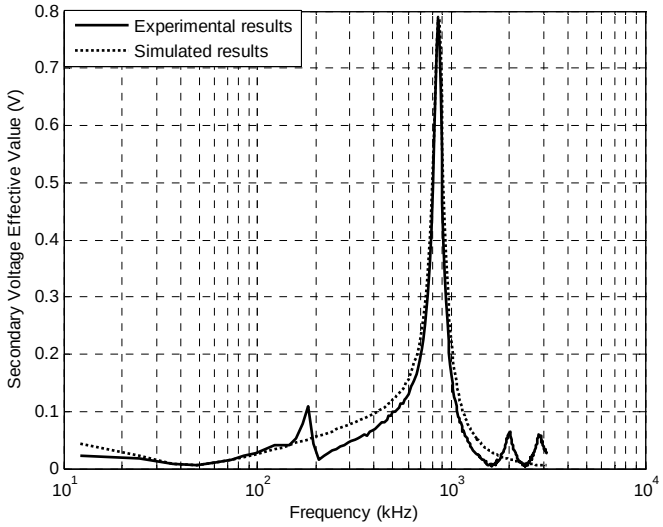

b. Frequency response of transfer voltage magnitude.

Figure 3.34 Secondary transferred voltage under unloaded condition for T2.

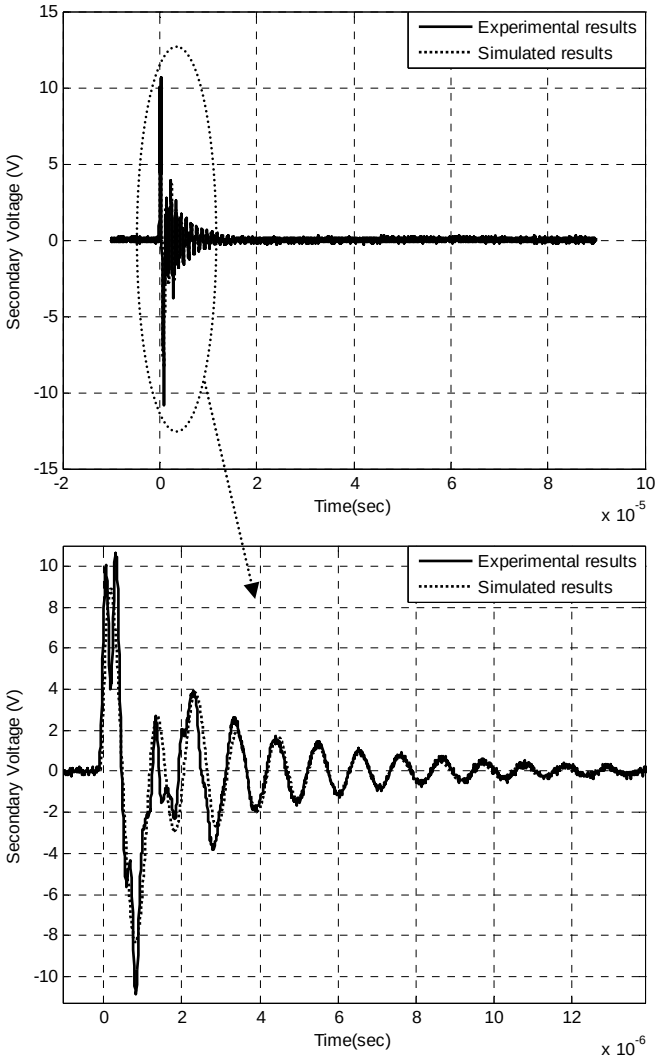

a. Time response of voltage transferred to the Secondary side.

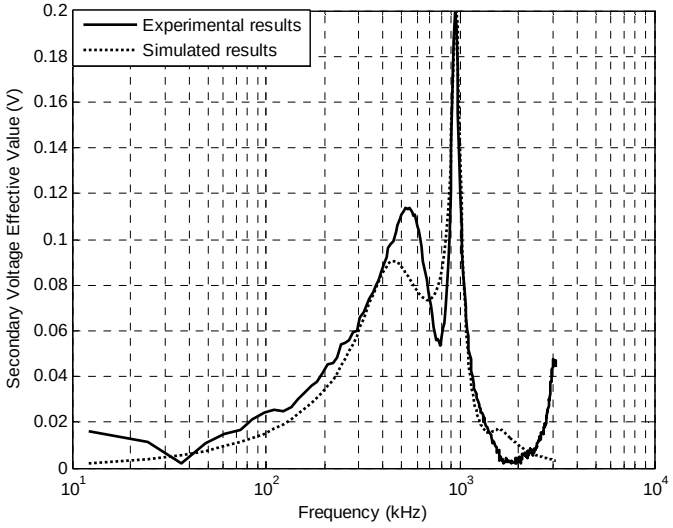

b. Frequency response of transfer voltage magnitude.

Figure 3.35 Secondary transferred voltage under paralleled resistive-capacitive load for T2.

3.2.4 Model Validation with Spark-Gap Operation Connected at Transformer Primary Side

In order to experimentally implement the MV spark-gap operation, a spark-gap is connected at the transformer primary side. Due to spark-gap flashover, a chopping in the impulse waveform is occurred. As the impulse amplitude is low value 450 V, a suitable spark-gap with small rating was used to dynamically give discharging consistence with this voltage. Figure 3.36 shows a comparison between the experimental and simulated chopped impulse waveforms where the spark-gap is simply presented by a time controlled switch in ATPDraw connected at the primary side of the transformer.

A validation of the proposed high frequency transformer model under the condition of spark-gap operation is carried out through unloaded and loaded cases as well as testing in both time and frequency domains as shown in Figures 3.37-3.39. These responses concluded that the proposed model under spark-gap operation is very accurate under unloaded conditions as shown in Figure 3.37; however this accuracy decreases only at the instant of spark-gap operation under loaded conditions as shown in Figures 3.38 and 3.39.

Concerning spark-gap operation connected at the primary side, the secondary transferred voltage is higher than when MV spark-gap is not operated. This can be observed by comparing for the measured results concerning unloaded and loaded conditions. Comparing Figures 3.31 and 3.37 for unloaded conditions, the maximum peak secondary transferred voltage is increased in time domain from 40 V to 150 V due to MV spark-gap operation and as well the magnitude is increased from 2 V to 4.5 V in frequency domain. Also Comparing Figures 3.32 and 3.38, the secondary transferred voltage is increased in case of resistive load from 25 V to 120 V in time domain and in the frequency domain the voltage magnitude is increased from 0.25 V to 0.8 V. Similarly, for paralleled resistive-capacitive load shown in Figures 3.33 and 3.39, the secondary transferred voltage is increased in time domain from 22 V to 120 V and in frequency domain it increased from 0.4 V to 1.3 V. Such experimental results confirm increasing the voltage transferred over the transformer due to MV spark-gap operation.

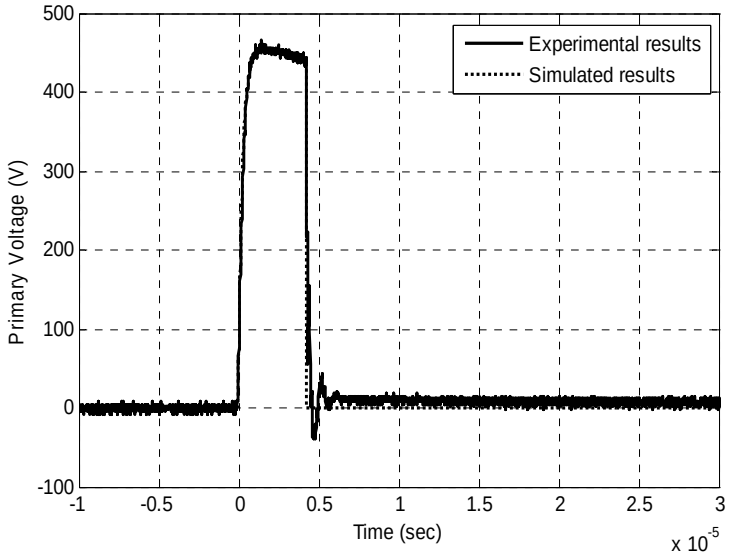

Figure 3.36 Chopped impulse waveforms.

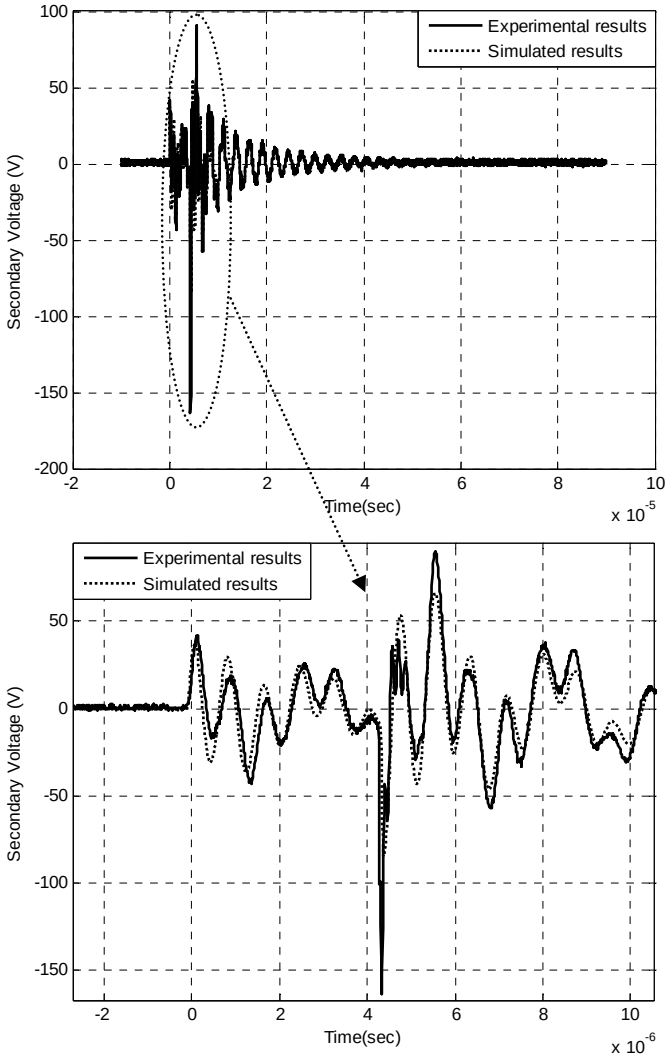

a. Time response of voltage transferred to secondary side.

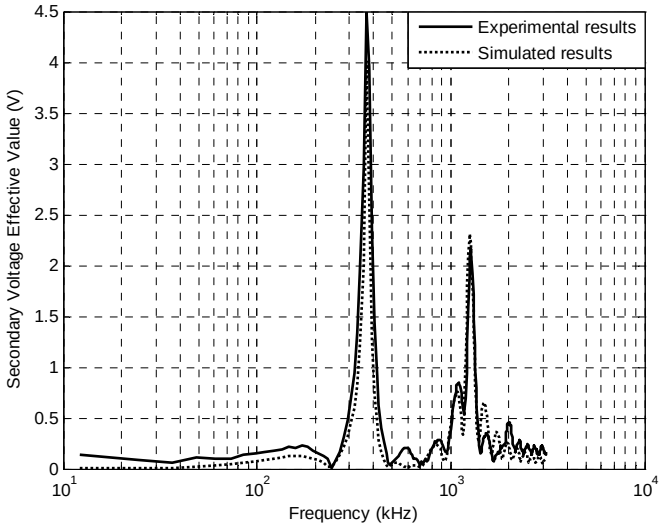

b. Frequency response voltage transferred to secondary side.

Figure 3.37 Secondary transferred voltage under unloaded condition with spark-gap operation (T1).

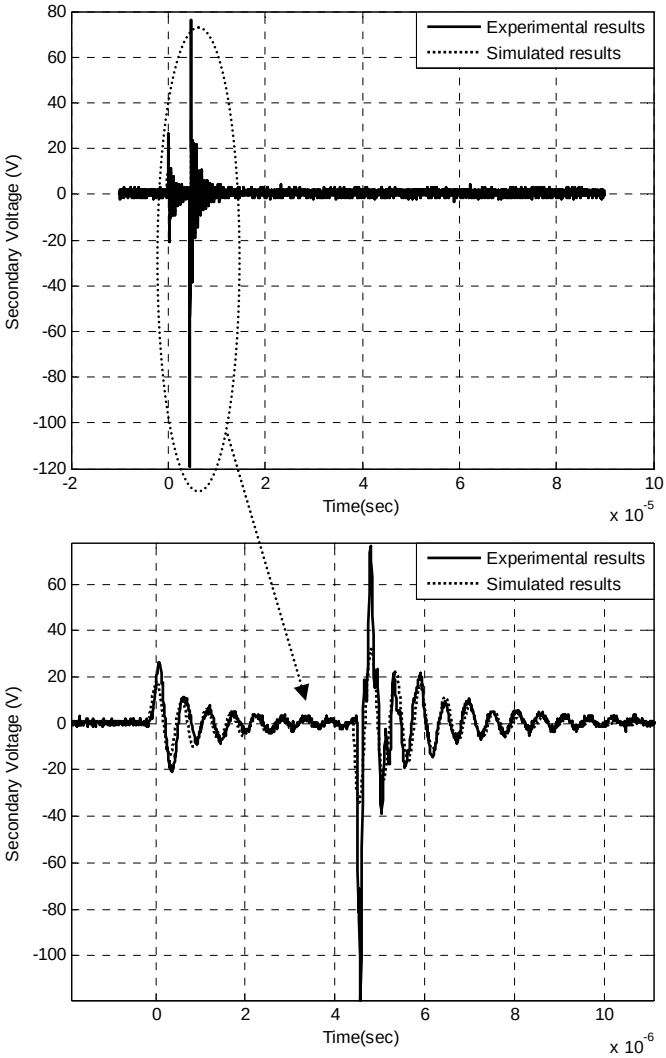

a. Time response of voltage transferred to secondary side.

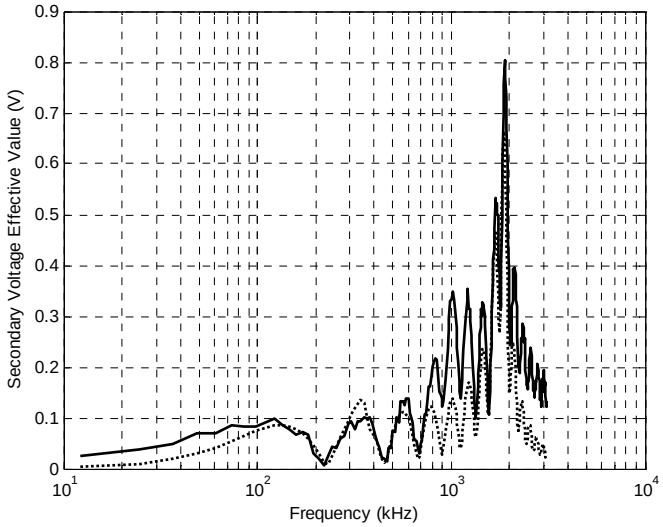

b. Frequency response voltage transferred to secondary side.

Figure 3.38 secondary transferred voltage under resitive load with spark-gap operation (T1).

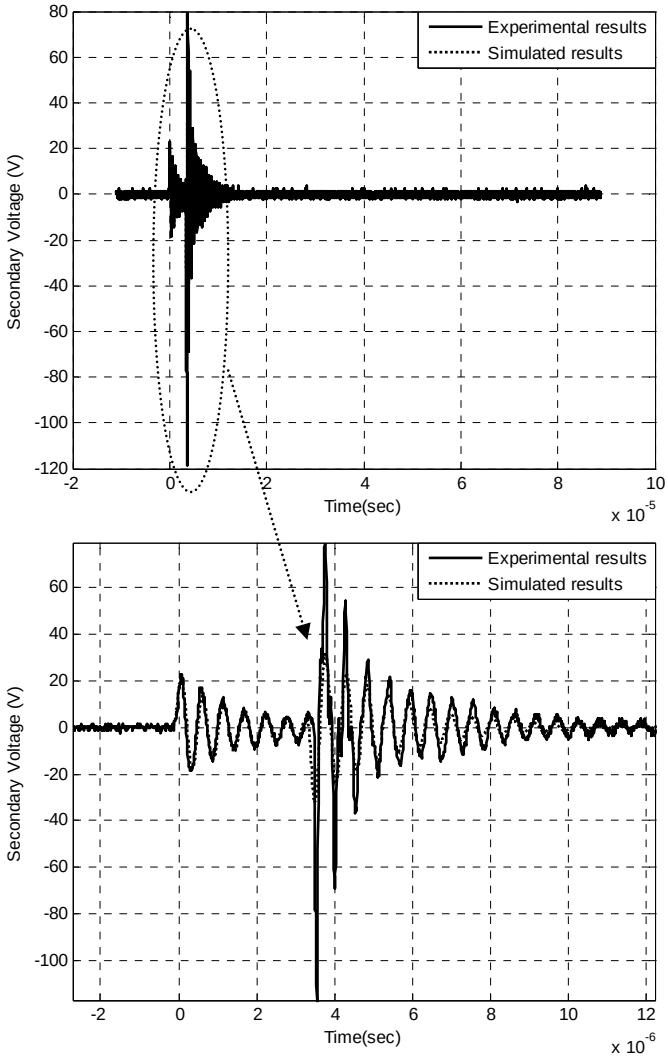

a. Time response of voltage transferred to secondary side.

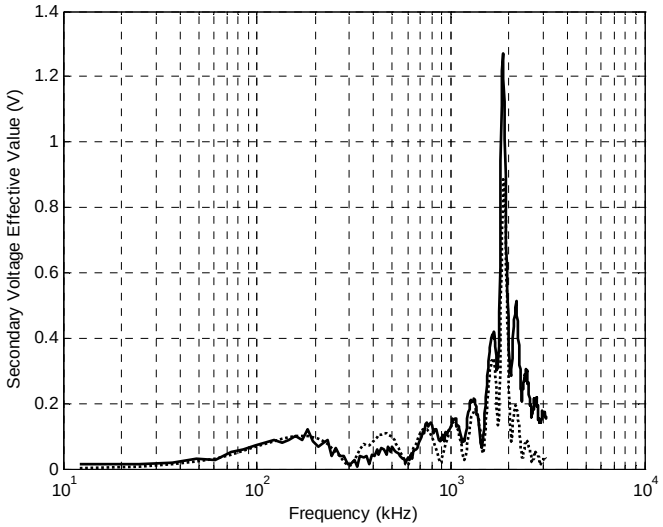

b. Frequency response voltage transferred to secondary side.

Figure 3.39 Secondary transferred voltage under resistive-capacitive load with spark-gap operation (T1).

4- Surge Arrester Model for LV Network Protection

Overvoltage protection devices play an important role for mitigating the performance of power system exposed to overvoltage due to lightning, switching … etc. In this chapter, modeling of the low voltage surge arrester is investigated using Pinceti surge arrester model where the model parameters are extracted and evaluate using ABB data sheet. This model is used to study the protection of the customer from the lightning surges coming through distribution transformer when the lightning strikes the transformer primary side. Therefore, its installation at the transformer secondary side can be studied as discussed in chapter 5. A brief introduction regarding customer overvoltage protection is declared as well as an introduction on the surge arrester in the following sections.

4.1 Overvoltage Protection Devices

The overvoltage protection devices of low voltage system can be divided to two major types [131]. They are called primary and secondary protection devices and they are discussed as follows.

4.1.1 Primary Protection Devices (Protection of Installations against Lightning)

The primary protection devices are usually used to protect installations against lightning direct strokes. Also, their function is to dissipate the lightning energy induced in the installations. The highest structure is the most attractive lightning path such as effect produced by a pole, building or very high metallic structure. There are three types of primary protection where these types are lightning conductors, overhead earth wires and meshed cage. More information about these types can be found in [131].

4.1.2 Secondary Protection Devices (Protection of Internal Installations against Lightning)

There are two types of the secondary protection devices where they are serial protection and parallel protection devices. Serial protection devices can be specified to a system and appliances. Parallel protection devices are used for distributed lines such as in power network, telephone network and furthermore at switching busbars. The parallel protection is the most applied protection principles in electrical power networks.

4.2 LV Surge Arresters

When the low voltage windings exposed to impulse, the tests showed that the low voltage windings have been damage under surges exceeding 30 kV [132-133]. The other occasion was that the high voltage windings have been damage under small impulse (as

low as 3 kV) but with long duration applied on low voltage windings. For the transformer connected to the overhead line with length more than 100 m, it is recommended to fit surge arrester with the transformer. However, in case of overhead line less than 100 m, there is no need for fitting the surge arrester. Under the condition that the line length is less than 100 m, the applied voltage on the low voltage windings is decreased in addition to the frequency is decreased by factor 10 where in this case the overhead line capacitance is less than the winding capacitance.

In [134], it is not recommended connecting the arrester on the transformer secondary side. The argument is that the arrester, in this case, does not protect the consumer when the lightning hits the low voltage network in addition to the consumer load duty cycle is increased. On the other hand, the arrester on the service entrance does not protect the transformer in addition to the current flows to the transformer from the arrester contributing to high duty on the transformer. From another point of view, an arrester on the transformer secondary side can protect the customer load from the overvoltage transferred through the distribution transformer due to lightning-induced overvoltage from the primary side of the transformer.

4.3 Modes of Protection

The overvoltage protections in the power networks can be classified into two modes. These modes are common mode and differential mode [131]. The difference between these modes is coming from a voltage surge occurrence. For the common mode, it is used to protect the voltage surge occurring between the live parts and the earth where its connection is phase to earth or it is neutral to earth. Therefore, this type of mode is very dangerous to the equipment that its frame has earthed. Regarding the differential mode, it is used to protect overvoltages between live parts. For example, it is connected between phases or phase and neutral. Therefore, this mode is expected to be dangerous for electronic devices.

Using surge arrester to protect equipment depends on the power distribution system configuration and the equipment connection [135]. For example, if the power distribution system is three-phase star, three-wire system, therefore the available modes of protection is only the differential mode.

4.4 Surge Protective Device Life Time

The surge arrester is as any device has a definite life time where it is impossible for its life to be infinity. The life time of metal oxide varistor depends on the magnitude and number of strokes. There are other factors that the life time can increase by increasing the number of varistors, the varistor size or these two factors together. The surge arrester can be damaged when it is subjected to surge strokes exceeding the maximum voltage or current rating. The ideal surge arrester has the same life time of the power distribution network where it is installed [135].

The required conditions for any used surge arrester are [136]:

1. To not absorb current (energy) at the power frequency voltage,
2. To operate correctly based on its setting designed based on the electric power system rating,
3. To work in the same environment of the protected equipment.

4.5 Surge Protective Device Coordination

The surge protective device (SPD) coordination has been used to provide proper installation of two or more surge protective devices allocated at different points in the network. The full understand of the right and suitable position of surge protective devices must be gained as well as the variables affecting on its function. The successful coordination can be achieved taking into consideration the following items [135]:

a) Surge waveform and duration,

b) The location of surge protective device with respect to the power distribution system,

c) Distance between the lightning stroke and the protected equipment,

d) The SPDs measured limiting voltage,

e) The SPDs surge current capacity,

f) The SPDs age,

g) The earthing design in the substation,

h) Suitable modes of protection for each SPD,

i) Power distribution system Configuration,

4.6 Low-Side Surge Phenomena

The low-side surges can be generated by lightning strokes on overhead lines and underground cable. These surges causes flow part of the stroke current to the neutral of the service cable. The stroke locations under these conditions are [134]:

1. Phase conductor on the primary side,
2. Neutral conductor on the primary side,
3. Load structure,
4. Ground,
5. Service cable.

These locations are identified for an overhead system as shown in Figure 4.1.

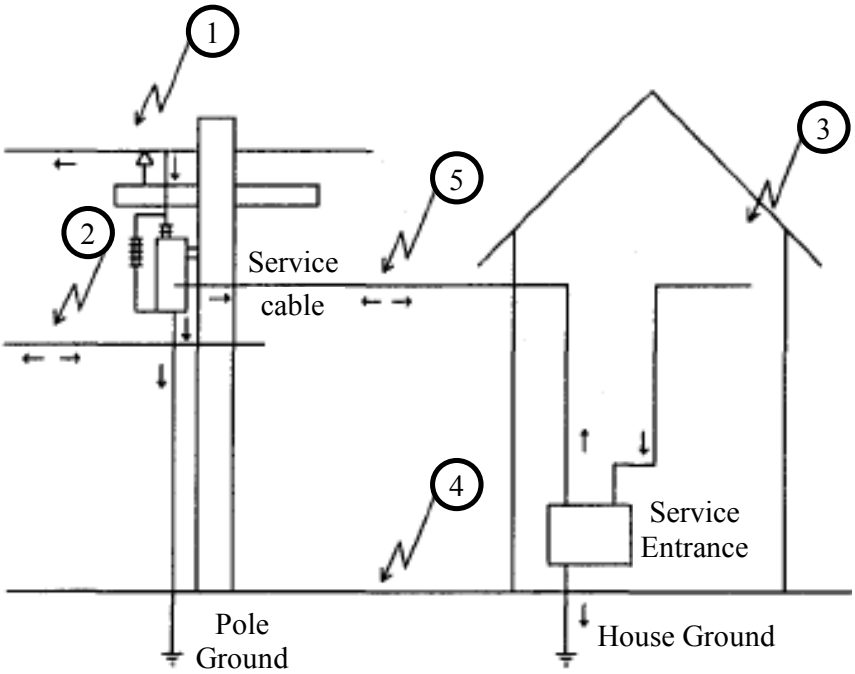

Figure 4.1 Possible strike locations and path for surge currents to enter the service drop [134].

4.7 Operation Principle of Surge Arrester

Inactive status of the surge arrester is achieved during normal operation conducting a very small current in μA. On the other hand, when the overvoltages come over the surge arrester, it operates and limits the voltage increasing by diverting the overvoltage charges on the line to the earth [137].

The surge arrester handles its operation under both normal and abnormal (overvoltage) conditions based on its nonlinearity (V-I characteristics). The metal oxide varistor, which is nonlinearly characterized, is the vital element in the surge arrester. Due to this nonlinearity, the voltage increasing across the surge arrester terminals is limited to a designed value which is the knee point in the nonlinear characteristics. The high current flowing through the arrester is at higher voltage comparing with the normal voltage operation. The surge arrester returns to its normal state after it is succeeded to quickly pass out the overvoltage. The surge arrester can be damaged when it is subjected to overvoltage of too high energy [138].

An economic surge protection device based on sand has been developed for protecting rural network using hygroscopic materials as addressed in [139]. When the overvoltage still has a higher value, the sand can keep a residual voltage.

4.8 Selection of Surge Arrester

The continuous withstand voltage (U_c) is one of the parameters should be defined in order to select the surge arrester device. This voltage is in r.m.s. value and is often called maximum continuous operating voltage (MCOV). The other voltage should be defined is the maximum permissible r.m.s. value of power frequency voltage. When the arrester is tested under this voltage for 10 s, it is designed to operate correctly under temporary conditions. These two voltages can be used together for the selection of arresters as reported in [140]. The third parameter is the voltage peak value which is at a flow of the nominal discharge current (I_n). In the nonlinear characteristics, the point of this voltage against the nominal current is the knee point.

In this chapter the low voltage surge arrester is modeled based on the data of low voltage surge arrester (LOVOS) recommended by ABB [138]. There are two products LOVOS 5 and LOVOS 10 which means that nominal discharge current in 8/20 μs is 5 and 10 kA (peak value), respectively. Therefore, the protection of low voltage network against lightning and switching overvoltages can be done using these products (LOVOS 5 and 10).

4.8.1 Selection of U_c

There are two factors have to be taken into consideration for selecting U_c. The first factor is the surge arrester location where it can be, as aforementioned, connected between phases, phase to earth or between the transformer neutral point to earth. The second factor is the maximum phase voltage (U_o). Lower protection level of the arrester is attained under lower U_c [140].

According to earthing systems, the maximum continuous operating voltage U_c of the surge protection devices will be equal to or higher than values computed with the aid of Table 4.1. This table is designed based on IEC 61643-1 amendment 1. Different earthing schemes (system configuration of distribution network) are summarized in appendix K [138].

In the current study, the low voltage surge arrester is inserted between the phase and earth, and in this case U_c can be calculated by:

$$U_c \geq 1.1 \times U_o \tag{4.1}$$

where U_o is the line-to-neutral voltage of the low-voltage system. Also, U_c value for this study can be taken equal to 280 V as a standardized voltage for 240/400V networks as illustrated in [138].

Table 4.1 Minimum required *Uc* of the SPD dependent on supply system configuration [131].

SPDs connected between	System configuration of distribution network				
	TT	TN-C	TN-S	IT with distributed neutral	IT without distributed neutral
Line conductor and neutral conductor	1.1 U_o	*NA*	1.1 U_o	1.1 U_o	*NA*
Each line conductor and PE conductor	1.1 U_o	*NA*	1.1 U_o	$\sqrt{3}$ U_o	Line-to-line voltage
Neutral conductor and PE conductor	U_o	*NA*	U_o	U_o	*NA*
Each line conductor and PEN conductor	*NA*	1.1 U_o	*NA*	*NA*	*NA*

NA: not available,
TT, TN-C, TN-S and IT are different earthing scheme illustrated in Appendix K.

4.8.2 Protection Level Selection

The protection level of surge arrester can be defined by U_p/U_c ratio where U_p is the voltage peak value on arrester terminals during flow of nominal discharge current (I_n). This ratio (U_p/U_c) is very important during the selection of arrester type. Decreasing the ratio contributes to increasing the protected equipment insulation protective margin.

In the current study, arrester type LOVOS-5 is selected with the following guaranteed data [138]:
Continuous operating voltage (U_c): 280 V,
Nominal discharge current (I_n) 8/20 μs: 5 kA,
Maximum discharge current (I_{max}) 8/20 μs: 25 kA,
Voltage protection level (U_p) at I_n: 1100 V,
Voltage protection level (U_p) at I_{max}: 1500 V,
Voltage protection level (U_p) at long lasting surge 2000 μs: 850 V,
Energy absorption capability: 1800 J.

This selected surge arrester is modeled and simulated in the ATPDraw environment where the above mentioned data in accordance with Pinceti et al. model are used in order to verify the model parameters as discussed in the following section.

4.9 Surge Arrester Models

Several models have been proposed to describe the arrester behavior as reported in [141-143]. The difficult point of these models is the identification of their parameters and their field tests to determine acceptable values. The well-known used models are discussed in following subsections.

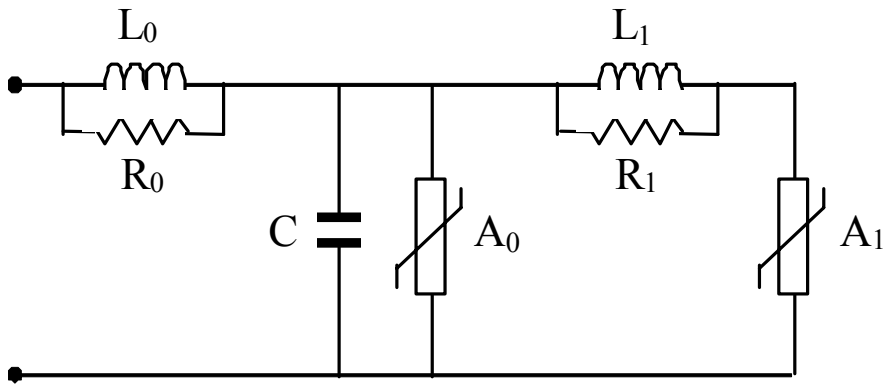

Figure 4.2 Frequency-dependent model [141].

4.9.1 Frequency-Dependent Model (IEEE Model)

IEEE working group (WG) 3.4.11 [141] recommended metal oxide surge arrester model shown in Figure 4.2. In this model, the arrester nonlinearity is represented using two nonlinear resistors (A_0 and A_1). They are separated by R-L filter that has very little impedance under slow front surges. However, the impedance of the filter increases under fast front surges and contributes to flow higher current in A_0 than A_1. Therefore, A_0 has a higher voltage than A_1, so increasing voltage excites the arrester. More section of nonlinear resistances can be added into the model in order to attain more accuracy. However, the model will be sophisticated with small improvement in its accuracy. Therefore, modeling using two sections has been found sufficient for an accurate dynamic modeling of the arrester.

The model parameters have been determined using iterative procedure until a satisfactory behavior of the implemented element is attained. The starting values in the iterative methodology have been determined using formulas that are function of electrical data (residual voltage) and physical parameters (the height, block dimension and number of columns).

4.9.2 Pinceti et al. Model

A simplified model has been presented deriving from the IEEE model [142]. This model is a simplified version of the IEEE model. The two resistances (R_0 and R_1) shown in Figure 4.2 have been eliminated and therefore the inductances (L_0 and L_1) are only considered in the new model as shown in Figure 4.3. A high resistance R of value 1 MΩ is added in order to avoid numerical instabilities during digital solving of the network. This numerical trouble can be occurred when the simulated surge arrester is tested using current source as mentioned in section 4.10. This simplified model has the same operating principles as the IEEE model. The model parameters were determined using only the electrical data and did not take into consideration any physical characteristics of the surge arrester. The inductances L_1 and L_0 in the model are defined in μH as:

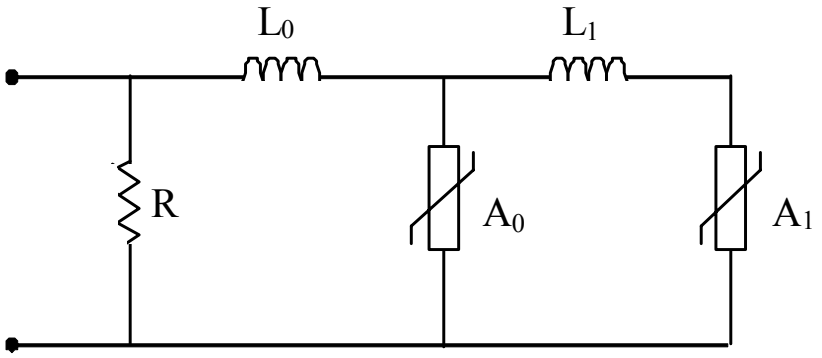

Figure 4.3 Pinceti et al. model [142].

$$L_1 = \frac{1}{4}.\frac{U_{r1/T2} - U_{r8/20}}{U_{r8/20}}.U_n \tag{4.2}$$

$$L_0 = \frac{1}{12}.\frac{U_{r1/T2} - U_{r8/20}}{U_{r8/20}}.U_n \tag{4.3}$$

where U_n is the arrester rated voltage in kV, $U_{rl/T2}$ is the residual voltage at 10 kA fast front current surge (l/*T*2 μs). $U_{r8/20}$ is the residual voltage at 10 kA current surge with 8/20 μs time parameters. The non-linear characteristics proposed by IEEE WG 3.4.11has been used to evaluate the nonlinear resistors (R_0 and R_1) with referring to $U_{r8/20}$.

The main obstacle in this model is that the $U_{rl/T2}$ is not available in most of the data sheets. Therefore, the parameter identification of this model is difficult. It is presented in [143] a procedure to overcome this problem where the model parameters are defined using the flowchart shown in Figure 4.4. Furthermore, this concept can help in case of missing data in datasheet where the parameter identification was modified with the aid of the following two forms:

$$L_1 = 0.03\ U_n \tag{4.4}$$

$$L_0 = 0.01 U_n \tag{4.5}$$

The flowchart in Figure 4.4 shows the procedure for evaluating the dynamic parameters under all conditions (with and without considering $U_{r1/T2}$). First, the voltage $U_{rl/T2}$ is checked. If it is available, the parameters are calculated using (4.2) and (4.3) under the condition that $K < 1.18$ where the parameter K is computed using $K=U_{r1/T2}/U_{r8/20}$. Otherwise, the parameters are calculated using (4.4) and (4.5). On the other hand, if $U_{r1/T2}$ value is not available, the parameters are calculated using (4.4) and (4.5). This is helped to find initial parameters helping to find more accurate values as it is discussed in the following section.

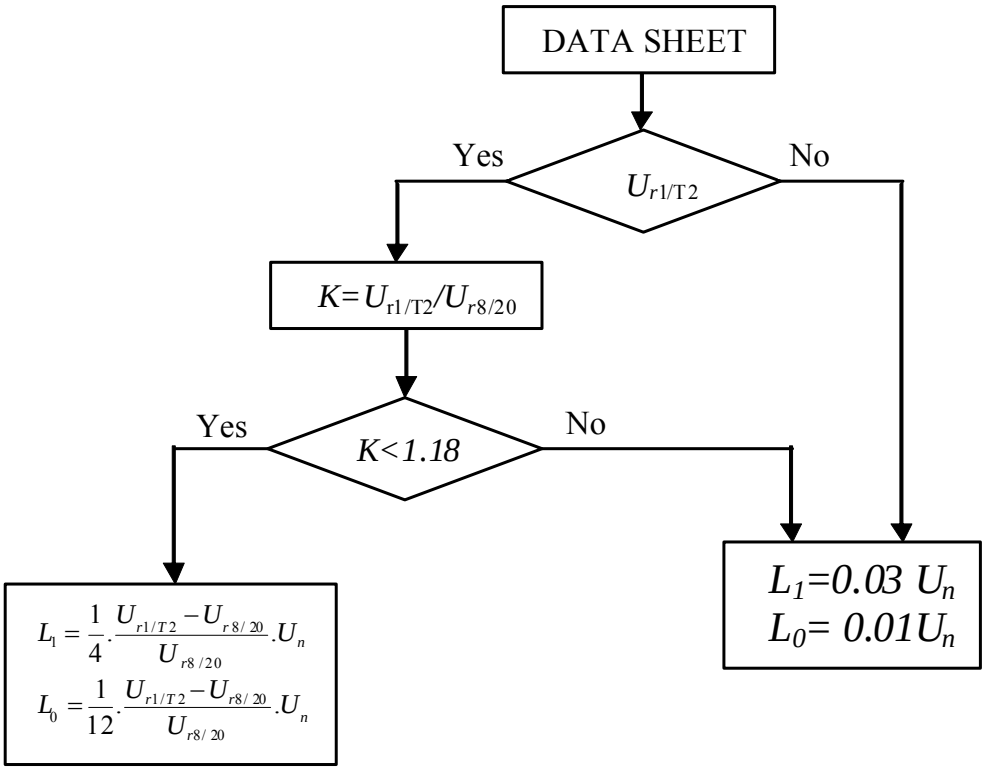

Figure 4.4 Flowchart to calculate elements L_0 and L_1 [143].

4.10 Surge Arrester Model Validation

In this work, Pinceti et al. model is used because of its simplicity. However, its inductance parameters are calculated using relations (4.4) and (4.5) [143], where $U_{r1/T2}$ is not available in the data sheet. So, L_1 and L_0 are found equal to 0.0084 and 0.0028 μH, respectively. The nonlinear characteristics of the two elements A_0 and A_1 are based on the pu data published in [142] and summarized in Appendix L. The corresponding nonlinear characteristics of A_0 and A_1 are shown in Figure 4.5.

The surge arrester model is simulated and tested using ATPDraw circuit shown in Figure 4.6. A discharge current 8/20 μs, 5 kA and 25 kA for nominal and maximum conditions respectively are injected to the surge arrester that its parameters are defined above. Adding 1 MΩ resistance is used parallel with the current source in order to avoid the numerical instability of the combination of the current source and non-linear elements. Regularly, it is recommended to add high resistance parallel with the current source in the field of EMTP or ATP/EMTP programs. The error of residual voltage rather than the manufactured data is found -4.22% at the nominal discharge current and -18.63% at the maximum discharge current. This error is computed as $(U_{ps}-U_p)/U_p$, where U_{ps} is simulated residual voltage (the simulated voltage protection level). So, the parameters computed by (4.4) and (4.5) are taken as initial values. Then, these parameters are tuned and the corrected values are

therefore determined for L_1 and L_0 where they are found L_1= 0.0048 and L_0= 0.06 μH [144-145]. Consequently, the errors for nominal and maximum discharge currents reach to -1.5% and +0.55%, respectively. The injected current, the residual voltage and the absorbed energy are as shown in Figures 4.7 and 4.8 for nominal and maximum discharge currents, respectively, considering the corrected parameters. Comparing the simulated results of the surge arrester evaluation with its data sheet, provides evidence of the efficacy of this model.

Finally, the surge arrester model is connected at the transformer secondary side in order to mitigate the transmitted lightning-induced overvoltages coming from MV network due to lightning-induced overvoltages with concerning MV spark-gap operation. This mitigation is investigated in the next chapter through the voltage waveforms and the peak voltage profile along the low voltage feeder.

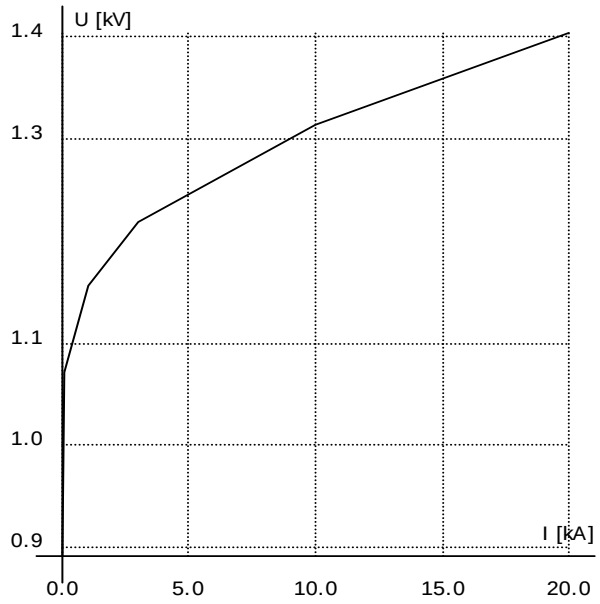

a. A_0 non-linear characteristics.

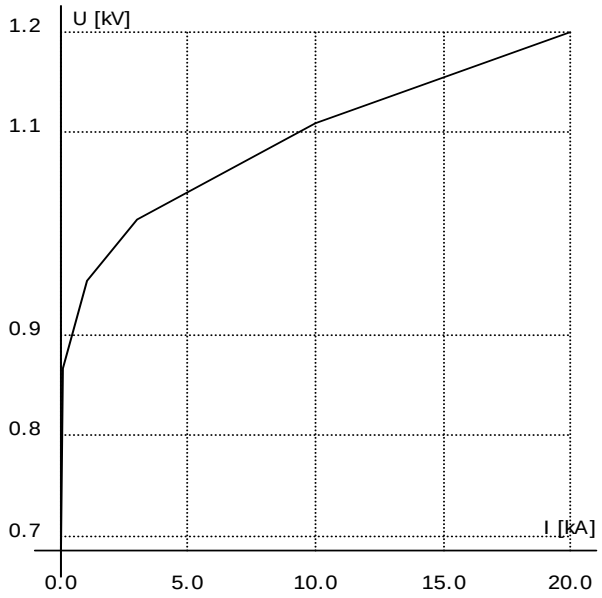

b. A_1 non-linear characteristic.

Figure 4.5 surge arrester elements nonlinear characteristics.

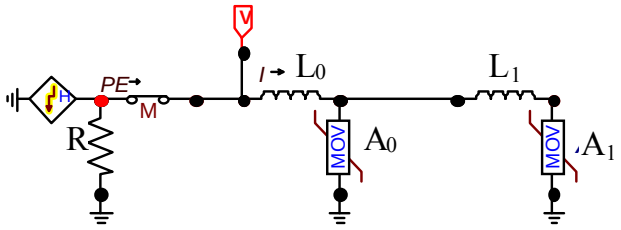

Figure 4.6 ATPDraw circuit for surge arrester.

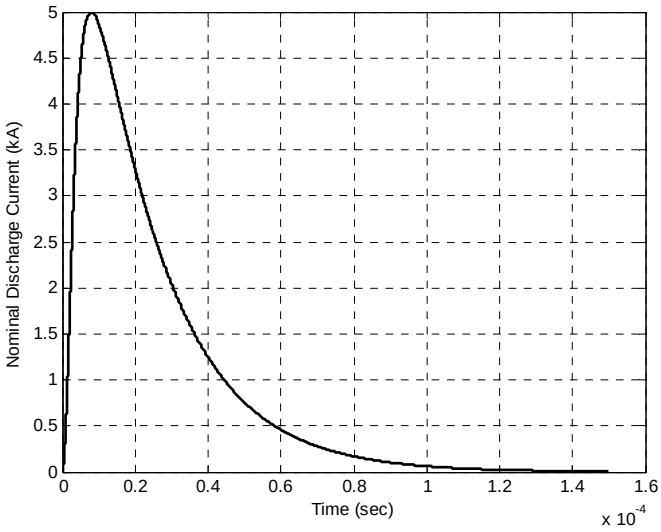

a. Injected current (nominal discharge current).

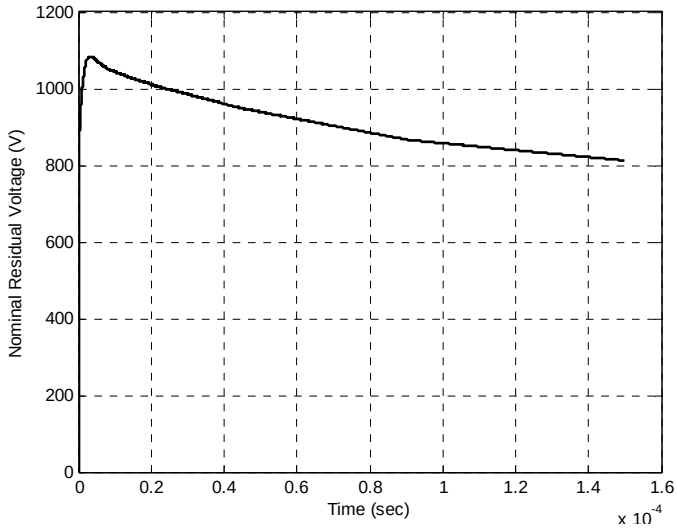

b. Residual voltage.

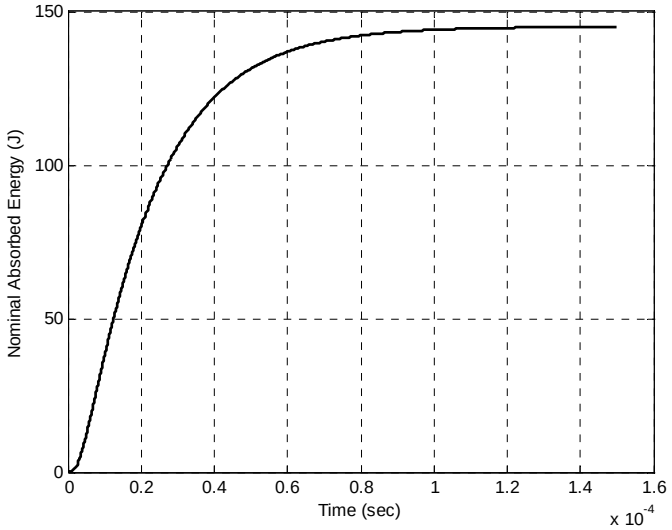

c. Absorbed energy.

Figure 4.7 injected nominal discharge current.

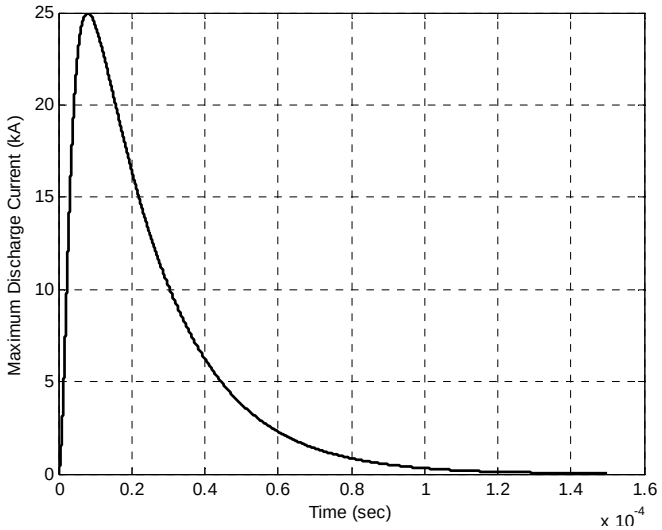

a. Injected current (maximum discharge current).

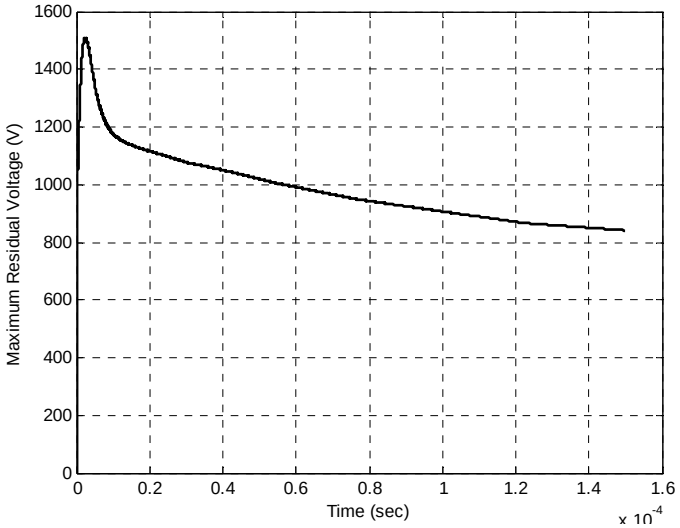

b. Discharge voltage.

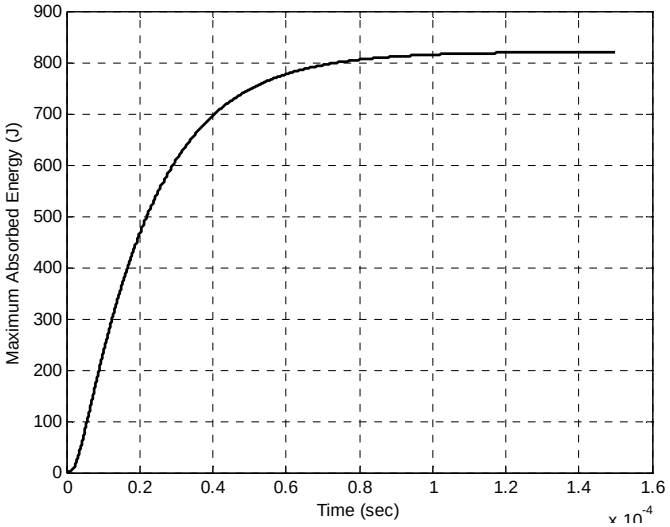

c. absorbed energy.

Figure 4.8 injected maximum discharge current.

5- Investigation of Lightning-Induced Overvoltages Transmitted to Customer Side under Spark-Gap Operation

The transference of surges from medium voltage to low voltage networks is the most frequent among all possible mechanisms of overvoltage generation on consumer loads which also threaten insulation of power distribution lines. So, many studies have been done to investigate the induced overvoltages on the distribution line caused by lightning stroke [144-154]. Other studies have been done through the observations of lightning induced voltage on distribution lines [155-157].

In order to generally interpret the probable transferred overvoltage from the medium voltage to low voltage networks, the coupling possibilities have to be considered [151]. These couplings are such as: (i) the high frequency coupling between the primary and secondary windings of the transformer, (ii) the electromagnetic coupling between them if they are installed in the same tower (the tower carries two circuits; one is the medium voltage and the second one is the low voltage), (iii) overvoltages in the low voltage networks generated by the coupling resulting from injected current due to flashovers across one of the medium voltage insulators.

In this chapter, the lightning induced-overvoltages transmitted to the low voltage network through the distribution transformer are investigated. Then the low voltage surge arrester installed at the distribution transformer secondary side is suggested to mitigate the induced overvoltage coming from distribution transformer primary side. Then influence of medium voltage spark-gap operation on the performance of low voltage network is studied through the voltage waveforms and the peak voltage profile along the feeder. Finally, the role of the low voltage surge arrester with spark-gap operation is investigated.

5.1 Simulated System

To investigate the effect of lightning strokes on the low voltage networks, an accurate model of the transformer is necessary as well as a model of low voltage network is required to obtain real response in this situation. So, an accurate and simplified model for the distribution transformer under lightning strokes proposed in chapter 3 (subsection 3.2.2) is used in this chapter. Where, the high frequency model representation of both the distribution transformer and low voltage network are combined in a single arrangement in the environment of ATP/EMTP.

The impact of feeder numbers, their lengths, their types (Overhead/underground cables) and loads on the lightning reached at the service entrance point is investigated with and without spark-gap operation [145]. The overall ATPDraw circuit is shown in Figure 5.1 where, the ATPDraw network of the distribution transformer shown in Figure 3.30 and the network of the overhead cable feeder are combined in a single ATPDraw file as well as the LV surge arrester model and spark-gap operation are added to this arrangement. The overall low voltage network circuit consists of 7 identical overhead cable feeders, 49 load and 350

m feeder length. Each feeder is divided to seven subsections with seven different loads where each subsection length equals to 50 m. At the end of each subsection, there is a resistive load which is randomly selected in a range of 1 to 2 kW. For example, the load distribution from point A1 to point G1 is 1, 2, 1.5, 1, 1, 2 and 1.5 kW, respectively. The simulation is carried out using induced overvoltage of 94.5 kV, 0.9/9.4 μs as lightning source applied on the primary side of the distribution transformer.

In Finland, the most common low voltage lines are aerial bundled cables where the most common cable types are AMKA 35, AMKA 70, and their multiplies [158]. In this section, AMKA 3×35+70 cable type is used where its identification is reported in [159]. More details supporting the ATPDraw simulation are illustrated in the Appendix M. The simulation of this cable was carried out using LCC JMarti model.

The evaluation of lightning-induced overvoltages transmitted to customer side is carried out by investigating the voltage profile concerning different scenarios. These scenarios are:

1. Different feeder number (one, two and seven feeders),
2. Different feeder lengths,
3. Different load values,
4. Replacing some sections of overhead cables by underground cables.

These scenarios are accomplished with and without considering the spark-gap operation of MV network. Furthermore, the mitigation of these overvoltages is presented using the surge arrester model discussed in the previous chapter. In order to accomplish these test cases, the ATPDraw network shown in Figure 5.1 is used where it is modified according to each scenario condition.

5.2 Impact of Feeder Number

The effect of the parallel feeder on the consumer side when the lightning-induced overvoltages occur at the primary terminals of the distribution transformer is investigated. This study is carried out concerning a network of one, two and seven feeders in Figure 5.1.

5.2.1 LV Network Performance without MV Spark-Gap Operation

When the LV network is not protected, the corresponding voltage waveforms at points SEND, A1 and G1 are shown in Figures 5.2 and 5.3 for one-feeder and two-feeder networks, respectively. Where all simulation measurements are carried out all over one feeder as the feeders are identical. For one-feeder network, the highest peak is at SEND where its value is 12.2 kV and reduced at A1 to 7.9 kV. Then, the signal peak is more reduced until the feeder end which is 0.395 kV at G1.

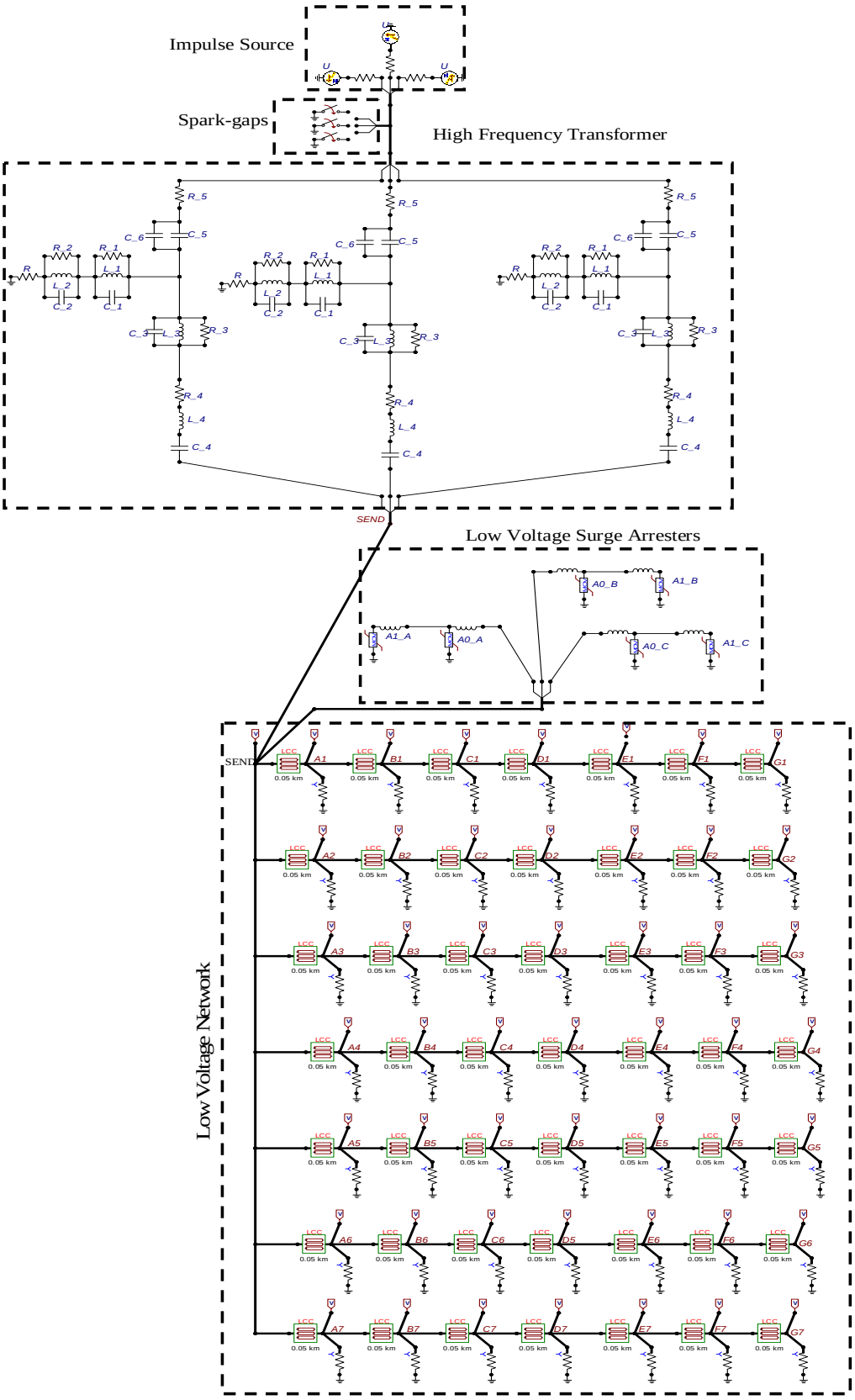

Figure 5.1 ATPDraw overall circuit.

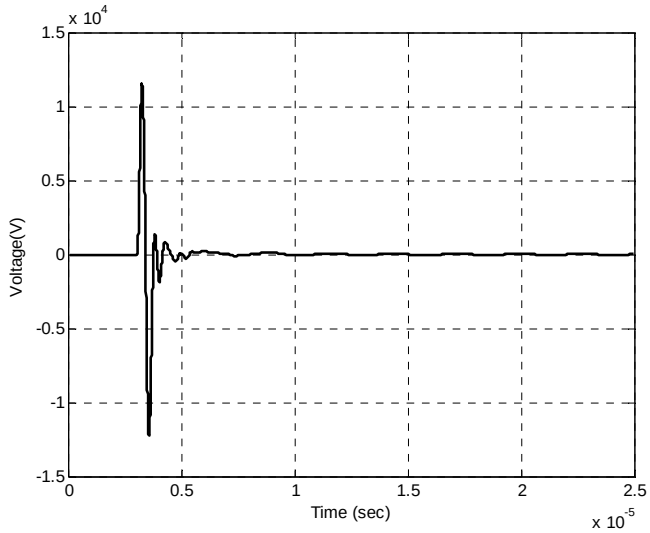

a. Voltage at SEND.

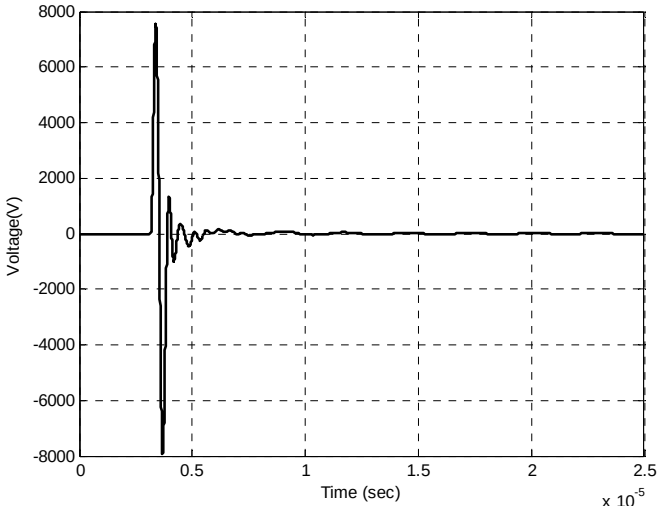

b. Voltage at point A1

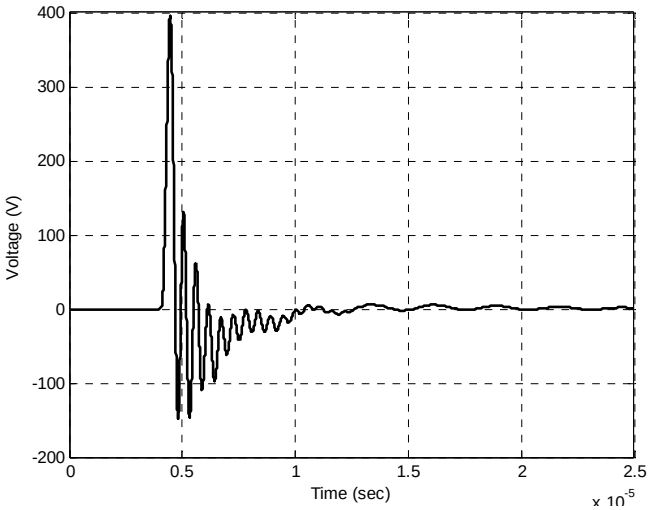

c. Voltage at point G1.

Figure 5.2 Secondary voltage transferred at different points considering one-feeder network, no LV SA, no MV spark-gap operation.

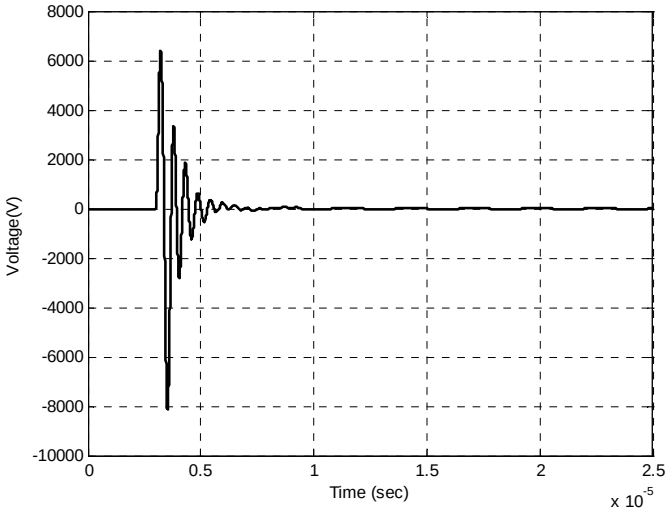

a. Voltage at SEND.

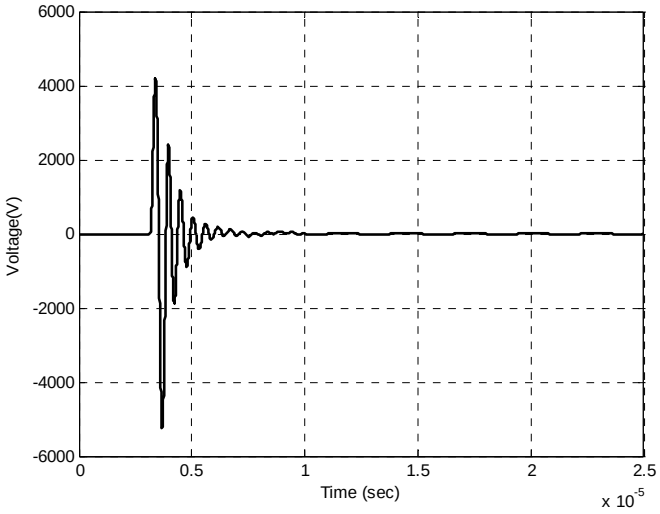

b. Voltage at point A1.

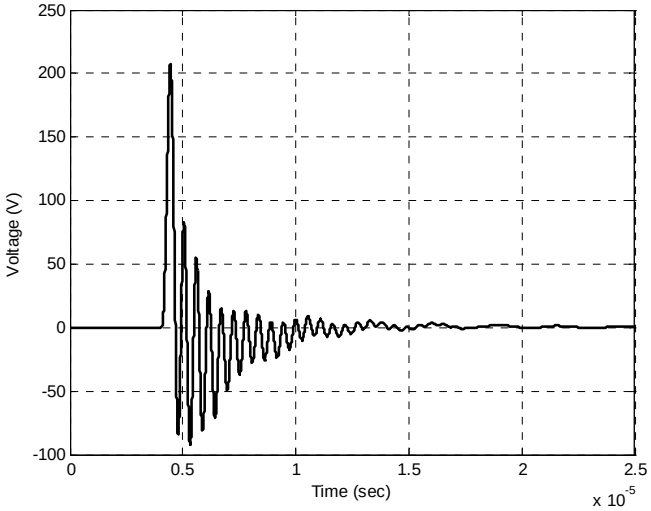

c. Voltage at point G1.

Figure 5.3 secondary voltage transferred at different points considering two-feeder network, no LV SA, no MV spark-gap operation.

The peak voltage profile is shown in Figure 5.4 for one-feeder, two-feeder and seven-feeder depicted by solid, dashed and dashdot curves, respectively. By comparing with the voltage profile of a network with a single feeder, the voltage peaks are reduced with increasing the feeder numbers. In order to interpret the obtained behavior, the parallel feeder characteristic impedances are the transmitted impedance. If this impedance is reduced, the transmitted signal is reduced where increasing parallel feeders reduces the equivalent impedance [160].

When the LV network is protected with low voltage surge arresters connected at the point SEND, the corresponding voltage waveforms at points SEND, A1 and G1 are shown in Figure 5.5 where the voltage is limited due to the dynamic effect of the surge arrester. The surge arrester influence is studied through the peak voltage profile along the feeder with and without surge arrester as shown in Figure 5.6. The overvoltages is mitigated and reduced from 12.2 kV to 850 V. When the number of feeders becomes two the voltage waveforms at the same mentioned points are shown in Figure 5.7. A comparison of the peak voltage profile with and without SA protection is shown in Figure 5.8. The Figure shows how much the limited voltage is due to the SA protection. Increasing the number of feeders to reached overall network feeder number (7 feeders), the corresponding peak voltage profile is shown in Figure 5.9. As shown in Figures 5.6, 5.8 and 5.9, surge arrester device limits the overvoltage in the line beginning to constant 850 V in all the cases.

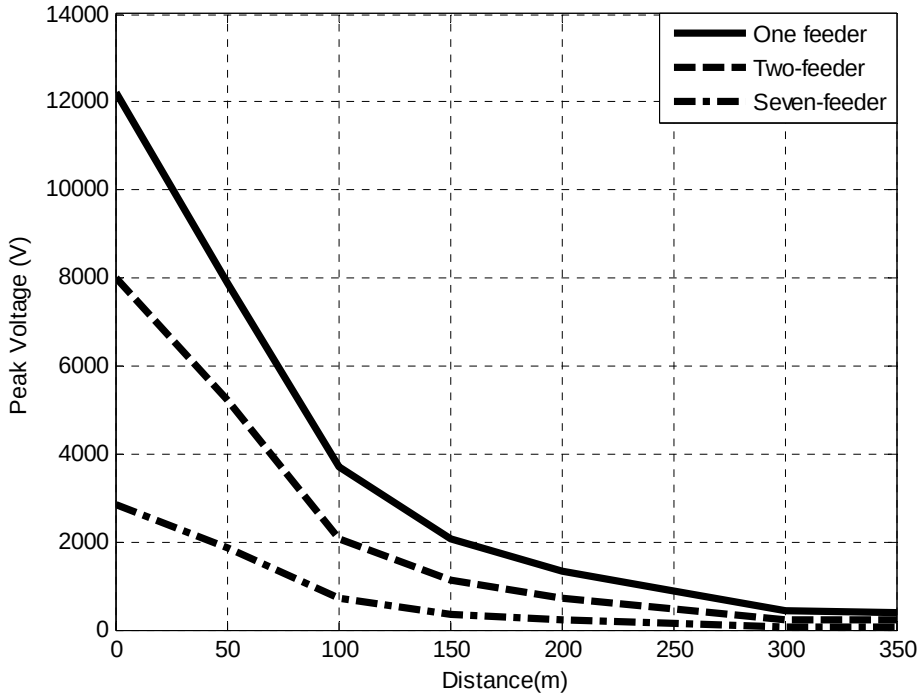

Figure 5.4 Number of Feeders Impact, no LV SA, no MV spark-gap operation.

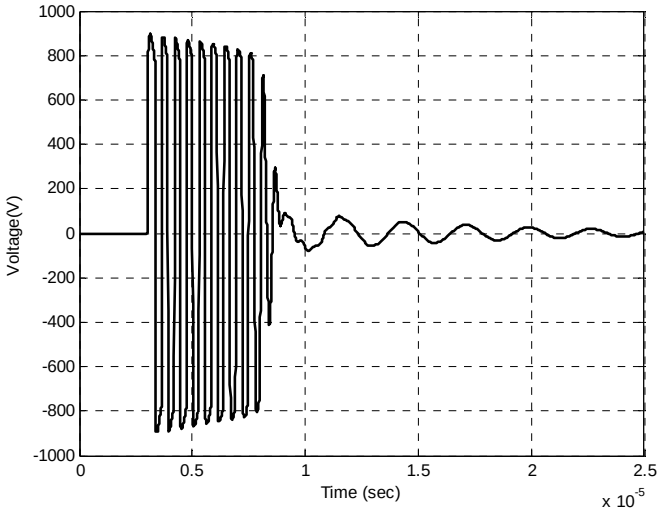

a. Voltage at SEND

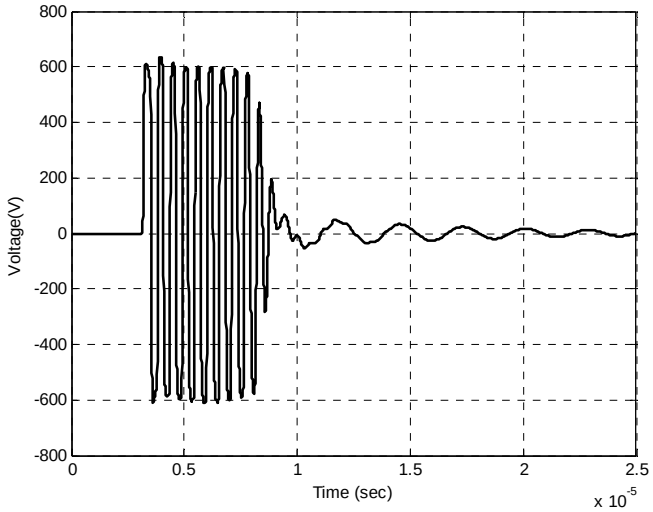

b. Voltage at Point A1

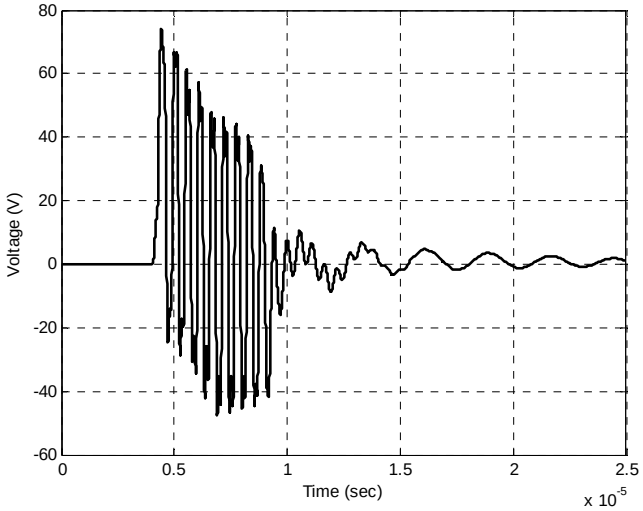

c. Voltage at Point G1

Figure 5.5 Surge arrester-based mitigation of secondary voltage of one-feeder network, no MV spark-gap operation.

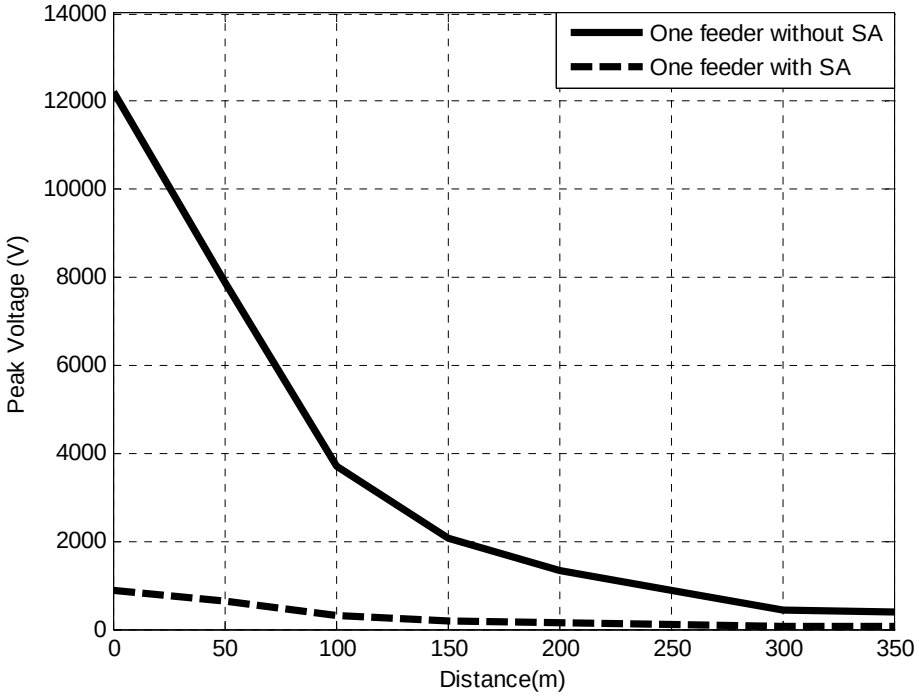

Figure 5.6 Impact of LV surge arrester on one feeder network, no MV spark-gap operation.

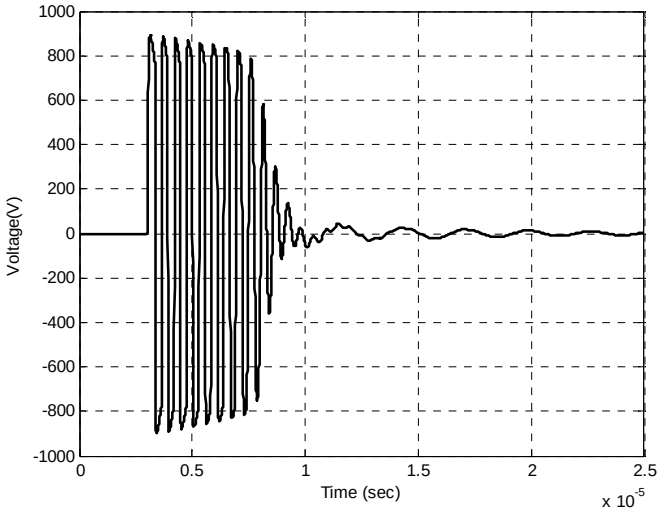

a. Voltage at SEND

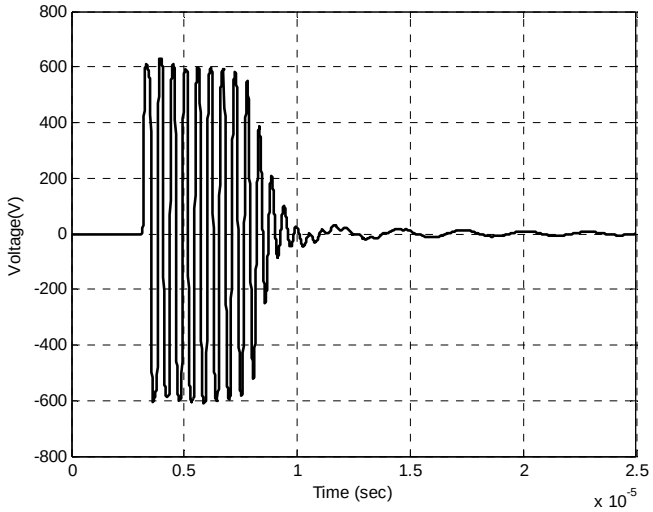

b. Voltage at Point A1

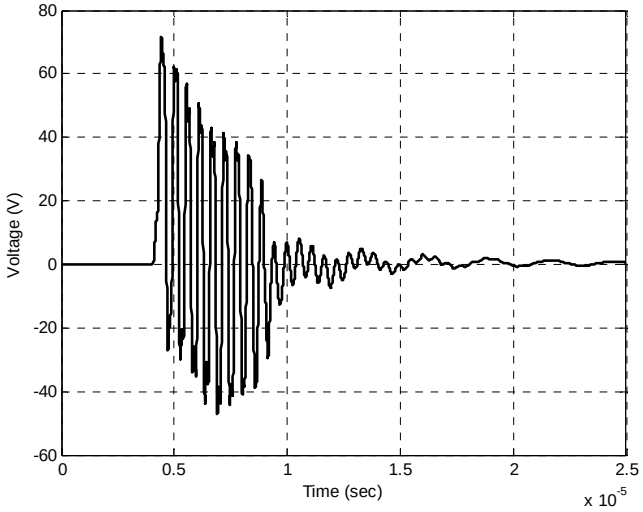

c. Voltage at Point G1

Figure 5.7 Surge arrester-based mitigation of secondary voltage of two-feeder network, no MV spark-gap operation.

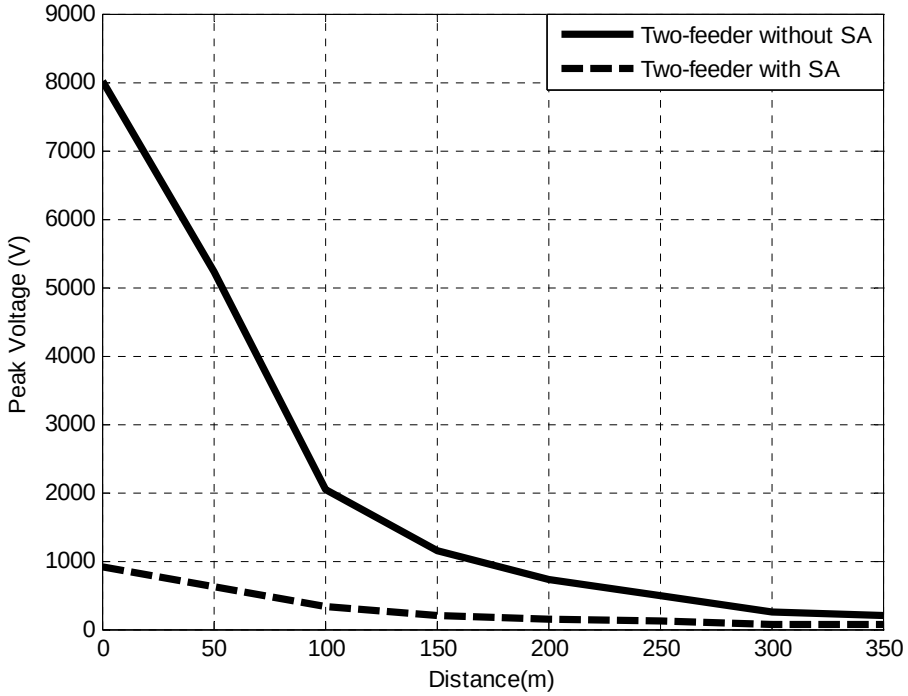

Figure 5.8 Impact of LV surge arrester on two-feeder network, no MV spark-gap operation.

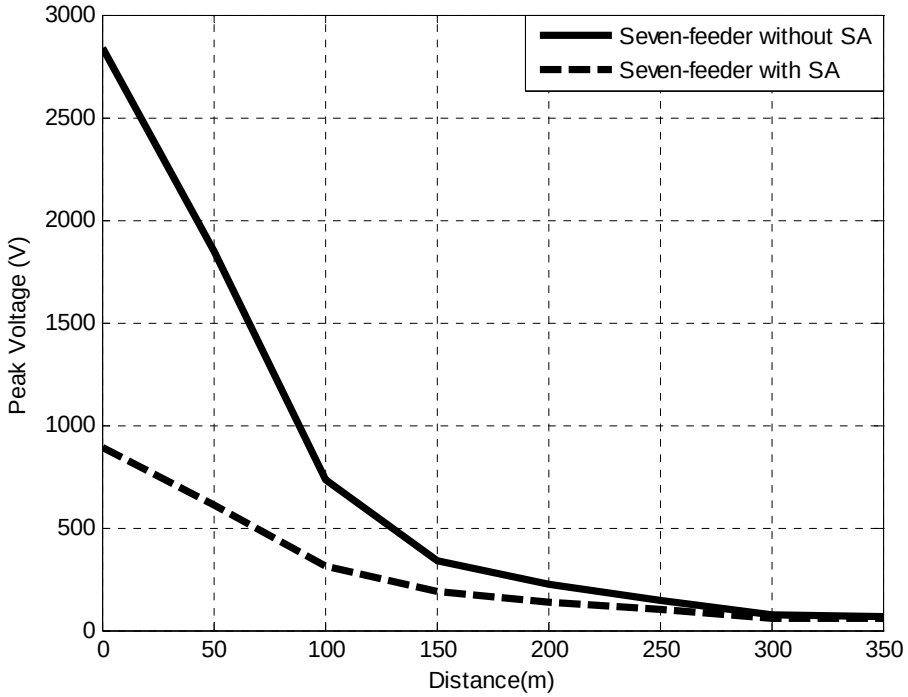

Figure 5.9 Impact of LV surge arrester on seven-feeder network, no MV spark-gap operation.

5.2.2 LV Network Performance with MV Spark-Gap Operation

When MV spark-gap operates and LV network is not protected, the corresponding waveforms of voltage at points SEND, A1 and G1 are shown in Figure 5.10 for one-feeder network. For the comparison point of view, the MV spark-gap operation impact is studied through the peak voltage profile along the feeder with and without MV spark-gap operation as shown in Figure 5.11. When the number of feeders becomes two the corresponding voltage wave forms at the same mentioned points are as shown in Figure 5.12 with peak voltage profile shown in Figure 5.13. Increasing the number of feeders to reached overall network, the corresponding peak voltage profile is shown in Figures 5.14. As shown from Figures 5.11, 5.13 and 5.14, MV spark-gap operation increases the overvoltages transmitted to the LV network through the distribution transformer. This is due to steep voltage collapse in MV spark-gap and hence stronger coupling through the distribution transformer capacitances.

When the LV network is protected with surge arrester, the corresponding voltage waveforms at points SEND, A1 and G1 are shown in Figure 5.15 for one feeder network. The corresponding peak voltage profiles along the feeder with and without surge arrester are shown in Figure 5.16. The voltage waveforms, when the number of feeders becomes two, are shown in Figure 5.17 and peak voltage profile shown in Figure 5.18. Increasing the number of feeders to reached overall network, the peak voltage profile is shown in Figures 5.19. As shown from Figures 5.16, 5.18 and 5.19, the overvoltages transmitted through the distribution transformer due to spark-gap operation are limited by the LV surge arrester to be less than 1000 V.

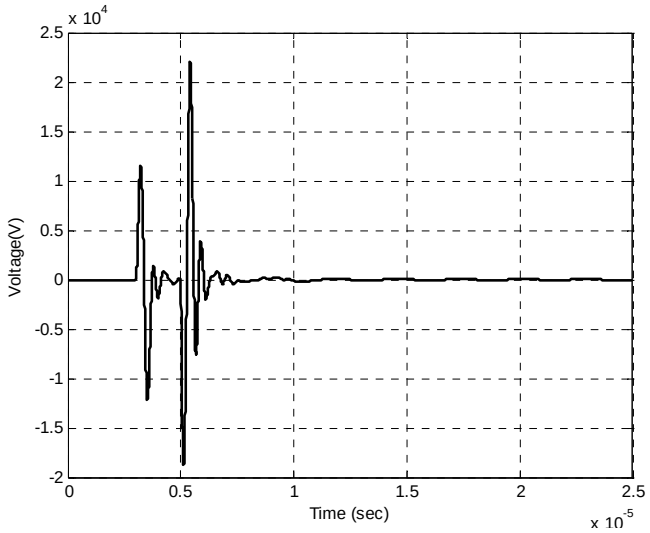

a. Voltage at SEND

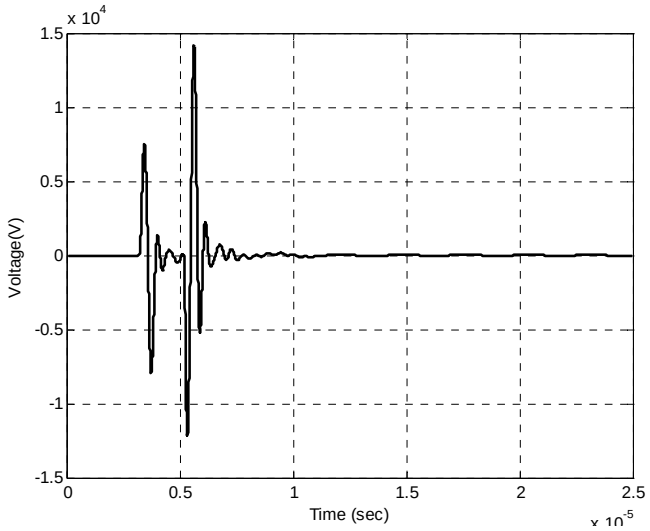

b. Voltage at Point A1

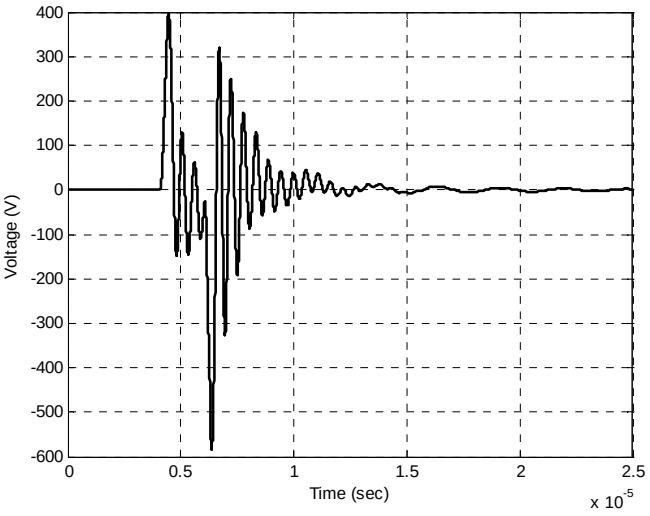

c. Voltage at Point G1

Figure 5.10 Secondary voltage transferred of one-feeder network under MV spark-gap operation, no LV SA.

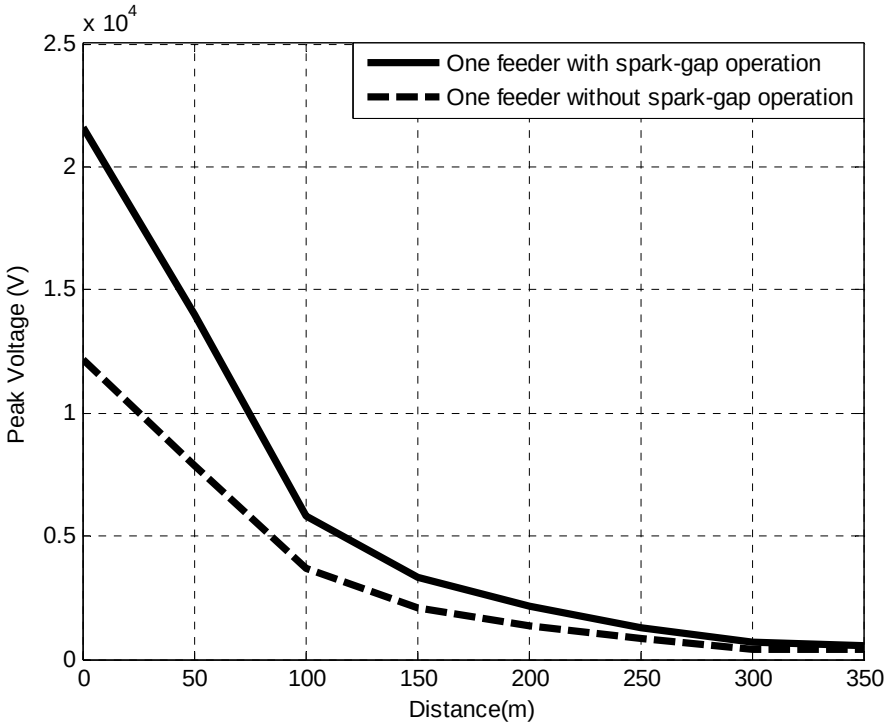

Figure 5.11 Impact of spark-gap operation on one feeder network, no LV SA.

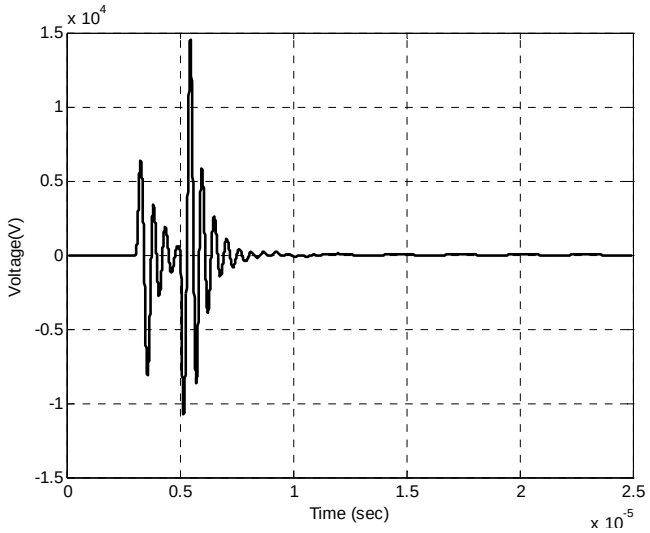

a. Voltage at SEND

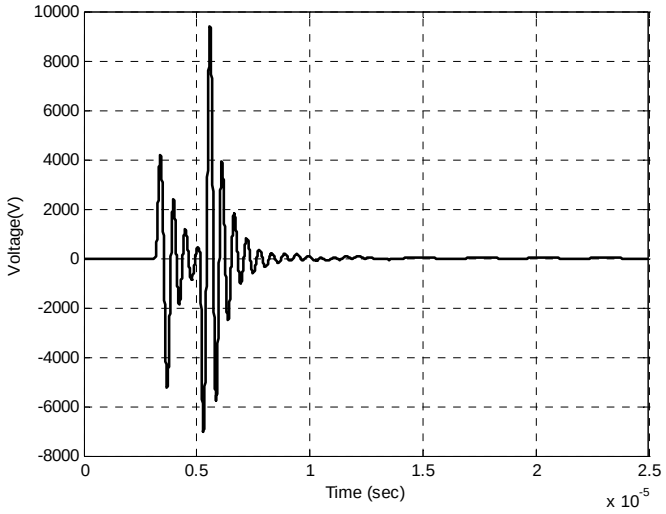

b. Voltage at Point A1

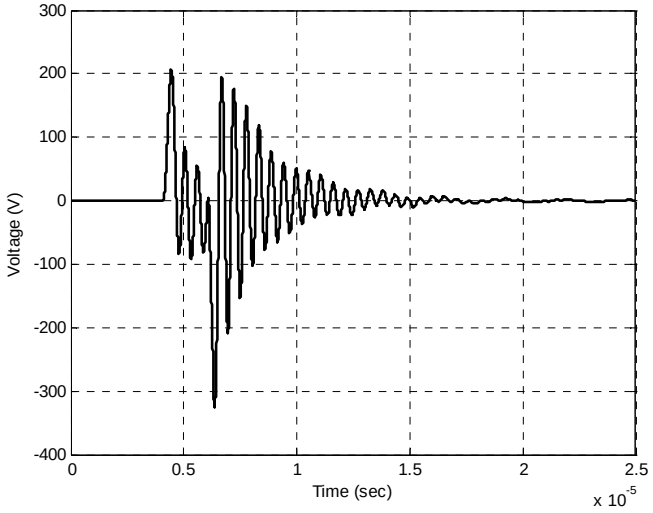

c. Voltage at Point G1

Figure 5.12 Secondary voltage of two-feeder network under MV spark-gap operation, no LV SA.

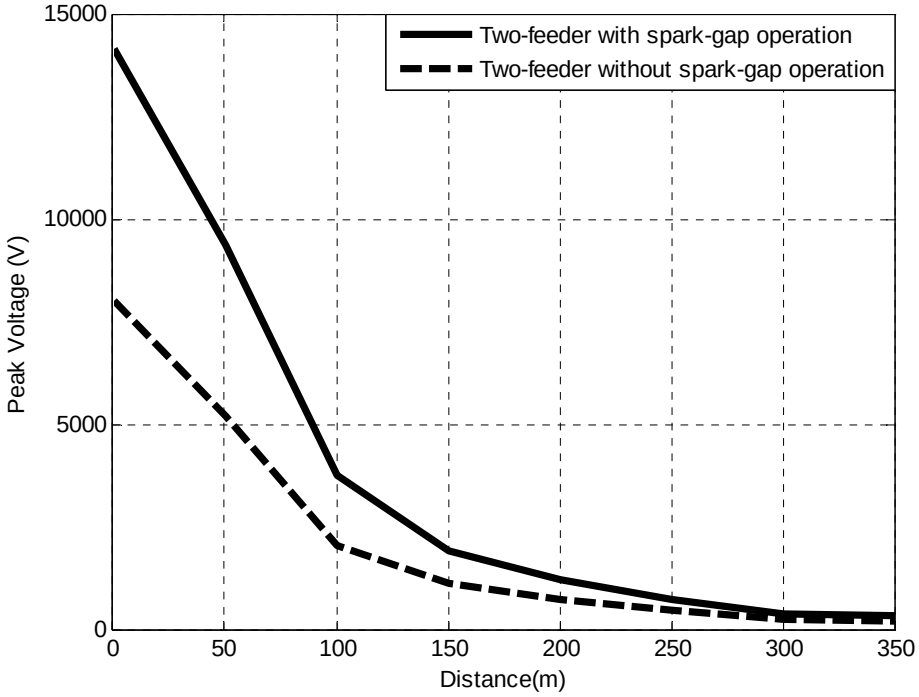

Figure 5.13 Impact of spark-gap operation on two-feeder network, no LV SA.

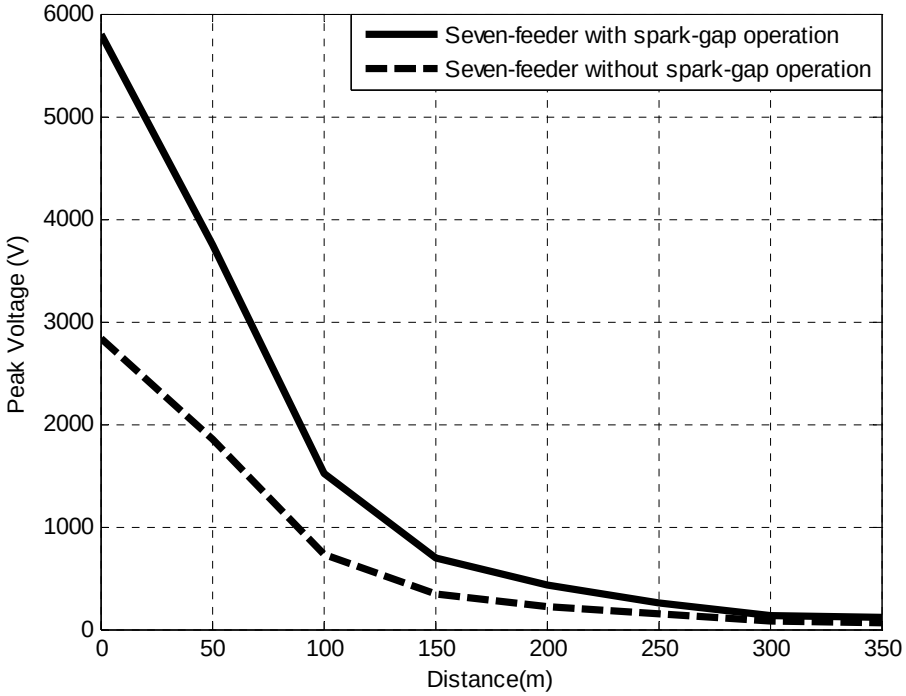

Figure 5.14 Impact of spark-gap operation on seven-feeder network, no LV SA.

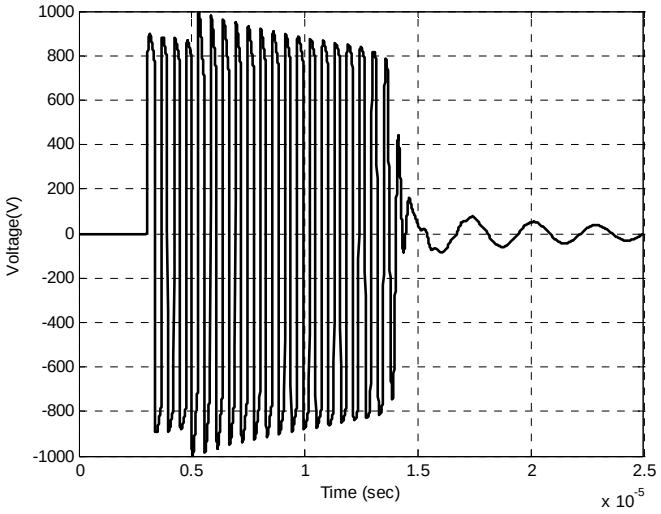

a. Voltage at SEND

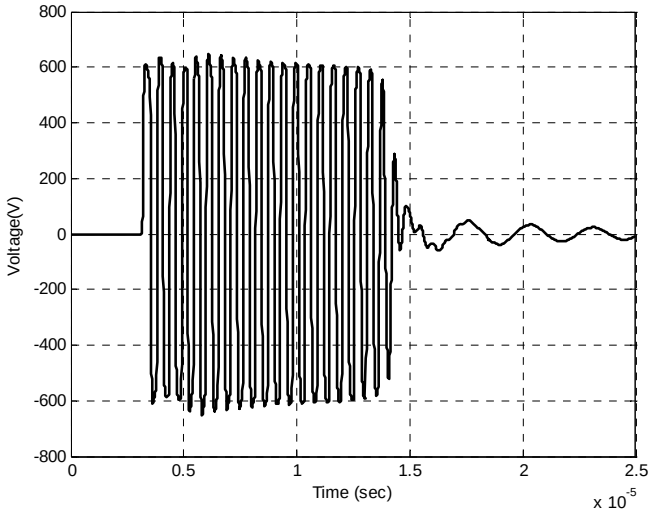

b. Voltage at Point A1

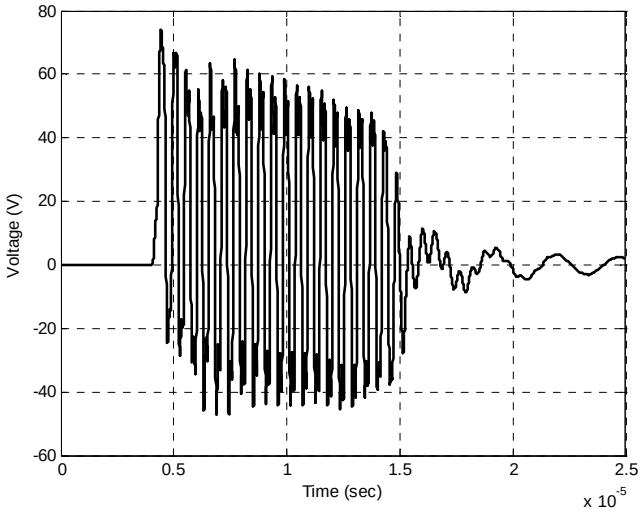

c. Voltage at Point G1

Figure 5.15 Surge arrester-based mitigation for one-feeder network under MV spark-gap operation.

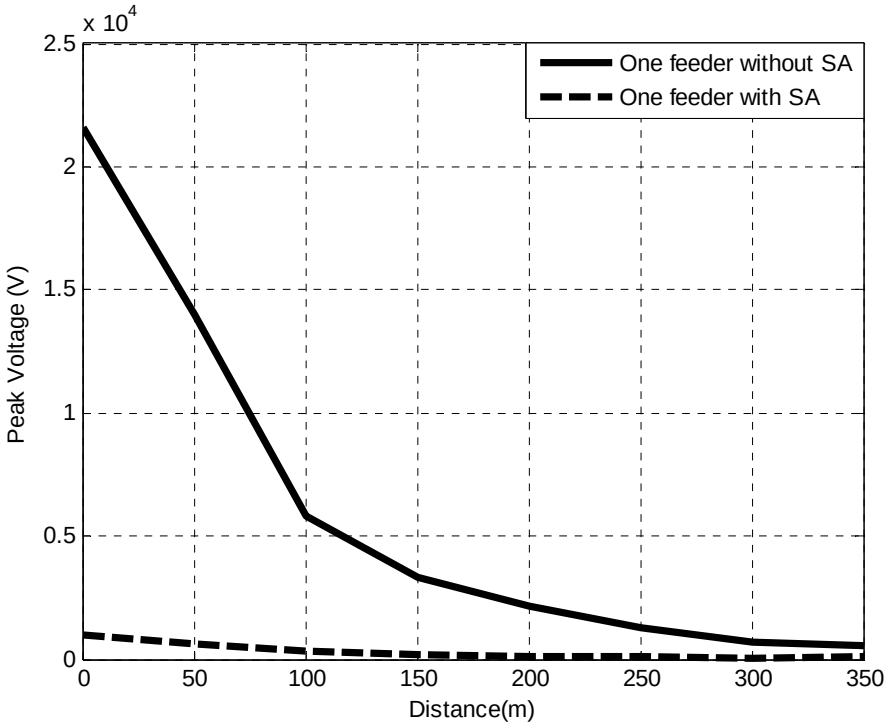

Figure 5.16 LV surge arrester impact on one feeder network under MV spark-gap operation.

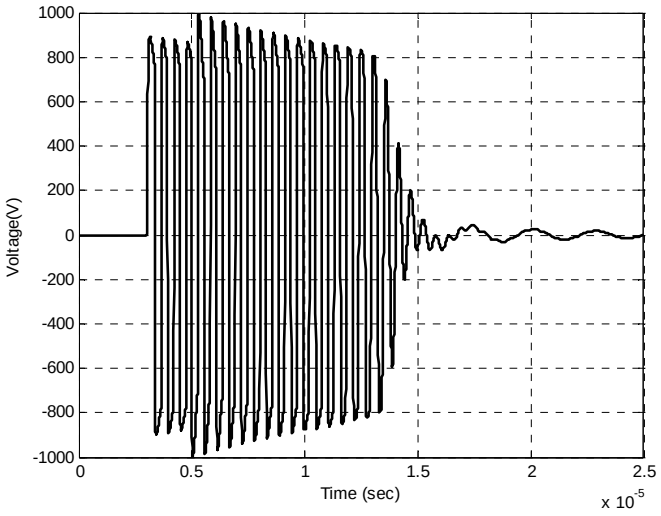

a. Voltage at SEND

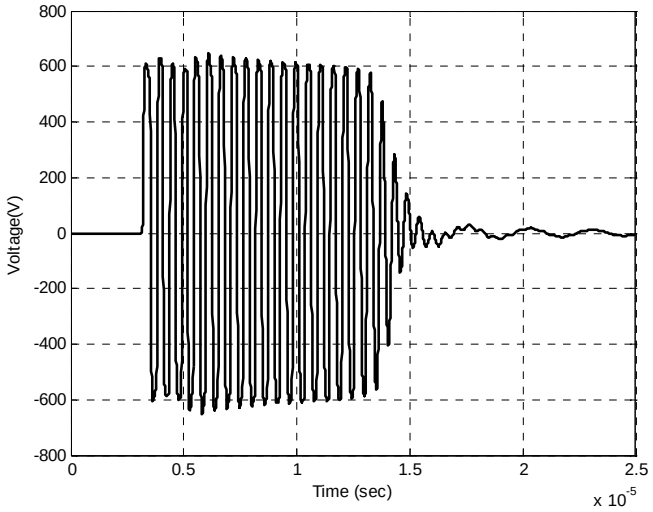

b. Voltage at Point A1

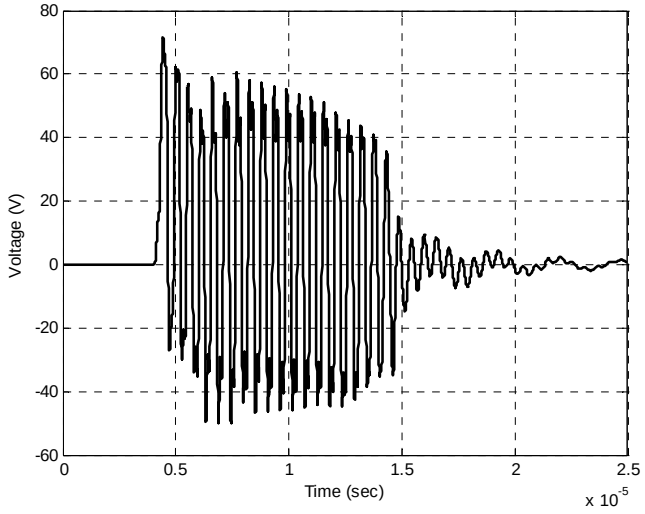

c. Voltage at Point G1

Figure 5.17 Surge arrester-based mitigation for two-feeder network under MV spark-gap operation.

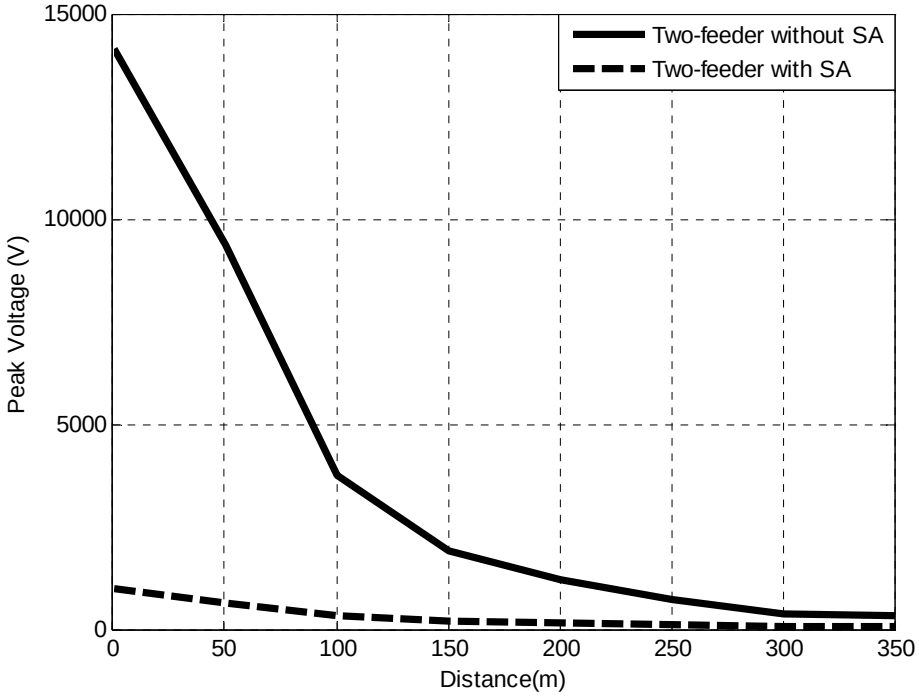

Figure 5.18 LV surge arrester impact on two-feeder network under MV spark-gap operation.

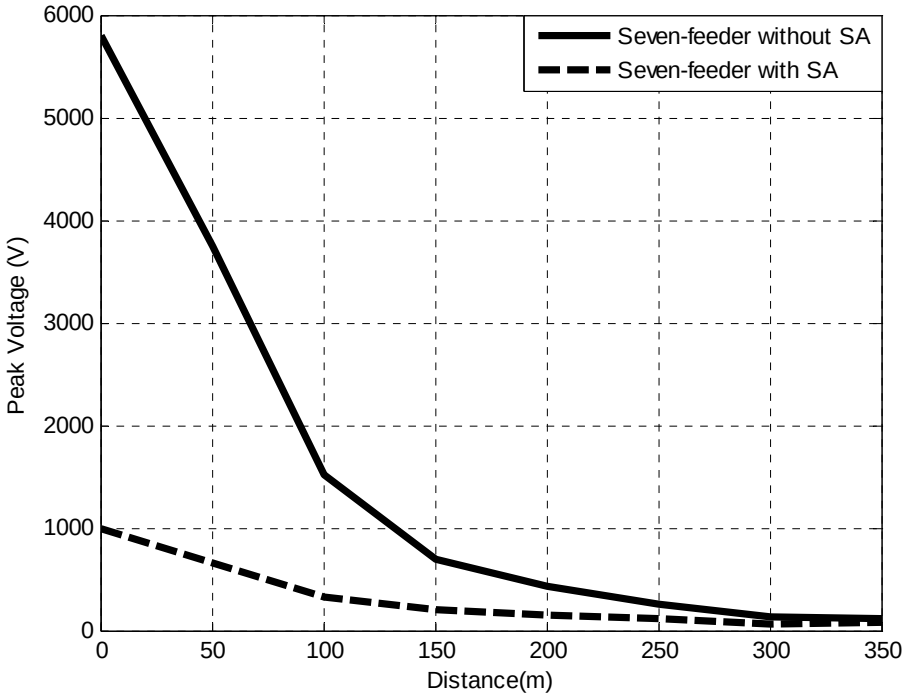

Figure 5.19 LV surge arrester impact on seven-feeder network under MV spark-gap operation.

5.3 Impact of Feeder Length

This study is carried out on only one feeder with different lengths, the feeder lengths under study are 350 m, 175 m (by reducing the subsection length to its half value) and 700 m (by increasing each subsection length to its double value). The same load is considered.

5.3.1 The Performance without MV Spark-Gap Operation

When LV network is without operation of MV spark-gap, Figure 5.20 shows the corresponding voltage profile for different feeder lengths of 700 m, 350 m and 175 m feeder length by solid, dashed and dashdot curves, respectively. For each feeder length, the peak voltage is reduced as propagated over the feeder. The induced voltage measured at the feeder beginning is not influences by the feeder length as the input characteristics impedance is the dominant at this point. As the feeder total length is increased, as the propagated voltage peak curve is moved up which means that the peak voltage is increased when the feeder length behind the measuring point is increased.

When LV network is protected without operation of MV spark-gap Figure 5.21 shows peak voltage profile for different feeder lengths of 700 m, 350 m and 175 m feeder length by solid, dashed and dashdot curves respectively. The LV surge arrester limits the transferred overvoltages to less than 900 V.

5.3.2 The Performance with MV Spark-Gap Operation

Influence of MV spark-gap operation on the low voltage network is depicted in Figure 5.22. By comparing the peak voltage profile with and without MV spark-gap operation, the spark-gap effect increases the overvoltages transmitted to low voltage network through the distribution transformer. Such increasing is very obvious in Figure 5.22 when the feeder lengths are 175, 350 and 700 m.

The effect of LV surge arrester on limiting the overvoltages transmitted to LV network due to MV spark-gap operation is depicted in Figure 5.23.

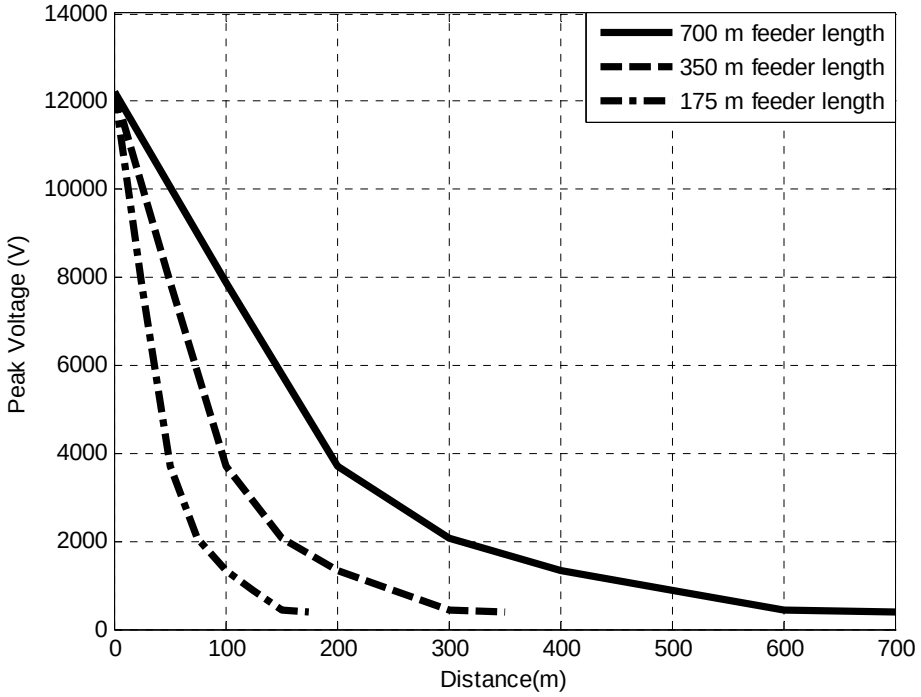

Figure 5.20 Feeder length impact, no LV SA, no MV spark-gap operation.

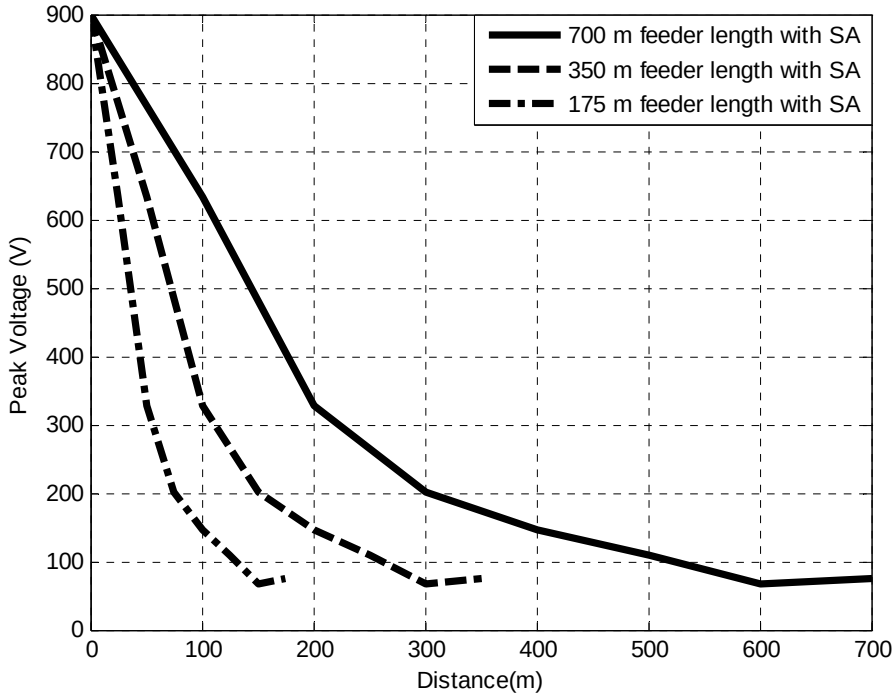

Figure 5.21 Impact of LV surge arrester on different feeder lengths, no MV spark-gap operation.

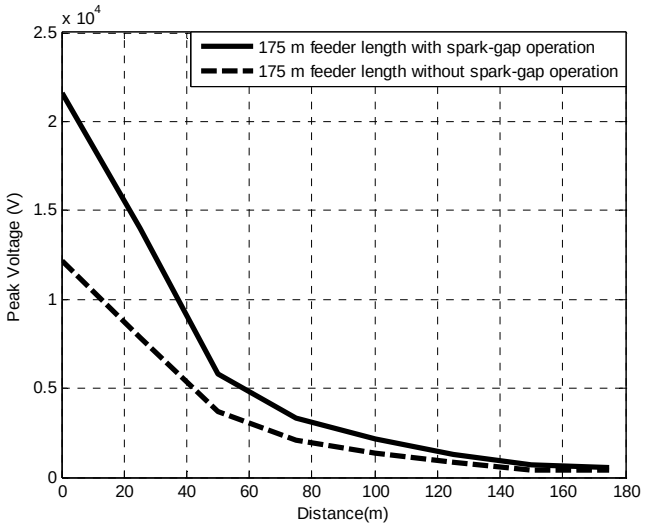

a. 175 m feeder length.

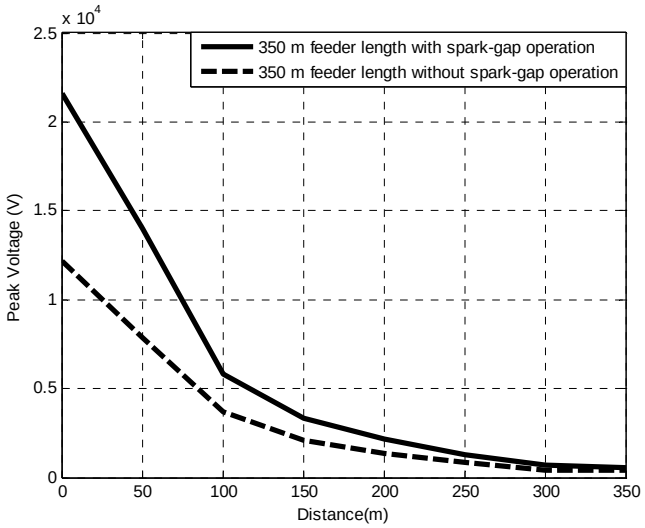

b. 350 m feeder length.

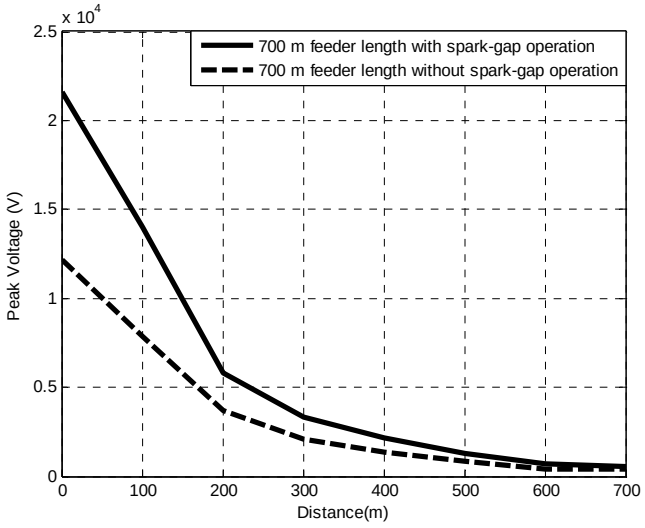

c. 700 m feeder length

Figure 5.22 Impact of spark-gap operation under different one-feeder network lengths, no LV SA.

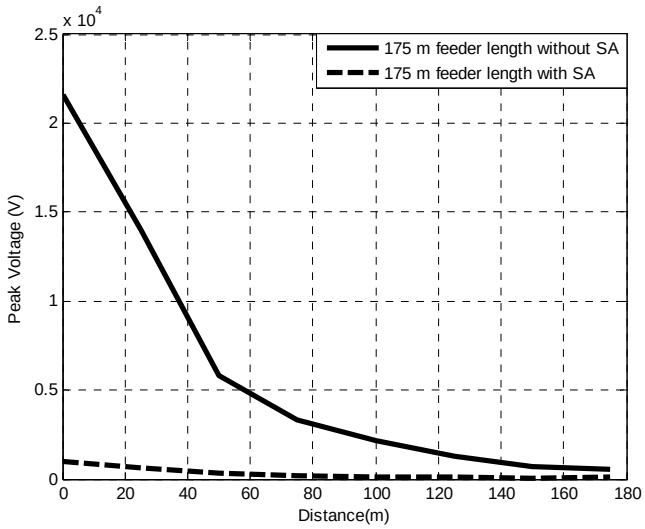

a. 175 m feeder length

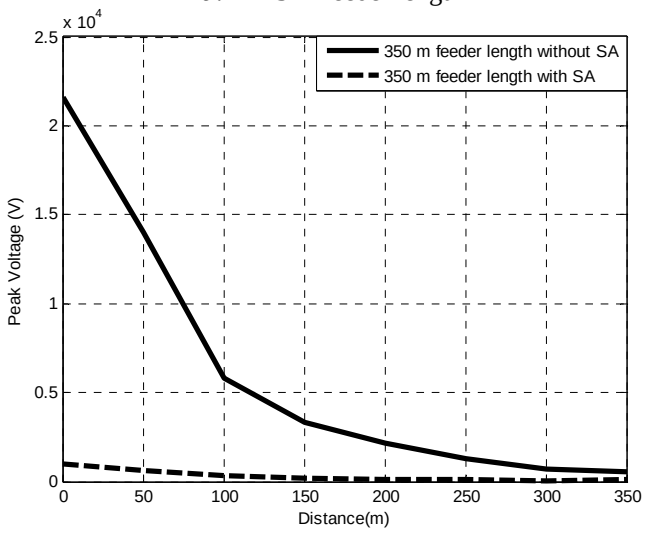

b. 350 m feeder length

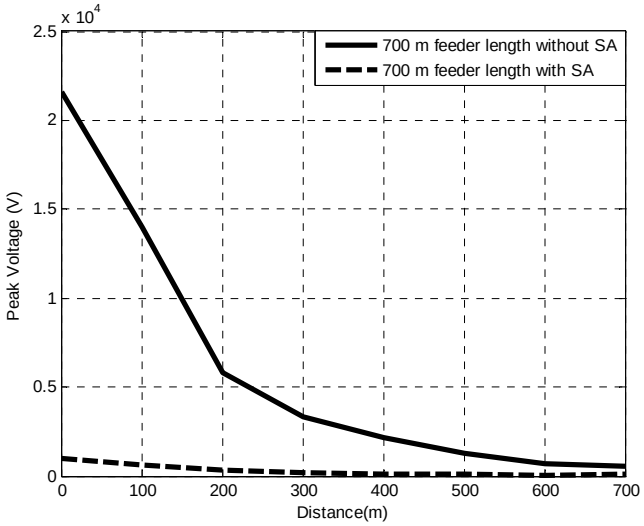

c. 700 m feeder length

Figure 5.23 Impact of LV surge arrester under MV spark-gap operation.

5.4 Impact of Load Reduction

In this case, the loads are reduced to their half values concerning one-feeder network; also, unloaded condition is taken into account.

5.4.1 The Performance without MV Spark-Gap Operation

When LV network is not protected using the surge arrester and as well it is without the operation of MV spark-gap, the corresponding peak voltage profile along the feeder length is shown in Figure 5.24. Solid, dashed and dashdot curves are for unloaded, half-load and full-load conditions respectively. The peak voltage profile is increased when the loads are reduced that is because the network damping is reduced where this increasing reached to its maximum values along the feeder under unloaded conditions.

When LV network is protected without operation of MV spark-gap, the influence of LV surge arrester on limiting the overvoltages transmitted to the LV network is shown in Figure 5.25 where it only limits the overvoltages to 1600 V at the end of the feeder in case of unloaded condition; however, less than 900 V in case of half and full load conditions. Although the network is protected, the voltage is high under unload conditions because of full reflection at the end of the feeder.

5.4.2 The Performance with MV Spark-Gap Operation

With considering the operation of MV spark-gap, the corresponding voltage waveforms at the same points aforementioned under unloaded and half load conditions are shown in Figures 5.26 and 5.27, respectively. The voltage waveforms under full load conditions are aforementioned and shown in Figure 5.10. The corresponding peak voltage profile for different loaded conditions is shown in Figure 5.28. As concluded above, peak voltage profile increased when the loads are reduced that is because the network damping is reduced where this increase reached to the maximum values along the feeder under unloaded conditions. Comparing the two Figures 5.24 and 5.28, the transmitted overvoltages to the LV network is more increased due to spark-gap operation.

When LV network is protected with spark-gap operation the corresponding voltage waveforms under unloaded and half load conditions are shown in Figures 5.29 and 5.30, respectively and the voltage waveforms under full load conditions are aforementioned in Figure 5.15. The corresponding peak voltage profile for different loaded conditions is shown in Figure 5.31. Also as concluded above, peak voltage profile increased when the loads are reduced. Comparing the two Figures 5.28 and 5.31, the transmitted overvoltages to the LV network is limited to less than 1000 V in case of half load and full load as well due to LV surge arrester operation; however incase of unloaded conditions, the surge arrester limits the transmitted overvoltages to 1600 V.

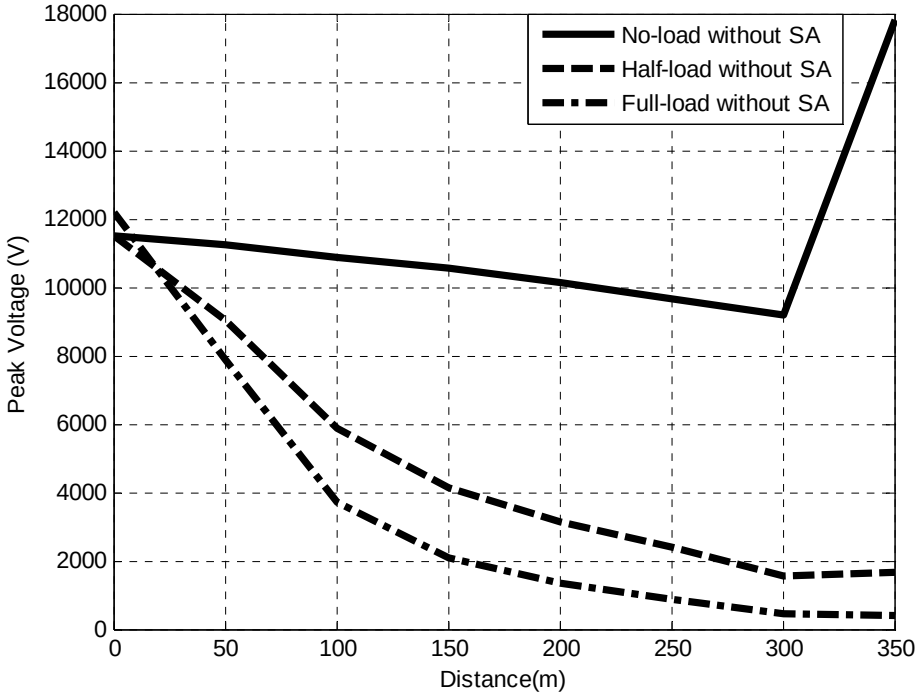

Figure 5.24 Load size Impact, no LV SA, no MV spark-gap operation.

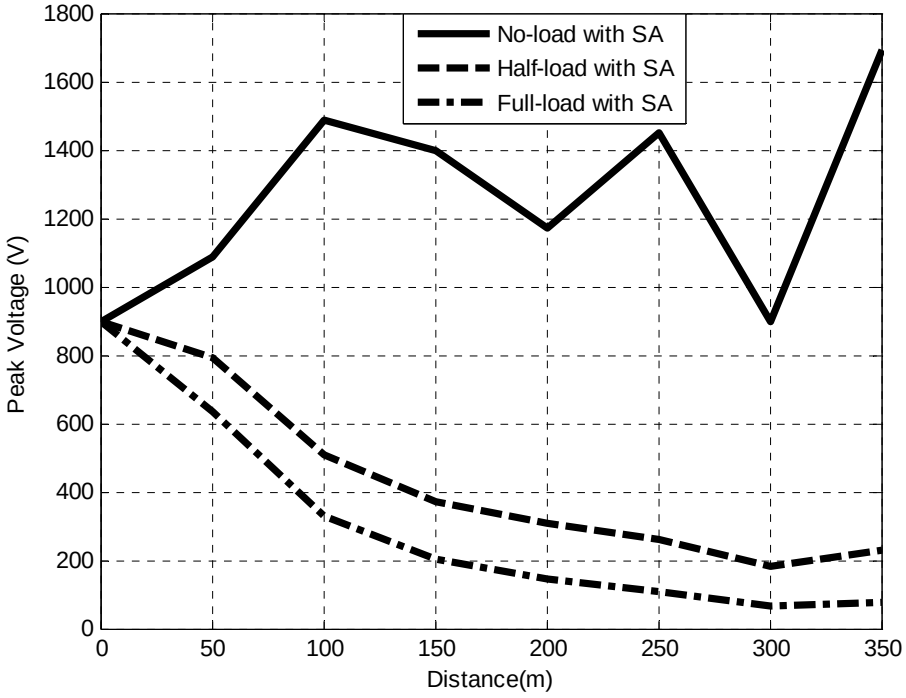

Figure 5.25 Impact of LV surge arrester on different load size, no MV spark-gap operation.

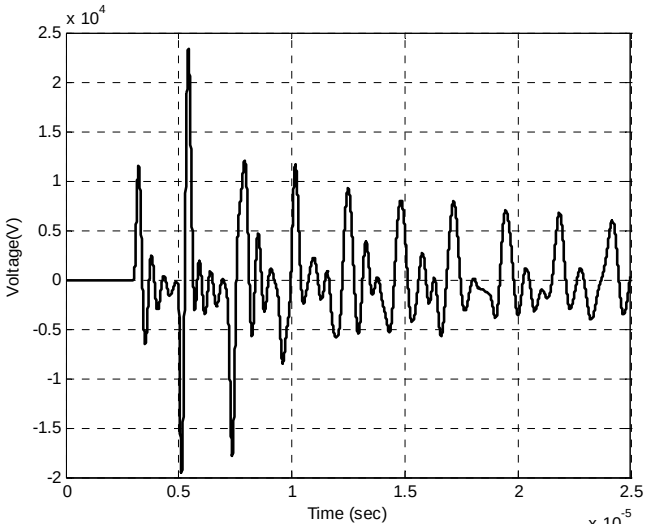

a. SEND

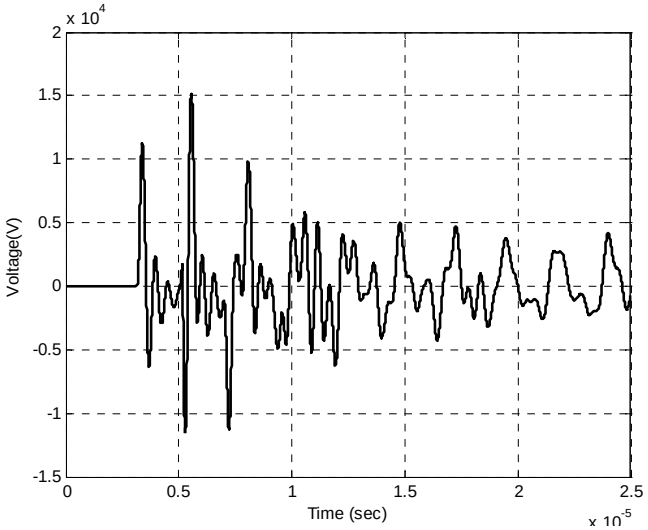

b. Piont A1

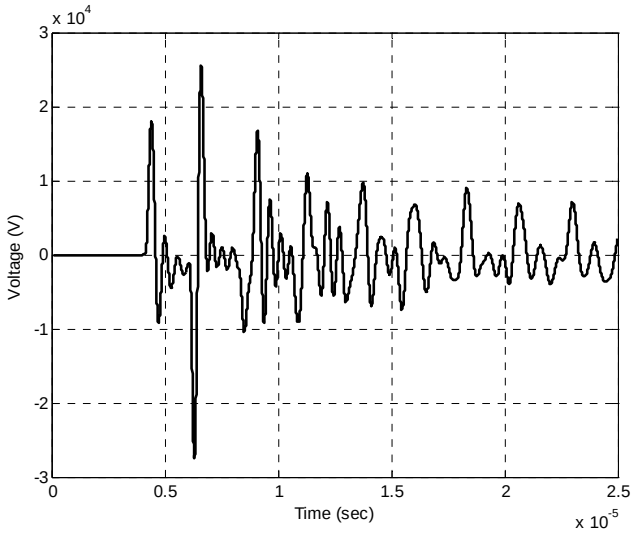

c. Point G1

Figure 5.26 Secondary voltage with MV spark-gap operation under unloaded conditions, no LVSA.

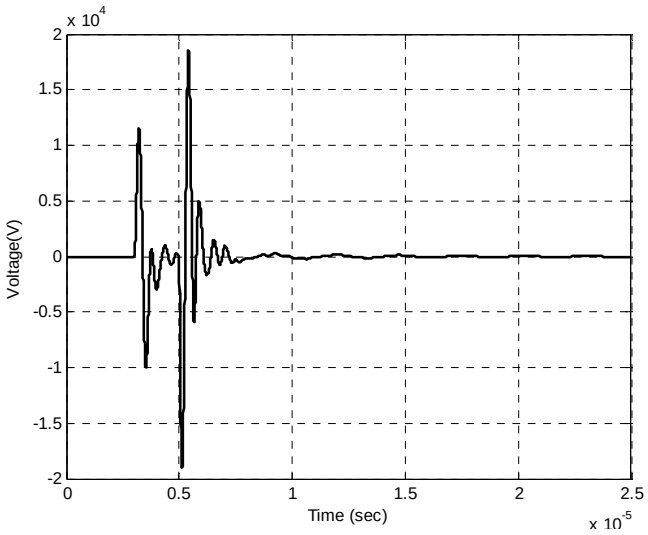

a. Voltage at SEND

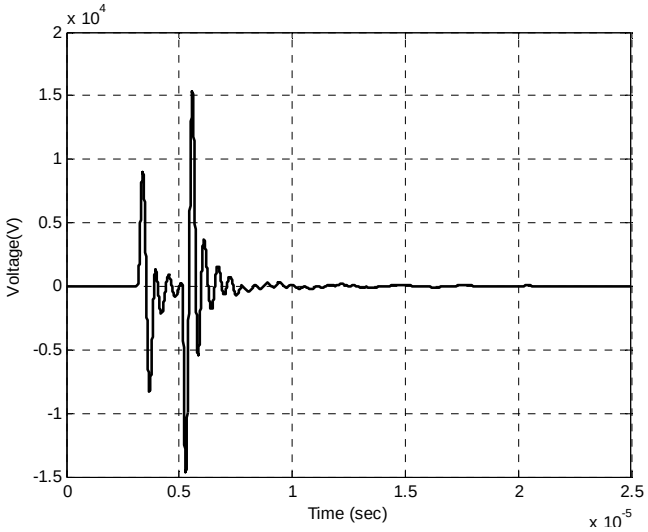

b. Voltage at Point A1

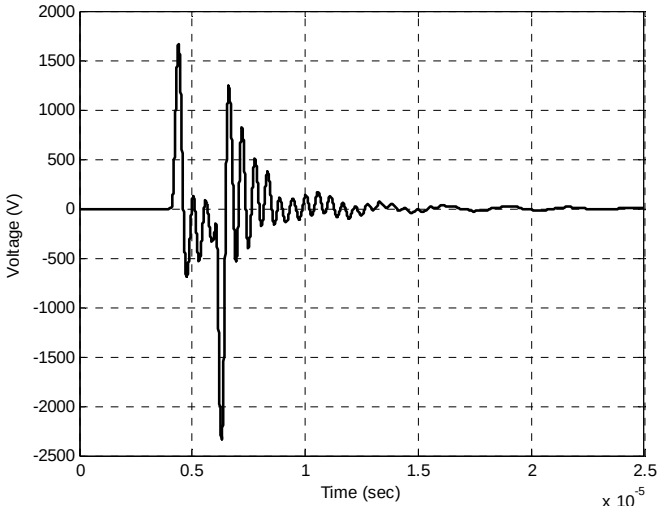

c. Voltage at Point G1

Figure 5.27 Secondary voltage transferred with MV spark-gap operation under half-load conditions, no LV SA.

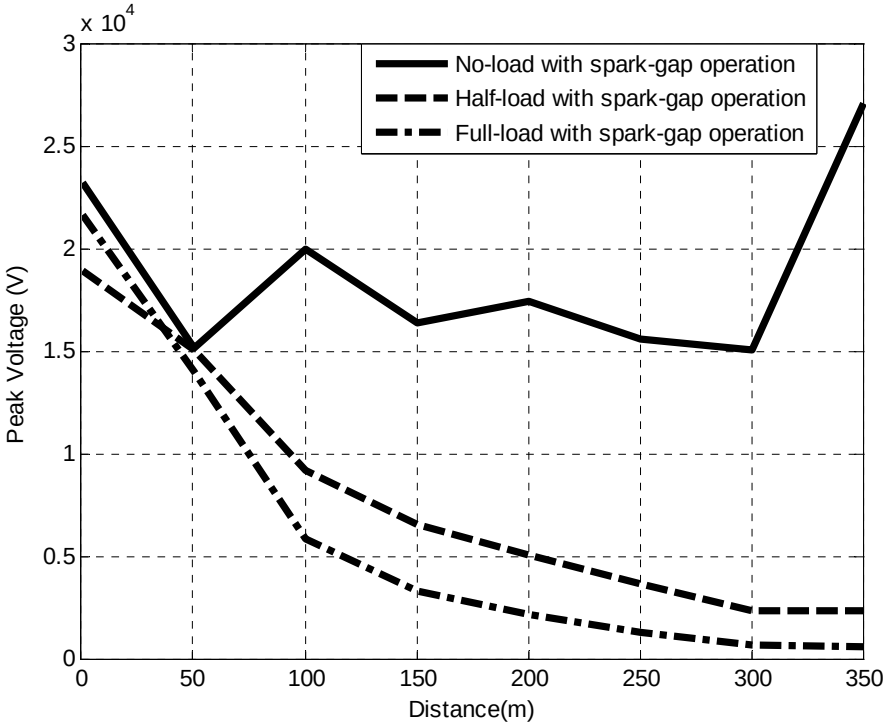

Figure 5.28 Load size impact under MV spark-gap operation, no LV SA.

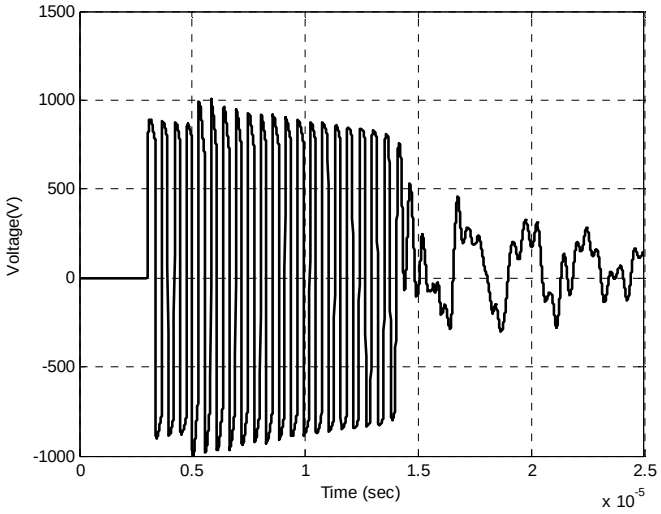

a. Voltage at SEND

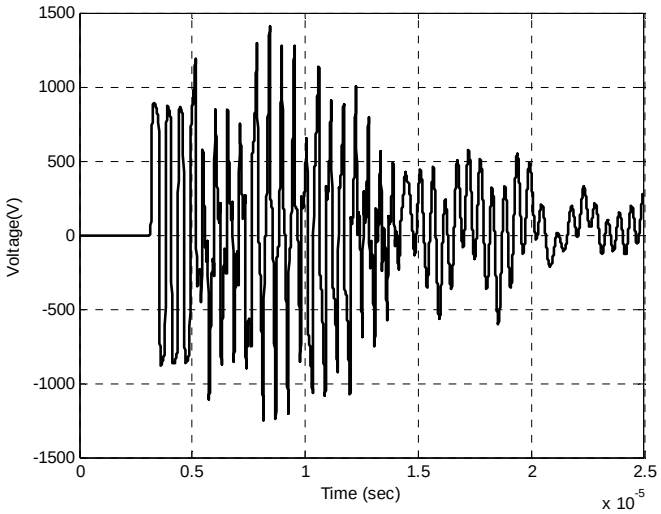

b. Voltage at Point A1

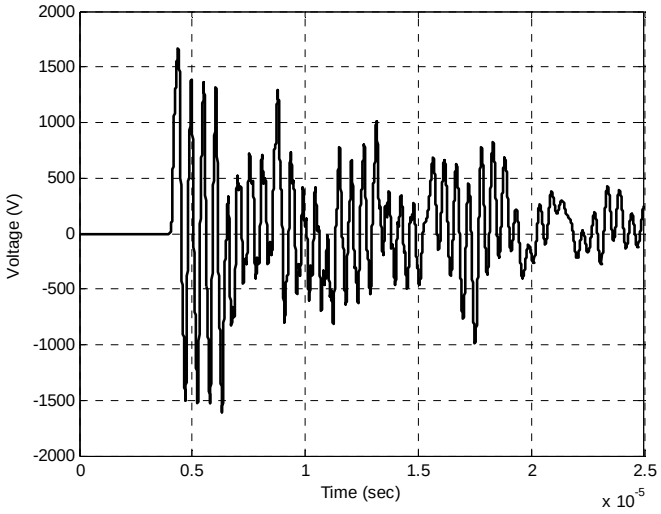

c. Voltage at Point G1

Figure 5.29 secondary voltage transferred with LV surge arrester under noload conditions with MV spark-gap operation.

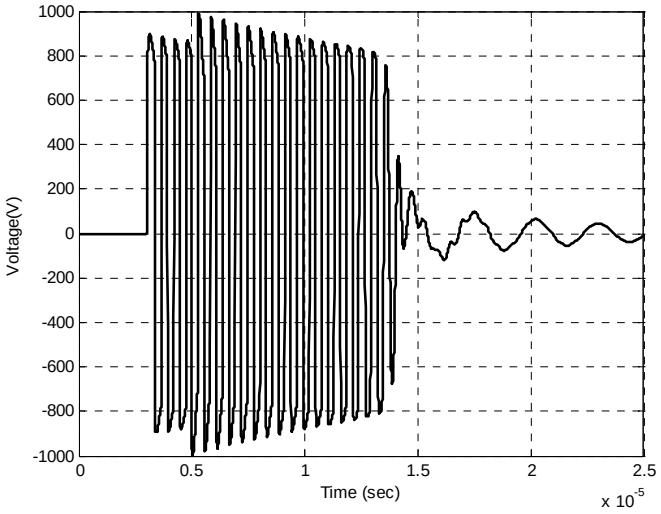

a. Voltage at SEND

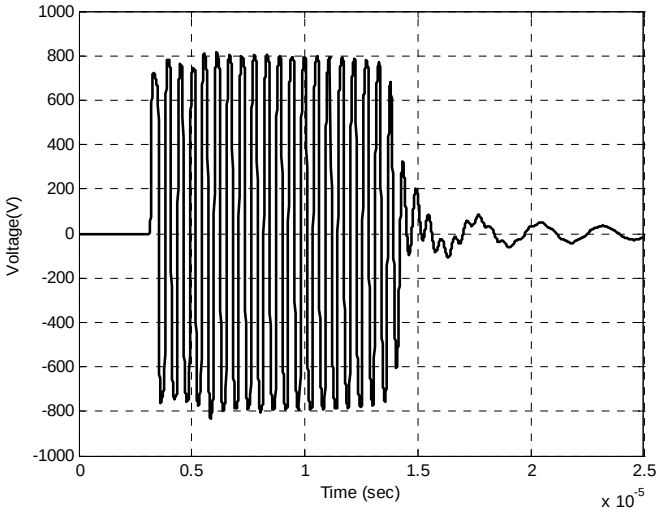

b. Voltage at Point A1

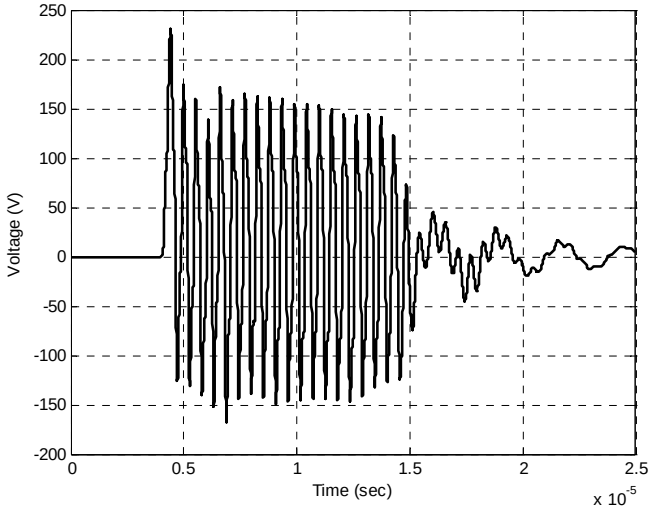

c. Voltage at Point G1

Figure 5.30 Secondary voltage transferred with LV surge arrester under half-load conditions with MV spark-gap operation.

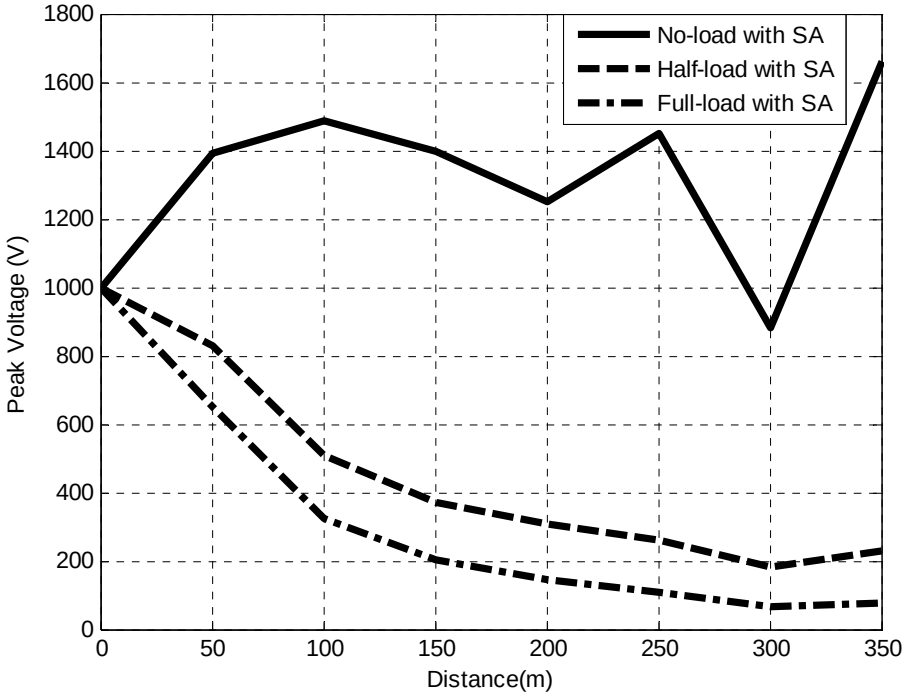

Figure 5.31 Impact LV surge arrester different load size with MV spark-gap operation.

5.5 Impact of Underground Cable

To study the impact of underground cable (UGC) on the transmitted overvoltages through the distribution transformer to the LV network, the overhead cable feeder is first totally replaced by underground cable as shown in Figure 5.32 then the combination between the OHC and UGC at the same feeder is taken into consideration concerning one feeder network. The considered underground cable model is for four-core, XLPE/PVC cable. The cable data are reported in [161] and summarized in the Appendix N.

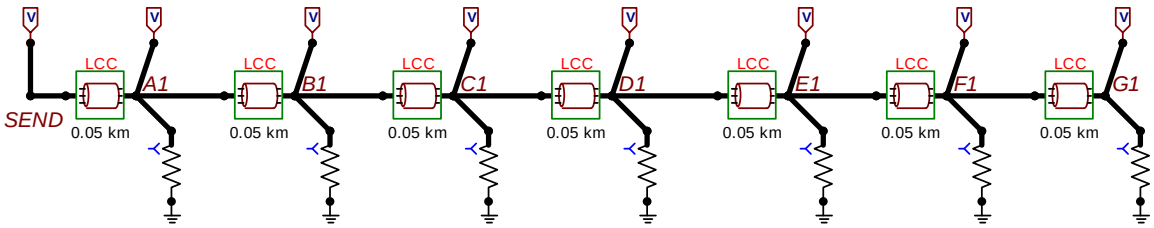

Figure 5.32 UGC configuration.

5.5.1 Impact of UGC without MV Spark-Gap Operation

When LV network is not protected and there is no MV spark-gap operation, the effect of UGC can be investigated through the peak voltage profile. The corresponding voltage waveforms and peak voltage profile are as shown in Figures 5.33 and 5.34, respectively. This peak voltage profile is compared with the profile when the network is constructed of overhead cables as shown in Figure 5.34. The voltage peaks close to the transformer are reduced when the network is of underground cables; however, the voltages at loads behind 250 m are higher when the network is underground cables.

Figure 5.35a illustrates the voltage profile when the network feeder is overhead cable; however, when the first section is underground cable (UGC) and when the last section is underground cable. Then, when two subsections are underground cable at the beginning of the feeder and when two subsections are underground cable at the end of the feeder, the corresponding results are shown in Figure 5.35b. The impact of underground cables at the beginning is bigger than their impact when they are at the feeder end. As depicted in Figure 5.35, there is an increase in the voltage at the point connecting between underground cable and overhead one when the UGC exist at the beginning of the feeder. The reason is that at this point, the characteristic impedance is increased from UGC impedance to OHC impedance value. When the UGC is at the beginning, the apparent impedance is the UGC which is less than OHC impedance.

Finally, the peak voltage profile for one, two, three and four sections of underground cable at the feeder beginning is shown in Figure 5.36a and as well at the feeder end, it is shown in Figure 5.36b. It also confirms that the underground cable impact is higher when the underground cable is installed at the feeder beginning.

When LV network is protected and there is no MV spark-gap operation the corresponding voltage waveforms and the peak voltage profile are as shown in Figures 5.37 and 5.38 respectively. Inserting the surge arrester provides more protection for the loads. In another case, a comparison of surge arrester performance is carried out for OHC and UGC feeder network where this comparison results are shown in Figure 5.39. The influence of surge arrester limits the voltage less than 900 V.

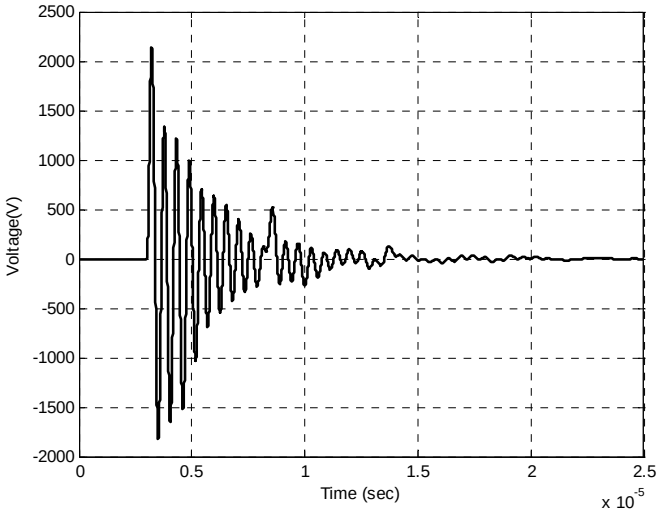

a. Voltage at SEND.

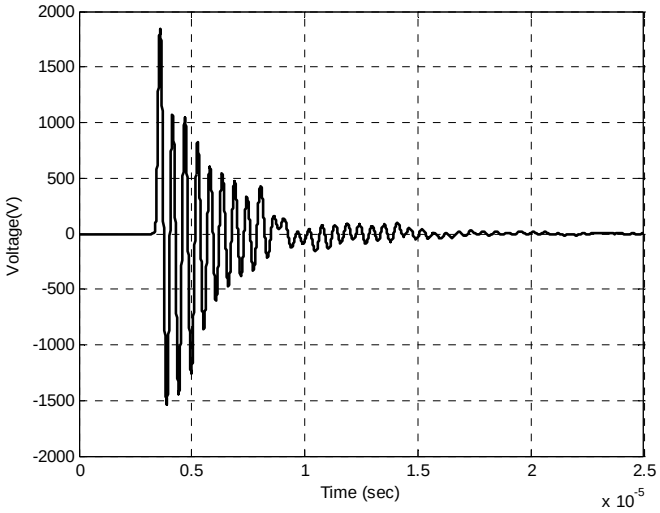

b. Voltage at Point A1.

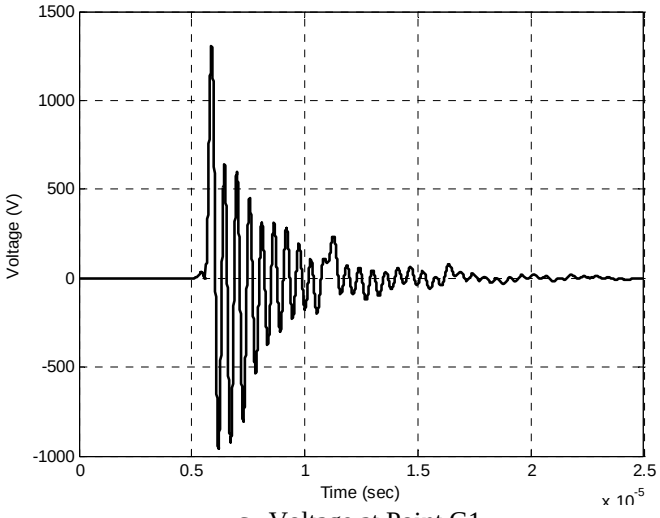

c. Voltage at Point G1.

Figure 5.33 Secondary voltage waveforms transferred when the network is underground cable, no LV SA, no MV spark-gap operation.

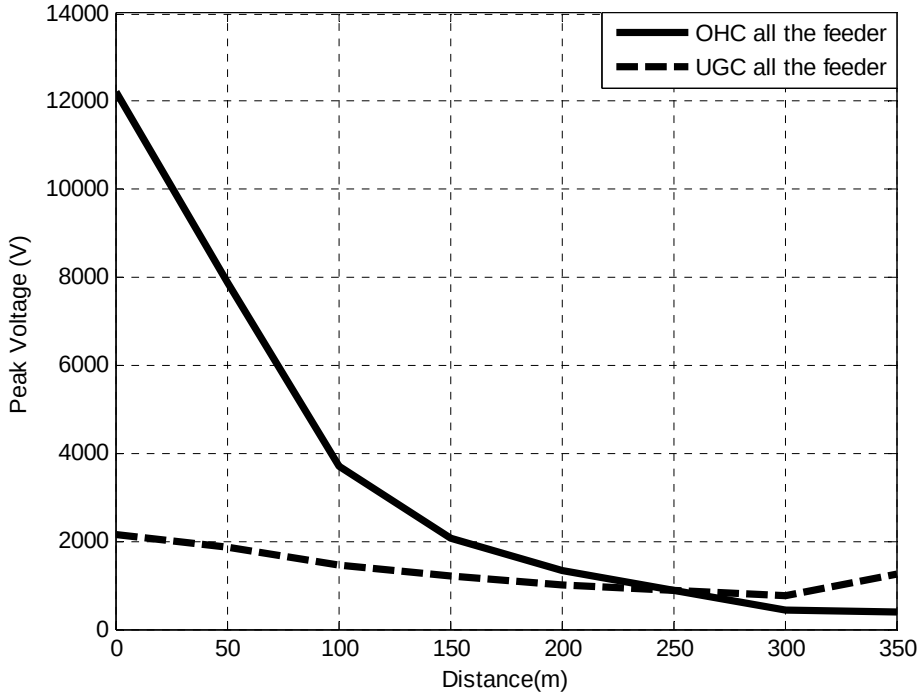

Figure 5.34 Comparing overhead cable and underground cable networks, no LV SA, no MV spark-gap operation.

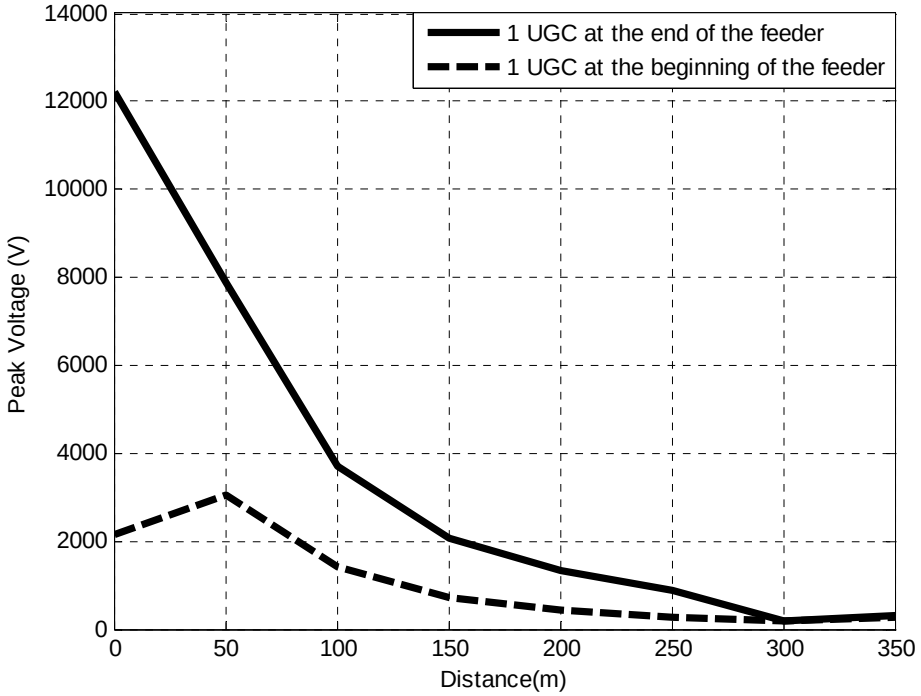

a. Only one section underground cable.

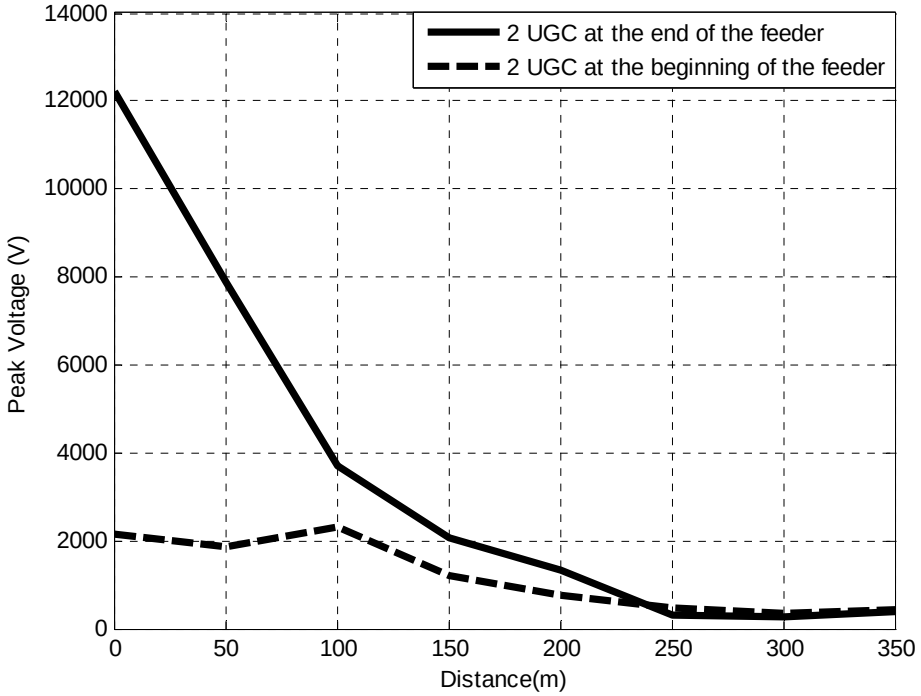

b. Two sections are underground cable.

Figure 5.35 Impact of underground cable position, no LV SA, no MV spark-gap operation.

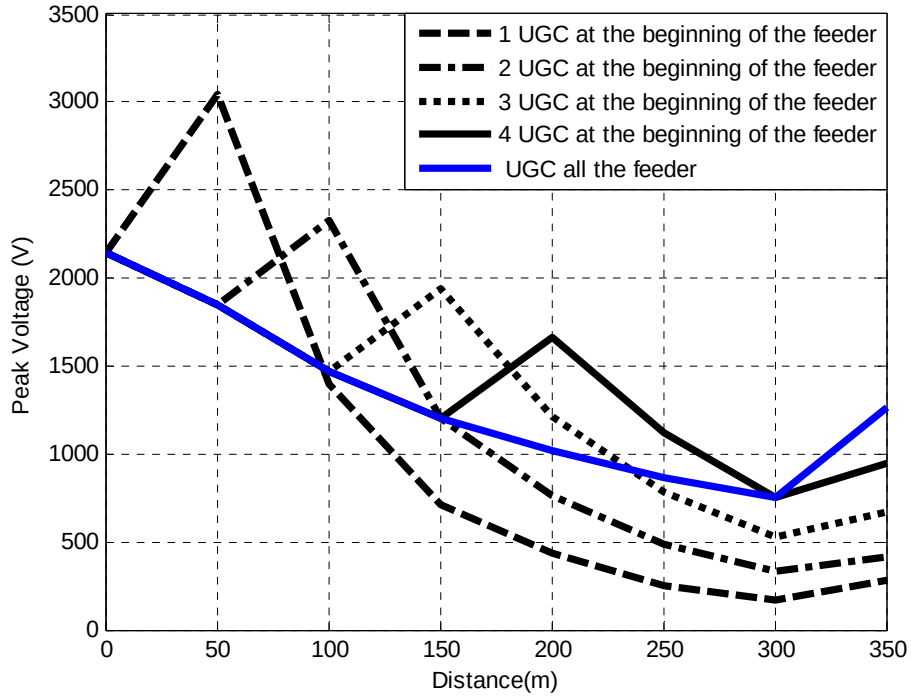

a. Cable sections at the feeder beginning

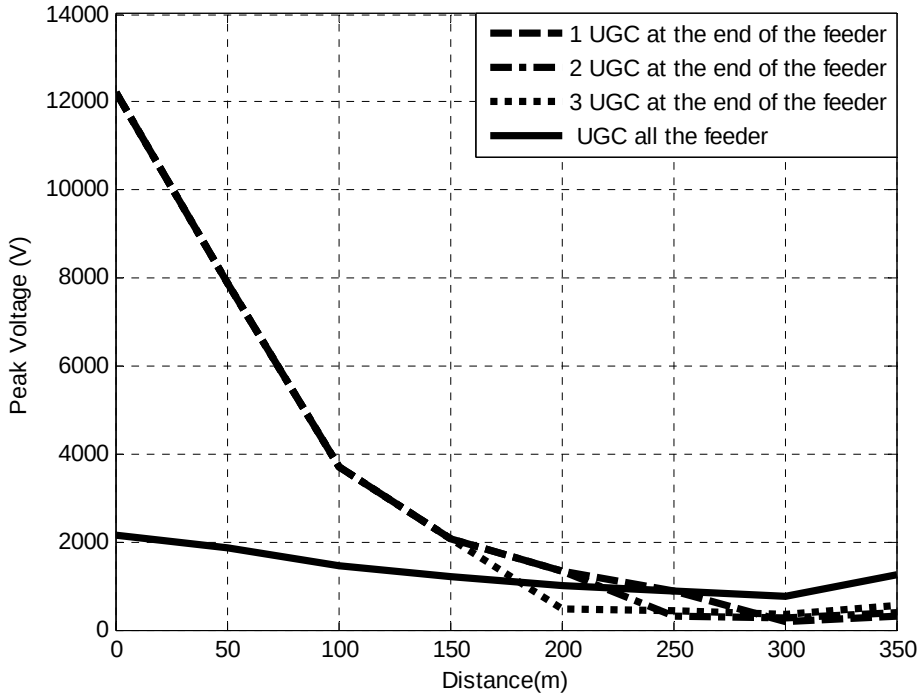

b. Cable sections at the feeder end.

Figure 5.36 UGC shares impact, no LV SA, no MV spark-gap operation.

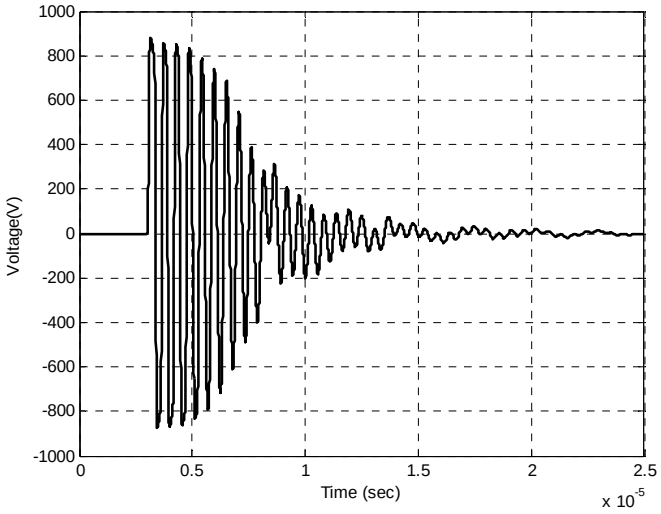

a. Voltage at SEND

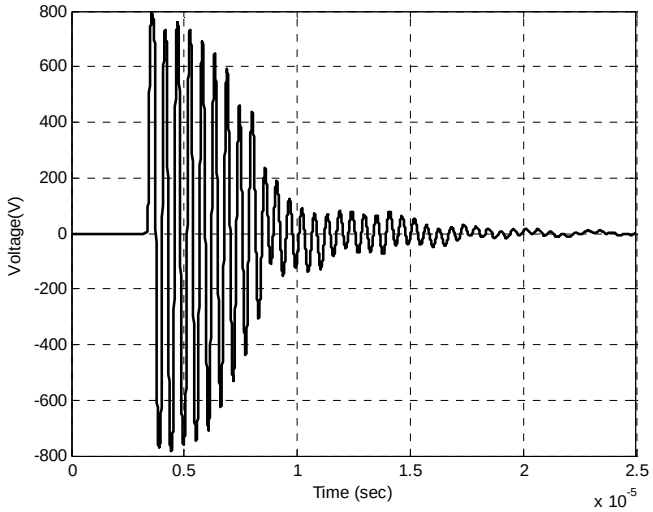

b. Voltage at Point A1

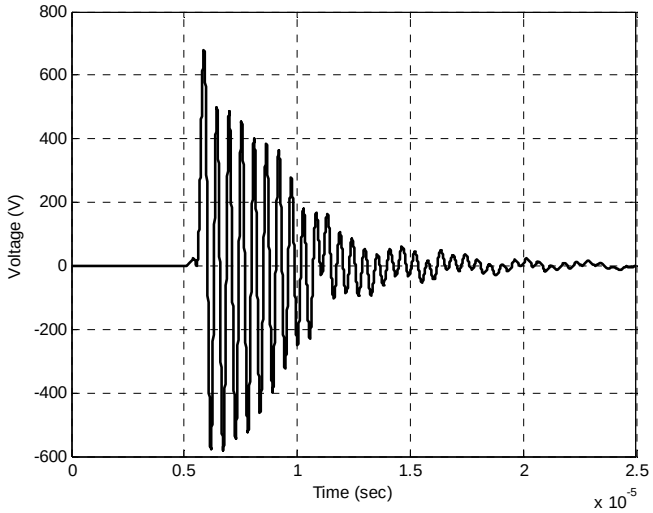

c. Voltage at Point G1

Figure 5.37 Surge arrester-based mitigation for one feeder UGC, no MV spark-gap operation.

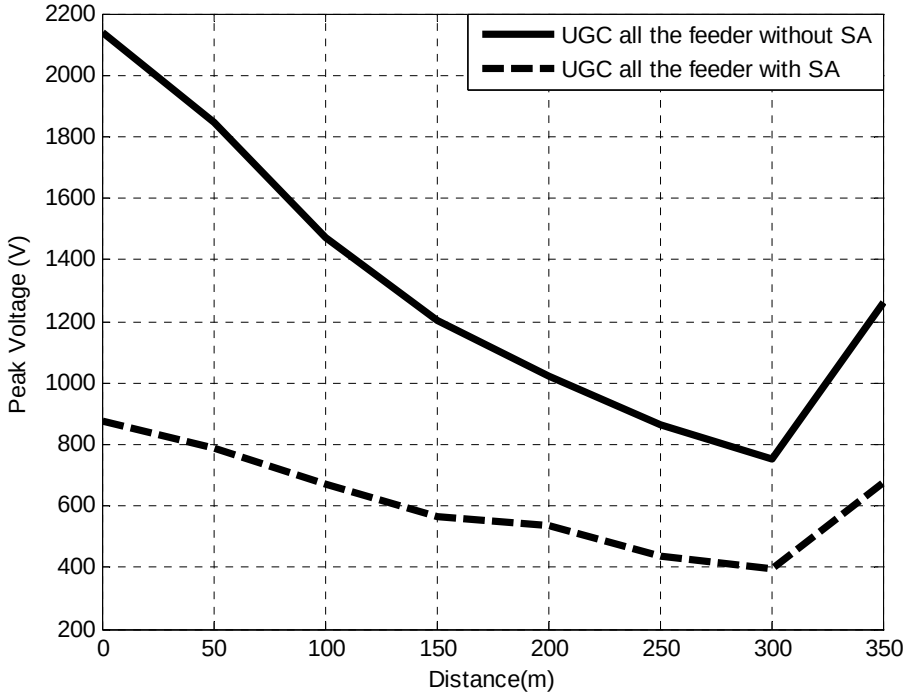

Figure 5.38 Impact of LV surge arrester on UGC one feeder network, no MV spark-gap operation.

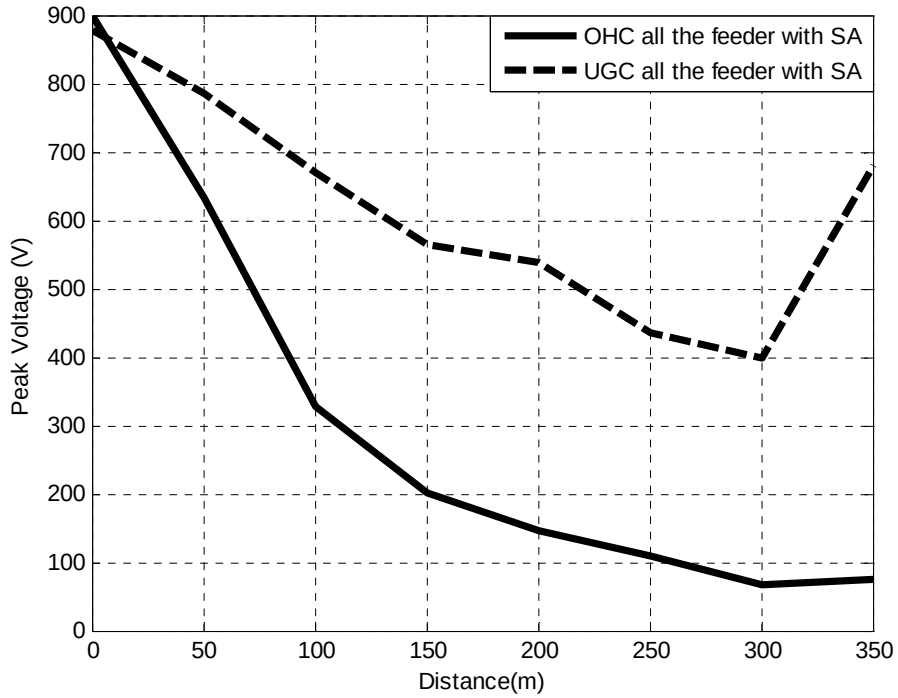

Figure 5.39 Comparison between OHC and UGC feeder with LV surge arrester, no MV spark-gap operation.

The voltage profiles when the one and two frst sections are underground cable (UGC) without and with LV surge arrester are shown in Figure 5.40. Although the overvoltages are low when the UGC segment is added at the feeder beginning and more reduced by installing surge arrester, there is an increase in the voltage at the junction between the UGC and OHC. Figure 5.41 more illustrates the effect of different two positions of the protection device when UGC exists at the feeder beginning. These positions are before UGC and at its junction with the OHC. Inserting surge arrester at the UGC termination with the OHC has lower voltage profile comparing with surge arrester before UGC. This observation is correct except at the feeder beginning where it is not protected. Installing two surge arresters highly protects the feeder. however, if it is assumed to using only one surge arrester in the LV network, it can be recommended to install it at UGC beginning to protect all over the feeder and the parallel feeders if they are found.

The results for one UGC section and two UGC sections at the end of the feeder are shown in Figures 5.42. Using one UGC at the end of the feeder makes the influence of surge arrester become noticeable until distance 300 m. However, using two- UGC at the end of the feeder makes the influence of the arrester become noticeable until distance 250 m. The value of induced overvoltage is high where the underground cable sections couldn’t reduce the overvoltage as well as these sections are at the feeder end. Therefore, the overvoltage protection has to be added under these circumstances at the feeder beginning in order to reduce such overvoltages.

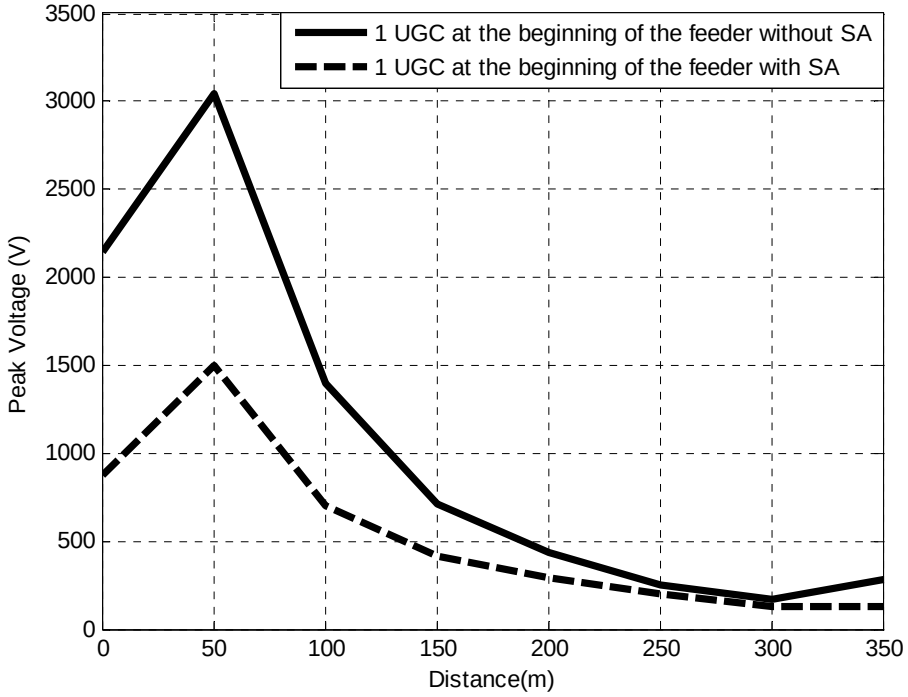

a. Using 1 UGC at the beginning of the feeder

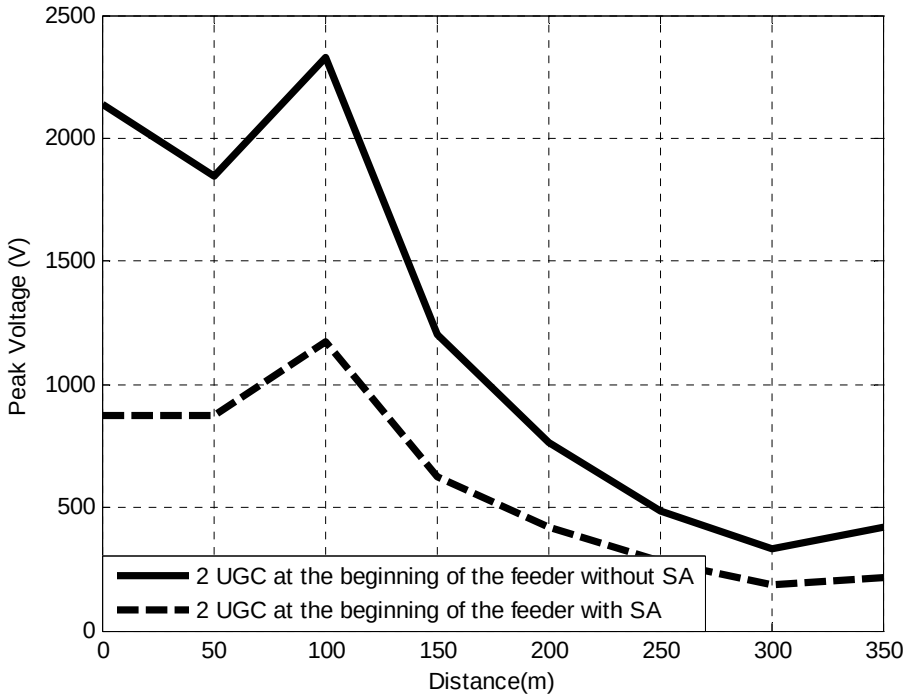

b. 2 UGC at the beginning of the feeder

Figure 5.40 Impact of LV surge arrester on the UGC at the feeder beginning, no MV spark-gap operation.

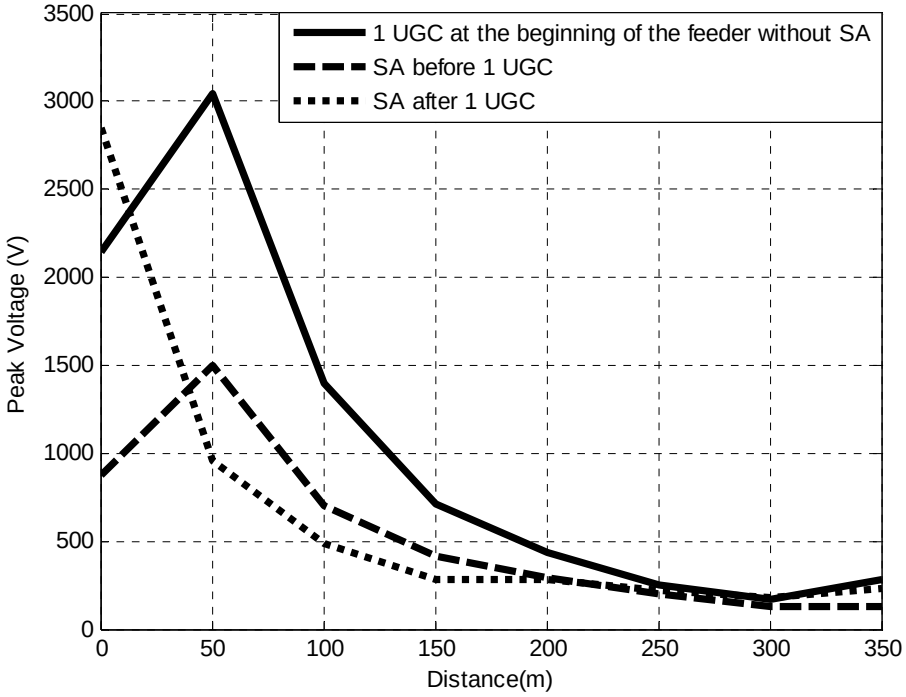

Figure 5.41 Effect of SA position using one UGC, no MV spark-gap operation.

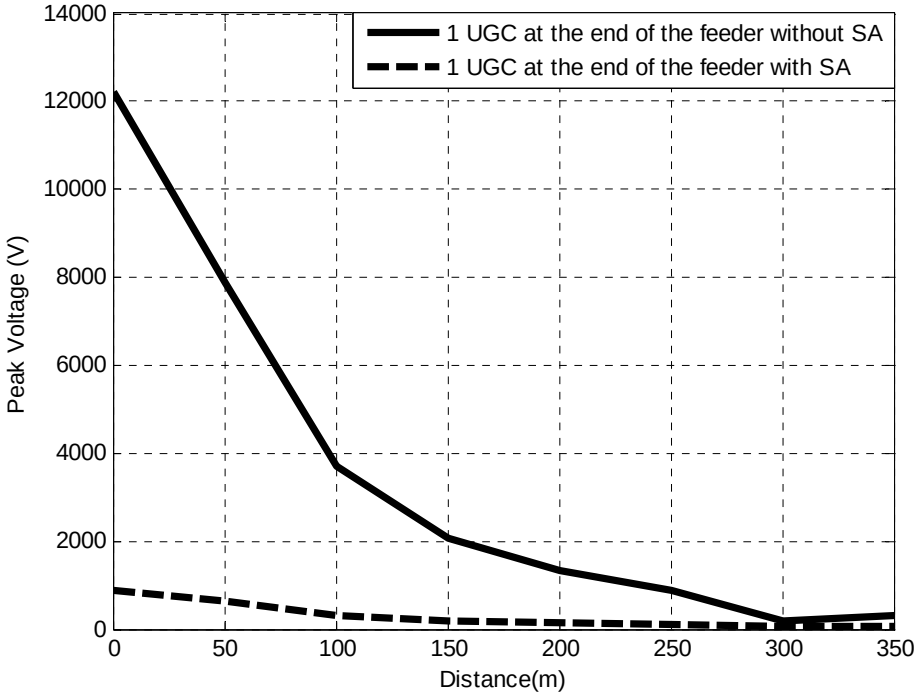

a. 1 UGC at the end of the feeder

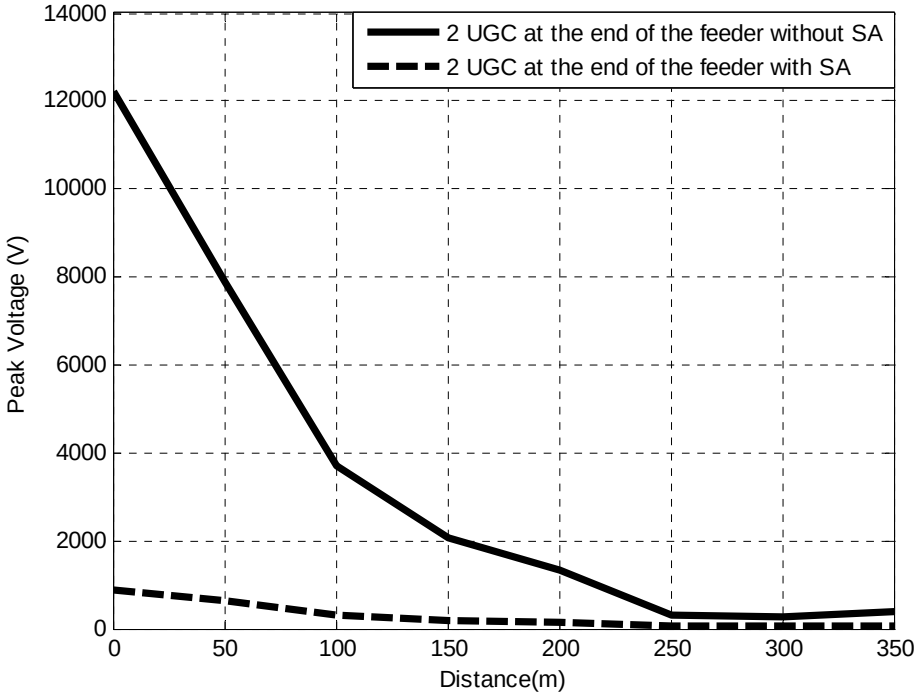

b. 2-UGC at the end of the feeder

Figure 5.42 Impact of LV surge arrester on the UGC at the feeder end, no MV spark-gap operation.

5.5.2 Impact of UGC with MV Spark-Gap Operation

When LV network is not protected by the surge arrester and with considering the MV spark-gap operation, the corresponding voltage waveforms and the peak voltage profile are shown in Figures 5.43 and 5.44, respectively where the network is UGC one-feeder. Figure 5.44 shows how much the spark-gap operation increases the transmitted overvoltages through the distribution transformer. The same influence can be depicted also when one UGC section is at the beginning and at the end of the feeder and when two-UGC sections are at the beginning and at the end of the feeder as shown in Figures 5.45 and 5.46, respectively.

When LV network is protected, the corresponding voltage waveforms and the peak voltage profile are as shown in Figures 5.47 and 5.48, respectively for UGC all the feeder. Figure 5.48 shows the effect of LV surge arrester on limiting the transmitted overvoltages through the distribution transformer. The same influence can be depicted also when one UGC section is at the beginning and at the end of the feeder and when two-UGC section are at the beginning and at the end of the feeder as shown from Figures 5.49 and 5.50, respectively.

Under circumstances of MV spark-gap operation, the LV network should be protected where the transferred overvoltages over the transformers are high whatever the LV network construction (OHC or UGC). This information is highlighted in this study as some network designers suppose that the UGC can kill the overvoltage. However, the overvoltages are still high enough to be hazard. Installing a surge arrester at the LV network beginning can protect the network and prevent these overvoltages to reach at the customer entrance.

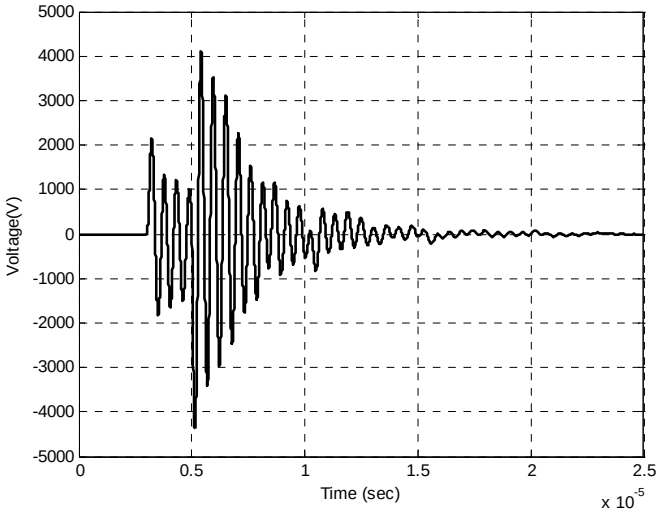

a. Voltage at SEND

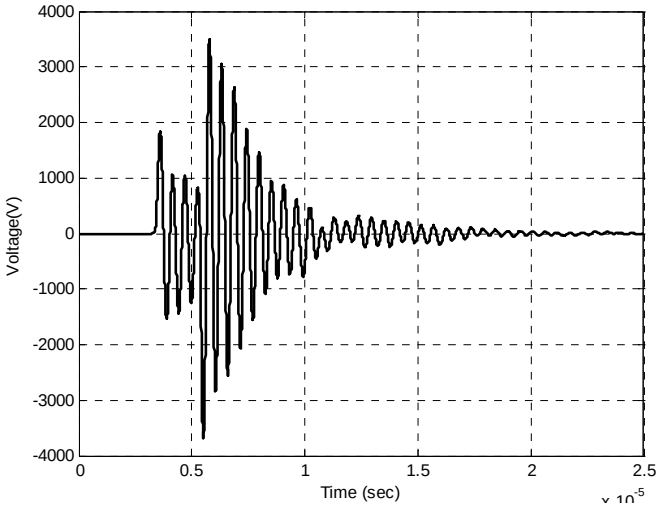

b. Voltage at Point A1

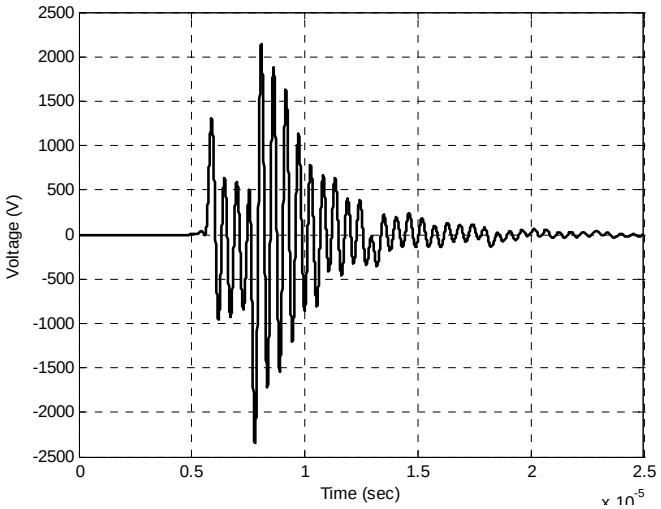

c. Voltage at Point G1

Figure 5.43 Secondary voltage waveforms transferred for UGC all the feeder under MV spark-gap operation, no LV SA.

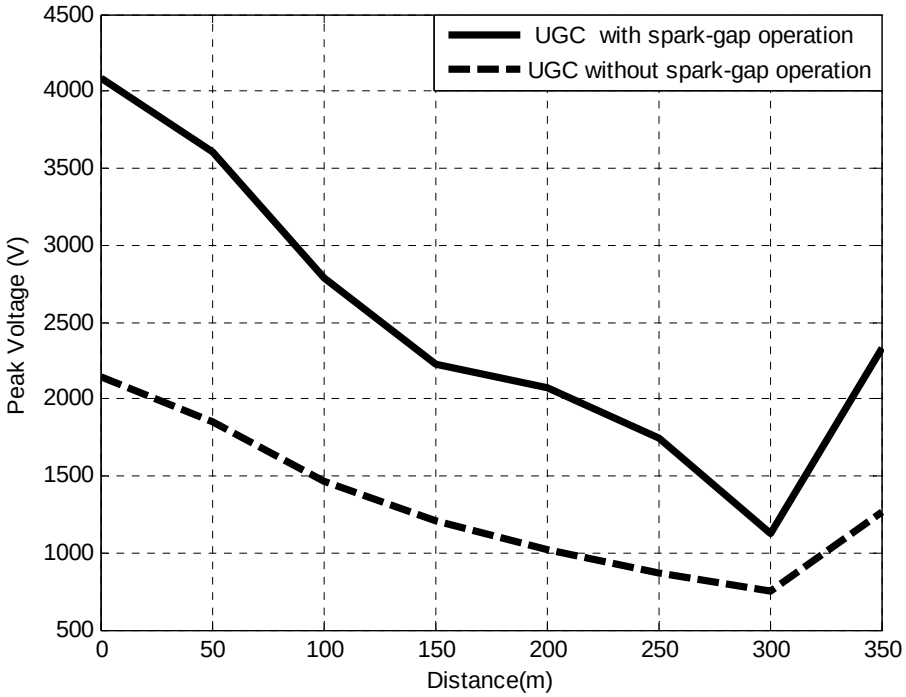

Figure 5.44 UGC behavior with and without MV spark-gap operation, no LV SA.

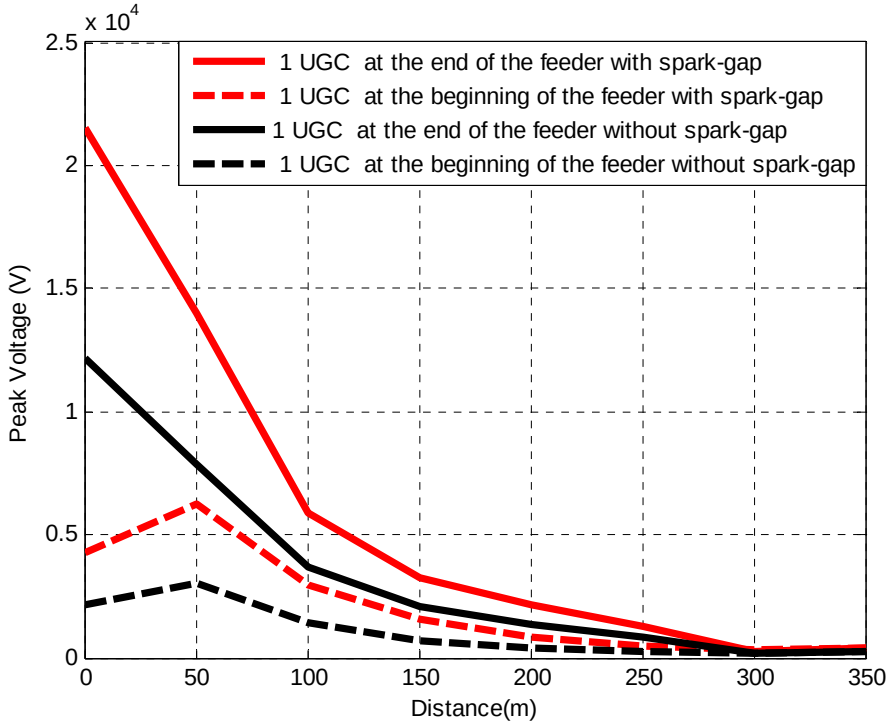

Figure 5.45 Impact of MV spark-gap operation for 1 UGC, no LV SA.

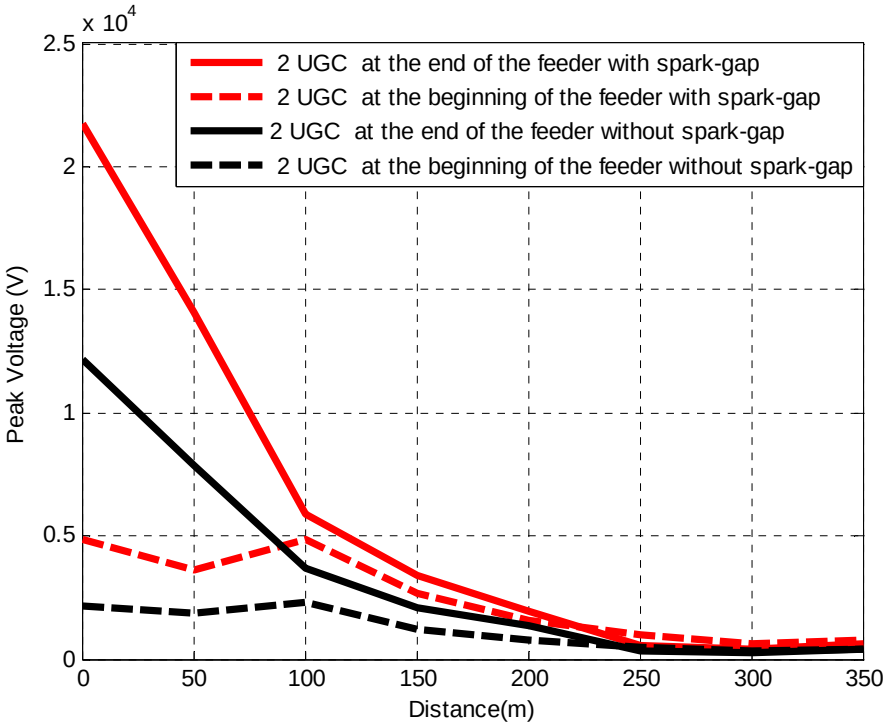

Figure 5.46 Impact of MV spark-gap operation for 2 UGC, no LV SA.

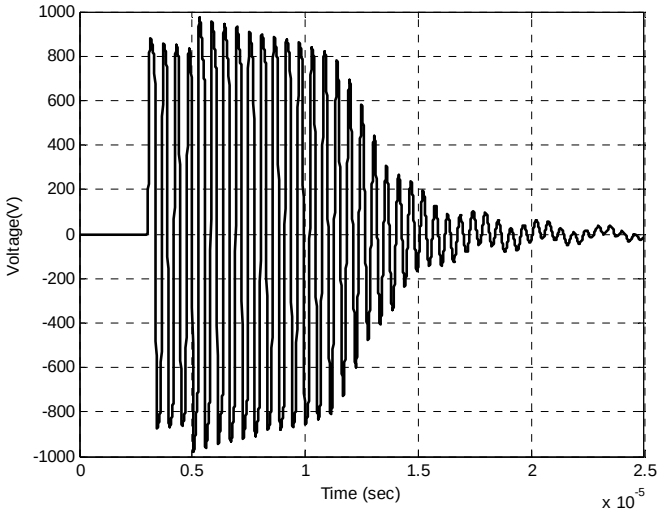

a. Voltage at SEND

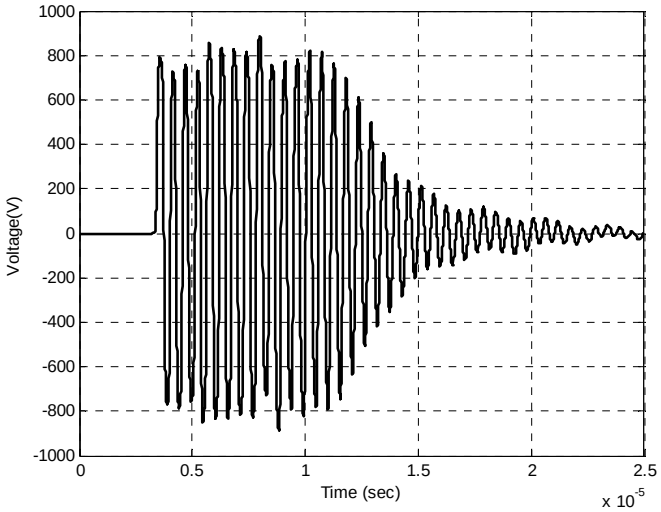

b. Voltage at Point A1

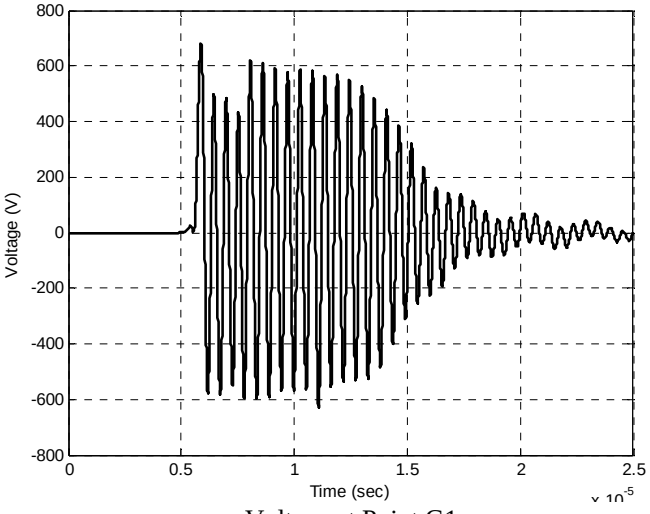

c. Voltage at Point G1

Figure 5.47 Secondary voltage transferred of UGC all over the feeder with LV surge arrester under MV spark-gap operation.

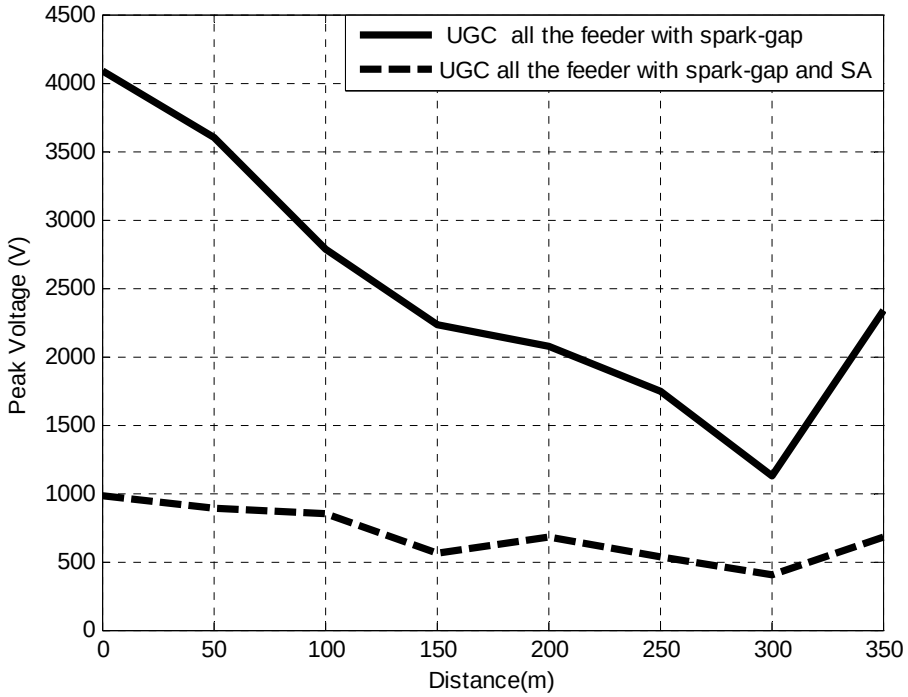

Figure 5.48 Impact of LV surge arrester under MV spark-gap operation.

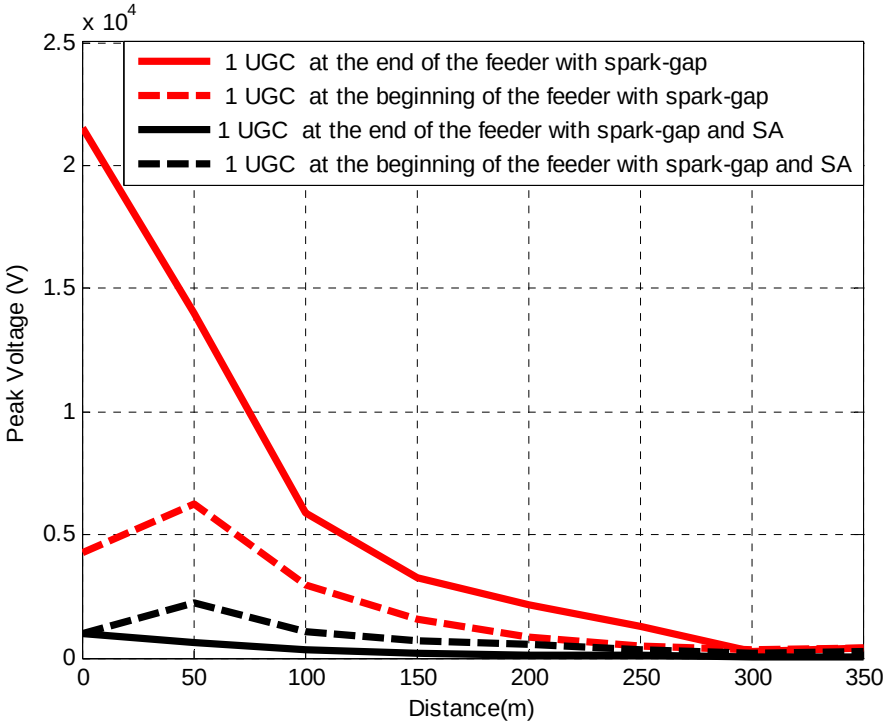

Figure 5.49 Impact of LV surge arrester under MV spark-gap operation.

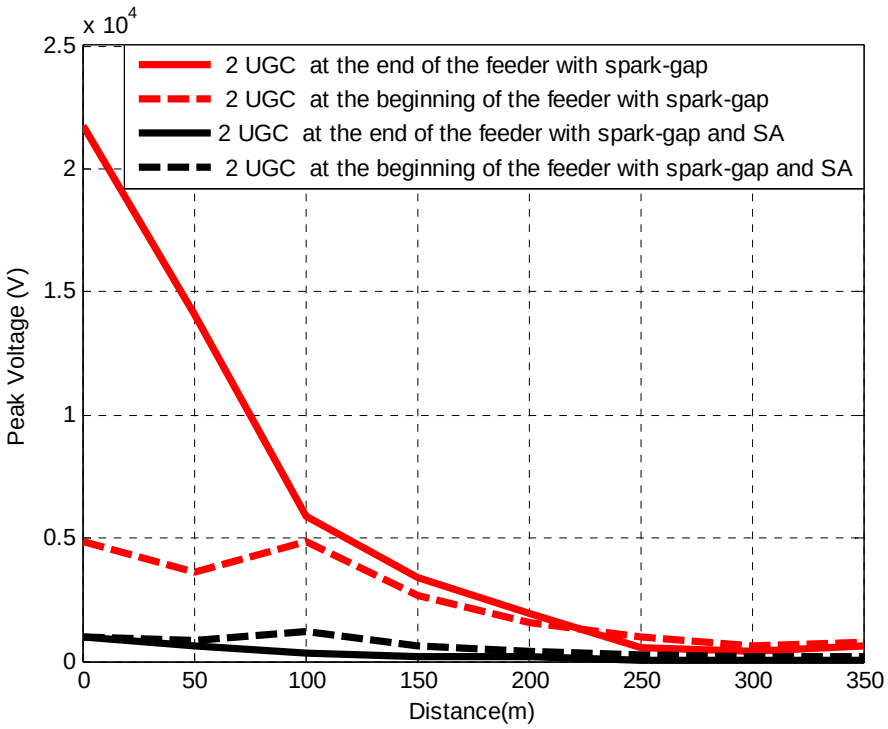

Figure 5.50 Impact of LV surge arrester under MV spark-gap operation.

6- Conclusions

The breakdown probability of a spark-gap subjected to combined impulse and ac voltages has been modeled. In order to ascertain the probabilistic model parameters, which are the standard deviation and mean values, the first part of the experiments was accomplished when the spark-gap was only exposed to impulse voltages. Considering these parameters and the ac voltage peak value, the proposed model has been experimentally verified and it showed a good agreement. Then the model was used in calculating the probability of the single-phase, two-phase and three-phase operation of the spark-gaps for different levels of lightning-induced overvoltages superimposed on the ac voltage. The fault type probability due to lightning-induced overvoltage in an MV network protected by spark-gaps has been investigated using the simplified Rusck expression to estimate the induced voltage above a perfectly conducting ground. This induced voltage is assumed to be randomly distributed using the well-known formula of Anderson.

The high frequency transformer model under unloaded conditions by Piantini has been modified. This modification has improved the transient voltage waveforms as taking more than one resonance frequency into consideration in the modeling process. The results have ensured the modified model accuracy as well as the model simplicity is still achieved. However, this model is not suitable for loaded conditions. So, a new high frequency transformer model has been proposed under unloaded as well as balanced loaded conditions. The model compromise between the simplicity and also accuracy. A very simple circuit to evaluate the transformer performance under lightning strokes was taken, in addition a very easy procedure was achieved to determine the model parameters at two different frequencies. Concerning two resonance frequencies in the transformer modeling has enhanced the model accuracy. The proposed model showed a good agreement between the experimental and the simulated results.

Using the proposed high frequency transformer model, the effect of lightning-induced overvoltages penetrating through the transformer to the customer side has been investigated. Also, the impact of feeder numbers, lengths, types and loads on the overvoltage reached at the service entrance point has been investigated through the peak voltage profile along the feeder. These voltage profiles for different conditions show reasonable results. Finally, a low voltage surge arrester has been modeled using Pinceti surge arrester model. This surge arrester has been installed at the distribution transformer secondary side in order to mitigate the induced overvoltage transferred from medium voltage to low voltage side in case of spark-gap operation and for the case that the overvoltage is too small to trigger the spark-gap as well. This mitigation has been studied through peak voltage profile along the feeder. The feeder type, overhead cable, underground cable or combination between them has been studied installing surge arrester at the transformer secondary side. Also, the surge arrester location has been studied when underground cable section is created at the beginning of the feeder. Generally, installing surge arresters at the transformer secondary side can mitigate the induced overvoltage transferred from the primary side before going to the consumers in low voltage network. So, inserting only one surge arrester at the feeder beginning will be sufficient to protect the

entire customers connecting to the feeder. This protection is required for the Finnish low voltage networks either they are constructed from overhead or underground cables.

This dissertation can help to do some researches of interest in work to follow such as:

1. Evaluating the probabilistic model of MV spark-gap characteristics with concerning discontinuities due to surge arrester where the model representing such characteristic has been shortly presented at the end of chapter 2; however, it is not verified using experimental results and its impact on the statistical analysis of fault type is not investigated.
2. Investigating the dynamic characteristics of spark-gap when it is connected in series with surge arrester where such connection can improve the overvoltage protection.
3. Discussing more on the customer experienced voltage spikes with different lightning protections in MV networks.
4. Time-domain evaluation of induced overvoltage superimposed on AC voltage and concerning MV Spark-Gap operation.
5. Studying the conditional probability of fault type changes due to induction effect of spark-gap operation in distribution networks.
6. Experimentally verifying the high frequency model of distribution transformers under unbalanced flashovers of spark-gaps such as single-phase and two-phase operations where the three-phase operation has been only evaluated in this dissertation.

References

[1] http://en.citizendium.org/wiki/Lightning, 05.2009.

[2] T. Thanasaksiri, "Improving the Lightning Performance of Overhead Distribution Lines" TENCON 2004. 2004 IEEE Region 10 Conference, 21-24 Nov., 2004.

[3] EPRI, Lightning Protection Design Workstation, LPDW Version 5 References, 1999.

[4] IEEE Standards 1410 "IEEE Guide for Improving the Lightning Performance of Electric Power Overhead Distribution Lines", 2004.

[5] J. R. Lucas, *High Voltage Engineering*, 2001, Sri Lanka.

[6] Lightning and surge protection, M. SYSTEM, CO., LTD, http://www.m-system.co.ip, 06.2009.

[7] S. Viscaro, "Direct Strokes to Transmission Lines: Considerations on the mechanisms of Overvoltage Formation and their Influence on the Lightning Performance of Lines", Journal of Lightning Research, Vol. 1, pp. 60-68, 2007.

[8] S. Viscaro, "Lightning: an Engineering Approach" (in Portuguese), ArtLiber Edit-Sao Paulo, 2005, pp. 1-272.

[9] S. Sekioka, K. Aiba and S. Okabe, "Lightning Overvoltages on Low Voltage Circuit Caused by Ground Potential Rise", International Power System Transients, IPST2007, Lyon, France, June 4-7, 2007.

[10] H. Koga, T. Motomitsu, and T. Taniguchi, "Lightning Surge Waves Induced on Overhead Lines" Transactions on IECE of Japan, Vol. E62, No. 4, pp. 216-223, 1979.

[11] C. A. Nucci and F. Rachidi "Lightning-Induced Overvoltage", IEEE Transmission and Distribution Conference, New Orleans, April 14, 1999.

[12] M. A. Uman, D. K. Mclain, "Magnetic Field of Lightning Return Stroke", Journal of Geophysics Research, Vol. 74, 1969.

[13] F. Rachidi, C. A. Nucci, M. Ianoz, C. Mazzetti, "Influence of a Lossy Ground on Lightning-Induced Voltages on Overhead Lines", IEEE Transactions On Electromagnetic Compatibility, Vol. 38, No. 3, pp. 250-264, Aug. 1996.

[14] C. A. Nucci, "Lightning-Induced Voltages on Overhead Power Lines. Part II: Coupling Models for the Evaluation of the Induced Voltages", Electra, No.162, pp. 121-145, Oct. 1995.

[15] C. A. Nucci, "Lightning-Induced Voltages on Overhead Power Lines. Part I: Return Stroke Current Models with Specified Channel-Base Current for the Evaluation of the Return Stroke Electromagnetic Fields", Electra, No.161, pp. 75-102, Aug. 1995.

[16] D. Djalel, H. Ali and C. Fayçal, "The Return-Stroke of Lightning Current, Source of Electromagnetic Fields: Study, Analysis and Modelling", American Journal of Applied Sciences, Vol. 4, No. 1, pp. 42-48, 2007.

[17] V. A. Rakov, M. A. Uman, "Review and Evaluation of Lightning Return Stroke Models Including Some Aspects of Their Application", IEEE Transactions on Electromagnetic Compatibility, Vol. 40, No. 4, pp. 403-426, November 1998.

[18] C. E. Bruce, R. H. Golde, "The Lightning Discharge", Journal of the IEE, Vol. 88, pp. 487-520, London, Dec. 1941.

[19] J. L. Bermudez "Lightning Currents and Electromagnetic Fields Associated with Return Strokes to Elevated Strike Objects", Ph.D. Thesis No. 2741. EPFL, pp. 65-98, 2003.

[20] M. A. Uman and D. K. Mclain, "Magnetic Field of Lightning Return Stroke", Journal of Geophysics Research, Vol. 74, 1969.

[21] C. A. Nucci and F. Rachidi "Experimental Validation of a Modification to the transmission line model for LEMP calculations" 8th International Symposium on Electromagnetic Compatibility EMC, Zurich: 6-11, 1989.

[22] Y. T. Lin, M. A. Uman, R. B. Standler "Lightning Return Stroke Models" Journal of Geophysical Research, Vol. 85, No. C3, March, 1980.

[23] M. J. Master, M. A. Uman, Y. T. Lin and R. B. Standler "Calculations of Lightning Return Stroke Electric and Magnetic Fields above Ground", Journal of Geophysics Research, Vol. 86, No. C12, Dec. 1981.

[24] D. M. Jordan, M. A. Uman, "Variation in Light Intensity with Height and Time from Subsequent Lightning Return Strokes", Journal of Geophysics Research, Vol. 88, pp. 6555-6562, 1983.

[25] F. Heidler, "Travelling Current Source Model for LEMP Calculation", 6th International Symposium on Electromagnetic Compatibility, Zurich, March 5-7, 1985.

[26] C. A. Nucci, C. Mazzetti, F. Rachidi, M. Ianoz, "On Lightning Return Stroke Models for LEMP Calculations", 19th International Conference on Lightning Protection, Graz, April 1988.

[27] F. Rachidi, C. A. Nucci, "On the Master, Uman, Lin Standler and the Modified Transmission Line Lightning Return Stroke Current Models", Journal of Geophysics Research, Vol. 95, No. D12, pp. 20389-20393, Nov. 1990.

[28] V. A. Rakov, A. A. Dulzon. 1987, "Calculated Electromagnetic Fields of Lightning Return Strokes", Russia. Teknicheskaya Electrodinamika,(1): 87-89.

[29] G. Diendorfer, M. A.Uman, "An Improved Return Stroke Model with Specified Channel-Base Current", Journal of Geophysics Research, Vol. 95, No. D9, pp. 13621-13644, Aug. 20, 1990.

[30] C. A. Nucci, Tutorial on Lightning-Induced Effects on Transmission Lines, 4th International Symposium on Electromagnetic Compatibility EMC, pp. 69-75, Zurich, 2000.

[31] R. Montano, "The Effects of Lightning on Low Voltage Power Networks", Ph.D Thesis, Uppsala university, 2005.

[32] S. Rusck, “Induced Lightning Overvoltages on Power Transmission Lines with Special Reference to the Overvoltage Protection of Low Voltage Networks”, Transactions of the Royal Institute of Technology, Stockholm, No. 120, 1958.

[33] V. Cooray, “Calculating Lightning-Induced Overvoltages in Power Lines: A Comparison of Two Coupling Models”, IEEE Transactions on Electromagnetic Compatibility, Vol. 36, No. 3, Aug. 1994.

[34] S. Rusck, Protection of Distribution Lines in Lightning, Vol. 2, R. H. Golde, London: Academic Press, pp. 747-771, 1977.

[35] V. P. Idone, and R. E. Orville, “Lightning Return Stroke Velocities in the Thunderstorm Research International Program”, Journal of Geophysical Research, Vol. 87, pp. 4903-4915, 1982.

[36] V. Cooray, “*The Lightning Flash*”, Institution of Electrical Engineers, London, United Kingdom, 2003.

[37] C.D. Taylor, Satterwhite R.S., Harrison C.W., “The response of a Terminated Two-Wire Transmission Line Excited by a Non-Uniform Electromagnetic Field”, IEEE Transaction on Antenna Propagation, Vol. AP-13, 1965.

[38] A. K. Agrawal, H. J. Price and S. H. Gurbaxani, “Transient Response of a Multiconductor Transmission Line Excited by a Non Uniform Electromagnetic Field”, IEEE Transactions on Electromagnetic Compatibility, Vol. EMC-22, pp. 119-129, 1980.

[39] C. A. Nucci, F. Rachidi, M. Ianoz, C. Mazzetti, “Comparison of Two Coupling Models for Lightning-Induced Overvoltage Calculations", IEEE Transactions on Power Delivery, Vol. 10, No. 1, pp. 330-339, Jan. 1995.

[40] F. Rachidi, “Formulation of the Field-to-Transmission line Coupling Equations in Terms of Magnetic Excitation Field”, IEEE Transactions on Electromagnetic Compatibility, Vol. 35, No. 3, Aug. 1993.

[41] P. Chowdhuri, E.T.B. Gross, “Voltage Surge Induced on Overhead Lines by Lightning Strokes”, Proceeding of IEE, Vol. 114, No. 12, pp. 1899-1907, Dec. 1967.

[42] P. Chowdhuti, “Lightning Induced Voltages on Multiconductor Overhead Lines”, IEEE Transaction on Power Delivery, Vol. 5, No. 2, pp.658-667, April 1990.

[43] A. E. Araujo, J. O. Paulino, J. P. Silva and H. W. Dommel, “Calculation of Lightning-Induced Voltages with RUSCK’s Method in EMTP. Part I: Comparison with Measurements and Agrawal’s Coupling Model”, Electric Power System Research, Vol. 60, pp.49-54, 2001.

[44] P. P. Barker, T. A. Short, A. R. Eybert-Berard, J. P. Berlandis, “Induced Voltage Measurements on an Experimental Distribution Line during Nearby Rocket Triggered Lightning Flashes”, IEEE Transactions on Power Delivery, Vol. 11, No. 2, pp. 98-995, April 1996.

[45] V. Jankov, “Estimation of the Maxital Voltage Induced on an Overhead Line due to the Nearby Lightning”, IEEE Transactions on Power Delivery, Vol. 12, No. 1, pp. 315-324, Jan. 1997.

[46] V. A. Rakov, "Rocket-Triggered Lightning Experiments at Camp Blanding, Florida", SIPDA 1999. http://plaza.ufl.edu/rakov/sipda1999.htm#top, 1.07.2009.

[47] F. Rachidi, C.A. Nucci, M. Ianoz, C. Mazzetti, "Response of Multiconductor Power Lines to Nearby Lightning Return Stroke Electromagnetic Fields", IEEE Transactions on Power Delivery, Vol. 12, pp. 1404-1411, July 1997.

[48] E. Perez, J. Herrera and H. Torres, "Sensitivity Analysis of Induced Voltages on Distribution Lines", IEEE Bologna PowerTech Conference, June 23-26, Bologna, Italy, 2003.

[49] P. D. Kannu and M. J. Thomas "Lightning Induced Voltages on Multiconductor Power Distribution Line", IEE Proceeding Generation, Transmission and Distribution, Vol. 152, No. 6, pp. 855-863, Nov. 2005.

[50] S. Yokoyama, "Calculation of Lightning-Induced Voltages on Overhead Lines", IEEE Transactions PAS, Vol. 103, No. 1, pp. 100-108, Jan. 1984.

[51] M. Paolone, C. A. Nucci, E. Petrache and F. Rachidi, "Mitigation of Lightning-Induced Overvoltages in Medium Voltage Distribution Lines by Means of Periodical Grounding of Shielding Wires and of Surge Arresters: Modeling and Experimental Validation", IEEE Transactions on Power Delivery, Vol. 19, No. 1, Jan. 2004.

[52] P. D. Kannu and M. J. Thomas "Lightning Induced Voltages on Overhead Conductors at Different Heights", IEEE Bologna PowerTech Conference, June 2 3-26, Bologna, Italy, 2003.

[53] S. M. A. Razzak, M. M. Ali, M. Z. I. Sarkar and H. Ahmad, "Lightning Induced over Voltages on Overhead Distribution Lines Including Lossy Ground Effects", 3rd International Conference on Electrical and Computer Engineering ICECE 2004, Dhaka, Bangladesh, 28-30 December 2004.

[54] P. D. Kannu, M. J. Thomas, "Influence of Lightning Electric Field Components on the Induced Voltages on a Power Distribution Line", Electric Power System Research, Vol. 64, pp. 247-255, 2003.

[55] A. Borghetti, C. A. Nucci, M. Paolone and F. Rachidi, "Characterization of the Response of an Overhead Line to Lightning Electromagnetic Fields", 25th International Conference on Lightning Protection, ICLP'2000, Rhodos, Greece, Sep. 2000.

[56] S. Guerrieri, C. A. Nucci and F. Rachidi, "Influence of the Ground Resistivity on the Polarity and Intensity of Lightning Induced Voltages", Proceedings of 10th International Symposium on High Voltage Engineering, Montreal, 24-30 Aug. 1997.

[57] C. A. Nucci, S. Guerrieri, M. T. Correia de Barros and F. Rachidi, "Influence of Corona on the Voltages Induced by Nearby Lightning on Overhead Distribution Lines", IEEE Transactions on Power Delivery, Vol. 15, No.4, pp. 1265-1273, Oct. 2000.

[58] M. T. Correia de Barros, J. Festas, C. A. Nucci and F. Rachidi, "Corona on Multi Conductor Overhead Lines Illuminated by LEMP", International Power System Transients, IPST1999, Budapest, June 1999.

[59] J. P. Silva, A. E. A. Araujo, J. O. S. Paulino, "Calculation of lightning-induced voltages with RUSCK's method in EMTP, Part II: Effects of Lightning Parameter Variations", Electric Power System Research, Vol. 61, pp. 133-137, 2002.

[60] C. A. Nucci, F. Rachidi, M. Ianoz and C. Mazzetti, "Lightning Induced Voltages on Overhead Power Lines", IEEE Transactions on Electromagnetic Compatibility, Vol. 35, pp. 75-86, 1993.

[61] http://www.hs.fi/english/article/Powerful+thunderstorm+hits+Helsinki+area+on+Wednesday+morning/1135229709338, 05.2009.

[62] T. J. Tuomi and A. Mäkelä, "Lightning observations in Finland", Report of Finnish Metrological Institute, Helsinki, Finland, No. 5, 2008.

[63] P. Verho, M. Marttila, K. Kannus, J. Pylvänäinen and M. Pouttu "Optimization of Overvoltage Protection of Distribution Networks", 19th International Conference on Electricity Distribution, CIRED 2007, Vienna, 21-24, May 2007.

[64] M-L. Pykälä, and V. Palva, "Protection Characteristics of Spark Gaps" Report 27, Helsinki University of Technology, High Voltage Institute, Espoo, Finland, 1997.

[65] W. Hauschild and W. Mosch, "Statistical Techniques for High-Voltage Engineering", Peter Peregrinus Ltd., London, 1992.

[66] E. Kuffel, W.S. Zaengl and J. Kuffel "High Voltage Engineering Fundamentals", published by Butterworth-Heinemann, pp. 472-489, 2nd Ed., 2000.

[67] S. Meijer, P. H. F. Morshuis and J. J. Smil "Breakdown Probability of SF6 due to Voltage Transient", Annual Report Conference on Electrical Insulation and Dielectric Phenomena, 2004.

[68] A. Haddad, D. M. German, R. T. Waters and Z. Abdul-Malek "Co-ordination of Spark-Gap Protection with Zinc-Oxide Surge Arresters", IEE Proceedings Generation, Transmission and Distribution, Vol. 148. No. 1, Jan. 2001.

[69] R. D. Yates, D. J. Goodman, Probability and Stochastic Processes, John Wiley and Sons, Inc. 2005.

[70] http://www.stats.gla.ac.uk/steps/glossary/probability_distributions.html#probdistn 05.2009.

[71] *NIST/SEMATECH e-Handbook of Statistical Methods*, http://www.itl.nist.gov/div898/handbook/, 05.2009

[72] W. Hauschild and W. Mosch, "Statistical Techniques for High-Voltage Engineering", Peter Peregrinus Ltd., London, 1992.

[73] http://wapedia.mobi/en/Q-function#3. 05.2009.

[74] M. K. Simon, "Probability Distributions involving Gaussian Random Variables: a Handbook for Engineers and Scientists", Kluwer Academic Publishers, Boston/Dordrecht/London, 2002.

[75] D. E. Parrish and D. J. Kvaltine “Lightning Faults on Distribution Lines”, IEEE Transactions on Power Delivery, Vol. 4, No, 4, Oct. 1989.

[76] A. Inoue and S. Kanao “Observation and Analysis of Multiple-Phase Grounding Faults Caused by Lightning”, IEEE Transactions on Power Delivery, Vol. 11, No, 1, Jan. 1996.

[77] A. Borghetti, C. A. Nucci and M. Paolone “Statistical Evaluation of Lightning Performances of Distribution Lines”, International Conference on Power Systems Transients, IPST 2001, Brazil June 24-28.

[78] I. M. Dudurych, T. J. Gallagher and M. Holly “A Novel Stochastic Approach to the Assessment of the Lightning Performance of HV Transmission Lines Using EMTP” PowerTech Conference Proceedings, 2003 IEEE Bologna.

[79] M. S. Savic “Medium Voltage Distribution Systems Lightning Performance Estimation”, IEEE Transactions on Power Delivery, Vol. 18, No. 3, July 2003.

[80] R. B. Anderson, “A Summary of Lightning Parameters for Engineering Applications,” CIGRE International Conference on Large High Voltage Electrical Systems, Paris, Aug. 1980.

[81] A. J. Eriksson, “The Incidence of Lightning Strikes to Power Lines”, IEEE Transactions on Power Delivery, Vol. PWRD-2, 1987.

[82] A. Borghetti, C. A. Nucci, M. Paolone and M. Bernardi “A Statistical Approach for Estimating the Correlation Between Lightning and Faults in Power Distribution Systems”, 9th International Conference on Probabilistic Methods Applied To Power Systems KTH, Stockholm, Sweden, June 11-15, 2006.

[83] J. A. Martinez and F. G. Molina “Statistical Evaluation of Lightning Overvoltages on Overhead Distribution Lines Using Neural Networks”, IEEE Transactions on Power Delivery, Vol. 20, No. 3, July 2005.

[84] Joint CIGRE/CIRED Working Group 05, “Lightning Protection of Distribution Networks. Part I: Basic Information”, 14th International Conference and Exhibition on Electricity Distribution, Birmingham, June 2-5, 1997.

[85] A. Joint CIGRE/CIRED Working Group 05, “Lightning Protection of Distribution Networks. Part II: Application to MV networks”, 14th International Conference Exhibition on Electricity Distribution, Birmingham, UK, Conference Publication No.438, 1997.

[86] Y. Kamata, K. Endoh, S. Furukawa, F. Endoh, K. Nonmmura, Y. Iwata, S. Horiuchi and N. Takasu, “Dielectric Strength of Oil-Immersed Transformer Insulation with Superimposed AC and Lightning Impulse Voltage”, IEEE Transactions on Electrical Insulation Vol. 25 No. 4, Aug. 1990.

[87] Y. Murata, S. Katakai and M. Kanaoka, “Impulse Breakdown Superposed on AC Voltage in XLPE Cable Insulation”, IEEE Transactions on Dielectrics and Electrical Insulation Vol. 3 No.3, June 1996.

[88] T. Yamazaki, Y. Takino, R. Matsuoka and S. Ito, “Flashover Voltage Characteristics of Contaminated Station Insulators under Temporary AC Overvoltages in the AC System Connected with a Frequency Converter Station”, Electrical Engineering Journal in Japan, Vol. 113, No. 8, March 2007.

[89] P. Hessen, W. Lampe, “PD Triggered by Switching Surges in Power Transformers”, IEEE Transactions on Power Apparatus and Systems, Vol. 91, pp. 1225-1234, 1972.

[90] J. Sletbak, A. Rein, and S. Haraldsen, “Breakdown Strength of Transformer Oil with Impulse Voltage Superimposed AC Voltage”, 1st ISH, H-7, 1972.

[91] International standard IEC 60060-1, High Voltage Test Techniques. Part 1: General Definitions and Test Requirements, 2nd edition, 1989-11.

[92] N. Sabiha, M. Lehtonen, N. Tarhuni, P. Hyvönen, “Probabilistic Model for MV Spark-gap Characteristics with Lightning Induced Overvoltage Superimposed on AC Voltage”, IEEE Transactions on Dielectric and Electrical Insulation, Vol. 16, No. 5, pp. 1404-1412, October 2009.

[93] J. G. Anderson “Lightning Performance of Transmission Lines”, Transmission Line Reference Book, 345 kV and above, Electric Power Research Institute: Palo Alto, CA, 1982, Ch. 12.

[94] M. A. Omidiora and M. Lehtonen “An Approach to the Lightning Overvoltage Protection of Medium Voltage Lines in Severe Lightning Areas”, World Congress on Engineering and Computer Science, 8 May 2008, Vol. 1007, pp. 140-151.

[95] M. Parviainen, P. Heine, M. A. Omidiora, M. Lehtonen, J. Niskanen and A. Oikarinen “Short Interruptions Caused by Lightning in Overhead Line Medium Voltage Networks”, Power Quality and Supply Reliability Conference, PQ 2008, Aug. 27-29, 2008.

[96] R. C. Dugan, M. F. McGranaghan, H.W. Beaty, *Electrical Power Systems Quality*, 1996 by the McGraw-Hill Companies.

[97] P. T. M. Vaessen, “Transformer Model for High Frequencies”, IEEE Transactions on Power Delivery, Vol. 3, No. 4, Oct. 1988.

[98] A. Piantini, C. V. S. Malagodi,.: “Modeling of Three-Phase Distribution Transformers for Calculating Lightning Induced Voltages Transferred to the Secondary”, IEEE, 5th International Symposium on Lightning Protection, Sao Paulo, 1999.

[99] V. Wyrebski, “Transmission of Overvoltage Spikes from Medium Voltage to Low Voltage Distribution Networks”, Master thesis 2006, tkk.

[100] N. Sabiha and M. Lehtonen “Experimental Verification of Distribution Transformers Model under Lightning Strokes” IEEE/PES, Power Systems Conference and Exposition, PSCE2009, 15-18 March 2009, Seattle, Washington, USA.

[101] L. Prikler and H. Hoildalen, *ATPDraw Users Manual*, SINTEF TR A4790, 1998.

[102] W. J. McNutt, T. J. Blalock, R. A. Hinton, “Response of transformer Windings to System Transient Voltages”, IEEE PES Summer Meeting and EHV/UHV Conference, Vancouver, Canada, July 15-20, 1973.

[103] O. Honorati, E. Santini, “New Approach to the Analysis of Impulse Voltage Distribution in Transformer Windings”, IEE Proceedings, Vol. 137, No. 4, July 1990.

[104] S. Okabe, M. koutou, T. Teranishi, S. Takeda and T. Saida “A High-Frequency Model of an Oil-Immersed Transformer, and its Use in Lightning Surge Analysis”, Electrical Engineering in Japan, Vol. 134, No. 1, 2001.

[105] Y. Shibuya, S. Fujita, “High Frequency Model and Transient Response of Transformer Windings”, Transmission and Distribution Conference and Exhibition, Asia Pacific. IEEE/PES, Vol. 3, pp. 1839-1844, 6-10 Oct. 2002.

[106] Y. Shibuya, S. Fujita, “High frequency Model Of Transformer Winding”, Electrical Engineering in Japan, Vol. 146, No. 3, 2004.

[107] M. Popov, L. Van der Sluis, R. P. P. Smeets, J. Lopez-Roldan and V. V. Terzija, “Modelling, Simulation and Measurement of Fast Transients in Transformer Windings with Consideration of Frequency-Dependent Losses”, IET Electric Power Applications, Vol. 1, No. 1, Jan. 2007.

[108] Y. Wang, W. Chen, C. Wang, L. Du and J. Hu, “A Hybrid Model of Transformer Windings for Very Fast Transient Analysis Based on Quasi-Stationary Electromagnetic Fields”, Electric Power Components Systems, 36:540-554, 2008.

[109] F. D. Leon and A. Semlyen, “Complete Transformer Model for Electromagnetic Transients”, IEEE Transactions on Power Delivery, Vol. 9, No. 1, Jan. 1994.

[110] V. Rashtchi, E. Rahimpour and E. M. Rezapour, “Using a Genetic Algorithm for Parameter Identification of Transformer R-L-C_M Model”, Electrical Engineering, Vol. 88, No. 5, June 2006.

[111] D. J. Wi lcox, W.G. Hurley, T.P. McHale and M. Conlon, “Application of modified Modal Theory in the Modelling of Practical Transformers”, IEE Proceedings-C, Vol. 139, NO. 6, Nov. 1992.

[112] P. Purkait and S. Chakravorti, “Investigations on the Usefulness of an Expert System for Impulse Fault Analysis in Distribution Transformers”, Electric Power Systems Research 65 (2003) 149-157.

[113] T. Noda, H. Nakamoto and S. Yokoyama, “Accurate Modelling of Core-Type Distribution Transformers for Electromagnetic Transient Studies”, IEEE Transactions on Power Delivery, Vol. 17, No. 4, Oct. 2002.

[114] T. Noda, M. Sakae and S. Yokoyama, “Simulation of Lightning Surge Propagation from Distribution Line to Consumer Entrance via Pole-Mounted Transformer”, IEEE Transactions on Power Delivery, Vol. 19, No. 1, Oct. 2004.

[115] V. Woivre, J. P. Arthaud, A. Ahmad, N. Burais, "Transient Overvoltage Study and Model for Shell-Type Power Transformers", IEEE Transactions on Power Delivery, Vol. 8, No. 1, Jan. 1993.

[116] D. R. Smith, J. L. Puri, "A Simplified Lumped Parameter Model for Finding Distribution Transformer and Secondary System Responses to Lightning", IEEE Transactions on Power Delivery, Vol. 4, No. 3, July 1989.

[117] J. Biernacki, D. Czarkowski, "High Frequency Transformer Modelling", IEEE International Symposium on Circuits and Systems (ISCAS), Vol. 3, pp. 676-679, 6-9 May 2001.

[118] J. Pleite, E. Olias, A. Lazaro, J. Vazquez, "Modeling the Transformer Frequency Response to Develop Advanced Maintenance Techniques", 14th PSCC, Sevilla, 24-28 June 2002.

[119] A. Piantini, W. Bassi, J. M. Janiszewski and N. M. Matsuo, "A Simple Transformer Model for Analysis of Transferred Lightning Surges from MV to LV Lines", Proceedings of the 15th International Conference on Electricity Distribution (15th CIRED), Nice, 1999.

[120] A. G. Kanashiro, A. Piantini, G. F. Burani, "A Methodology for Transformer Modelling Concerning High Frequency Surge", Proceedings of the VI International Symposium on Lightning Protection (VI SIPDA), pp. 275-280, Sao Paulo, Nov. 2001.

[121] A. G. Kanashiro A. Piantini, "Surges Transferred to the Low-Voltage Network via Transformer, the Influence of the Load Connected to the Secondary" International Conference on Grounding and Earthing and 3rd Brazilian Workshop on Atmospheric Electricity Rio de Janeiro - Brazil Nov. 4-7, 2002.

[122] R. J. Bachega, M. L. B. Martinez, "Transformer Modeling for Transferred Voltages", Transmission and Distribution Conference And Exposition, Latin America 2004.

[123] A. Morched, L. Marti, J. Ottevangers, "A High Frequency Transformer Model for the EMTP", IEEE Transactions on Power Electronics, Vol. 8, No. 3, July 1993.

[124] E. Dallago, G. Sassone and G. Venchi, "High-Frequency Power Transformer Model for Circuit Simulation", IEEE Transactions on Power Electronics, Vol. 12, No. 4, July 1997.

[125] T. Tran-Anh, P. Auriol, T. Tran-Quoc, "High Frequency Power Transformer Modeling for Power Line Communication Applications" Power Systems Conference and Exposition, 2006. PSCE '06. 2006 IEEE PES, Oct. 29 2006-Nov. 1 2006 pp. 1069 – 1074.

[126] N. Sabiha and M. Lehtonen "Lightning Induced Overvoltages Transmitted over Distribution Transformer with MV Spark-Gap Operation, Part I: High Frequency Transformer Model with MV Spark-Gap" Accepted to be Published in IEEE Transactions on Power Delivery.

[127] httpsclassshares.student.usp.ac.fjEE102LecturesWeek%2013%20Two%20Port%20Network.pdf.

[128] C. K. Alexander, M. N. O. Sadiku "*Fundamentals of Electric Circuits*", 3rd Edition, McGraw-Hill Higher Education, 2006.

[129] http://www.tina.com/course/28resonant/resonant.htm, 06.2008.

[130] J. Christian and R. Wimmer "Comparability of Transfer Function Results", European Transactions on Electrical Power 2006, Vol. 16, pp. 137-146.

[131] http://www.electrical-installation.schneider-electric.com/ei-guide/pdf_files/EIG-J-protection-voltage-surges.pdf, 06.2009.

[132] M. Darveniza and D. R. Mercer, "Lightning Protection of Pole Mounted Transformers", IEEE Transactions on Power Delivery, Vol. 4, No. 2, pp. 1087-1095, April 1989.

[133] J. F. Carter, M. Darveniza, N. Logothetis and T. M. Parneli, "Investigations of Selected High Voltage Tests on the Windings of 11 kV Transformers", ibid. Vol 6612. pp 89-97, 1976.

[134] Task Force Report, "Secondary (Low-Side) Surges in Distribution Transformers", IEEE Transactions on Power Delivery, Vol. 7, No. 2, April 1992.

[135] IEEE Std C62.72™-2007, IEEE Guide for the Application of Surge-Protective Devices for Low-Voltage (1000 V or Less) AC Power Circuits.

[136] S. S. Kershaw, G. L. Gaibrois and K.B. Stump, "Applying Metal-Oxide Surge Arresters on Distribution Systems", IEEE Transactions on Power delivery, Vol. 4, pp. 301-307, Jan. 1989.

[137] http://apa19.apator.com.pl/pdf/ASA_en.pdf, 06.2009.

[138] Catalogue card 2617pl082-W1-en. Edition 08.2008, Low Voltage Surge Arrester. http://www.cablejoints.co.uk/upload/Surge_Arresters.pdf, 07.2009.

[139] L. Arevalo, A. Mejia and O. Diaz, "Design and Construction of Surge Protection Devices for Rural Distribution Transformers Based on the Hygroscopic Properties of Sand", IX International Symposium on Lightning Protection, 26th -30th Nov. 2007, Foz do Iguaçu, Brazil.

[140] Joint CIGRE/CIRED Working Group 05, "Lightning Protection of Distribution Networks. Part II: Application to MV networks", 14th International Conference Exhibition on Electricity Distribution, Birmingham, UK, Conference Publication No.438, 1997.

[141] IEEE working group 3.4.11, Application of Surge Protective Devices Subcommittee, Surge protective devices committee, "Modeling of Metal Oxide Surge Arresters", Transactions on Power Delivery, Vol. 7 No.1, pp. 302-309, Jan. 1992.

[142] P. Pinceti and M. Giannettoni, "A simplified Model For Zinc Oxide Surge Arresters", IEEE Transactions on Power Delivery, Vol. 14, No. 2, April 1999.

[143] M. C. Magro, M. Giannettoni and P. Pinceti, “Validation of ZnO Surge Arresters Model for Overvoltage Studies”, IEEE Transactions on Power Delivery, Vol. 19, No. 4, Oct. 2004.

[144] N. Sabiha and M. Lehtonen “ATP/EMTP Simulation for Mitigation of Lightning Overvoltages at Customer Entrance” EEUG Meeting 2009, European EMTP-ATP Conference, 26, 27 and 28 October 2009, Delft, the Netherlands.

[145] N. Sabiha and M. Lehtonen “Lightning Induced Overvoltages Transmitted over Distribution Transformer with MV Spark-Gap Operation, Part II: Mitigation Using LV Surge Arrester” Accepted to be Published in IEEE Transactions on Power Delivery.

[146] N. Sabiha and M. Lehtonen “Investigating Lightning Induced Overvoltages Transmitted to Customer” The International Conference on Power Systems Transients, IPST2009, June 3-6 2009, Kyoto, Japan.

[147] S. Matsuura, T. Noda, A. Asakawa and S. Yokoyama “EMTP Modelling of a Distribution Line for Lightning Overvoltages Studies”, International Conference on Power Systems Transients, IPST2007, Lyon, France, June 4-7, 2007.

[148] K. Nakada, H. Sugimoto and S. Yokoyama “Experimental Facility for Investgation of Lightning Performance of Distribution Lines”, IEEE Transactions on Power Delivery, Vol. 18, No. 1, Jan. 2003.

[149] S. M. A. Razzak, M. M. Ali, M. Z. I. Sarkar and H. Ahmad “Lightning Induced Overvoltages on Overhead Distribution Lines Including Lossy Ground Effects”, 3rd International Conference on Electrical and Computer Engineering (ICECE) 2004, 28-30 December 2004, Dhaka, Bangladesh.

[150] S. Yokoyama and A. Askawa “Experimental Study of Response of Power Distribution Lines to Direct Lightning Hits”, IEEE Transactions on Power Delivery, Vol. 4, No. 4, Oct.1989.

[151] A. D. Conti and S. Visacro “Evaluation of Lightning surges Transferred from Medium Voltage to Low-Voltage Networks”, IEE Proceeding Generation Transmission Distribution, Vol. 152, No. 3, May 2005.

[152] S. Sekioka, K. Aiba and S. Okabe “Lightning Overvoltages on Low Voltage Circuit Caused by Ground Potential Rise”, International Conference on Power Systems Transients, IPST2007, Lyon, France, June 4-7, 2007.

[153] A. Borghetti, A.S. Morched, F. Napolitano, C.A. Nucci, M. Paolone, “Lightning-Induced Overvoltages Transferred Through Distribution Power Transformers”, IEEE Transactions on Power Delivery, Vol. 24, No. 1, pp. 360-372, Jan. 2009.

[154] H.K. Høidalen, J.H.F. Dahlslett, T. Aalborg, “Impacts of Lightning-induced Overvoltages on Power Quality in Low-Voltage Distribution Systems”, Proceeding of the 25th International Conference on Lightning Protection, Rhodes, Greece, 18-22 Sep. 2000.

[155] S. Yokoyama, K. Miyake and S. Fukui “Advanced Observations of Lightning Induced Voltage on Power Distribution Lines (II)”, IEEE Transactions on Power Delivery, Vol. 4, No. 4, Oct.1989.

[156] T. Miyazaki, S. Okabe and S. Sekioka “An Experimental Validation of Lightning Performance in Distribution Lines”, IEEE Transactions on Power Delivery, Vol. 23, No. 4, Oct., 2008.

[157] T. Hirai, S. Okabe, T. Takinami and T. Chindo “Statistical Analysis of Lightning Performance of Distribution Lines Based on Observation in Fields”, Electrical Engineering in Japan, Vol. 155, No. 2, 2006.

[158] 20/1/0.4 kV three voltage level distribution system, Report, LUT 2005, Available on Line on http://www.ee.lut.fi/fi/lab/sahkomarkkina/index.html.

[159] http://www.ru.prysmian.com/ru_RU/cables_systems/energy/product_families/pdf/amka_uk_n.pdf;jsessionid=KZI524UVIJSEZFYKJOPCFEY.

[160] R. H. Golde, “Lightning, Volume 2, Lightning Protection”, London. New York, San Francisco, chapter 24, 1977.

[161] http://www.ucable.com.my/catalogue/xlpe_insulated_power_cables.pdf.

Appendices

A. GFD Map in Finland

Figure A shows average ground flash density (GFD) per 100 km^2 in Finland from 1998-2008 which was collected from the FMI (Finnish Meteorological Institute) on thunderstorms days. Every stroke was located separately then they are grouped into full flashes by location system. The flash is found more appropriate climate quantity, and therefore, it can be used for the statistical study. More details can be found in [62].

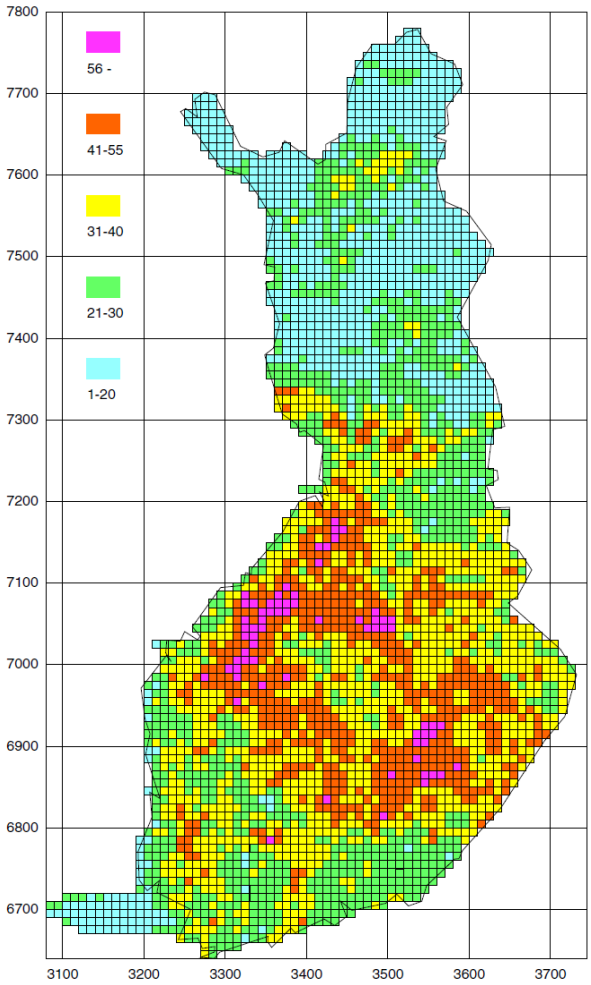

Figure A Flashes on 10 km × 10 km squares in 1998-2008 [62].

B. Probability Overview

The probability is a number between 0 and 1 computed using large number of experiments. If it is 0, the event will not be occurred and if it is 1, there is certainty that the event will occur. The value in between 0 and 1 declares the probability of the event to occur. The probability can be used to describe any random process by statistical approach.

B.1 Counting Methods

If there are subexperiments A and B where each one has N and n possible outcomes, there are Nn possible outcomes when both experiments are performed. The total number of possibilities is in the form [69]:

$$(N)_n = \frac{N!}{(N-n)!} \tag{1}$$

Assuming the number of k-combinations of n objects $\binom{N}{n}$, the following two subexperiments to assemble a n-permutation of n distinguishable objects:

1. Choose a n-combination out of the n objects which has $\binom{N}{n}$ possible outcomes.

2. Choose a n-permutation of the k objects in the k-combination which has $n!$ Possible outcomes.

Therefore the number of outcomes of the combined experiment is $(N)_n$ is in the form:

$$(N)_n = \binom{N}{n} n! \qquad \therefore \binom{N}{n} = \frac{(N)_n}{n!} = \frac{N!}{n!(N-n)!} \quad \text{(binomial coefficient)} \tag{2}$$

$$\binom{N}{n} = \binom{N}{N-n} \tag{3}$$

For an integer $N \geq 0$,

$$\binom{N}{n} = \begin{cases} \dfrac{N!}{n!(N-n)!} & n = 0,1,.....,N, \\ 0 & otherwise \end{cases} \tag{4}$$

B.2 Independent Trials

Considering independent repetition of a subexperiment of experiments, the probability models can be attained assuming a success occurs with probability p; otherwise, a failure occurs with probability *1-p*. The probability of n_0 failures and n_1 successes in $n = n_0 + n_1$ independent trials are in the form [69]:"

$$P\left[S_{n_0,n_1}\right] = \binom{n}{n_1}(1-p)^{n-n_1} p^{n_1} = \binom{n}{n_0}(1-p)^{n_0} p^{n-n_0} \tag{5}$$

B.3 Probability Distributions

The probability distribution for a random variable describes how probabilities are distributed over the values of the random variables and defined by a probability function. There are a large number of distributions used in statistical applications, which can be classified into two types of the probability distributions depending on the random variable, discrete and continuous distributions.

There are three main types of both discrete and continuous distributions, they are, probability density function (pdf), cumulative distribution function (cdf) and survival density function (sdf). These functions can be expressed as a function of each cdf=1- sdf and pdf = d(cdf)/dx.

B.3.1 Discrete Distributions

The probability distribution of a discrete random variable X produces the probability $p(xi)$ that the random variable is equal to xi, for each value xi [70]:

$$p(xi) = P(X=xi) \tag{6}$$

where the constraints are:

$$0 \leq p(xi) \leq 1 \tag{7}$$

$$\sum p(xi)=1 \tag{8}$$

Among the most well-known discrete probability distributions that are used for statistical modeling are single-point distribution, the discrete uniform distribution, the Poisson distribution, the Bernoulli distribution, the binomial distribution, the geometric distribution, the negative binomial distribution [71,72]. In this dissertation, the binomial distribution was used. So, a small overview of it is given below.

Binomial distribution

The binomial distribution is probably the most commonly used discrete distribution. The formula for the binomial probability mass function is expressed as [72]:

$$f(x, p, n) = \binom{n}{x}(1-p)^{n-x}\ p^{x} \text{ for } x= 0,1,2,\ldots\ldots n. \tag{9}$$

The formula for the binomial cumulative probability function is:

$$F(x, p, n) = \sum_{i=0}^{x}\binom{n}{i}(p)^{i}(1-p)^{n-i} \tag{10}$$

As two status decision (either yes or no), the binomial distribution can be suitable for all testing problems of such decisions

B.3.2 Continuous Distributions

The continuous random distributions is in the form [70]:

$$f(x) = \frac{d}{dx} F(x) \text{ , F(x)= P(X} \le \text{x) leads to } \int f(x)\, dx = F(b) - F(a) = P(a < X < b) \quad (11)$$

where $f(x)$ is the probability density function of a continuous random variable X and $F(x)$ is the cumulative distribution function.

This type contains a large number of distributions used in statistical applications [71, 72]. Such as, continuous uniform distribution, normal distribution, uniform distribution, cauchy distribution, t distribution, F distribution, chi-square distribution, exponential distribution, weibull distribution, lognormal distribution, fatigue life distribution, gamma distribution, double exponential distribution, power normal distribution, power lognormal, tukey-Lambda distribution, extreme value type I distribution and beta distribution. In this dissertation, the normal distribution was used. So, a small overview of it is given below

Normal distribution

It is also well known by Gaussian functions and it is expressed by (12), where, m is the mean and σ is the standard deviation which means that the probability distribution is characterized by location and scale parameters. The standard normal distribution is the case where $m = 0$ and $\sigma = 1$ expressed by (13).

The mean is the average of the data points as given by (14), $\overline{Y}$ is the mean of the data, ND is the number of data point. Standard deviation is the square root of the variance (15) and the variance is defined as (16).

$$f(x) = \frac{e^{-(x-m)^2/(2\sigma^2)}}{\sigma\sqrt{2\pi}} \quad (12)$$

$$f(x) = \frac{e^{-x^2/2}}{\sqrt{2\pi}} \quad (13)$$

$$\overline{Y} = \frac{\sum_{i=1}^{N} Y_i}{ND} \quad (14)$$

$$\sigma = \sqrt{\sum_{i=1}^{N} (Y_i - \overline{Y})^2 / (ND-1)} \tag{15}$$

$$\sigma^2 = \sum_{i=1}^{N} (Y_i - \overline{Y})^2 / (ND-1) \tag{16}$$

The normal distribution is the most important distribution in statistics for theoretical as well as practical reasons [71].

B.4 Gaussian *Q*- Function *Q*(*x*)

The *Q*-function is the defined as the tail probability of the normalized Gaussian distribution. The *Q*-function take the form [73,74]:

$$Q(k) = \frac{1}{\sqrt{2\pi}} \int_{k}^{\infty} \exp(-\frac{w^2}{2})\, dw \tag{17}$$

Thus, $Q(k)=1-\phi(k)$ (18)

where $\phi(k)$, is the cumulative function of the Gaussian distribution.

The *Q*-function can be related to the error and complementary error functions as:

$$Q(k) = \frac{1}{2} - \frac{1}{2} erf(\frac{k}{\sqrt{2}}) = \frac{1}{2} erfc(\frac{k}{\sqrt{2}}) \tag{19}$$

where, *erf* (*k*) is the error function and *erfc*(*k*) is the complementary error function. They are expressed as:

$$erf(k) = \frac{2}{\sqrt{\pi}} \int_{0}^{k} e^{-t^2}\, dt. \tag{20}$$

$$erfc(k) = 1 - erf(k) = \frac{2}{\sqrt{\pi}} \int_{k}^{\infty} e^{-t^2}\, dt. \tag{21}$$

C. Number of Strikes to Distribution Lines

The number of strikes to distribution lines are depend on three important factors must which are [75]:

1. Accurate *ground* flash density data.

2. The number of strikes to lines of known length and height.

3. Shielding from other nearby structures.

So, Eriksson equation can be modified to take the form (22) instead of (23).

$$N_s = N_g\,(b+28h^{0.6})\times 10^{-1}\times(1-Sf) \quad (22)$$

$$N_s = N_g\,(b+28h^{0.6})\times 10^{-1} \quad (23)$$

Where N_s is the number of strikes to the line. N_g is the ground flash density, it is the number o lightning flashes striking one square kilometer on the earth in a year. It was obtained by lightning flash counter but nowadays it is obtained by lightning localization systems. In general it will range between less than one ground flash km^{-2} yr^{-1} to about 10 km^{-2} yr^{-1}. b (m) is the width of the line, is considered for multi-conductor lines with the conductor arranged horizontally. h is the height of the line. Sf is shielding factor.

D. Experiments' Devices

With the aid of the experimental configuration shown in Figure 2.4, the capacitor divider is used for transforming the breakdown voltage to be suitable input to the oscilloscope. Voltage measurements were achieved using a coaxial probe. The experimental setup data are:

Impulse voltage source: 800 kV (4-stage), 1.6/50 μs,
Capacitive divider: 500PF, 100kV rms, 400 kV impulse, response time < 100 ns,
Spark-gap: double spark-gap horn to horn,
Current limiting resistor: 50 kΩ,
Transformer (AC voltage source): 20000/ 400 V), Δ/Y,
Oscilloscope: 100 MHz, 500 Ms/s DSO.

E. Spark-gap Dimensions

The used spark-gap configuration and its dimensions are depicted in Figure B. It is horn to horn type.

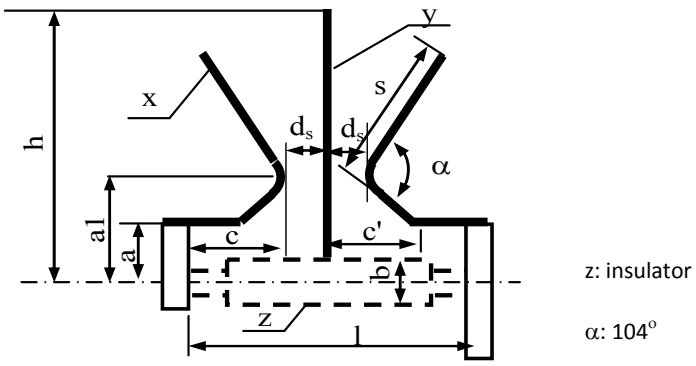

Dimensions	a	a1	d_s	c	c'	b	h	l	S	x	y
(mm)	75	160	40	80	80	100	335	255	125	ϕ8	ϕ6

Figure B Spark-gap configuration and dimensions.

F. Segment of Matlab Script File

```
n = 1; % initiating a counter
Um = 86.9e3; % Mean
Us = 2.75e3; % Standard deviation
Uo = 17.0e3; % Peak supply Voltage
U = 20e3:2e3:140e3; % Voltage range 20 to 140 kV.
Px=1-qfunc((U-Um)./Us); % The model of the impulse
for Ut = U;
    % The model of the combined waveforms is
    Pu(n) = 1 - 1/(2*pi)...
       *quadl(@(x)qfunc((Ut-Uo.*cos(x)-Um)./Us) ...
       ,0,2*pi);
    n=n+1
end
```

G. Experimental Devices

Requirements components for experiment shown in Figure 3.3 are:

1- Impulse voltage source 940 V, 0.87/50 μs,

2- Transformer (T1): 100 kVA Dyn5 21000 V ± 2 x 2.5 %/420 V 2.75 A / 137.5 A,

3- Transformer (T2): 50 kVA Yzn11 20500 V/410 V 1.41 A / 70.4 A,

4- Pearson current monitor Model 110A has been used to measure the phase current, with frequency range 1 Hz- 20MHz.,
5- A probe 100:1 to measure the voltage,
6- Digital recorder LeCroy LP142 controlled by HPVEE program for the measurements.

H. Step-by-Step Piantini Model Parameters Determination

The values of the circuit parameters shown in Figure 3.7 can be derived for each transformer from the analysis of its input impedance and frequency response as depicted below.

Step 1: Input impedance analysis

$$Z_{in} = \frac{U_1}{i_1} = R + j(\omega L - \frac{1}{\omega C}) \tag{24}$$

where, $R=R\_1+R\_2$ and $L=L\_1+L\_2$.
The modulus value of input impedance is:

$$|Z_{in}| = \sqrt{R^2 + (\omega L - \frac{1}{\omega C})^2} \tag{25}$$

At the resonance frequency (f_r),

$$\omega L = \frac{1}{\omega C}, \qquad f_r = \frac{1}{2\pi\sqrt{LC}} \tag{26}$$

$$|Z_{in}| = R = R\_1 + R\_2 \tag{27}$$

So, f_r and R were graphically obtained from the frequency response of input impedance.

Step 2: Frequency response analysis of the transformer

$$\frac{U_2}{U_1} = \frac{R\_2 + j\omega L\_2}{Zin} \tag{28}$$

Then, its modulus is:

$$\left|\frac{U2}{U1}\right| = \frac{\sqrt{R\_2^2 + (\omega L\_2)^2}}{\sqrt{R^2 + (\omega L - \frac{1}{\omega C})^2}} \tag{29}$$

At the resonance frequency f_r

$$\left|\frac{U2}{U1}\right| = \frac{\sqrt{R\_2^2 + (\omega L\_2)^2}}{R} \tag{30}$$

Where $\left|\frac{U2}{U1}\right|$ was graphically obtained from the frequency response of the transformer.

At a phase angle φ=0, $\left|\frac{U2}{U1}\right| \approx \frac{R\_2}{R}$ (31)

Where, $\frac{R\_2}{R}$ was graphically determined from the frequency response of the transformer

For very high frequencies, when w → ∞

$$\left|\frac{U_2}{U_1}\right| \approx \frac{L\_2}{L} \approx \frac{L\_2}{L\_1 + L\_2} \quad (32)$$

$\frac{L\_2}{L}$ was determined graphically from the frequency response of the transformer.

After obtaining the values (f_r, R, $|\frac{U2}{U1}|$ at f_r, $\frac{R\_2}{R\_1}$ and $\frac{L\_2}{L}$), the circuit parameters can deduced from the above equations as following:

- *R_2* was deduced from equation (31), and then *R_1* was deduced from equation (27).
- *L_2* was deduced from equation (30) then *L* and *L_1* were deduced from equation (32).
- The capacitance *C* was deduced from equation (26).

These parameters were tuned to get the optimum values. The tuning process was carried out to compensate the approximation during the parameters calculations.

I. Two-Port Networks

There are four types of two-port networks shown in Figure C, they are impedance parameters, admittance parameters, hybrid parameters and transmission parameters. The conditions to use such these networks with the following analysis are:

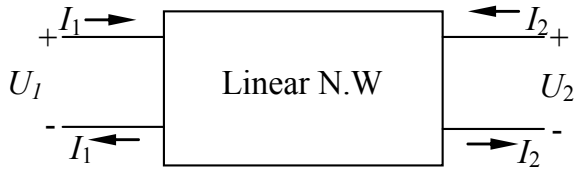

Figure C Two-port network.

1. Impedance parameters

The values of the parameters can be evaluated using open circuit tests for both of input port and out port as declared from Figure D. the corresponding equations in this case are:

$U_1=Z_{11}I_1+Z_{12}I_2$ (33)

$U_2=Z_{21}I_1+Z_{22}I_2$ (34)

where, Z_{11} : open circuit input impedance, Z_{12} : open circuit transfer impedance from port 1 to port 2, Z_{21} : open circuit transfer impedance from port 2 to port 1 and Z_{22} : open circuit output impedance.

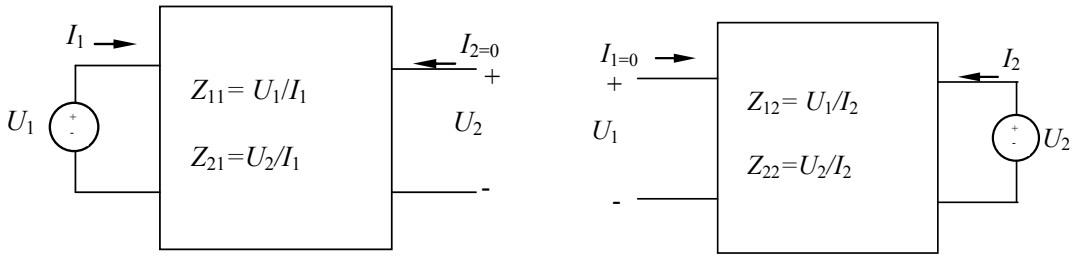

a. Finding Z_{11} and Z_{21} b. Finding Z_{12} and Z_{22}

Figure D Impedance parameters measurements for parameters determination.

2. Admittance parameters

The values of the parameters can be evaluated by setting $U_2 = 0$ (output port short circuit) or $U_1 = 0$ (input port short circuit) as declared from Figure E. the corresponding equations are:

$$I_1=Y_{11}U_1+Y_{12}U_2 \quad (35)$$

$$I_2=Y_{21}U_1+Y_{22}U_2 \quad (36)$$

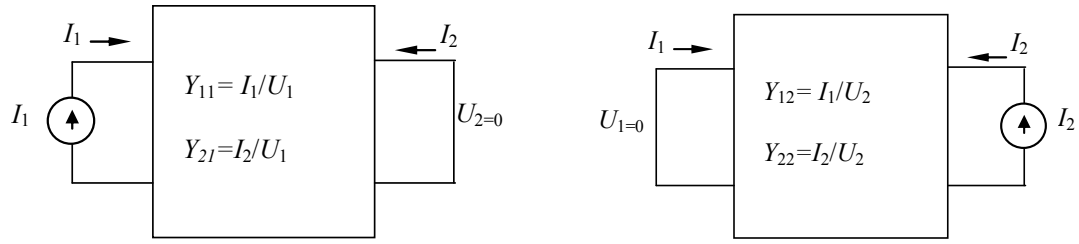

a. Finding Y_{11} and Y_{21} b. Finding Y_{12} and Y_{22}

Figure E Admittance parameters measurements for parameters determination.

3. Hybrid parameters

The values of the parameters can be evaluated by setting $U_2 = 0$ (output port short circuit) or $I_1 = 0$ (input port open circuit) as declared from Figure F. the corresponding equations are:

$$U_1=h_{11}I_1+h_{12}U_2 \quad (37)$$

$$I_2=Y_{21}I_1+h_{22}U_2 \quad (38)$$

where h_{11} is the short-circuit input impedance, h_{12} is the open-circuit reverse voltage gain, h_{21} is the short-circuit forward current gain and h_{22} is the open-circuit output admittance.

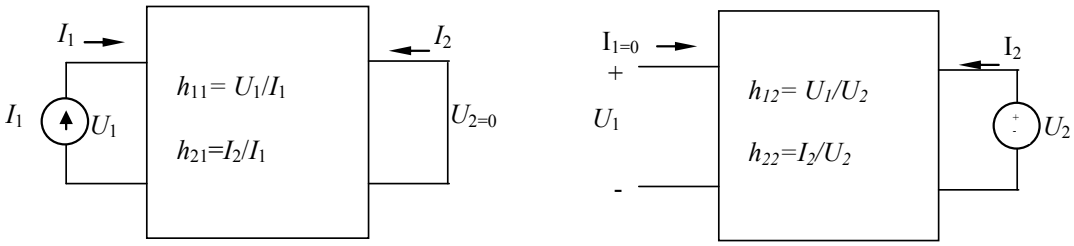

b. Finding h_{11} and h_{21} b. Finding h_{12} and h_{22}

Figure F Hybrid parameters measurements for parameters determination.

4. Transmission parameters

The values of the parameters can be evaluated by setting $U_2 = 0$ (output port short circuit) or $I_2 = 0$ (output port open circuit) as declared from Figure G. the corresponding equations are:

$$U_1 = AU_2 - BI_2 \quad (39)$$

$$I_1 = CU_2 - DI_2 \quad (40)$$

where, A : open-circuit voltage ratio, B : Negative short-circuit transfer impedance, C :open-circuit transfer admittance and D : Negative short-circuit current ratio.

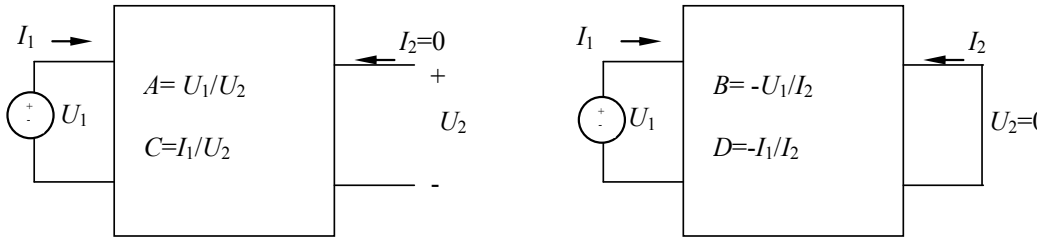

a. Finding A and C b. Finding B and D

Figure G Transmission parameters measurements for parameters determination.

J. Procedure For Parameter Determination Of The Proposed Transformer Model

Using impedance analysis (input impedance (Z_{11}), output impedance (Z_{22}) and transfer impedance (Z_{12}), the elements value of the high frequency transformer model shown in Figure 3.30 can be evaluated as illustrated below.

I. From the impedance analysis in frequency domain, the connections of the elements R, L and C can be estimated (either parallel connected or series connected).

II. The values of the high frequency transformer model elements can be calculated using the frequency response of the mentioned impedances by the following concepts.

A. <u>At resonance frequency (F_r)</u>

$$Z = R\Big|_{Series\ resonance} \ \&\ \ Y = 1/R\Big|_{Parallel\ resonance} \tag{41}$$

$$LC = \frac{1}{4\pi^2 F_r^{\,2}} \tag{42}$$

B. <u>At very high frequency</u>
For series resonance circuit

$$\frac{1}{\omega C} = 0 \quad \& L = \left(\sqrt{|Z|^2 - R^2}\right)/\omega \tag{43}$$

From Equation 42, the capacitive element can be calculated as:

$$C = \frac{1}{4\pi^2 F_r^{\,2} L} \tag{44}$$

For parallel resonance circuit

$$\frac{1}{\omega L} = 0 \quad \& C = \left(\sqrt{|Y|^2 - \frac{1}{R^2}}\right)/\omega \tag{45}$$

From Equation 42, the inductive element can be calculated as:

$$L = \frac{1}{4\pi^2 F_r^{\,2} C} \tag{46}$$

K. Different Network Configurations

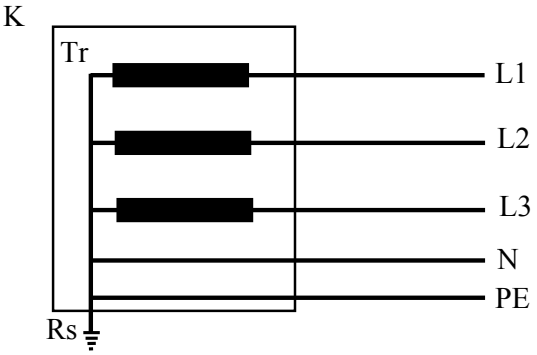

a. TN-S the supply network has a connection of the neutral conductor with the earthing conductor at the feeding transformer only.

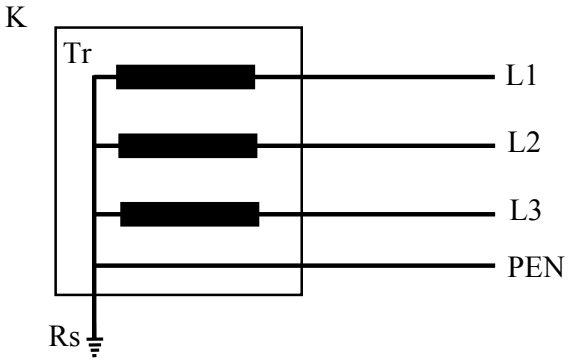

b. TN-C neutral and earthing conductor are common (PEN) and earthed at the transformer or near it.

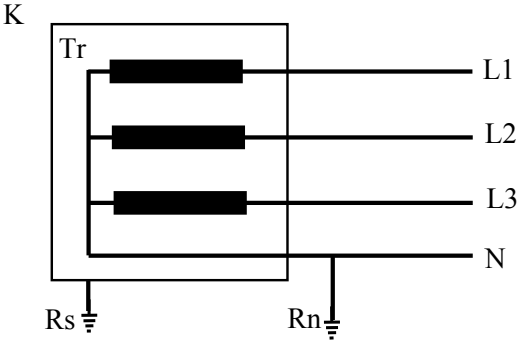

c. TN-C-S the neutral conductor is earthed at the transformer and in other network points.

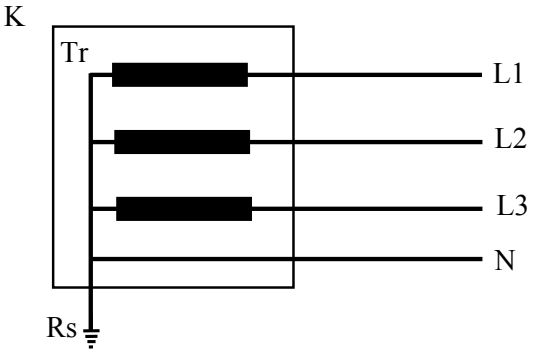

d. TT neutral point of transformer is earthed directly, while the reciever's installation is earthed by a separate earth electrode.

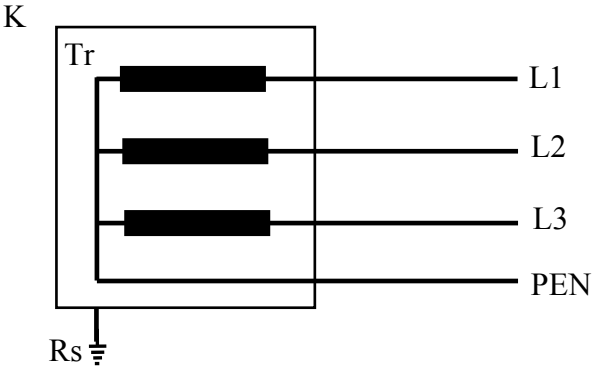

e. IT in this system there is no direct connection of active network parts with earth, while accessible conducting parts of installation elements are earthed.

Marking
L1,2,3 phase conductor, N is the neutral conductor, PE is the earthing conductor, PEN is the common earthing and neutral conductor, K is the transformer tank, Rs is the protective earthing of station, Rn is the earthing of transformer neutral point..

Figure H Network configurations.

L. Nonlinear Resistors of Surge Arrester

The nonlinear characterstics of the surge arrester nonlinear elements are shown in Table A.

Table A V-I characteristics of A_0 and A_1

I(kA)	A_0(PU)	A_1(PU)
2×10^{-6}	0.81	0.623
0.1	0.974	0.788
1	1.052	0.866
3	1.108	0.922
10	1.195	1.009
20	1.277	1.091

M. Overhead Cable

The feeders are represented using LCC JMarti model. The configuration of the overhead cable and the corresponding dimensions and parameters are shown in Figure I. In Overhead cable, the messenger conductor has two dual functions, it is earthed in addition to it is uncovered for the protection purpose. The dimensions and parameters are:

- Conductor cross-section = 35 mm^2,
- Outer insulation thickness = 1.6 mm,
- Over messenger area =70 mm^2,
- Conductor resistivity = 2.84×10^{-9} Ω.m,
- Relative permeability of the conductor material = 1,
- Relative permeability of the insulator material outside the conductor = 1,
- Relative permittivity of the insulator material outside the conductor = 2.3.

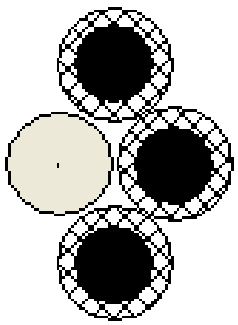

Figure I Three phase conductors + one messenger overhead cable.

N. Underground Cable

The underground cable sections are considered four core cables buried 0.7 m deep under earth and arranged as shown in Figure J.

Underground cable dimensions and parameters are:

- Conductor cross-section = 35 mm2,
- Outer insulation thickness = 0.9 mm,
- Overall diameter =25.4 mm,
- Conductor resistivity = 2.84×10^{-9} Ω.m,
- Relative permeability of the conductor material = 1,
- Relative permeability of the insulator material outside the conductor = 1,
- Relative permittivity of the insulator material outside the conductor = 5.1.

Pipe data are :

- Depth= 0.7 m,
- Inner radius= 0.0105 m,
- Outer radius= 0.0109 m,
- Insulator radius= 0.0127 m,
- Conductor resistivity = 2.84×10^{-9} Ω.m,
- Relative permeability of the conductor material = 1,
- Relative permittivity of the insulator material = 5.1.

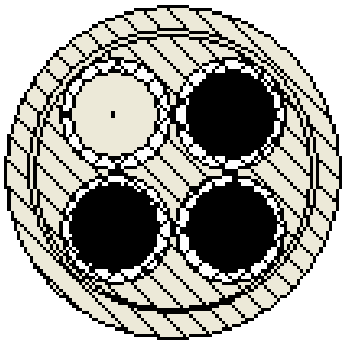

Figure J Four cores, XLPE/PVC underground cable.

ISBN 978-952-60-3045-6
ISBN 978-952-60-3046-3 (PDF)
ISSN 1795-2239
ISSN 1795-4584 (PDF)